A STUDY OF A REDOX NON-INNOCENT TETRADENTATE DIAMIDE-DIIMINE LIGAND CHELATED TO TITANIUM, CHROMIUM, AND IRON: FROM CATALYTIC NITRENE GROUP TRANSFER TO ELECTRONIC STRUCTURE

A Dissertation

Presented to the Faculty of the Graduate School

of Cornell University

In Partial Fulfillment of the Requirements for the Degree of

Doctor of Philosophy

by

Spencer Palmerlee Heins

August 2018

A STUDY OF A REDOX NON-INNOCENT TETRADENTATE DIAMIDE-DIIMINE LIGAND CHELATED TO TITANIUM, CHROMIUM, AND IRON: FROM CATALYTIC NITRENE GROUP TRANSFER TO ELECTRONIC STRUCTURE

Spencer Palmerlee Heins, Ph. D.

Cornell University 2018

Redox non-innocent (RNI) or “redox-active” ligands have become an essential part of inorganic chemistry. RNI dithiolate ligands studied in the 1960’s contributed to our understanding of electronic structure and utilized the recently developed ligand field theory. Since then, RNI ligands have been discovered in naturally occurring sources such as cytchrome P-450, and have found myriad applications in synthetic transition metal chemistry and catalysis. RNI ligands can be leveraged to tune the electronic structure of transition metal complexes to confer nobility upon first row transition metals or promote desirable one electron processes.

While RNI ligands of various forms have been studied for over 50 years, there is still much to be explored. Modern analytical techniques and computational methods have expanded the chemist’s ability to study these systems to gain a deeper understanding of the effects of electronic structure on reactivity. The purpose of this work is to expand the knowledge of RNI ligands and to understand how redox non-innocence manifests reactivity and affects the electronic structure of first row transition metal complexes. To achieve this goal, a detailed synthetic and reactivity study of the tetradentate diamide-diimine (dadi) ligand chelated to titanium, chromium, and iron was

pursued.

The study began initially with synthesis of the dadi ligand and the titanium, chromium, manganese, and iron complexes, which was performed by Dr. Wesley Morris in this laboratory. Following the early work of Dr. Morris, the reactivity of the chromium and iron dadi complexes was explored. This work found RNI was responsible for the processes observed in the system that ultimately lead to formal insertion of imidyls into the C-C bond of the ligand backbone. Along the same vein, the RNI of the dadi ligand was found to be critical for nitrene group transfer that generated adamantyl isocyanate, catalyzed by a titanium imido species.

In between these highlights of chemistry, various metal complexes were synthesized to probe the electronic structure, and to discover new and interesting chemistry. The diversity of reactions available to a single RNI ligand is exemplified in the later chapters of this work. A direct carbene transfer was discovered to be effected by the RNI dadi ligand, providing insight into the mechanism of metal catalyzed cyclopropanations. In the final expansion of this work, radical type reactions were discovered that diverge from the previously studied nitrene transfer, a 2-electron process.

BIOGRAPHICAL SKETCH

Spencer Heins grew up spending his school years in Denver, CO with his mother, and spending his summers in Alaska with his father. His love for skiing was kindled as a young child in Montana and continued to affect his decisions later on in life, particularly his choice of undergraduate institution. Besides being the only college he was accepted into, Fort Lewis' proximity to world class skiing made the decision very easy. Spencer began his undergraduate studies as a physics major, but quickly realized that his math background was not suited for physics, and instead he switched majors to Chemistry, not knowing the long path it would lead him down.

At Fort Lewis College, Spencer carried out research with Dr. Kenny Miller working on the total synthesis of the natural product (+)-satazzolin. After completing the synthesis, Spencer's disdain for column chromatography was deeply rooted, but his love for synthesis remained strong. Naivety lead Spencer to believe that he would find gainful employment as a bachelor level scientist after graduating, but this turned out to be particularly difficult. He had impressed his undergraduate inorganic professor Dr. Monte Helm enough during classes that he was offered a position at Pacific Northwest National Laboratory (PNNL), where Monte had recently started as a Senior Staff Scientist.

At PNNL Spencer worked with Elliott Hulley, who convinced someone at Cornell University that Spencer would be a worthy graduate student, despite his mediocre GRE scores. Once Spencer was accepted into Cornell he quickly found his place in the Wolczanski Group. Since then he has enjoyed studying RNI ligands with first row metals, and beers once or twice a week.

Dedicated to Mom and Dad

ACKNOWLEDGMENTS

I have been extremely lucky over the years to have had incredible mentors in my life. First I would like to thank Monte for believing in me as a researcher and giving me the opportunity to grow as a scientist and become ready for graduate school. Your advice during grad school when I was down, letters of recommendation, and your unwavering support even when your obligations to me had long passed are deeply appreciated. It is because of you that I am here now, and for that I am eternally indebted. Of course, Pete deserves a large thank you as well, for training me to become a Ph.D. scientist from meager beginnings. You exemplify what a Ph.D. advisor should be, which I have been watching and hope to be able to repeat in my own career.

There are many friends and colleagues to thank, starting with Russ Algera, the kinetics extraordinaire. Russ probably deserves an authorship, but would never accept because his genuine curiosity was the only motivation he needed to help me. I would also like to thank Kyle Mack and Anton Chavez for countless adventures and for providing much needed reprieves from the real world. While Anton will not be forgiven for moving to Chicago, he should know that his company is always welcome. I would also like to thank Wes for the most valuable advice I have ever received in graduate school: ‘he will probably yell at you, but at least you’ll learn something and everyone will forget about it once we get to beers’. I would also like to thank the former group members Valerie, Wes, Lindley, OB, and Elliott for training me and getting me started in lab. Without you all I certainly would have floundered. Shekie deserves a thanks as well, for staying in touch and taking time away from the beam to remind me that there is a better world out there. Thank you to Emil Lobkovsky

and Sam MacMillan for helping me with crystallography over the years. I would also like acknowledge and thank Tom Cundari, our indispensable theoretical collaborator. None of the mechanisms or molecular orbital calculation in this thesis were done by me, Tom is solely responsible and for that I am very grateful.

Lastly, I would like to thank Avery, for being my reason to stay in this far away humid and gray land. We have had such an amazing time together, I am forever grateful that you were with me along this bumpy road. I love you and I cannot wait to continue my life, full of adventures, with you.

TABLE OF CONTENTS

LIST OF SCHEMES

LIST OF FIGURES

LIST OF TABLES

LIST OF ABBREVIATIONS

Ad:	1-adamantyl
$DadiH_2$:	N,N'-Di-2-(2,6-diisopropylphenylamine)-phenylglyox-aldiimine
Dadi:	diamide-diimine; $\{-CH=N(1,2-C_6H_4)N(2,6-^iPr_2-C_6H_3)\}_2$
$(dadi)Na_2$:	Bis(tetrahydrofuran-2-yl)sodium(II)(((1E,1'E)-ethane-1,2-diylidenebis(azanylylidene))bis(2,1-phenylene))bis((2,6-diisopropylphenyl)amide)
DaIm:	Diamide-imidazole; N^1-Ar-N^2-((1-Ar-1-benzo[d]imidazol-2-yl)methyl)benzene-1,2-diamide
1-Br_2:	(dadi)$TiBr_2$; Titanium N, N'-di-2-(2,6-diisopropylphenylamide)-phenylglyoxaldiimine-dibromide
1-CCPh·Li:	$[(dadi)TiCCPh]Li(THF)_2$; Titanium (N,N'-di-2-(2,6-diisopropylphenylamide)-phenylglyoxaldiimine-phenylacetylide)lithium bis-tetrahydrafuran
1-CCTMS·Li:	$[(dadi)TiCCTMS]Li(THF)_2$ **;** Titanium (N,N'-di-2-(2,6-diisopropylphenylamide)-phenylglyoxaldiimine-trimethylsilyacetylide)lithium bis-tetrahydrafuran
1-$CH=CH_2$·Li:	$[(dadi)TiC_2H_3]Li(THF)_{2.5}$; Titanium (N,N'-di-2-(2,6-diisopropylphenylamide)-phenylglyoxaldiimine-vinyl)lithium bis-tetrahydrafuran
1-CH_3·Li:	$[(dadi)TiCH_3]Li(THF)_2$; Titanium (N,N'-di-2-(2,6-diisopropylphenylamide)-phenylglyoxaldiimine-methyl)lithium bis-tetrahydrafuran
1-Cl_2:	(dadi)$TiCl_2$; Titanium N,N'-di-2-(2,6-diisopropylphenylamide)-phenylglyoxaldiimine-dichloride
1-Cl·Li:	$[(dadi)TiCl]Li(THF)_4$; Titanium N,N'-di-2-(2,6-diisopropylphenylamide)-phenylglyoxaldiimine- chloride)lithium bis-tetrahydrafuran
1-$(CNMe)_2$:	$(dadi)Ti(CNMe)_2$; Titanium N,N'-di-2-(2,6-diisopropylphenylamide)-phenylglyoxaldiimine-bis(methylisocyanide)

1-Cr(THF): (dadi)Cr(THF); RN(-CH=N(1,2-C_6H_4)NH(2,6-$^{i}Pr_2$-C_6H_3))}$_2$Cr(THF)

1-Fe: (dadi)Fe; RN(-CH=N(1,2-C_6H_4)NH(2,6-$^{i}Pr_2$-C_6H_3))}$_2$Fe

1-H·Li: [(dadi)TiH]Li(THF)$_2$; Titanium (N,N'-di-2-(2,6-diisopropylphenylamide)-phenylglyoxaldiimine-hydride)lithium-bis-tetrahydrafuran

1-I_2: (dadi)TiI_2; Titanium N,N'-di-2-(2,6-diisopropylphenylamide)-phenylglyoxaldiimine-diiodide

1-N_3·Na: [(dadi)TiN_3]Na(15-crown-5)(THF)$_2$; Titanium (N,N'-di-2-(2,6-diisopropylphenylamide)-phenylglyoxaldiimine-azide)sodium-1,4,7,10,13-pentaoxacyclopentadecan-bis-tetrahydrafuran

1-N_2CPh_2: (dadi)Ti(η^2-N_2CPh_2) Titanium (N,N'-di-2-(2,6-diisopropylphenylamide)-phenylglyoxaldiimine-η^2-diphenyldiazomethane

1-^{neo}Pe·Li: [(dadi)Ti^{neo}Pe]Li(THF)$_{2.4}$; Titanium (N,N'-di-2-(2,6-diisopropylphenylamide)-phenylglyoxaldiimine-neopentyl)lithium bis-

1-OPMe$_3$: (dadi)TiOPMe$_3$; Titanium N,N'-di-2-(2,6-diisopropylphenylamide)-phenylglyoxaldiimine-trimethylphosphineoxide

1-O^{i}Pr·Li: [(dadi)TiO^{i}Pr]Li(THF)$_3$; Titanium (N,N'-di-2-(2,6-diisopropylphenylamide)-phenylglyoxaldiimine-isopropoxide)lithium-tris-tetrahydrafuran

1-PMe_2Ph: (dadi)Ti(PMe2Ph); Titanium N,N'-di-2-(2,6-diisopropylphenylamide)-phenylglyoxaldiimine-dimethylphenyphosphine

1-THF: (dadi)Ti(THF); Titanium N,N'-di-2-(2,6-diisopropylphenylamide)-phenylglyoxaldiimine-tetrahydrofuran

2-CrAd: (dadi-NAd)Cr; *{AdN(-CH=N(1,2-C_6H_4)NH(2,6-$^{i}Pr_2$-C_6H_3)}$_2$Cr*

2-CrAr: (dadi-N$^{2,6\text{-dipp}}$ Ar)Cr; {(2,6-$^{i}Pr_2$-C_6H_3)N(-CH=N(1,2-C_6H_4)NH(2,6-$^{i}Pr_2$-C_6H_3)}$_2$Cr

2-FeAd: (dadi-NAd)Fe; {AdN(-CH=N(1,2-C_6H_4)NH(2,6-$^{i}Pr_2$-C_6H_3)}$_2$Fe

2-FeAr: (dadi-$N^{2,6\text{-dipp}}$Ar)Fe, {(2,6-$^{i}Pr_2$-C_6H_3)N(-CH=N(1,2-C_6H_4)NH(2,6-$^{i}Pr_2$-C_6H_3)}$_2$Fe

2=NAd: (dadi)TiNAd; Titanium N,N'-di-2-(2,6-diisopropylphenylamide)-phenylglyoxaldiimine-1-imidoadamantane

2=O: (dadi)TiO; Titanium N,N'-di-2-(2,6-diisopropylphenylamide)-phenylglyoxaldiimine-oxide

3: {PhC_3H_3(-NC_6H_4-2-Ar)$_2$}Ti(THF); Ar = 2,6-$^{i}Pr_2$-C_6H_3

3-Cr: (dadi-NTs)$_2Cr_2$; [(-(CH=N(1,2-C_6H_4)NH(2,6-$^{i}Pr_2$-C_6H_3)(C(=NS(O)(=O-)-tol)N(1,2-C_6H_4)NH(2,6-$^{i}Pr_2$-C_6H_3)Cr]$_2$; Ts = tosylate

4: {PhC(CNC_6H_4-2-NAr)$_2$}Ti(η^2-HNNCPh$_2$) ; Ar = 2,6-$^{i}Pr_2$-C_6H_3

5-Cl: (dadi-Bz)TiCl; dadi-Bz = (C_6H_5-CH_2)-C[=N(1,2-C_6H_4)NAr]-[CH_2-N(1,2-C_6H_4)NAr], Ar = 2,6-$^{i}Pr_2$-C_6H_3

5-Br: (dadi-Bz)TiBr; dadi-Bz = (C_6H_5-CH_2)-C[=N(1,2-C_6H_4)NAr]-[CH_2-N(1,2-C_6H_4)NAr], Ar = 2,6-$^{i}Pr_2$-C_6H_3

6-Cl: (dadi-CH_3)TiBr ; dadi-CH_3 = (CH_3-CH_2)-C[=N(1,2-C_6H_4)NAr]-[CH_2-N(1,2-C_6H_4)NAr], Ar = 2,6-$^{i}Pr_2$-C_6H_3)

6-Br: (dadi-CH_3)TiBr dadi-CH_3 = (CH_3-CH_2)-C[=N(1,2-C_6H_4)NAr]-[CH_2-N(1,2-C_6H_4)NAr], Ar = 2,6-$^{i}Pr_2$-C_6H_3)

7: (dadi-CH_2PPh_2)TiCl ; (dadi-CH_2PPh_2) = ((C_6H_5)$_2$P-CH_2)-[C(=N(1,2-C_6H_4)NAr)]-[CH_2-N(1,2-C_6H_4)NAr], Ar = 2,6-$^{i}Pr_2$-C_6H_3)

8: (diamide-benzimidazole)$TiCl_2$; (DaIm) = N^1-Ar-N^2-((1-Ar-1-benzo[d]imidazol-2-yl)methyl)benzene-1,2-diamide; Ar = 2,6-^{i}Pr-C_6H_3)

9: ^{c}Hex-dadi = 2,5-(C=N(1,2-C_6H_4)NAr)-1,4-(CH-N(1,2-C_6H_4)NAr)cyclohexane, Ar = 2,6-$^{i}Pr_2$-C_6H_3).

10: (DaIm)Ti=NAd($OPMe_2Ph$); (DaIm) = N^1-Ar-N^2-((1-Ar-1-benzo[d]imidazol-2-yl)methyl)benzene-1,2-diamide; Ar = 2,6-^{i}Pr-C_6H_3)

11: 1,4,6-trimethyl-6-nitro-1,4-diazepane

12: 1,4,6-trimethyl-1,4-diazepan-6-amine

13: DPyIm; DPyIm = (E)-1-(pyridin-2-yl)-N-(1,4,6-trimethyl-1,4-diazepan-6-yl)methanimine)

14-Cl_2 (DPyIm)$FeCl_2$; DPyIm = (E)-1-(pyridin-2-yl)-N-(1,4,6-trimethyl-1,4-diazepan-6-yl)methanimine)

14-Br_2: (DPyIm)$FeBr_2$; DPyIm = (E)-1-(pyridin-2-yl)-N-(1,4,6-trimethyl-1,4-diazepan-6-yl)methanimine)

15-Cl: $[(DPyAm)FeCl]_2$; DPyA = 1,2-di(pyridin-2-yl)-N1,N2-bis(1,4,6-trimethyl-1,4-diazepan-6-yl)ethane-1,2-diamide)

15-Br: $[(DPyAm)FeBr]_2$; DPyA = 1,2-di(pyridin-2-yl)-N1,N2-bis(1,4,6-trimethyl-1,4-diazepan-6-yl)ethane-1,2-diamide)

15-crown-5: 1,4,7,10,13-pentaoxacyclopentadecane

CHAPTER 1

A Redox Non-Innocent Diamide-diimine Ligand with Iron and Chromium: Nitrene Insertion into CC and CH Bonds

Introduction:

Jorgensen's definition of 'redox non-innocent (RNI) ligands'[1] and the early discovery of RNI in dithiolene ligands by Gray and Eisenberg[2,3] in the mid 1960's and laid the groundwork for a flourishing area of chemical research. RNI ligands can act as electron reservoirs, or sinks, to stabilize a metal center prior to reaction with substrate, and provide reducing or oxidizing equivalents for catalysis. Nature has found uses for RNI ligands in galactose oxidase, a Cu enzyme that converts alcohols to aldehydes utilizing a tyrosinate redox-active cofactor that is oxidized to a tyrosinyl radical during turnover.[4] Additionally, the heavily studied cytochrome P450 site in peroxidase enzymes reacts with molecular oxygen, generating a porphyrin based radical cation with an Fe(IV) oxo center (Compound I), which can hydroxylate unactivated C-H bonds.[5,6]

RNI exists when metal and ligand orbitals are similar in energy, resulting in molecular orbitals of mixed composition. Iminopyridine [7,8] and *o*-phenylenediamido[9–12] ligands behave in a redox non-innocent (RNI) manner. Hence, the tetradentate diamide-diimine (dadi) ligand, (dadi = [{-CH=N- (1,2-C_6H_4)NH(2,6-$^{i}Pr_2$-C_6H_3)}$_2$]^n, n = 0 to -4), combining two amides and an α-diiimine moiety was surmised to behave in a RNI fashion. Scheme 1.1 shows five plausible redox states available to the dadi ligand upon double deprotonation of the amines. The π-electron count of the dadi ligand in its different redox states are also shown in Scheme 1.1. As will be discussed later

in further detail, the π-electron count can be used to rationalize reactivity upon coordination to transition metals, depending on whether it exists as a conjugated 4n+2 or 4n π-electron system.

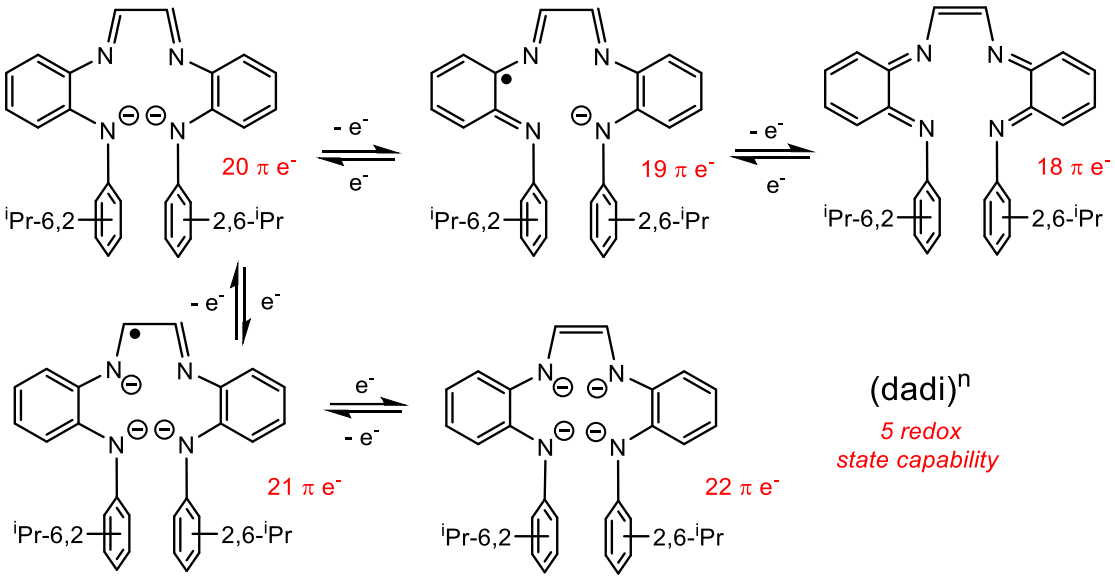

Scheme 1.1. Five plausible redox states of the (dadi)^n (n = 0 to -4) ligand with the π-electron count given for each state.

Of particular interest are nitrene group transfers from metal imidos for hydroamination and aziridination reactions. Isolable mononuclear Fe imidos have been reported with varying metal oxidation states (Fe(II/III)), spin states, and geometries[9,13–23] but predominantly contain trigonal ligand fields.[24] Fe(IV) imidos have been invoked as reactive intermediates during the formation of Fe(III) amido complexes[25] but only a few examples of stable Fe(IV) imidos have been reported.[26,27] In contrast, mononuclear Cr imido complexes tend to exist as high valent species (Cr(IV-VI))[28–37] and nitrene group transfer is limited to complexes with corrole[38,39] and porphyrin[40] supporting ligands.

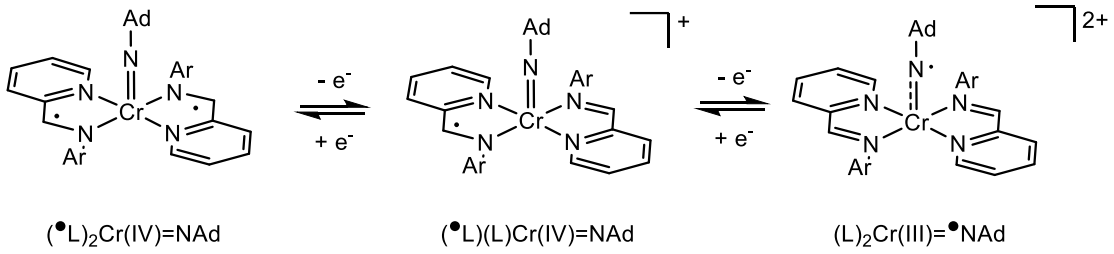

Scheme 1.2. Electronic buffering of Cr center upon oxidation and ultimate reduction by adamantyl imide generating and imidyl coordinated to Cr(III) center.

Wieghardt's [(L•)$_2$Cr(II)] (L = 2,6-bis(1-methylethyl)-*N*-(2-pyridinylmethylene)phenylamine) complex with a RNI α-iminopyridine ligand (Scheme 1.2), reacts with adamantyl azide to generate a [(L•)$_2$Cr(IV)NAd] imido.[41] 2-electron oxidation of the diradical complex generates an imidyl species [(L)$_2$Cr(III)(•NAd)]$^{2+}$ where the RNI ligands are in their imine form. This counterintuitive overall reduction of the Cr center under oxidative conditions is a prime example of RNI ligands acting to electronically buffer a transition metal center. Furthermore, this provided early evidence supporting the formation of an imidyl radical, suggesting that metal nitrogen multiply bonded species could react out of their closed shell dianoinic $(NR)^{2-}$ or open shell anionic monoanion $(^{\bullet}NR)^{1-}$ forms, depending on the electronics of the supporting ligand.

The (dadi)M complexes (M = Cr(THF), **1**-Cr(THF); Fe, **1**-Fe) were previously synthesized in this laboratory and structurally characterized, but their reactivity had not been fully explored. The RNI dadi ligand may electronically buffer the metal centers, preventing the formation of high valent Fe imidos and support the formation of isolable mononuclear, low valent Cr imidos. At the launch of the investigation into **1**-Cr(THF) and **1**-Fe, it was envisioned that metal imidos could be formed by treating with organic azides, thereby facilitating a study into the nature of the RNI dadi ligand.

Results and Discussion:

1.1. Ligand and (dadi)M (M= Fe, Cr(THF)) syntheses

1.1.1. N,N'-Di-2-(2,6-diisopropylphenylamine)-phenylglyox-aldiimine (dadiH_2)

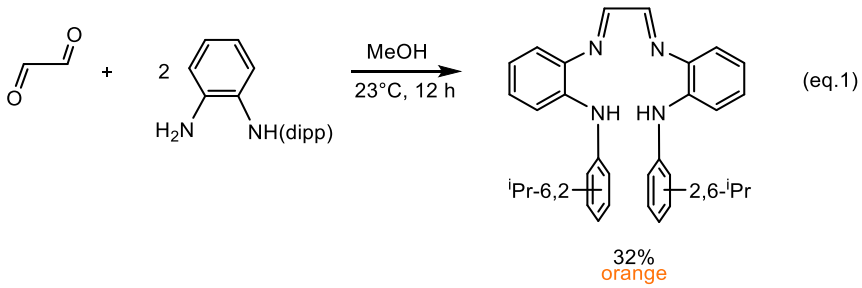

(eq.1)

The synthesis of N,N'-Di-2-(2,6-diisopropylphenylamine)-phenylglyox-aldiimine (dadiH_2) was achieved by condensation of glyoxal with two equiv of N-(2-aminophenyl)-2,6-diisopropylaniline[15,42] in methanol (eq.1). The diamine ligand precursor precipitates from solution as a bright orange solid. After filtration and washing with cold ethanol, dadiH_2 is isolated in 32% yield. Attempts to synthesize derivatives using less bulky anilines (Ph, ^{i}Pr, ^{t}Bu) resulted in clean formation of the N-subsituted benzimidazoles.[15] With the bulkier 2,6-^{i}Pr-C_6H_3 substituted aniline, this cyclization also occurs but the formation of dadiH_2 is driven by its precipitation from solution.

*1.1.2. Synthesis of (dadi)Cr(THF) (**1**-Cr(THF)) and (dadi)Fe (**1**-Fe)*

Treatment of dadiH_2 with Cr(N(TMS)$_2$)$_2$(THF)$_2$ [43,44] or Fe(N(TMS)$_2$)$_2$(THF)[45–47] in benzene generated two equiv of hexamethyldisilazane (HMDS) and (dadi)M(THF)$_x$ (**1**-M; M = Cr(THF), **1**-Cr(THF), x = 1, 76%; Fe, **1**-Fe, x = 0, 75%) as maroon and dark green

crystals, respectively (Scheme 1.3). Evans' method magnetic susceptibility measurements[48,49] are consistent with an intermediate spin system for **1**-Cr(THF) (μ_{eff} = 2.7(1) μ_B, *S* = 1) and a high spin **1**-Fe complex (μ_{eff} = 4.7(1) μ_B, *S* = 2).

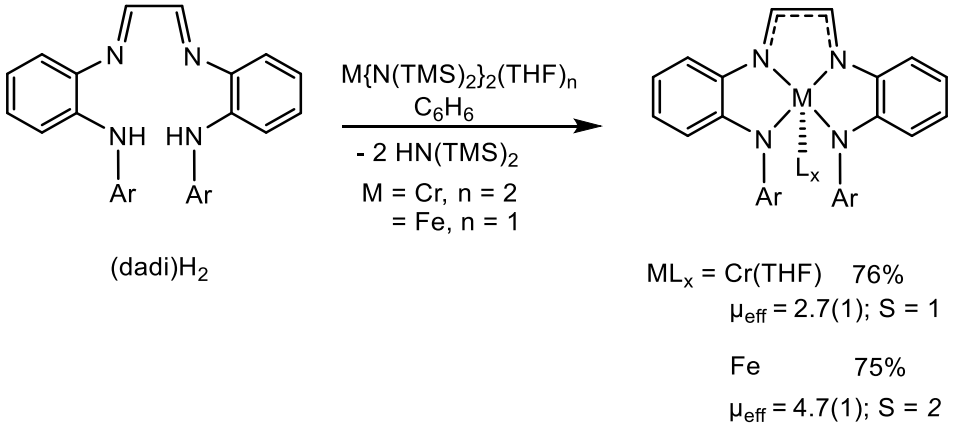

Scheme 1.3. Synthesis of **1**-Cr(THF) and **1**-Fe. Ar = 2,6-iPr-C_6H_3.

*1.1.3. Electronic structure description of (dadi)Cr(THF) (**1**-Cr(THF)) and (dadi)Fe (**1**-Fe)*

The interatomic distances in ligands have been shown to be a useful metric when assessing the ligand redox state.[8,50,51] Figure 1.1 shows the bond distances in the diimine backbone of the dadi ligand. For **1**-Fe, the CN distances of 1.293(3) Å (ave) and CC distance of 1.437(3) Å are consistent with C_{sp2}=N double bonds and C_{sp2}-C_{sp2} single bonds, respectively, indicative of the $(dadi)^{2-}$ ligand and a high spin Fe(II) metal center. Calculations also support the $(dadi)^{2-}$ quintet d^6 electronic structure implicated by magnetic susceptibility measurements and its solid state structure. Ambiguity in the ligand redox state arises when comparing the metrics of the dadi ligand backbone in **1**-Cr(THF). The elongated CN distances of 1.377(3) Å (ave) and

the contracted CC distance of 1.361(3) Å in **1**-Cr(THF) relative to **1**-Fe clearly indicates deviation from the $(dadi)^{2-}$ redox state.

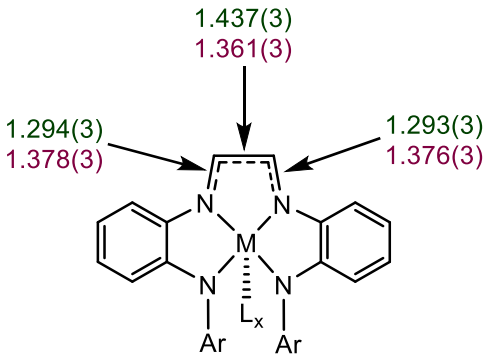

Figure 1.1. Selected interatomic distances of **1**-$M(L)_X$ (M = Cr, L = THF, X = 1, red; M = Fe, X = 0, green).[15]

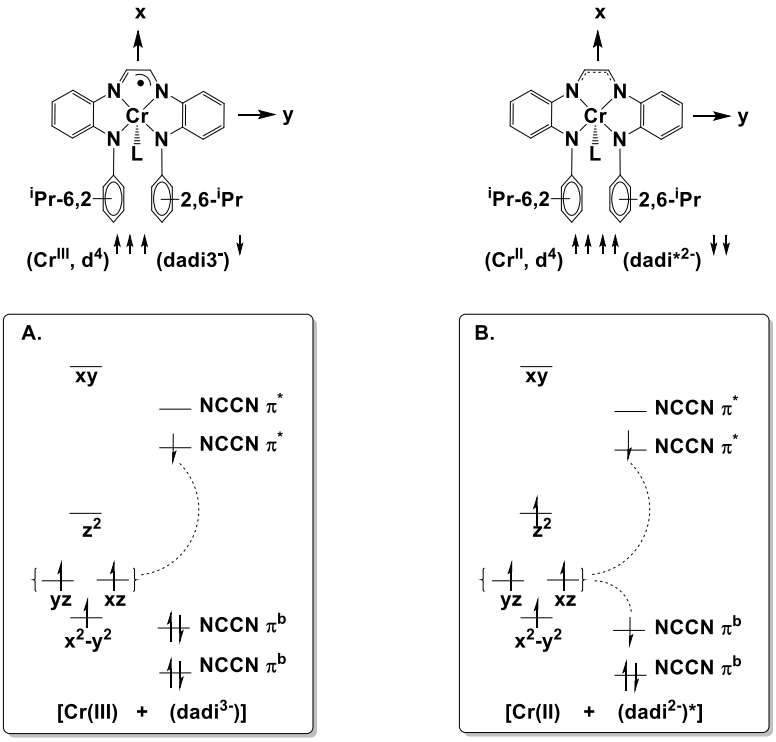

Figure 1.2. Plausible electronic structure descriptions for **1**-Cr(THF).

The magnetic susceptibility of 2.7 μ_B for **1**-Cr(THF) prompts several explanations. A standard ligand field description for **1**-Cr(THF) with an

intermediate spin Cr(II) center chelated by a $(dadi)^{2-}$ ligand is clearly not valid given the ligand metrics shown in Figure 1.1. This leads to two plausible descriptions for **1**-Cr(THF): (A) antiferromagnetic (AF) coupling between Cr(III) and a reduced $(dadi)^{3-}$ ligand (Figure 1.2.), and (B) AF-coupling between an $S = 1$ excited state of $[(dadi)^{2-}]^*$, containing electrons in π and π^* orbitals, and a high spin chromous center (Figure 1.2). The computed spin density on the Cr center in **1**-Cr(THF) is 3.75 electrons suggesting that (B) is the dominant description, although the ground state likely contains significant admixture from (A).[15]

1.2 Nitrene insertions into CC- and CH-bonds of 1-Fe and 1-Cr(THF)

*1.2.1. Synthesis of {RN(-CH=N(1,2-C_6H_4)NH(2,6-^{i}Pr$_2$-C_6H_3))}$_2$M (M=Cr, R = Ad, **2**-CrAd; Ar, **2**-CrAr; M = Fe, R = Ad, **2**-FeAd; Ar, **2**-FeAr)*

Treatment of **1**-Cr(THF) with organic azides AdN_3 and ArN_3 (Ad = adamantyl, Ar = 2,6-^{i}Pr-C_6H_3) at -78 ^{o}C did not result in the expected formation of chromium imido species. Instead, these reactions afforded products derived from the formal insertion of a nitrene into the CC-bond of the diimine unit (Scheme 1.4). Blue and purple {RN(-CH=N(1,2-C_6H_4)NH(2,6-^{i}Pr$_2$-C_6H_3))}$_2$Cr (R = Ad, **2**-CrAd; Ar, **2**-CrAr) were crystallized from cold pentane solutions and isolated in 86% and 65% yields respectively. Solution magnetic moment measurements (**2**-CrAd, μ_{eff} = 4.4(1) μ_B; **2**-CrAr, μ_{eff} = 4.5(1) μ_B) are consistent with $S = 2$ spin systems. The maroon iron analogues, {RN(-CH=N(1,2-C_6H_4)NH(2,6-^{i}Pr$_2$-C_6H_3))}$_2$Fe (R = Ad, **2**-FeAd; Ar, **2**-FeAr), were synthesized in a similar manner with slightly lower yields (Scheme 1.4; **2**-FeAd = 67%; **2**-FeAr = 40%). $S = 2$ spin centers were also found via Evans' method measurements (**2**-FeAd, μ_{eff} = 4.8(1) μ_B; **2**-FeAr, μ_{eff} = 4.9(1) μ_B).

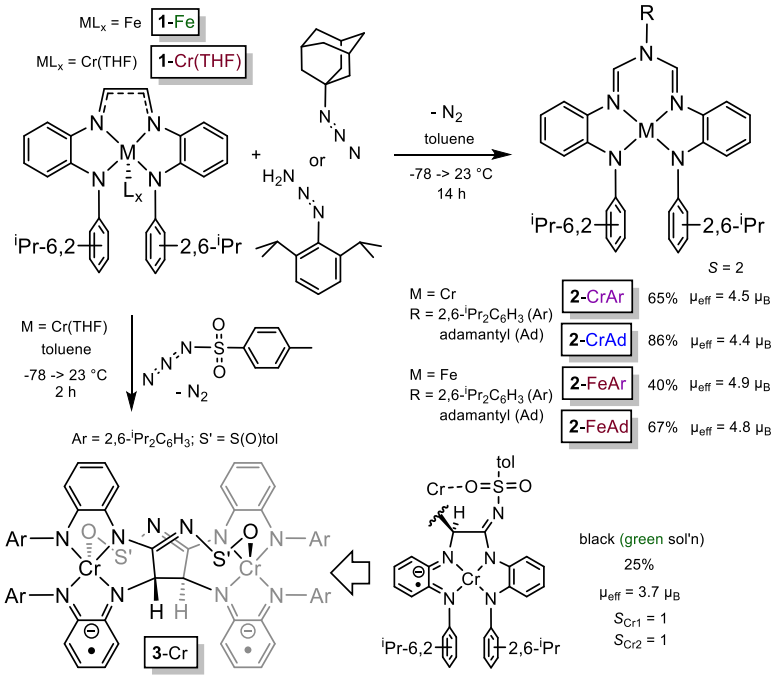

Scheme 1.4. Products resulting from treatment of **1**-Cr(THF) and **1**-Fe with organic azides.

*1.2.2. Synthesis of [(-(CH=N(1,2-C$_6$H$_4$)NH(2,6-^{i}Pr$_2$-C$_6$H$_3$)(C(=NS(O)(=O-)-tol)N(1,2-C$_6$H$_4$)NH(2,6-^{i}Pr$_2$-C$_6$H$_3$)Cr]$_2$ (**3**-Cr)*

Treatment of **1**-Cr(THF) with electron deficient TsN_3 (Ts = tosyl) afforded **3**-Cr in 25% yield after fractional crystallization from benzene solutions layered with pentane. **3**-Cr is consistent with an initial nitrene insertion into the CH-bond on the diimine backbone. CC-bond formation at one side of the original diimine unit forms the dimer **3**-Cr. The adjacent carbon has lost its hydrogen to the formation of the CN bond of the η^1-amidinate. The IR spectrum of **3**-Cr does not show an NH stretch and a C-NH-S unit is ruled out due to spatial overlap with the coplanar aryl CH. Thus, the gas evolved from the reaction was analyzed (Toepler pump) revealing 1 equiv of N_2, but no H_2

evolution. Unfortunately, the fate of the lost hydrogen was not identified but it is likely to be found in the byproducts of the reaction.

*1.2.3. Crystal structures of **2**-CrAr, **2**-CrAd and **2**-FeAd*

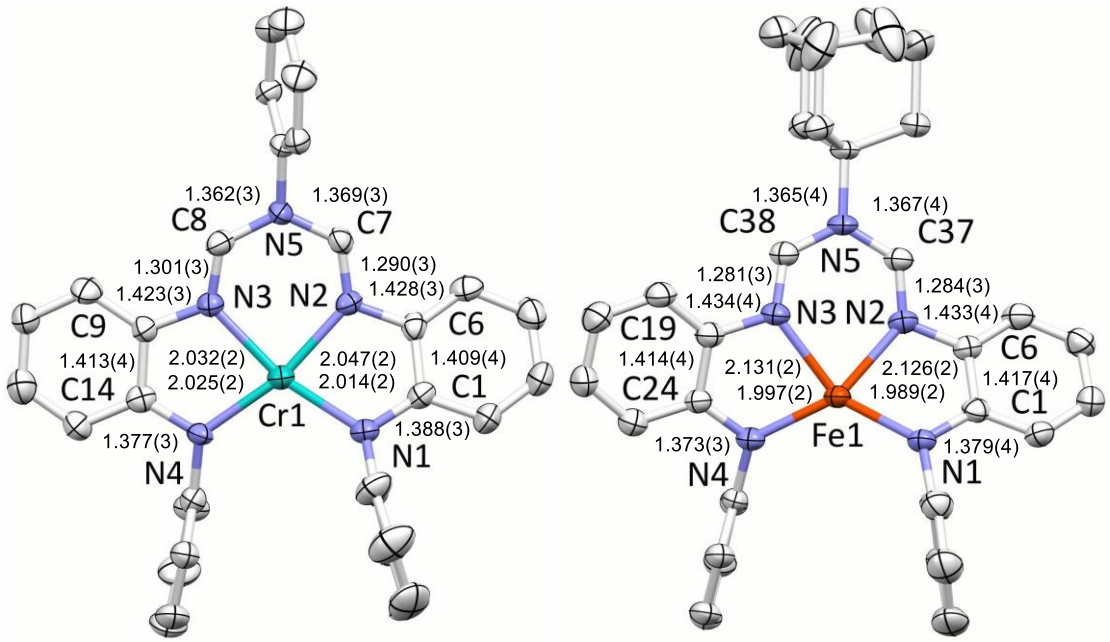

Figure 1.3. Molecular structures of **2**-CrAr and **2**-FeAd obtained from single crystal X-ray crystallography (^{i}Pr groups have been removed for clarity), with pertinent distances (Å) and core angles (°) listed. (Left) One of two independent {2,6-$^{i}Pr_2C_6H_3$-N(-CH=N(1,2-C_6H_4)NH(2,6-$^{i}Pr_2$-C_6H_3)}$_2$Cr (**2**-CrAr) molecules: ∠N1-Cr-N2, 80.22(13); ∠N1-Cr-N3, 163.82(13); ∠N1-Cr-N4, 113.28(13); ∠N2-Cr-N3, 86.75(13); ∠N2-Cr-N4, 164.64(12); ∠N3-Cr-N4, 81.02(13). (Right) {AdN(-CH=N(1,2-C_6H_4)NH(2,6-$^{i}Pr_2$-C_6H_3)}$_2$Fe (**2**-FeAd):∠N1-Fe-N2, 79.94(9)°; ∠N1-Fe-N3, 149.39(9)°; ∠N1-Fe-N4, 127.03(9); ∠N2-Fe-N3, 80.77(8)°; ∠N2-Fe-N4, 148.03(9)°; ∠N3-Fe-N4, 79.85(8)°.

The solid state structures of **2**-CrAr and **2**-FeAd shown in figure 1.3 reveal pseudo square planar coordination environments around each metal center. The 26.5° twist in the Fe-N_4 frame is significantly greater than that observed in **2-**CrAd (10.3°). This distortion is also evident in the core angles listed in Figure 1.3. Of note are the diimine C-N distances that exhibit clear

double bond character [7] (M = Cr, d(C-N_{imine}) = 1.296(3) Å (ave); M = Fe, d(C-N_{imine}) = 1.283(3) Å (ave)). In conjunction, the C-N_{amine} distances in the ligand backbone are consistent with C_{sp2}-N_{sp3} single bonds [7] (M = Cr, d(C-N5) = 1.366(3) Å (ave); M = Fe, d(C-N5) = 1.366(4) Å (ave)), revealing a dianionic ligand chelating high spin Cr(II) and Fe(II) centers. The 2.030(14) Å (ave) Cr-N distances are in contrast to elongated Fe-N imine distances (2.129(4) Å (ave)). Occupation of the M-N σ*-orbital (d_{xy}, x-axis defined by Fe1-N5) in the case of **2**-FeAd, but not in **2**-CrAr, undoubtedly contributes to the angular and bond distortions in the former.

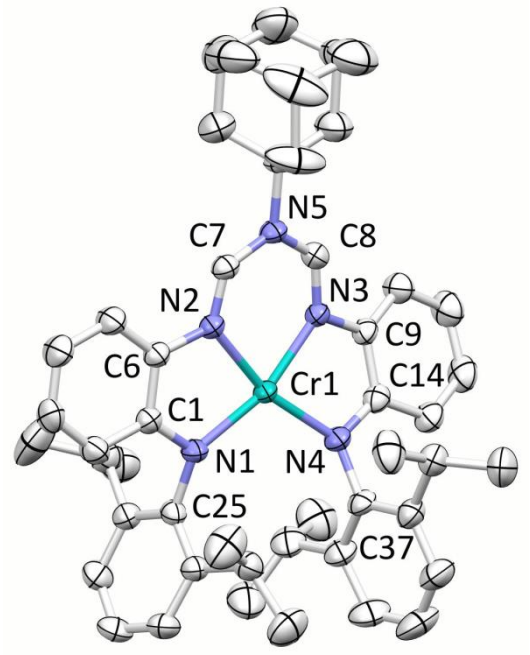

Figure 1.4. Molecular view of {AdN(-CH=N(1,2-C_6H_4)NH(2,6-^{i}Pr$_2$-C_6H_3)}$_2$Cr (**2**-CrAd). Select interatomic distances (Å) and angles (°): Cr-N1, 2.014(2); Cr-N2, 2.047(2); Cr-N3, 2.032(2); Cr-N4, 2.025(2); N1-C1, 1.388(3); C1-C6, 1.409(4); N2-C6, 1.428(3); N2-C7, 1.290(3); N5-C7, 1.369(3); N5-C8, 1.362(3); N3-C8, 1.301(3); N3-C9, 1.423(3); C9-C14, 1.413(4); N4-C14, 1.377(3); ∠N1-Cr-N2, 81.58(8); ∠N1-Cr-N3, 164.76(9); ∠N1-Cr-N4, 112.69(9); ∠N2-Cr-N3, 85.40(8); ∠N2-Cr-N4, 164.23(9); ∠N3-Cr-N4, 81.27(8).

Single crystals of **2**-CrAd (Ad = adamantyl) were grown by diffusion of hexanes vapor into a saturated diethyl ether solution. The asymmetric unit

contains two molecules of **2**-CrAd, one of which is shown in Figure 1.4. Examination of the metric parameters reveal no significant deviation of those in **2**-CrAr, with Cr-N distances of 2.030(2) Å (ave), d(C-N_{imine}) = 1.314(6) Å (ave), and d(C-N_{amine}) = 1.365(6). A detailed list of interatomic distances and core angles are listed in Figure 1.4.

*1.2.4 Crystal structure of **3**-Cr.*

A single crystal of **3**-Cr, suitable for X-ray diffraction, was obtained by the diffusion of pentane vapor into a saturated THF solution at -20 °C. The molecular structure of **3**-Cr, shown in Figure 1.5, reveals dimer formation *via* coupling of two carbons of the original diimine backbone and coordination of the tosylate oxygen to the neighboring Cr atom. An inspection of the metric parameters affiliated with **3**-Cr (Figure 1.5) expose subtle differences between

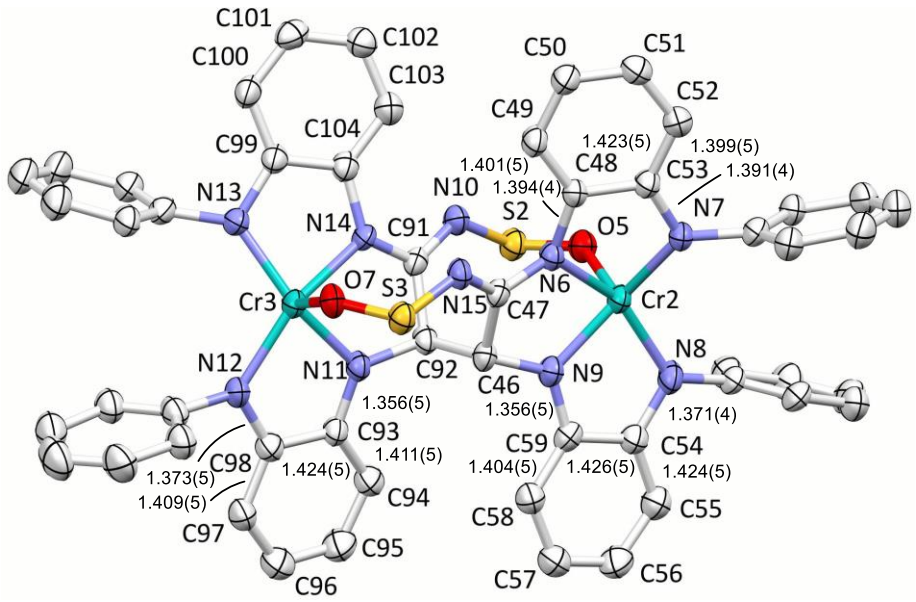

Figure 1.5. A molecular view of dimer **3**-Cr (an additional 1/2 dimer in the asymmetric unit is not shown) obtained from a single crystal X-ray study, with ^{i}Pr groups, tolyl, and sulfoxide oxygen removed.

the amide-amidinate-arene and the diamide-arene. The average CN, C(N)C(N), and CC distances affiliated with diamide-arene are 1.364(9),1.428(5) and 1.411(10) Å, respectively, while the corresponding distances of the amide-amidinate-arene average 1.408(12), 1.410(11) and 1.397(5) Å, suggesting 1-electron reduction of the diamide-arene.[7]

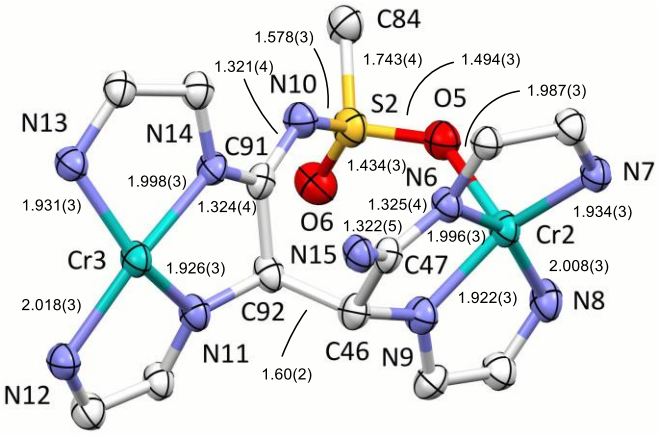

Figure 1.6. A core view of **3**-Cr, and selected metric parameters (°):∠N6-Cr2-N7, 80.60(12); ∠N6-Cr2-N8, 155.92(13); ∠N6-Cr2-N9, 78.40(12); ∠N7-Cr2-N8, 111.99(12); ∠N7-Cr2-N9, 146.24(13); ∠N8-Cr-N9, 80.52(12); ∠O5-Cr2-N6, 93.32(11); ∠O5-Cr2-N7, 106.70(12); ∠O5-Cr2-N8, 101.92(12); ∠O5-Cr2-N9, 100.65(12); similar angles describe Cr3.

The core structure of **3**-Cr is shown in Figure 1.6. The new CC-bond is relatively long (d(C46-C92) = 1.60(2) Å) suggesting reversible bond formation may be possible, similar to azaallyl couplings,[52] although no evidence of dynamic behavior in solution to generate a monomeric form of **3**-Cr has been observed. The sulfur bond distances (d(S-N) = 1.577(3) Å (ave); d(S-C = 1.743(4) Å (ave); d(S-O) = 1.459(2) Å (ave)) are consistent with single SN, single SC, and double SO bonds.[7] CN distances for the η^1-amidinate average 1.323(2) Å, and the square pyramidal cores, shown in Figure 1.6, have varied d(CrN) bond lengths that support a Cr(III) formulation. Furthermore,

calculations support the assignment of a Cr(III) center AF-coupled to an arene radical resulting in two *S* = 1 centers.

1.2.5 Mechanism of nitrene insertions

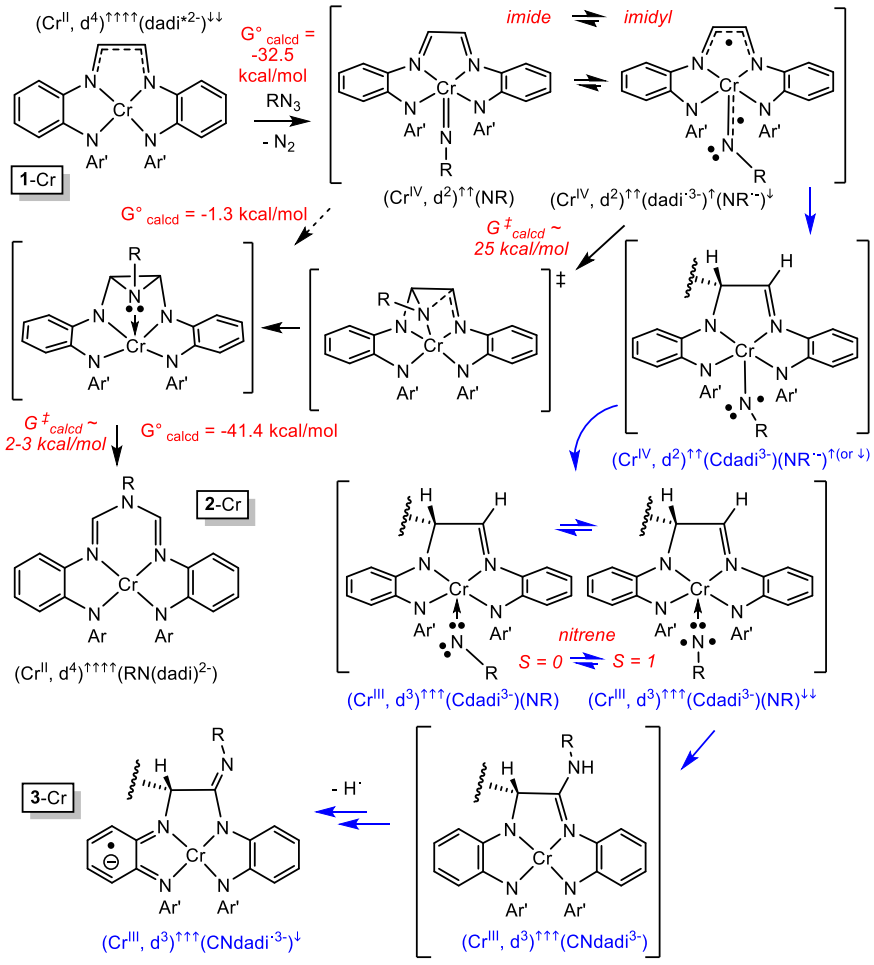

Scheme 1.5. Proposed imidyl (aziridination ring opening to **2**-Cr, black; calculated free energies in red) and nitrene reactivity (to **3**-Cr, blue) from (dadi)M(NR) (**1**-Cr).

Depicted in Scheme 1.5 is a proposed mechanism to form **2**-Cr, and by inference **1**-Fe. The initial reaction between **1**-Cr and azide, generates a Cr(IV) center chelated to a dadi^{3-} ligand with an azaallyl radical AF-coupled to an

imidyl radical, i.e $(Cr^{IV})^{\uparrow\uparrow}(dadi^{\cdot 3-})^{\uparrow}(NR^{\cdot -})^{\downarrow}$ ($\Delta G°_{calcd}$ = -32.5 kcal/mol). This is based upon calculation of a truncated model, (dadi`)CrNMe (H in place of 2,6-^{i}Pr-C_6H_3) shown in Figure 1.7. Lying 3 kcal/mol above the triplet is an *S* = 0 broken symmetry solution with like-spin imidyl and $dadi^{3-}$ ligands AF-coupled to d^2 Cr(IV). Both solutions indicate imidyl character, with an unpaired spin density of *ca.* 1 electron for the imidyl nitrogen (triplet, ρ_{spin} ~ - 1 e^-; singlet, ρ_{spin} ~ + 1 e^-), accompanied by *ca.* 2 electrons on the Cr(IV) d^2 center (triplet, ρ_{spin} ~ + 2 e^-; singlet, ρ_{spin} ~ - 2 e^-), and *ca.* 1 electron for the $dadi^{3-}$ ligand (triplet, ρ_{spin} ~ + 1 e^-; singlet, ρ_{spin} ~ + 1 e^-).

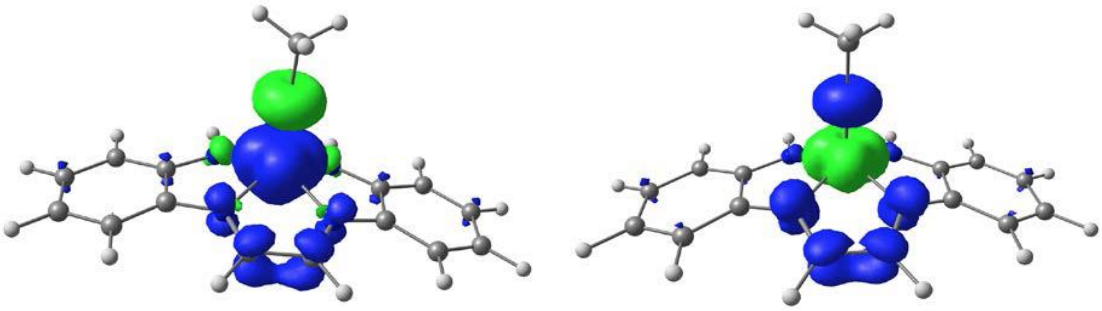

Figure 1.7. Spin density (IsoValue = 0.01) of triplet (left) and singlet (right) (dadi`)Cr=NMe. Note for the triplet the positive spin density on the metal (ρ_{spin} ~ +2 e^-) and dadi ligand (ρ_{spin} ~ +1 e^-), and the negative spin density on the imidyl nitrogen (ρ_{spin} ~ -1 e^-). For the broken-symmetry singlet, the spin density on the imidyl (ρ_{spin} ~ +1 e^-) and dadi (ρ_{spin} ~ +1 e^-) ligand are positive, while the Cr has negative spin density (ρ_{spin} ~ -2 e^-).

Use of a truncated model with –NCH=NHN- in place of the flanking phenylene groups, permitted a more efficient search of the reaction space to locate transition states (TSs). Nitrene transfer to the ligand backbone occurs through the formation of a transient aziridine that is only -1.3 kcal/mol below the imidyl, with a TS for nitrene transfer about 25 kcal/mol (ΔG) above the imidyl species. Aziridination does not appear to occur stepwise, but the TS is asymmetric, in such a way that imidyl and azaallyl coupling occurs while the

RN: fragment is aligned to undergo nucleophilic attack at the adjacent carbon. Aziridine ring-opening has a modest barrier of about 5 kcal/mol, affording **2**-Cr in a process that is overall substantially exoergic (ΔG = -41.4 kcal/mol).

Scheme 1.5 illustrates a plausible sequence of steps to form **3**-Cr, beginning with the formation of an imidyl species related to those forming **2**-Cr. Divergence from the aziridination mechanism occurs with the electron withdrawing tosyl-N fragment which may stabilize the azaallyl radical allowing intermolecular CC-coupling (dimerization) to occur. Reduction of Cr(III) by the imidyl would generate a nitrene, a group known to insert into CH-bonds. Due to the low yield of **3**-Cr and the complexity its formation, which includes a formal loss of $H^{\bullet}$, the mechanism was not investigated computationally. It should be noted that when attempting to trap the putative imidyl species with alkenes (styrene, cis-2-pentene) or hydrogen atom sources (dihydroanthracene, 1,4-cyclohexyldiene), products resulting from intermolecular alkene aziridination or H atom transfer were not detected by ^{1}H nuclear magnetic resonance (NMR) spectroscopy or direct analysis in real time mass spectroscopy (DART-MS) of quenched crude reaction mixtures.

Conclusions:

The $dadi^{2-}$ ligand contains 20 π-electrons, a 4n conjugated system, rendering the ligand prone to reduction, a factor that is taken to be critical for productive RNI. The 20 π-electron $dadi^{2-}$ ligand effectively competes for electron density with the RN moiety, resulting in radical character on both ligands. This interplay between the dadi redox state and the imide/imidyl group drives product formation. In the case of more electron rich RN groups (R = adamantyl, 2,6-^{i}Pr-C_6H_3), intramolecular radical coupling occurs. With the

electron deficient tosyl-N group, stabilization of the dadi ligand radical facilitates intermolecular C-C coupling. Furthermore, the nitrene insertion products **2**-Cr and **2**-Fe possess 22 π-electrons, resulting in compounds that are thermally stable and resistant to further oxidation by azides.

The observed imide-imidyl chemistry presented herein coincides with transient imidyl species of the first row presented by Betley,[14,18,20,22,53] Holland,[54] and de Bruin,[40] but stands in contrast to Wieghardt's "normal" $(pyridineimine)_2CrNAd$ complex.[41] It is possible that the combination of the imide with two hard amide donors of the dadi force the Cr and Fe away from their preferred charge state (Cr = ~ +2.6,Fe = ~ 2),[55] leading to a more reactive imidyl compared to Wieghardt's chromium imido/imidyl complexes containing neutral pyridineimine ligands. In any case, a balance must be struck between the electronics of a RNI ligand and substrate, in order to achieve productive chemistry. For example, the energy gained from conjugated 4n+2 π-system may be leveraged to generate imidyl character, but in the case of the dadi ligand, the presence of a low lying LUMO within proximity of a reactive imidyl group results in detrimental intramolecular reactivity, preventing nitrene group transfer to exogenous substrates. These are factors that must be considered when rationally designing RNI ligands for catalysis.

*Experimental**:***

A. General Considerations

All manipulations were performed using either glovebox or high-vacuum techniques unless otherwise indicated. Hydrocarbon and ethereal solvents were dried over sodium and vacuum transferred from sodium benzophenone ketyl (3-4 mL tetraglyme/L were added to hydrocarbons). Benzene-d_6 and THF-d_8 were sequentially dried over sodium and stored over sodium. All glassware was oven dried at 165°C prior to use.

Lithium bis(trimethylsilyl)amide was purchased from Aldrich and recrystallized from hexanes prior to use. Metal amides $Cr\{N(SiMe_3)_2\}_2(THF)_2$[43,44] and $Fe\{N(SiMe_3)_2\}_2(THF)$[45–47] were prepared according to literature procedures, as were all organoazides. ^1H and ^{13}C NMR spectra were obtained on Varian 300 MHz (Mercury), 400 MHz, and 500 MHz (INOVA) spectrometers. Spectra are referenced to benzene-d_6 (^1H, δ 7.16 ppm; $^{13}C\{^1H\}$ δ 128.39 ppm), THF-d_8 (^1H, δ 3.58 (OCHD) ppm; $^{13}C\{^1H\}$ δ 67.21 ppm), and $CDCl_3$ (^1H, δ 7.26 ppm; $^{13}C\{^1H\}$ δ 77.16 ppm). Solution magnetic moments were determined via Evans' method in benzene-d_6.[48,49] Elemental analyses were performed by Robertson Microlit Laboratories, Madison, New Jersey.

B. Procedures

1. *N-(2-nitrophenyl)-2,6-diisopropylaniline.* This is a modified literature procedure.[56] To a 250 mL round bottom flask equipped with a reflux condenser was added 2,6-diisopropylaniline (50.0 g, 282 mmol), potassium fluoride (13.27 g, 141 mmol) and 1-fluoro-2-nitrobenzene (19.87 g, 141 mmol). The reaction mixture was heated to 180 °C and refluxed for 24 h. The resulting

amber reaction mixture was washed with distilled water (3 x 100 mL), extracted with dichloromethane (3 x 50 mL) dried over magnesium sulfate and concentrated. Excess 2,6- diisopropylaniline was removed by vacuum distillation (1 x 10^{-5} torr, b.p. = 70 °C), and the remaining crude product was dissolved in 125 mL boiling ethanol and cooled to 0 °C for 12 h. 2,6-Diisopropyl-N-(2-nitrophenyl)aniline was collected by filtration as a golden crystalline solid (15.93 g, 38 %). ^{1}H NMR ($CDCl_3$): δ 1.11 (d, *J* = 7 Hz, 6H, Me), 1.18 (d, *J* = 7 Hz, 6H, Me), 3.04 (sept, *J* = 7 Hz, 2H, CH), 6.38 (d, *J* = 9 Hz, 1H, ArH), 6.68 (m, 1H, ArH), 7.27 (m, 3H, ArH), 7.38 (m, 1H, ArH), 8.23 (d, *J* = 9 Hz, 1H, ArH), 9.21 (s, 1H, NH). ^{1}H NMR (C_6D_6, 295K): δ 0.97 (d, *J* = 7.0 Hz, 6H), 1.00 (d, *J* = 7.0 Hz, 6H), 3.00 (sp, *J* = 7.0 Hz, 2H), 6.16 (t, *J* = 7.8 Hz, 1H), 6.23 (d, *J* = 8.6 Hz, 1H) 6.67 (t, *J* = 7.8 Hz, 1H), 7.09 (m, 2H), 7.20 (m, 1H), 8.13 (d, *J* = 8.6 Hz, 2H), 9.41(s, 1 H).

2. *N-(2-aminophenyl)-2,6-diisopropylaniline.* This is a modified literature procedure.[56] 2,6-Diisopropyl-N-(2-nitrophenyl)aniline (15.9 g, 53 mmol) was dissolved in a mixture of ethanol and ethyl acetate (75 mL and 150 mL, respectively) and added to a 500 mL round bottom flask charged with Raney Ni (ca. 10 g in water). The reaction mixture was cooled to -78 ^{o}C and degassed, then placed under 1 atm of H_2 and stirred to 16 h. The hydrogen atmosphere was periodically replenished every 6-10 h. The resulting purple solution was filtered and the solvents were removed by vacuum to afford a purple crystalline solid (12.3 g, 86 %). ^{1}H NMR ($CDCl_3$): δ 1.14 (d, *J* = 7 Hz, Me), 3.06 (sept, *J* = 7 Hz, 2H, CH), 3.57 (s, 2H, NH_2), 4.90 (s, 1H, NH), 6.19 (d, *J* = 8 Hz, 1H, ArH), 6.64 (m, 1H, ArH), 6.71 (m, 1H, ArH), 6.79 (d, *J* = 8 Hz, 1H, ArH), 7.23 (m, 3H, ArH). ^{1}H NMR (C_6D_6, 295K): δ 1.09 (bd, *J* = 7.0 Hz, 12H), 2.81 (s, 2H), 3.13 (hept, *J* = 6.9 Hz, 2H), 4.86 (s, 1H), 6.35 (dd, *J* = 7.9,

1.4 Hz, 1H), 6.48 (dd, *J* =7.6, 1.5 1H), 6.66 (td, *J* = 7.6, 1.5 1H), 6.74 (td, *J* = 7.5, 1.5 Hz, 1H), 7.2 (m, 3 H).

3. *N,N'-Di-2-(2,6-diisopropylphenylamine)-phenylglyox-aldiimine ((dadi)H$_2$).* N-(2-aminophenyl)-2,6-diisopropylaniline (4.7 g, 18 mmol) was dissolved in 60 mL MeOH. A 40 wt% glyoxal solution (1.3 g, 8.8 mmol) was dissolved in 60 mL MeOH and added dropwise. The solution turned orange and was stirred for 12 h as an orange solid precipitated. The bright orange solid was collected by filtration and washed with cold MeOH (1.2 g, 2.2 mmol, 24%). ^{1}H NMR ($CDCl_3$): δ 1.17 (m, 24H, Me), 3.24 (sept, *J* = 7 Hz, 4H, CH), 6.21 (d, *J* = 8 Hz, ArH), 6.68 (m, 4H, ArH), 7.03 (m, 2H, ArH), 7.31 (m, 6H, ArH), 8.65 (s, 2H, NCH). ^{13}C{^{1}H} NMR ($CDCl_3$): δ 23.31, 24.86, 28.50, 112.30, 116.44, 116.98, 123.97, 127.57, 130.04, 133.90, 135.43, 145.08, 148.07, 156.07. ^{1}H NMR (C_6D_6): δ 1.14 (d, *J* = 7 Hz, 12H, Me), 1.19 (d, *J* = 7 Hz, 12H, Me), 3.46 (sept, *J* = 7 Hz, 4H, CH), 6.37 (d, *J* = 8 Hz, ArH), 6.54 (t, *J* = 8 Hz, 2H, ArH), 6.92 (m, 4H, ArH), 7.05 (s, 2H, NH), 7.31 (m, 6H, ArH), 8.48 (s, 2H, NCH). Anal. for $C_{38}H_{46}N_4$ (calc) C 81.68, H 8.30, N 10.03; (found) C 82.37, H 8.33, N 9.58.

4. *(dadi)Cr(THF) (**1**-Cr(THF)).* To a 50 mL flask charged with Cr{N(SiMe$_3$)$_2$}$_2$(THF)$_2$ (400 mg, 0.774 mmol) and (dadi)H$_2$ (432 mg, 0.774 mmol) was added 25 mL benzene via vacuum transfer at -78 °C. Upon warming to 23 °C, the solution turned deep purple, and after stirring for 12 h the volatiles were removed. The maroon solid was triturated with benzene (3 x 5 mL), redissolved in 15 mL benzene and filtered. Solvent was removed under vacuum, pentane was added, and the resulting slurry was cooled to -78 °C, and filtered to yield a maroon solid (360 mg, 76%). A single crystal suitable for X-ray diffraction was acquired by slow diffusion of pentane into a concentrated

THF solution. ^{1}H NMR (C_6D_6): δ -1.38 ($\nu_{1/2}$ = 880 Hz, 2H), 1.78 ($\nu_{1/2}$ = 720 Hz, 10H), 2.85 ($\nu_{1/2}$ = 120 Hz, 6H), 4.20 ($\nu_{1/2}$ = 250 Hz, 12H), 4.71 ($\nu_{1/2}$ = 70 Hz, 2H), 6.78 ($\nu_{1/2}$ = 580 Hz, 2H), 18.07 ($\nu_{1/2}$ = 570 Hz, 2H), 20.92 ($\nu_{1/2}$ = 190 Hz, 2H), 71.47 ($\nu_{1/2}$ = 1800 Hz, 2H), 77.97 ($\nu_{1/2}$ = 2600 Hz, 2H). μ_{eff} (Evans, C_6D_6): 2.7 μ_B. Anal. for $C_{42}H_{52}CrN_4O$ (calc) C 74.09, H 7.70, N 8.23; (found) C 74.52, H 7.95, N 8.14.

5. *(dadi)Fe (**1**-Fe).* To a 25 mL flask charged with Fe{N(SiMe$_3$)$_2$}$_2$(THF) (116 mg, 0.259 mmol) and (dadi)H$_2$ (145 mg, 0.259 mmol) was added 12 mL benzene via vacuum transfer at -78 °C. Upon warming to 23 °C, the dark olive green solution was stirred for 2 d. The volatiles were removed under vacuum, and the green solid was triturated with benzene (2 x 5 mL). Diethyl ether (30 mL) was added and the reaction was filtered. The filter cake was washed until colorless, and the Et$_2$O was removed and 10 mL pentane added. After cooling to -78 °C, a dark green solid (120 mg, 75%) was collected by filtration. A single crystal suitable for X-ray diffraction was obtained by slow evaporation of a concentrated pentane solution. ^{1}H NMR (C_6D_6): δ -33.32 ($\nu_{1/2}$ = 104 Hz, 2H), -23.32 ($\nu_{1/2}$ = 1040 Hz, 12H), -10.94 ($\nu_{1/2}$ = 134 Hz, 2H), 8.26 ($\nu_{1/2}$ = 290 Hz, 2H), 13.80 ($\nu_{1/2}$ = 200 Hz, 12H), 18.50 ($\nu_{1/2}$ = 660 Hz, 2H), 32.95 ($\nu_{1/2}$ = 160 Hz, 4H), 54.93 ($\nu_{1/2}$ = 284 Hz, 2H), 72.59 ($\nu_{1/2}$ = 186 Hz, 2H). μ_{eff} (Evans, C_6D_6): 4.7 μ_B. MS for $C_{38}H_{44}FeN_4$ (calc) 613.2949; (found) 613.2982.

6. *{AdN(-CH=N(1,2-C$_6$H$_4$)NH(2,6-^{i}Pr$_2$-C$_6$H$_3$)}$_2$Cr (**2**-CrAd).* To a 50 mL flask charged with (dadi)Cr (**1**-Cr, 260 mg, 0.427 mmol) and 1-azidoadamantane (75 mg, 0.423 mmol) at -78 °C was vacuum transferred 20 mL of toluene. The reaction mixture warmed to 23 °C over 4 h, then stirred for an additional 8 h. The reaction mixture was cooled to -78 °C, degassed, warmed to 23 °C, and filtered. The solvent was removed under vacuum and

the resulting solid was triturated with 2 x 25 mL of pentane. The resulting solid was dissolved in 45 mL of pentane and cooled to -78 °C to precipitate the product as a microcrystalline violet solid (280 mg, 0.369 mmol, 86 %). A single crystal suitable for X-ray diffraction was obtained by diffusion of hexanes into a saturated diethyl ether solution. ^{1}H NMR (C_6D_6, 295K): δ -20.20 ($\nu_{1/2}$ = 760 Hz), 4.07 ($\nu_{1/2}$ = 110 Hz), 7.48 ($\nu_{1/2}$ = 1950 Hz). μ_{eff} (Evans, C_6D_6): 4.5 μ_B. Anal. for $C_{48}H_{59}CrN_5$ (calc), C 76.06, H 7.85, N 9.24; (found) C 73.14, H 8.04, N 8.94.

7. *{(2,6-^{i}Pr$_2$-C$_6$H$_3$)N(-CH=N(1,2-C$_6$H$_4$)NH(2,6-^{i}Pr$_2$-C$_6$H$_3$)}$_2$Cr (**2**-CrAr).* To a 50 mL flask charged with (dadi)Cr (**1**-Cr, 165 mg, 0.271 mmol) and 25 mL of toluene at -78 °C, was dropwise added a solution of 2,6-diisopropylphenylazide (55 mg, 0.271 mmol) via syringe. The reaction mixture was degassed, warmed to 23 °C over 2 h, and stirred for an additional 10 h. The solvent was removed under vacuum, and the resulting solid was triturated with 2 x 25 mL of pentane. The solid was dissolved in benzene, filtered, and the solvent was removed under vacuum. The blue solid was dissolved in 30 mL of pentane and cooled to -78 °C to afford a denim-blue microcrystalline solid (138 mg, 0.176 mmol, 65 %). A single crystal suitable for X-ray diffraction was obtained by slow evaporation of a saturated diethyl ether solution layered with hexanes at -20 °C. ^{1}H NMR (C_6D_6, 295K): δ -24.34 ($\nu_{1/2}$ = 600 Hz), 0.84 ($\nu_{1/2}$ = 26 Hz), 1.19 ($\nu_{1/2}$ = 26 Hz), 3.85 ($\nu_{1/2}$ = 150 Hz), 4.77 ($\nu_{1/2}$ = 750 Hz), 8.09 ($\nu_{1/2}$ = 850 Hz). μ_{eff} (Evans): 4.9 μ_B. Anal. for $C_{50}H_{61}CrN_5$ (calc), C 76.59, H 7.84, N 8.93; (found) C 75.39, H 8.01, N 9.09.

8. *{AdN(-CH=N(1,2-C$_6$H$_4$)NH(2,6-^{i}Pr$_2$-C$_6$H$_3$)}$_2$Fe (**2**-FeAd).* To a 50 mL flask charged with (dadi)Fe (**1**-Fe, 200 mg, 0.326 mmol) and 1-azidoadamantane (58 mg, 0.327 mmol) at -78 °C was vacuum transferred 25

mL of toluene. The reaction mixture warmed to 23 °C over 2 h, and stirred for an additional 10 h. The reaction mixture was cooled to -78 °C, degassed, warmed to 23 °C, filtered, and concentrated. Pentane (45 mL) was added at -78 °C to precipitate **1**-Fe as a maroon microcrystalline solid (165 mg, 0.217 mmol, 67 %). A single crystal suitable for X-ray diffraction was obtained by slow evaporation of a concentrated benzene solution. ^{1}H NMR (C_6D_6, 295K): δ -42.99 ($\nu_{1/2} \approx$ 425 Hz, 4H), -20.19 ($\nu_{1/2}$ = 25 Hz, 2H), -7.44 (($\nu_{1/2}$ = 25 Hz, 2H), -4.30 ($\nu_{1/2}$ = 130 Hz, 4H), 1.60 ($\nu_{1/2}$ = 18 Hz, 4H), 1.73 ($\nu_{1/2}$ = 18 Hz, 4H), 2.65 ($\nu_{1/2}$ = 100 Hz, 3H), 3.48 ($\nu_{1/2}$ = 90 Hz, 3H), 4.50 ($\nu_{1/2}$ = 10 Hz, 3H), 6.75 ($\nu_{1/2}$ = 140 Hz, 11H), 20.78 ($\nu_{1/2}$ = 150 Hz, 2H), 26.91 ($\nu_{1/2}$ = 116 Hz, 2H), 35.16 ($\nu_{1/2}$ = 120 Hz, 2H), 36.82 ($\nu_{1/2}$ = 110 Hz, 2H), 48.75 ($\nu_{1/2}$ = 36 Hz, 2H). μ_{eff} (Evans): 4.8 μ_B. Anal. for $C_{48}H_{59}FeN_5$ (calc), C 75.67, H 7.81, N 9.19; (found) C 75.39, H 8.01, N 9.09.

9. *{(2,6-^{i}Pr$_2$-C$_6$H$_3$)N(-CH=N(1,2-C$_6$H$_4$)NH(2,6-^{i}Pr$_2$-C$_6$H$_3$)}$_2$Fe (**2**-FeAr).* To a 50 mL flask charged with (dadi)Fe (**1**-Fe, 120 mg, 0.196 mmol) and 22 mL of diethyl ether at -78 °C was dropwise added a solution of 2,6-diisopropylphenylazide (40 mg, 0.197 mmol) in 0.5 mL of diethyl ether via syringe. The reaction mixture was stirred for 3 h at -78 °C, warmed to 23 °C, and stirred for an additional hour. The reaction mixture was filtered and the solvent removed by vacuum. Pentane (15 mL) was added and the solution was cooled to -78 °C to afford **2**-FeAr as a dark maroon/purple precipitate (60 mg, 0.076 mmol, 39 %). ^{1}H NMR (C_6D_6, 400MHz, 295K): δ -51.34 ($\nu_{1/2}$ = 390 Hz, 2H), -21.02 ($\nu_{1/2}$ = 25 Hz, 2H), -10.26 ($\nu_{1/2}$ = 110 Hz, 2H), -7.75 ($\nu_{1/2}$ = 130 Hz, 5H), -6.84 ($\nu_{1/2}$ = 30 Hz, 3H), -5.44 ($\nu_{1/2}$ = 125 Hz, 7H), -0.66 ($\nu_{1/2}$ = 65 Hz, 7H), 1.39 ($\nu_{1/2}$ = 8 Hz, 2H), 6.86 ($\nu_{1/2}$ = 15 Hz, 2H), 7.70 ($\nu_{1/2}$ = 200 Hz, 7H),

24.11 ($\nu_{1/2}$ = 110 Hz, 1H), 26.29 ($\nu_{1/2}$ = 80 Hz, 1H), 34.46 ($\nu_{1/2}$ = 100 Hz, 2H), 39.15 ($\nu_{1/2}$ = 100 Hz, 2H), 50.70 ($\nu_{1/2}$ = 41 Hz, 2H). μ_{eff} (Evans): 4.9 μ_B.

10. *[(-(CH=N(1,2-C_6H_4)NH(2,6-^{i}Pr$_2$-C_6H_3)(C(=NS(O)(=O-)-tol)N(1,2-C_6H_4)NH(2,6-^{i}Pr$_2$-C_6H_3)Cr]$_2$ (**3**-Cr).* To a 50 mL round bottom flask charged with (dadi)Cr (**1**-Cr, 119 mg, 0.195 mmol) and 20 mL of toluene at -78 °C was dropwise added a solution of tosyl azide (40 mg, 0.203 mmol) in 3 mL of toluene via syringe. The reaction mixture warmed to 23 °C over 4 h, and stirred for an additional 20 h. The solvent was removed under vacuum, and the resulting solid dissolved in 5 mL of benzene and filtered through a celite plug into a 20 dram scintillation vile. The product was crystallized by diffusion of pentane into the benzene solution yielding the product as green brittle needles (38 mg, 0.024 mmol, 25%). A single crystal suitable for X-ray diffraction was obtained by the diffusion of pentane into a saturated THF solution at -20 °C. ^{1}H NMR (C_6D_6, 295K): δ -12.53 ($\nu_{1/2}$ = 162 Hz), -7.31 ($\nu_{1/2}$ = 170 Hz), 0.42 ($\nu_{1/2}$ = 180 Hz), -2.93 ($\nu_{1/2}$ = 100 Hz), -2.10 ($\nu_{1/2}$ = 150 Hz), -0.42 ($\nu_{1/2}$ = 140 Hz), 0.42 ($\nu_{1/2}$ = 180 Hz), 2.46 ($\nu_{1/2}$ = 64 Hz), 6.25 ($\nu_{1/2}$ = 70 Hz), 15.49 ($\nu_{1/2}$ = 76 Hz), 37.00 ($\nu_{1/2}$ = 460 Hz), 40.00 ($\nu_{1/2}$ = 530 Hz), 61.94 ($\nu_{1/2}$ = 730 Hz). μ_{eff} (Evans): 3.8 μ_B. Anal. for $C_{90}H_{100}Cr_2N_{10}O_4S_2$ (calc), C 69.56, H 6.49, N 9.01; (found) C 69.42, H 6.49, N 8.91.

C. Crystallographic data

Upon isolation, crystals were covered in polyisobutenes and placed under a 173 K N_2 stream on the goniometer hed of a Siemend P4 SMART CCD area detector (graphite-monochromated Mo Kα radiation, λ = 0.71073 Å). The structures were solved by direct methods (SHELXS). All non-hydrogen

atoms were refined anisotropically unless otherwise stated, and hydrogen atoms were treated as idealized contributions (Riding model).

1-Cr(THF) (0.35 x 0.20 x 0.10 mm^3)**:** $C_{42}H_{52}CrN_4O$, M = 680.88, T = 173(2) K, λ = 0.71073 Å, triclinic, P1bar, a = 12.0237(5), b = 18.1933(9), c = 19.6461(9) Å, α = 65.547(2)°, β = 82.660(2)°, γ = 71.705(2)°, V = 3714.4(3) $Å^3$, Z = 4, ρ (calcd) = 1.218 g/cm^3, abs. coeff. = 0.345 mm^{-1}, 71009 reflections, 18259 independent, R_{int} = 0.0472, abs. correc. was semi-empirical from equivalents, $R_1(I > 2\sigma I)$ = 0.0487, wR_2 = 0.1240, R_1(all data) = 0.0868, wR_2 = 0.1430, GOF = 1.052, CCDC-1416745.

1-Fe (0.40 x 0.35 x 0.25 mm^3)**:** $C_{38}H_{44}FeN_4$, M = 612.62, T = 183(2) K, λ = 0.71073 Å, monoclinic, $P2_1/c$, a = 12.7432(6), b = 19.2721(9), c = 14.4594(6) Å, β = 98.966(2)°, V = 3505.7(3) $Å^3$, Z = 4, ρ (calcd) = 1.160 g/cm^3, abs. coeff. = 0.460 mm^{-1}, 32629 reflections, 8690 independent, R_{int} = 0.0383, abs. correc. was semi-empirical from equivalents, $R_1(I > 2\sigma I)$ = 0.0458, wR_2 = 0.1477, R_1(all data) = 0.0673, wR_2 = 0.1610, GOF = 1.043, CCDC-1416744.

2-CrAd (0.40 x 0.20 x 0.15 mm^3)**:** $C_{48}H_{59}CrN_5$, M = 758.00, T = 243(2) K, λ = 0.71073 Å, monoclinic, $P2_1/c$, a = 14.8982(17), b = 14.2012(16), c = 21.136(2) Å, β = 96.616(4)°, V = 4442.1(9) $Å^3$, Z = 4, ρ (calcd) = 1.133 g/cm^3, abs. coeff. = 0.294 mm^{-1}, 26817 reflections, 7564 independent, R_{int} = 0.0519, abs. correc. was semi-empirical from equivalents, $R_1(I > 2\sigma I)$ = 0.0533, wR_2 = 0.1482, R_1(all data) = 0.0800, wR_2 = 0.1625, GOF = 1.053, CCDC-1416746.

2-CrAr (0.30 x 0.20 x 0.03 mm^3)**:** $C_{50}H_{61}CrN_5$, M = 784.04, T = 223(2) K, λ = 0.71073 Å, triclinic, P1bar, a = 14.590(8), b = 16.190(10), c = 22.071(11) Å, α = 97.866(18)°, β = 99.639(18)°, γ = 109.04(2)°, V = 4754(5) $Å^3$, Z = 4, ρ (calcd) = 1.095 g/cm^3, abs. coeff. = 0.277 mm^{-1}, 28640 reflections, 11688 independent, R_{int} = 0.0657, abs. correc. was semi-empirical from

equivalents, $R_1(I > 2\sigma I)$ = 0.0526, wR_2 = 0.1147, R_1(all data) = 0.1045, wR_2 = 0.1294, GOF = 0.969, CCDC-1416748.

2-Fe-Ad (0.40 x 0.20 x 0.10 mm^3)**:** $C_{66}H_{74}FeN_5$, M = 993.15, T = 223(2) K, λ = 0.71073 Å, monoclinic, P2$_1$/n, a = 17.6231(12), b = 15.2157(11), c = 21.6061(16) Å, β = 105.117(3)°, V = 5593.1(7) Å^3, Z = 4, ρ (calcd) = 1.179 g/cm^3, abs. coeff. = 0.314 mm^{-1}, 44740 reflections, 9536 independent, R_{int} = 0.0464, abs. correc. was semi-empirical from equivalents, $R_1(I > 2\sigma I)$ = 0.0533, wR_2 = 0.1482, R_1(all data) = 0.0800, wR_2 = 0.1625, GOF = 1.053, CCDC-1416749.

2-CrAd (0.40 x 0.20 x 0.15 mm^3)**:** $C_{48}H_{59}CrN_5$, M = 758.00, T = 243(2) K, λ = 0.71073 Å, monoclinic, P2$_1$/c, a = 14.8982(17), b = 14.2012(16), c = 21.136(2) Å, β = 96.616(4)°, V = 4442.1(9) Å^3, Z = 4, ρ (calcd) = 1.133 g/cm^3, abs. coeff. = 0.294 mm^{-1}, 26817 reflections, 7564 independent, R_{int} = 0.0519, abs. correc. was semi-empirical from equivalents, $R_1(I > 2\sigma I)$ = 0.0533, wR_2 = 0.1482, R_1(all data) = 0.0800, wR_2 = 0.1625, GOF = 1.053, CCDC-1416746.

D. UV-vis spectra

In Figure 1.9, UV-vis spectra of **2**-FeAd and **2**-FeAr are shown, and indicate the similarity of the two species.

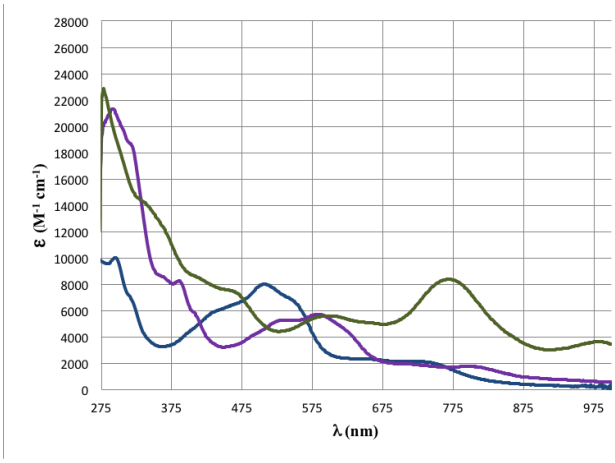

Figure 1.8. UV-vis spectra of **2**-CrAd (purple), **2**-CrAr (blue), and **3**-Cr (green).

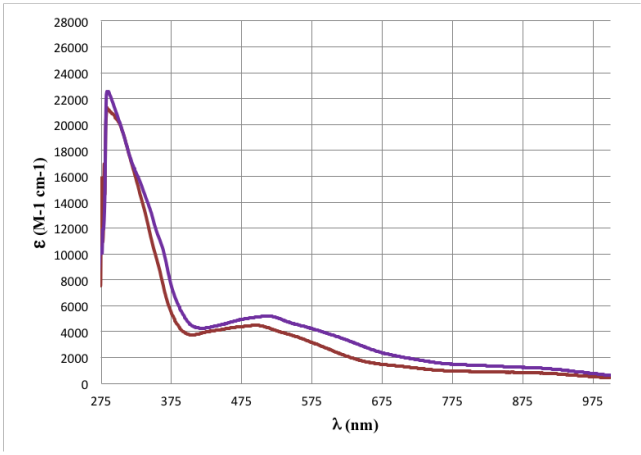

Figure 1.9. UV-vis spectra of **2**-FeAd (red) and **2**-FeAr (purple) (green).

E. Computations

All simulations employed the Gaussian 09[57] code. Geometries were optimized and energy Hessians were computed at the M06/6-31+G(d) level of theory. At these stationary points, M06[58]/6-311++G(d,p)/SMD[59]-THF single point electronic energies were determined, which were then converted to free

energies using the M06/6-31+G(d) vibrational frequencies (unscaled). Reported enthalpies and free energies for the transition metal complexes assume 1 atm and 298.15 K.

References:

(1) Jørgensen, C. K. *Coord. Chem. Rev.* **1966**, *1* (1), 164–178.

(2) Eisenberg, R.; Gray, H. B. *Inorg. Chem.* **2011**, *50* (20), 9741–9751.

(3) Baker-Hawkes, M. J.; Billig, E.; Gray, H. B. *J. Am. Chem. Soc.* **1966**, *88* (21), 4870–4875.

(4) Jazdzewski, B. A.; Tolman, W. B. *Coord. Chem. Rev.* **2000**, *200–202*, 633–685.

(5) Rittle, J.; Green, M. T. *Science.* **2010**, *330* (6006), 933–937.

(6) Dolphin, D.; Forman, A.; Borg, D. C.; Fajer, J.; Felton, R. H. *Proc. Natl. Acad. Sci. U. S. A.* **1971**, *68* (3), 614–618.

(7) Allen, F. H.; Kennard, O.; Watson, D. G.; Brammer, L.; Orpen, A. G.; Taylor, R. *J. Chem. Soc. Perkin Trans. 2*. **1987**, No. 12, S1–S19.

(8) Williams, V. A.; Hulley, E. B.; Wolczanski, P. T.; Lancaster, K. M.; Lobkovsky, E. B. *Chem. Sci.* **2013**, *4* (9), 3636–3648.

(9) Bart, S. C.; Lobkovsky, E.; Bill, E.; Chirik, P. J. *J. Am. Chem. Soc.* **2006**, *128* (16), 5302–5303.

(10) Zhou, W.; Patrick, B. O.; Smith, K. M. *Chem. Commun.* **2014**, *50* (69), 9958–9960.

(11) Zarkesh, R. A.; Heyduk, A. F. *Organometallics*. **2011**, *30* (18), 4890–4898.

(12) Blackmore, K. J.; Ziller, J. W.; Heyduk, A. F. *Inorg. Chem.* **2005**, *44* (16), 5559–5561.

(13) Spasyuk, D. M.; Carpenter, S. H.; Kefalidis, C. E.; Piers, W. E.; Neidig, M. L.; Maron, L. *Chem. Sci.* **2016**, *7* (9), 5939–5944.

(14) Wilding, M. J. T.; Iovan, D. A.; Betley, T. A. *J. Am. Chem. Soc.* **2017**, *139* (34), 12043–12049.

(15) Heins, S. P.; Morris, W. D.; Wolczanski, P. T.; Lobkovsky, E. B.; Cundari, T. R. *Angew. Chemie Int. Ed. 54* (48), 14407–14411.

(16) Mehn, M. P.; Peters, J. C. *J. Inorg. Biochem.* **2006**, *100* (4), 634–643.

(17) Saouma, C. T.; Peters, J. C. *Coord. Chem. Rev.* **2011**, *255* (7), 920–937.

(18) Iovan, D. A.; Betley, T. A. *J. Am. Chem. Soc.* **2016**, *138* (6), 1983–1993.

(19) Cowley, R. E.; Holland, P. L. *Inorg. Chem.* **2012**, *51* (15), 8352–8361.

(20) Hennessy, E. T.; Liu, R. Y.; Iovan, D. A.; Duncan, R. A.; Betley, T. A. *Chem. Sci.* **2014**, *5* (4), 1526–1532.

(21) Bowman, A. C.; Milsmann, C.; Bill, E.; Turner, Z. R.; Lobkovsky, E.; DeBeer, S.; Wieghardt, K.; Chirik, P. J. *J. Am. Chem. Soc.* **2011**, *133* (43), 17353–17369.

(22) King, E. R.; Hennessy, E. T.; Betley, T. A. *J. Am. Chem. Soc.* **2011**, *133* (13), 4917–4923.

(23) Cowley, R. E.; DeYonker, N. J.; Eckert, N. A.; Cundari, T. R.; DeBeer, S.; Bill, E.; Ottenwaelder, X.; Flaschenriem, C.; Holland, P. L. *Inorg. Chem.* **2010**, *49* (13), 6172–6187.

(24) Bucinsky, L.; Breza, M.; Lee, W.-T.; Hickey, A. K.; Dickie, D. A.; Nieto, I.; DeGayner, J. A.; Harris, T. D.; Meyer, K.; Krzystek, J.; et al. *Inorg. Chem.* **2017**, *56* (8), 4751–4768.

(25) Lucas, R. L.; Powell, D. R.; Borovik, A. S. *J. Am. Chem. Soc.* **2005**, *127* (33), 11596–11597.

(26) Searles, K.; Fortier, S.; Khusniyarov, M. M.; J., C. P.; Sutter, J.; Meyer, K.; Mindiola, D. J.; Caulton, K. G. *Angew. Chemie Int. Ed.* **2014**, *53* (51), 14139–14143.

(27) Thomas, C. M.; Mankad, N. P.; Peters, J. C. *J. Am. Chem. Soc.* **2006**, *128* (15), 4956–4957.

(28) Wa-Hung, L. *Eur. J. Inorg. Chem.* **2003**, *2003* (4), 583–593.

(29) Nugent, W. A.; Harlow, R. L. *Inorg. Chem.* **1980**, *19* (3), 777–779.

(30) Barron, A. R.; Salt, J. E.; Wilkinson, G.; Motevalli, M.; Hursthouse, M. B. *J. Chem. Soc. Dalt. Trans.* **1987**, No. 12, 2947–2954.

(31) Elliott, R. L.; Nichols, P. J.; West, B. O. *Polyhedron*. **1987**, *6* (12), 2191–2192.

(32) Danopoulos, A. A.; Hussain-Bates, B.; Hursthouse, M. B.; Leung, W.-H.; Wilkinson, G. *J. Chem. Soc. Chem. Commun.* **1990**, No. 23, 1678–1679.

(33) Danopoulos, A. A.; Leung, W.-H.; Wilkinson, G.; Hussain-Bates, B.; Hursthouse, M. B. *Polyhedron*. **1990**, *9* (21), 2625–2634.

(34) Coles, M. P.; Dalby, C. I.; Gibson, V. C.; Clegg, W.; Elsegood, M. R. J. *J. Chem. Soc.{,} Chem. Commun.* **1995**, No. 16, 1709–1711.

(35) Danopoulos, A. A.; Wilkinson, G.; Sweet, T. K. N.; Hursthouse, M. B. *Polyhedron*. **1996**, *15* (5), 873–879.

(36) Sydora, O. L.; Kuiper, D. S.; Wolczanski, P. T.; Lobkovsky, E. B.; Dinescu, A.; Cundari, T. R. *Inorg. Chem.* **2006**, *45* (5), 2008–2021.

(37) Beaumier, E. P.; Billow, B. S.; Singh, A. K.; Biros, S. M.; Odom, A. L. *Chem. Sci.* **2016**, *7* (4), 2532–2536.

(38) Edwards, N. Y.; Eikey, R. A.; Loring, M. I.; Abu-Omar, M. M. *Inorg. Chem.* **2005**, *44* (10), 3700–3708.

(39) Elpitiya, G. R.; Malbrecht, B. J.; Jenkins, D. M. *Inorg. Chem.* **2017**, *56* (22), 14101–14110.

(40) Goswami, M.; Lyaskovskyy, V.; Domingos, S. R.; Buma, W. J.; Woutersen, S.; Troeppner, O.; Ivanović-Burmazović, I.; Lu, H.; Cui, X.; Zhang, X. P.; et al. *J. Am. Chem. Soc.* **2015**, *137* (16), 5468–5479.

(41) Connie C., L.; Serena, D. G.; Thomas, W.; Eckhard, B.; Eberhard, B.; Karl, W. *Angew. Chemie Int. Ed.* **2008**, *47* (34), 6384–6387.

(42) Takacs, J. M.; Anderson, L. G.; Madhavan, G. V. B.; Creswell, M. W.; Seely, F. L.; Devroy, W. F. *Organometallics*. **1986**, *5* (11), 2395–2398.

(43) Bradley, D. C.; Hursthouse, M. B.; Newing, C. W.; Welch, A. J. *J. Chem. Soc., Chem. Commun.* **1972**, No. 9, 567–568.

(44) Horvath, B.; Strutz, J.; Horvath, E. G. *Zeitschrift für Anorg. und Allg. Chemie*. **2004**, *457* (1), 38–50.

(45) Olmstead, M. M.; Power, P. P.; Shoner, S. C. *Inorg. Chem.* **1991**, *30* (11), 2547–2551.

(46) Andersen, R. A.; Faegri, K.; Green, J. C.; Haaland, A.; Lappert, M. F.; Leung, W. P.; Rypdal, K. *Inorg. Chem.* **1988**, *27* (10), 1782–1786.

(47) Bürger, H.; Wannagat, U. *Monatshefte für Chemie und verwandte Teile anderer Wissenschaften*. **1963**, *94* (6), 1007–1012.

(48) Schubert, E. M. *J. Chem. Educ.* **1992**, *69* (1), 62.

(49) Evans, D. F. *J. Chem. Soc.* **1959**, 2003–2005.

(50) Williams, V. A.; Wolczanski, P. T.; Sutter, J.; Meyer, K.; Lobkovsky, E. B.; Cundari, T. R. *Inorg. Chem.* **2014**, *53* (9), 4459–4474.

(51) Lu, C. C.; Bill, E.; Weyhermüller, T.; Bothe, E.; Wieghardt, K. *J. Am. Chem. Soc.* **2008**, *130* (10), 3181–3197.

(52) Frazier, B. A.; Williams, V. A.; Wolczanski, P. T.; Bart, S. C.; Meyer, K.; Cundari, T. R.; Lobkovsky, E. B. *Inorg. Chem.* **2013**, *52* (6), 3295–3312.

(53) Wilding, M. J. T.; Iovan, D. A.; Wrobel, A. T.; Lukens, J. T.; MacMillan, S. N.; Lancaster, K. M.; Betley, T. A. *J. Am. Chem. Soc.* **2017**, *139* (41), 14757–14766.

(54) Cowley, R. E.; Eckert, N. a; Vaddadi, S.; Figg, T. M.; Cundari, T. R.; Holland, P. L. *J. Am. Chem. Soc.* **2011**, *133* (25), 9796–9811.

(55) Wolczanski, P. T. *Organometallics*. **2017**, *36* (3), 622–631.

(56) Khumsubdee, S.; Fan, Y.; Burgess, K. *J. Org. Chem.* **2013**, *78* (19), 9969–9974.

(57) Gaussian 09, Revision D.01, M. J. Frisch, G. W. Trucks, H. B. Schlegel, G. E. Scuseria, M. A. Robb, J. R. Cheeseman, G. Scalmani, V. Barone, B. Mennucci, G. A. Petersson, H. Nakatsuji, M. Caricato, X. Li, H. P. Hratchian, A. F. Izmaylov, J. Bloino, G. Zheng, J. L. Sonnenberg, J. M. Hada, M. Ehara, K. Toyota, R. Fukuda, J. Hasegawa, M. Ishida, T. Nakajima, Y. Honda, O. Kitao, H. Nakai, T. Vreven, J. A. Montgomery, Jr., J. E. Peralta, F. Ogliaro, M. Bearpark, J. J. Heyd, E. Brothers, K. N. Kudin, V. N. Staroverov, R. Kobayashi, J. Normand, K. Raghavachari, A. Rendell, J. C. Burant, S. S. Iyengar, J. Tomasi, M. Cossi, N. Rega, J. M. Millam, M. Klene, J. E. Knox, J. B. Cross, V. Bakken, C. Adamo, J. Jaramillo, R. Gomperts, R. E. Stratmann, O. Yazyev, A. J. Austin, R. Cammi, C. Pomelli, J. W. Ochterski, R. L. Martin, K. Morokuma, V. G. Zakrzewski, G. A. Voth, P. Salvador, J. J. Dannenberg, S. Dapprich, A. D. Daniels, Ö. Farkas, J. B. Foresman, J. V. Ortiz, J. Cioslowski, D. J. Fox, Gaussian, Inc., Wallingford CT, 2009.

(58) Zhao, Y.; Truhlar, D. G. *Theor. Chem. Acc.* **2008**, *120* (1), 215–241.

(59) Marenich, A. V; Cramer, C. J.; Truhlar, D. G. *J. Phys. Chem. B*. **2009**, *113* (18), 6378–6396.

CHAPTER 2

Redox Non-Innocence and Catalytic Nitrene Carbonylation with Titanium

Introduction:

Ligand redox non-innocence (RNI) is primarily a consequence of ligand and metal *d*-orbitals whose similar energies give rise to molecular orbitals of mixed metal and ligand composition.[1–9] This phenomenon can extend the capabilities of transition metals, particularly in the 1st row where 1-electron processes are common,[10,11] as well as with early metals were high oxidation states dominate.[12–18] By acting as an electronic buffer (Figure 2.1), RNI ligands can keep a metal in a stable configuration (M^{n+2}) by being in a reduced state (L^{p-2}), while supplying reducing equivalents required for the oxidative addition of XY ($L^{p-2}M^{m+2}$ -> $L^{p}M^{m}$ -> $L^{p}M^{m+2}XY$).[19] Transfer of XY to substrate, causes reduction of the metal, but its formal oxidation state (M^{m} -> M^{m+2}) is maintained by the RNI of the ligand.

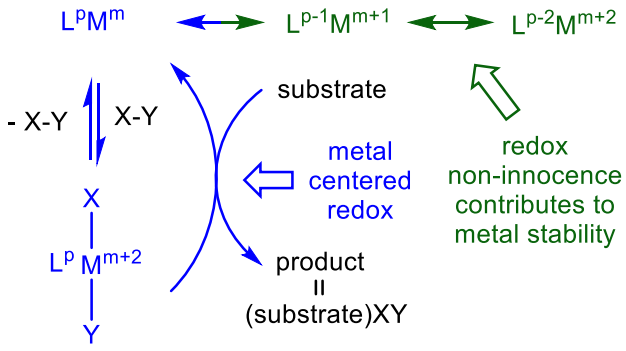

Figure 2.1. Conventional oxidative addition (blue), and corresponding 1- and 2-e^{-} redox non-innocent (RNI) configurations (green) that can electronically buffer the metal center. The ligand, L^{p}, π-system can be (4n+2) -> 4n or 4n -> (4n-2) depending on its compatibility with M^{m}.

Heyduk's work with a tris-amide (NNN) pincer ligands chelated to Zr(IV) effect the catalytic nitrene transfer to isocyanide, forming carbodiimides (Scheme 2.1).[12] The metal maintains a +4 oxidation state throughout, while the pincer ligand cycles through its monoanionic and trianionic forms. This represents the first example of a catalytic nitrene transfer from a non-porphyrin metal complex.[20] This has proven to be an effective strategy to elicit multi-electron processes from formally d^0 metals, and has been extended to Ta(V) complexes.[21] The previously introduced (*cf.* Chapter 1) diamide-diimine ligand $\{\text{-CH=N(1,2-C}_6\text{H}_4\text{)N(2,6-}^i\text{Pr}_2\text{-C}_6\text{H}_3\text{)}\}_2^m$ (m = 0 to -4), *i.e.* $(\text{dadi})^m$, has at least five available redox states, and was envisioned to behave in a similar manner with early, first row transition metals. Chelation of Ti(II) by $(\text{dadi})^{2-}$ was a target, with the expectation that RNI leading to $(\text{dadi})^{4-}\text{Ti}^{IV}$ could potentially stabilize the system, as the tetraanion has a 4n+2 conjugated π-system.

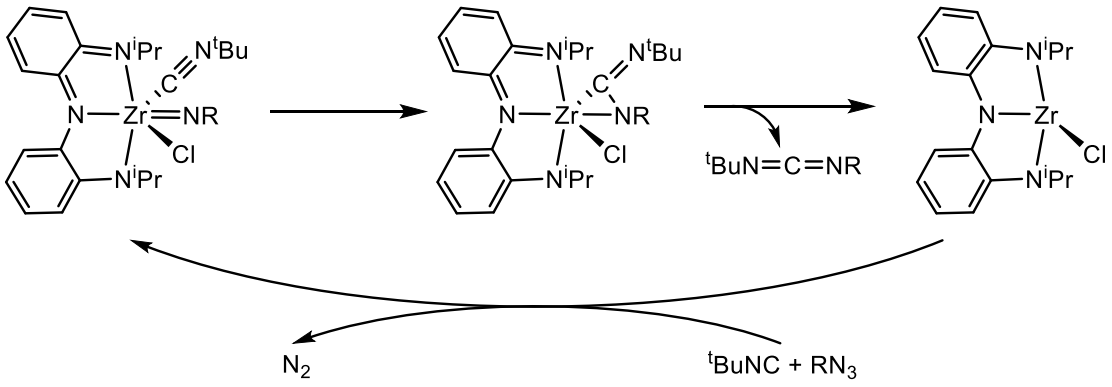

Scheme 2.1. Catalytic nitrene transfer by a Zr(IV) imido species.

The ligand metrics of the (dadi)Fe complex indicated a $(\text{dadi})^{2-}$ chelate with high spin Fe(II) complex.[22] RNI is more evident in the (dadi)Cr(THF) complex, where the ground state consists of an admixture of $(\text{dadi})^{3-}$ radical antiferromagnetically (AF) coupled to Cr(III) (S_T = 1), and an S = 1 excited

state of $(dadi)^{2-}$ AF-coupled to high spin Cr(II) (i.e., α $\{(dadi)^{2-}\}^{*\downarrow\downarrow}Cr^{\uparrow\uparrow\uparrow\uparrow}$ + (1-α) $\{(dadi)^{3-}\}^{\downarrow}Cr^{\uparrow\uparrow\uparrow}$ with $\alpha > 0.5$). The availability of multiple redox states, separated by two electrons was initially evident in the diamagnetic {(dadi)TiCl}Li$(THF)_4$ complex (*cf.* Chapter 3), hinting at the possibility of oxidative additions facilitated by the RNI dadi ligand.

Cr and Fe dadi complexes react with organic azides, generating transient imidyl species to afford products from an intramolecular aziridination-ring-opening sequence, or from intramolecular CH insertion.[22] Unfortunately, these intramolecular processes could not be circumvented, limiting the utility of the Cr and Fe dadi compounds as nitrene-group transfer catalysts. However, simultaneous studies of (dadi)Ti$(L)_x$ (x = 1, L = THF, PMe_2Ph; x = 2, L = CNMe) complexes suggested that metal imido species could be isolated. This prompted a more detailed investigation into the nature of the dadi RNI in conjunction with reactivity studies aimed at nitrene and oxo group transfers.

Results and Discussion:

2.1. Synthesis of (dadi)TiL_x (x = 1, L = THF, PMe_2Ph; x = 2, L = CNMe)

*2.1.1. (dadi)Ti(THF) (**1**-THF)*

Deprotonation of dadiH_2 (dadiH_2 = {-CH=N(1,2-C_6H_4)NH(2,6-^{i}Pr$_2$-C_6H_3)}$_2$), with 2 equiv $NaN(TMS)_2$ in THF afforded the disodium salt of $(dadi)^{2-}$ in 94% yield as a bright blue crystalline solid after precipitation with pentane (Scheme 2.2). The dianion is bright blue in THF solution, and exhibits a dominant absorption band at 770 nm (ε = 22,000 $M^{-1}cm^{-1}$) that features a ~1500 cm^{-1} progression plausible for a diimine. Treatment of $(TMEDA)_2TiCl_2$[23] with $(dadi)Na_2$ in THF at -30 ^{o}C for 12-18 hours resulted in a green solution. Removal of TMEDA by triturating with THF, followed by filtration and

crystallization from cyclohexane gave (dadi)Ti(THF) (**1**-THF) in 40-50% yield as an olive green solid with residual cyclohexane. Thorough removal of TMEDA and the use of cyclohexane were found to be critical to isolate pure **1**-THF. Crystallization from hexanes, n-pentane, or cyclopentane resulted in the isolation of (dadi)Ti(THF) contaminated with an unknown impurity that does not appear to affect subsequent chemistry, but could not be removed downstream.

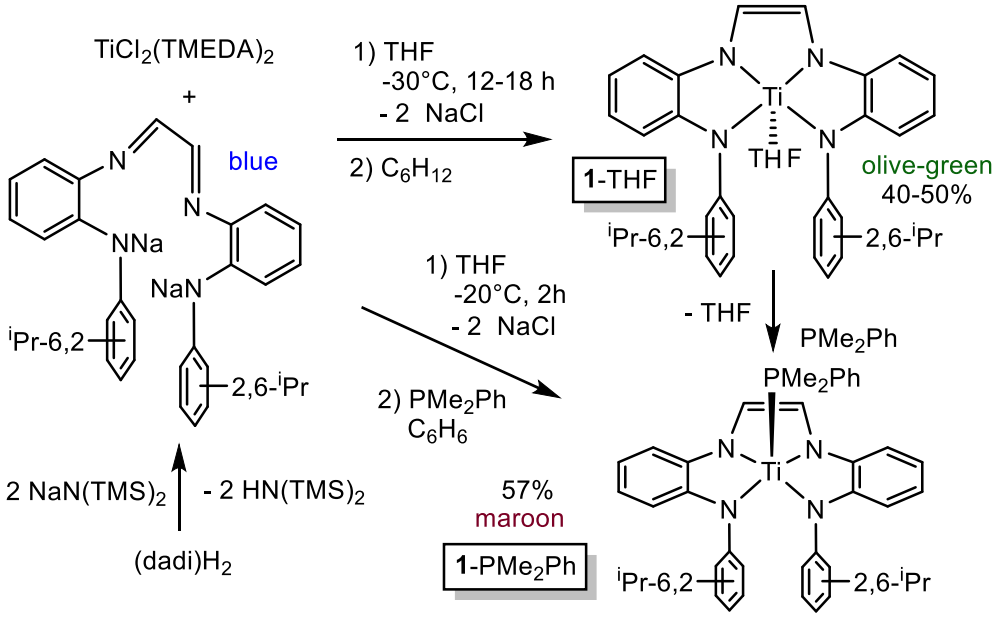

Scheme 2.2. Synthesis of (dadi)Na_2 and (dadi)TiL (L = THF, **1**-THF; PMe_2Ph, **1**-PMe_2Ph).

Diamagnetic **1**-THF appears to be five-coordinate by ^{1}H NMR spectroscopy. Due to hindered rotation of the 2,6-^{i}Pr-C_6H_3 groups around the *ipso*-carbon, the ^{i}Pr groups are rendered diastereotopic, therefore they are expected to appear as doublets in a ~6:6:6:6 ratio, but two coincident doublets in the^{1}H NMR spectrum of **1**-THF result in an observed 12:6:6 ratio of instead. The THF resonances are shifted from free solvent indicating coordination to

the metal center. Furthermore, addition of excess THF to C_6D_6 solutions of **1**-THF results in the coalescence of the four ^{i}Pr doublets (~12:6:6 ratio) to two doublets (~12:12 ratio) in the ^{1}H NMR spectrum, presumably due to coordination of a second THF molecule or rapid exchange of solvent molecules at the metal center.

In previous systems,[24] the ^{1}H NMR spectroscopic shift of the diimine protons was an indicator of the ligand redox state. The ^{1}H NMR chemical shift of the backbone diimines in (dadi)Ti(THF) (**1**-THF) appear at δ 6.64 ppm. This does not distinguish between a $(dadi)^{2-}$ and $(dadi)^{4-}$ ligand, as both states contain sp^2 carbons, which are unlikely to exhibit significantly different hydrogen chemical shifts in the ^{1}H NMR spectrum. However, the presence of a ligand based radical ($(dadi)^{3-\downarrow}$) is expected to affect the ^{1}H NMR chemical shift of the diimine protons. Calculations of pseudo-square planar (dadi)Ti suggest that it would be best considered $[(dadi)^{3-\downarrow}]Ti(III)^{\uparrow}$, a d^1 titanium AF-coupled to $(dadi)^{3-}$, but adduct formation causes an electronic reorganization to the $[(dadi)^{4-}](L)Ti^{IV}$configuration.

The electronic absorption spectra of related complexes (dadi)M (M = Fe, Mn)[22] feature absorptions at ~720 and ~940 nm (ε ~ 5-12,000 $M^{-1}cm^{-1}$) (*cf.* Chapter 1). The UV-vis spectrum of **1**-THF (Figure 2.2) features two similar, blue shifted bands at 495 (ε ~ 900 $M^{-1}cm^{-1}$) and 590 nm (ε ~ 700 $M^{-1}cm^{-1}$). It is difficult to assign these transitions but from a qualitative perspective, the appreciable decrease in molar absorptivities suggests a decrease in the transition moment integral,[25] and thus a more covalent electronic environment for **1**-THF compared to the Fe and Mn congeners. Calculations also support a $[(dadi)^{4-}](THF)Ti^{IV}$ configuration in which the tetraanionic chelate possesses $22e^-$, a 4n+2 π-system.

*2.1.2. (dadi)Ti(PMe_2Ph) (**1**-PMe_2Ph)*

Single crystals of **1**-THF for X-ray analysis have remained elusive, thus a PMe_2Ph adduct was prepared. **1**-PMe_2Ph can be prepared *in situ* by adding phosphine after metalation or by displacement of THF from **1**-THF (Scheme 2.2). The maroon phosphine adduct also exhibits a normal diimine ^1H NMR spectroscopic shift at δ 6.73.

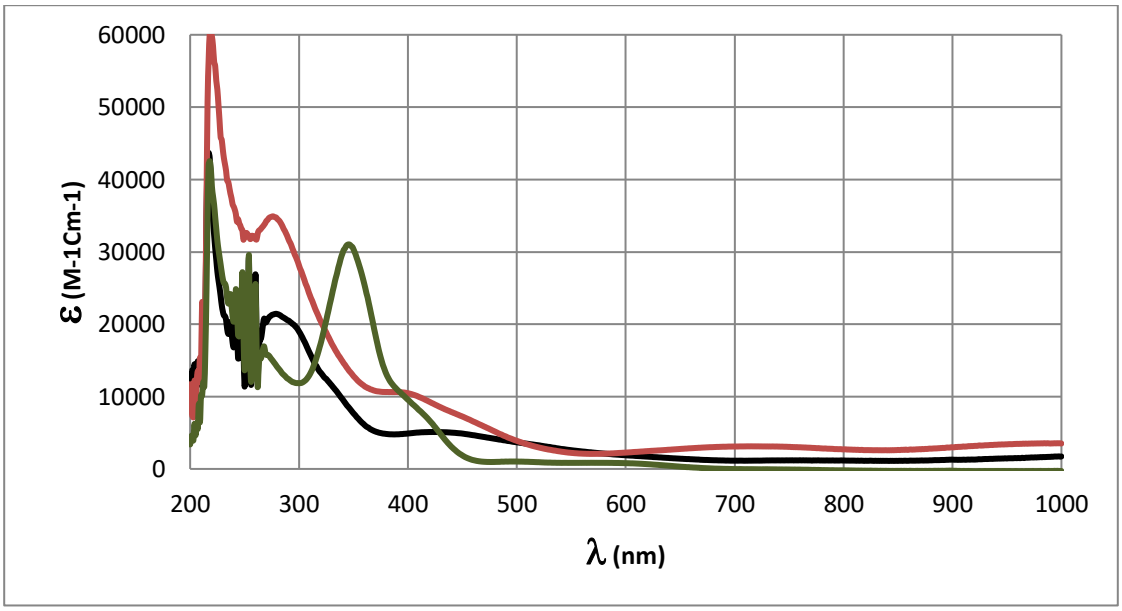

Figure 2.2. Electronic absorption spectra of **1**-THF (green), **2**=NAd (red), **2**=O (black) in C_6H_6.

*2.1.3. (dadi)Ti($CNMe)_2$ (**1**-$(CNMe)_2$)*

In contrast, exposure of **1**-THF to carbon monoxide (1 atm) did not result in displacement of THF by CO (Scheme 2.3), consistent with the presence of a d^0 Ti^{IV} center. A d^2 titanium center would likely provide a favorable backbonding situation to a carbonyl ligand, whereas a more electrophilic $[(dadi)^{4-}]Ti^{IV}$ configuration would favor σ-donors such as isocyanides and phosphines. Thus, THF was displaced from **1**-THF by treating

with MeNC, generating blood red (dadi)Ti(CNMe)$_2$ (**1**-(CNMe)$_2$) as the bis-methylisocyanide adduct (Scheme 2.3). Attempts to synthesize the 5-coordinate species using only 1 equiv MeNC were unsuccessful, resulting in a 1:1 mixture of **1**-(CNMe)$_2$ and **1**-THF. The IR spectrum of **1**-(CNMe)$_2$ has a broad absorption at 2199 cm^{-1} assigned to the isocyanide CN stretching mode. This is well above that of free MeNC (2164 cm^{-1}), consistent with a lack of π-backbonding, and indicative a d^0 Ti^{IV} center with a tetranionic ligand. As in the mono-adducts, **1**-(CNMe)$_2$ also exhibits a normal diimine proton chemical shift (δ 6.16) in the ^{1}H NMR spectrum, supplying additional evidence for the (dadi)$^{4-}$ formulation.

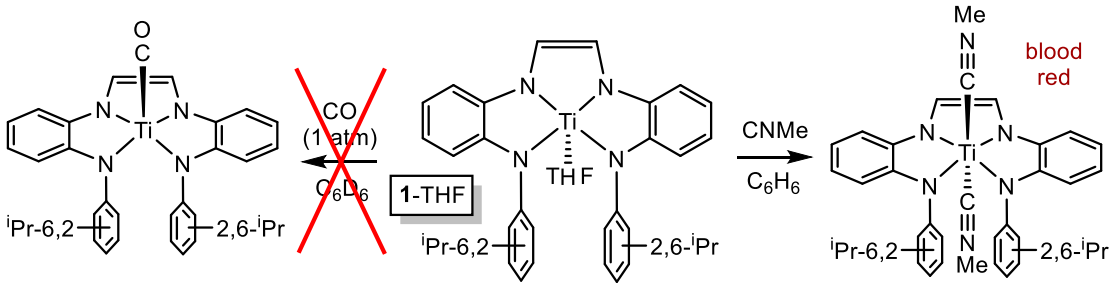

Scheme 2.3. Methylisocyanide binds to form **1**-(CNMe)$_2$, but CO does not bind.

2.2. Structural Studies of (dadi)TiL$_n$ (L = PMe$_2$Ph, L$_2$ = (CNMe)$_2$)

*2.2.1. (dadi)Ti(PMe$_2$Ph) (**1**-PMe$_2$Ph)*

Single crystals of **1**-PMe$_2$Ph, amendable for X-ray diffraction, were obtained by diffusion of hexanes vapor into a concentrated Et$_2$O solution. Figure 2.3 depicts the molecular structure of **1**-PMe$_2$Ph, revealing a pseudo-square pyramidal structure (τ_5 = 0.09).[26] The Ti-N distances of the ligand backbone are relatively short, at d(Ti-N2) = 2.0194(18) and d(Ti-N3) = 2.0332(18) Å. The titanium aryl amide-nitrogen bond length of 2.0029(18) and

2.0088)(18) Å are nearly identical to the “diimine” Ti-N distances, suggesting reduction of the diimine backbone to an ene-diamide. Furthermore, the tell-tale interatomic distances in the ligand backbone support the $[(dadi)^{4-}](PMe_2Ph)Ti^{IV}$ electronic configuration, with CN distances and a CC distance consistent with single and double bonds respectively (d(N2-C19) = 1.387(3), d(N3-C20) = 1.381(3), d(C19-C20) = 1.328(3) Å). Lastly, distortions around the Ti center from phosphine-isopropyl interactions are evident in the solid state structure.

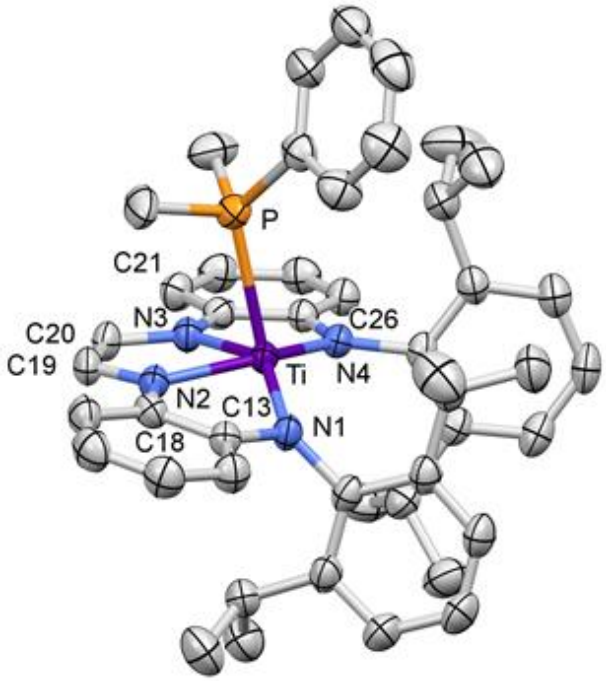

Figure 2.3. Molecular structure of (dadi)TiPMe$_2$Ph (**1**-PMe$_2$Ph). Interatomic distances (Å) and angles (°): Ti-P, 2.6049(7); Ti-N1, 2.0029(18); Ti-N2, 2.0194(18); Ti-N3, 2.0332(18); Ti-N4, 2.0088(18); N1-C13, 1.411(3); C13-C18, 1.413(3); N2-C18, 1.396(3); N2-C19, 1.379(3); C19-C20, 1.338(3); N3-C20, 1.381(3); N3-C21, 1.396(3); C21-C26, 1.408(3); N4-C26, 1.406(3); P-Ti-N1, 114.64(6); P-Ti-N2, 85.21(5); P-Ti-N3, 85.23(5); P-Ti-N4, 102.35(5); N1-Ti-N2, 78.10(7); N1-Ti-N3, 143.60(7); N1-Ti-N4, 123.37(7); N2-Ti-N3, 73.38(7); N2-Ti-N4, 148.83(7); N3-Ti-N4, 77.14(7).

The PMe$_2$Ph is tilted toward the ene-diamide (∠P-Ti-N$_{im}$ = 85.22(2)° (ave)) and the orientation of its phenyl group causes the P-Ti-N1 angle (114.64(6)°) to be greater than the other amide (∠P-Ti-N4 = 123.37(5)°).

*2.2.2. (dadi)Ti(*CNMe)$_2$ *(**1**-*(CNMe)$_2$)

Figure 2.4. illustrates the crystal structure of (dadi)Ti(CNMe)$_2$ (**1**-(CNMe)$_2$) with selected distances and angles. The ligand metric parameters are all within 0.015 Å of **1**-PMe$_2$Ph despite its pseudo-octahedral coordination environment. The interatomic distances in the backbone (d(C19-C20) = 1.350(3) Å, and d(CN$_{im}$) = 1.372(2) (ave)), are consistent with an ene-diamide

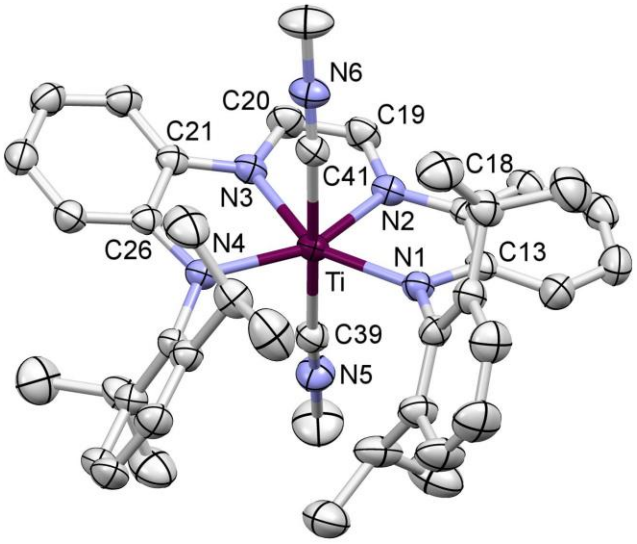

Figure 2.4. Molecular structure of (dadi)Ti(CNMe)$_2$ (**1**-(CNMe)$_2$). Interatomic distances (Å) and angles (°): Ti-N1, 2.0677(16); Ti-N2, 2.0331(15); Ti-N3, 2.0353(16); Ti-N4, 2.0636(15); Ti-C39, 2.2484(18); Ti-C41, 2.2364(18); N1-C13, 1.396(2); C13-C18, 1.418(3); N2-C18, 1.403(2); N2-C19, 1.373(2); C19-C20, 1.350(3); N3-C20, 1.371(2); N3-C21, 1.401(2); C21-C26, 1.423(2); N4-C26, 1.395(2); C39-N5, 1.141(2); C41-N6, 1.145(2); N1-Ti-N2, 77.04(6); N1-Ti-N3, 149.95(6); N1-Ti-N4, 132.75(6); N2-Ti-N3, 73.96(6); N2-Ti-N4, 150.05(6); N3-Ti-N4, 76.83(6); N1-Ti-C39, 91.41(6); N2-Ti-C39, 84.33(6); N3-Ti-C39, 93.42(6); N4-Ti-C39, 90.98(6); N1-Ti-C41, 91.37(6); N2-Ti-C41, 92.30(6); N3-Ti-C41, 82.13(6); N4-Ti-C41, 90.14(6); C39-Ti-C41, 175.04(7).

(dadi)$^{4-}$ chelated to a Ti^{IV} center, as predicted by its IR spectrum. The four nitrogen donors are best described as amides, evidenced by Ti-N distances that are within 0.035 Å of each other at 2.050(18) Å (ave), which are slightly longer than in **1**-PMe$_2$Ph (d(Ti-N) = 2.016(13) Å (ave)). The bite angles around

the metal center are 76.94(15)° (ave) and 73.96(6)° (∠N(1/3)-Ti-N(2/4) and ∠N(2)-Ti-N(3) respectively), which are nearly identical to the phosphine adduct. The steric interaction between the axial ligand and the isopropyl groups is relieved by the smaller isocyanides, and compared to **1**-PMe_2Ph, the titanium is almost coplanar with the four nitrogen donors. As a result, the two arylamide-nitrogens are forced open to an angle of 132.75(6)° (∠N1-Ti-N4 = 123.37(7)° for **1**-PMe_2Ph).

2.3. Electronic structure of (dadi)Ti(PMe_2Ph)

The ligand metrics found in (dadi)Ti(PMe_2Ph) (**1**-PMe_2Ph) prompted an investigation into its electronic structure to assess the proposed RNI. The truncated molecular orbital diagram for **1**-PMe_2Ph is shown in Figure 2.5 featuring three filled orbitals. The HOMO is comprised of the ene-diamide π-bonding orbital in the dadi backbone, which acts as the "electron reservoir" for the 2-electrons originating from the Ti(II) starting material. The unoccupied orbitals, representing the *3*d-manifold, are tightly packed and separated from the HOMO by ~3 eV, partly as a consequence of DFT calculations.[27] In line with the $(dadi)^{4-}$ formulation, the d_{xz} and d_{yz}, which possess modest π-character, are empty.

Intrinsic to low symmetry environments, σ- and π-components are highly mixed across the system. In combination with the RNI of the ligand (*i.e.* roughly degenerate ligand- and *3*d-orbitals), the unoccupied molecular orbitals that contain 3d-character (but not purely *3*d), are essentially non-bonding. Furthermore, all of the filled molecular orbitals shown in Figure 2.5 possess some *3*d-character, this metal-dadi admixture reflects the covalency of the (dadi)Ti(L) systems.

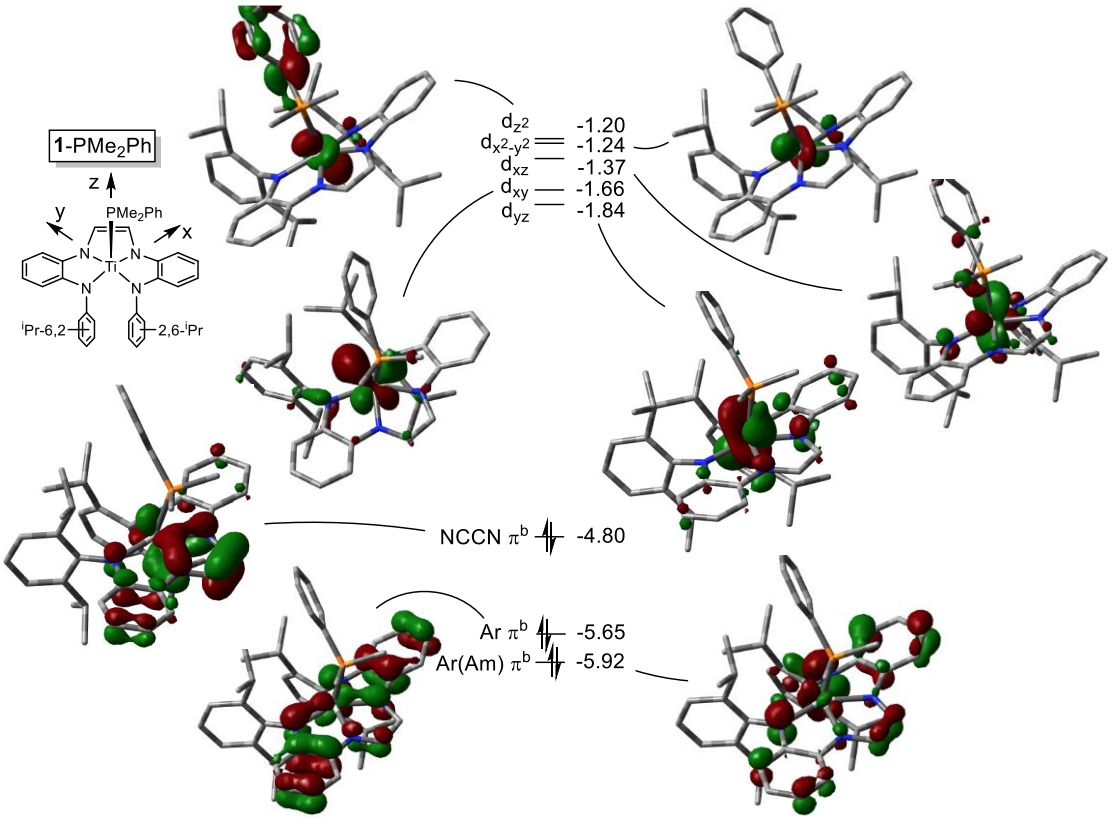

Figure 2.5. Truncated MO diagram of (dadi)TiPMe$_2$Ph (**1**-PMe$_2$Ph), showing the unfilled orbitals of the d^0 species, and three filled dadi-based orbitals (energies in eV). Assignments are tentative due to the low symmetry: M06/6-311+G(d) single point calculations for orbitals at the ONIOM(M06/6-311+G(d)) optimized minimum derived from the X-ray structure as an initial guess.

2.4. Synthesis of (dadi)Ti=X (X = NAd, O)

*2.4.1. (dadi)Ti=NAd (**2**=NAd)*

The use of organoazides was pursued as a route to access imido derivatives. Treating **1**-THF with 2,6-^{i}Pr-C$_6$H$_3$N$_3$ resulted in a complex product devoid of symmetry. Attempts to elucidate the structure *via* 2D-NMR spectroscopy suggested a reaction with at least one isopropyl group, although significant ambiguity in the molecular structure remains. Unfortunately, attempts to grow single crystals for X-ray diffraction experiments were unsuccessful and the structure of the product is still unknown. In contrast, NMR tube experiments using TMSN$_3$ lead to a single major product with

spectroscopic signals consistent with a 5-coordinate, (dadi)Ti=NSiMe$_3$ complex but was never isolated or fully characterized.

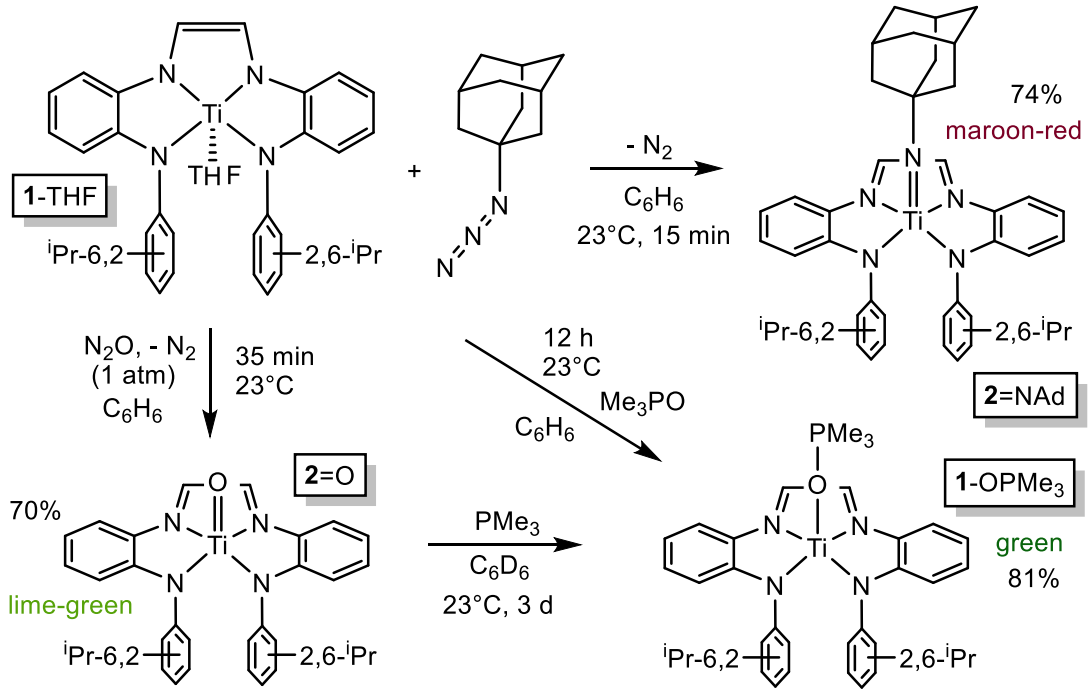

Scheme 2.4. Imide, (dadi)Ti=NAd (**2**=NAd), and oxo, (dadi)Ti=O (**2**=O), formation from (dadi)Ti(THF) (1-THF), AdN$_3$ and N$_2$O, respectively.

Treatment of **1**-THF with AdN$_3$ (Ad = adamantyl) in C$_6$H$_6$ led to immediate effervescence and a green to red color change. Maroon-red (dadi)Ti=NAd (**2**=NAd) was isolated in 74% yield after thorough removal of benzene by triturating with hexanes (Scheme 2.4). The ^{1}H NMR spectrum of **2**=NAd displays three isopropyl-methyl doublets in an integrated 6:12:6 ratio, indicating a five-coordinate imide complex.

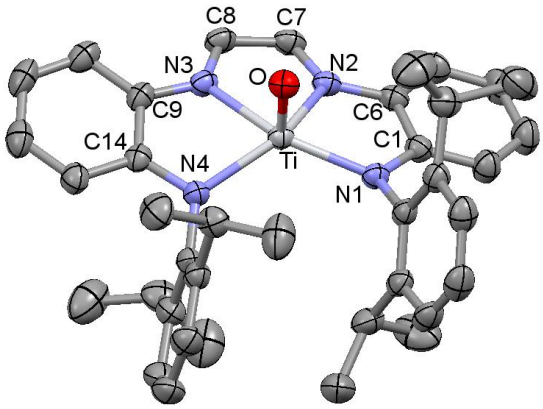

Figure 2.6. Molecular view of (dadi)TiO (**2**=O). Interatomic distances (Å) and angles (°): Ti-O, 1.6361(11); Ti-N1, 2.0538(13); Ti-N2, 2.1938(12); Ti-N3, 2.1603(13); Ti-N4, 2.0640(12); N1-C1, 1.3770(19); C1-C6, 1.419(2); N2-C6, 1.395(2); N2-C7, 1.301(2); C7-C8, 1.433(2); N3-C8, 1.297(2); N3-C9, 1.388(2); C9-C14, 1.418(2); N4-C14, 1.3750(19); O-Ti-N1, 105.18(5); O-Ti-N2, 104.88(5); O-Ti-N3, 94.71(5); O-Ti-N4, 105.66(5); N1-Ti-N2, 75.40(5); N1-Ti-N3, 144.73(5); N1-Ti-N4, 124.02(5); N2-Ti-N3, 71.44(5); N2-Ti-N4, 136.56(5); N3-Ti-N4, 75.94(5).

*2.4.2. (dadi)Ti=O (**2**=O)*

Generation of the corresponding oxo complex proved to be equally fruitful. Initial attempts using common oxygen atom transfer (OAT) reagents, such as PhIO, DMSO, Me_3N-O, PyN-O, *p*-^{t}Bu-PyN-O failed to cleanly generate the titanium-oxo. ^{1}H NMR spectroscopic analysis of the crude reaction mixture obtained from treating a benzene solution of (dadi)Ti(THF) (**1**-THF) with 1 equiv N_2O at 23 ^{o}C for 8 hours indicated the presence of a 5-coordinate complex, albeit in less than 10% yield. After optimization, **2**=O was isolated in 70% yield by exposing **1**-THF to N_2O (1 atm), in benzene for 30-35 min. Concentration of the reaction mixture followed by filtration of the product afforded the titanium-oxo as a lime-green microcrystalline solid (Scheme 2.4). Four sets of isopropyl-methyl doublets in a 6:6:6:6 ratio were observed in the ^{1}H NMR spectrum, and a resonance-enhanced Raman (λ = 475 nm) spectrum showed an absorption at 1015.4 cm^{-1}, tentatively assigned to the ν(Ti=O) stretch.

2.5. Structural studies of (dadi)Ti=X (X = NAd, O)

*2.5.1. (dadi)Ti=O (**2**=O)*

The molecular structure of (dadi)Ti=O (**2**=O) with selected interatomic distances and angles, is given in Figure 2.6, which reveals an oxidized dadi ligand. Relative to **1**-PMe_2Ph, the dadi backbone contains a shortened CN_{imine} distance of 1.299(3) Å (ave) and an elongated CC distance of 1.433(3) Å, consistent with a neutral diimine fragment of a $(dadi)^{2-}$ ligand. Furthermore, the titanium-nitrogen bond lengths to the diimines are 2.1603(13) and 2.1938(12) Å, substantially longer than the electrostatically contracted d(TiN) distances of **1**-PMe_2Ph and **1**-$(CNMe)_2$. The titanium-arylamide distances of 2.059(7) Å (ave) are consistent with anionic nitrogen donors. The oxo tilts slightly towards N3 (∠O-Ti-N3 = 94.71(5)°), and the other core O-Ti-N angles average 105.2(4)°. The titanium center sits out of the basal plane by ~0.491 Å, allowing a contraction of the N1-Ti-N4 angle to 124.02(5)°. Additionally, the diimine bite angle of 71.44(5)° and imine-arylamide bite angles of 75.7(4)° (ave) describe the slightly distorted square-pyramid (τ_5 = 0.13),[26] with basal nitrogens and an apical oxo. Lastly, the d(TiO) distance of 1.6361(11) Å is typical for 5-coordinate Ti^{IV} oxo species (1.63(1) Å ave for 15 examples).[19]

*2.5.1. (dadi)Ti=NAd (**2**=NAd)*

Attempts to isolate single crystals of **2**=NAd were challenging, and fraught with twinning issues. Eventually, single crystals were obtained from a benzene solution layered with TMS_2O after 2 months. These crystals yielded a data set that was also twinned, but could be refined to the extent that the imide structure, suggested by NMR spectroscopic analysis, could be confirmed. Figure 2.7 illustrates the molecular structure of **2**=NAd, from one of the

molecules in the asymmetric unit, revealing a pseudo square-pyramidal titanium center (τ_5 = 0.13).[26] The d(Ti=N) is 1.705(5) Å (ave), a typical value for Ti^{IV} imides.[28–34] The elongated diimine-titanium distances of 2.183(17) Å (ave) versus the titanium-arylamide Ti-N bond lengths of 2.100(2) Å (ave) are

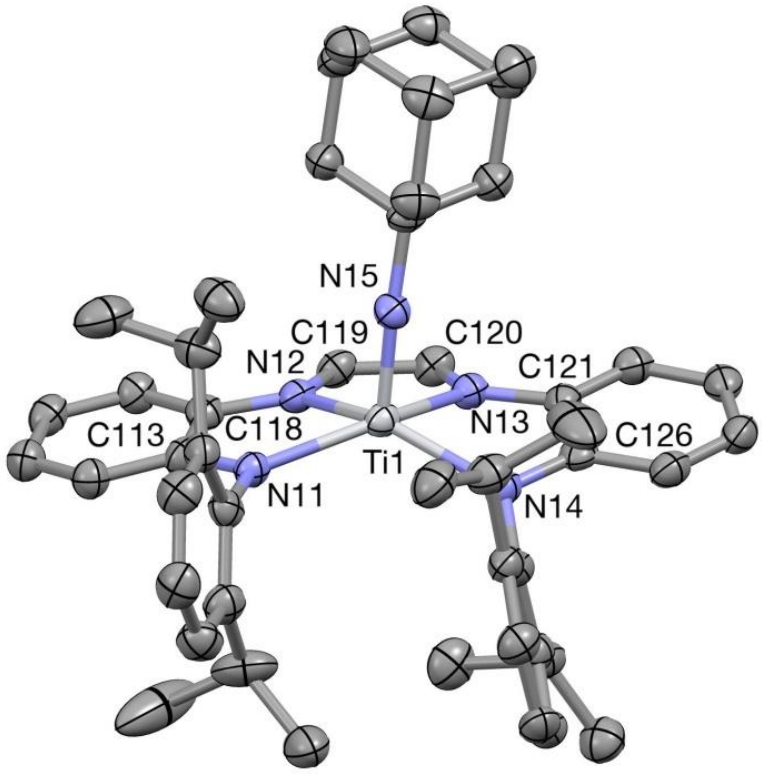

Figure 2.7. A view of one of two (dadi)Ti=NAd (**2**=NAd) molecules in the asymmetric unit. (°) are: N=Ti-N(11,21), 108.4(2), 108.1(2); N=Ti-N(14,24), 108.8(2), 108.7(2); N=Ti-N(12,22), 99.2(2), 91.7(2); N=Ti-N(13,23), 91.1(2), 100.0(3); N(11,21)-Ti-N(12,22), 75.52(18), 74.75(18); N(11,21)-Ti-N(13,23), 143.51(19), 136.08(19); N(11,21)-Ti-N(14,24), 123.73(19), 123.76(19); N(12,22)-Ti-N(13,23), 71.01(18), 71.37(19); N(12,22)-Ti-N(14,24), 135.79(19), 143.18(19); N(13,23)-Ti-N(14,24), 74.85(19), 74.99(19).

consistent with a dianionic $(dadi)^{2-}$ chelate. More importantly, the metrics of the dadi backbone ($d(CN_{imine})$ = 1.300(6) Å (ave), d(CC) = 1.437(3) Å (ave)) indicate 2-electron oxidation from the ene-diamide in **1**-THF to the diimine form of the $(dadi)^{2-}$ ligand.

2.6. Electronic structure of (dadi)Ti=O (2=O)

The electronic structure of (dadi)Ti=O (**2**=O) was investigated *via* DFT calculations since its experimental structure, with a quality data set, was available for comparison. A truncated molecular orbital diagram for **2**=O is featured in Figure 2.8, illustrating TiO π-bonding orbitals below a group of occupied dadi π-orbitals. The HOMO contains significant Npπ– and phenylene-character, but no metal constituent. The occupied ligand based orbitals possess some components of the NCCN bonding, but there are no discrete diimine orbitals. A pair of unoccupied orbitals, including the LUMO, can be distinguished as NCCN π* in character. This is consistent with a titanyl center and a delocalized $(dadi)^{2-}$ chelate. As a minor point, the distortion in **2**=O is reproduced by calculations and appears to be steric in origin, as removal of 2,6,-^{i}Pr-C_6H_3 groups results in a more symmetric species.

The molecular orbital diagram of **2**=O contains similarities to that of **1**-PMe_2Ph (Figure 2.5), mainly well-separated metal and ligand antibonding orbitals, a lower energy NCCN π* orbital, and dadi π-bonding orbitals. Both diagrams depict Ti^{IV} metal centers, but the middle π*-orbital for **2**=O is unoccupied, revealing disparate redox states for **1**-PMe_2Ph and **2**=O, as well as highlighting the RNI of the ligand. In the $(dadi)^{4-}$ state, the middle NCCN π-type orbital is well placed energetically, as it acts as an electron reservoir for oxidative chemistry to the formally d^0 Ti^{IV} center.

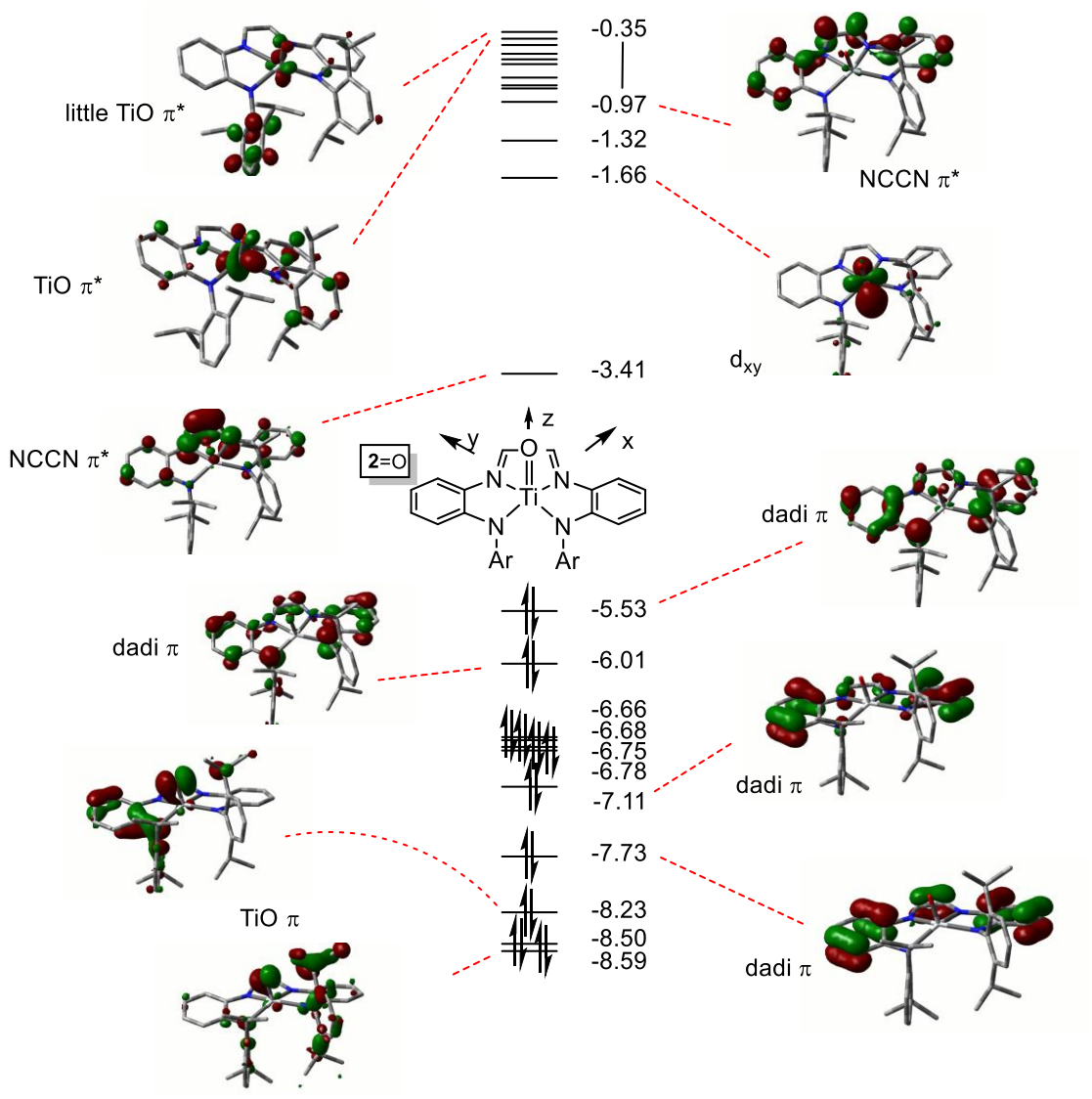

Figure 2.8. Truncated molecular orbital diagram of (dadi)TiO (**2**=O); orbitals not plotted are either diffuse virtual orbitals or pertain to 2,6-$^{i}Pr_2C_6H_3$. Energies are in eV.

2.7. Carbonylation of adamantyl azide

2.7.1. Catalytic carbonylation

Treatment of **2**=NAd with CO (1 atm) in the presence of THF generated adamantylisocyanate (AdNCO) and **1**-THF. Due to the failure of CO to compete with THF in binding to titanium, an implicit consequence of the (dadi)^{n}

RNI, it was envisioned that catalytic carbonylation without catalyst deactivation *via* CO coordination would be possible. It was found that the titanium-imido complex (**2**=NAd) does indeed catalytically carbonylate the nitrene derived from AdN_3 with a turnover number (TON) of ~20. A plausible mechanism for carbonylation of the nitrene is depicted in Scheme 2.5. Insertion of the

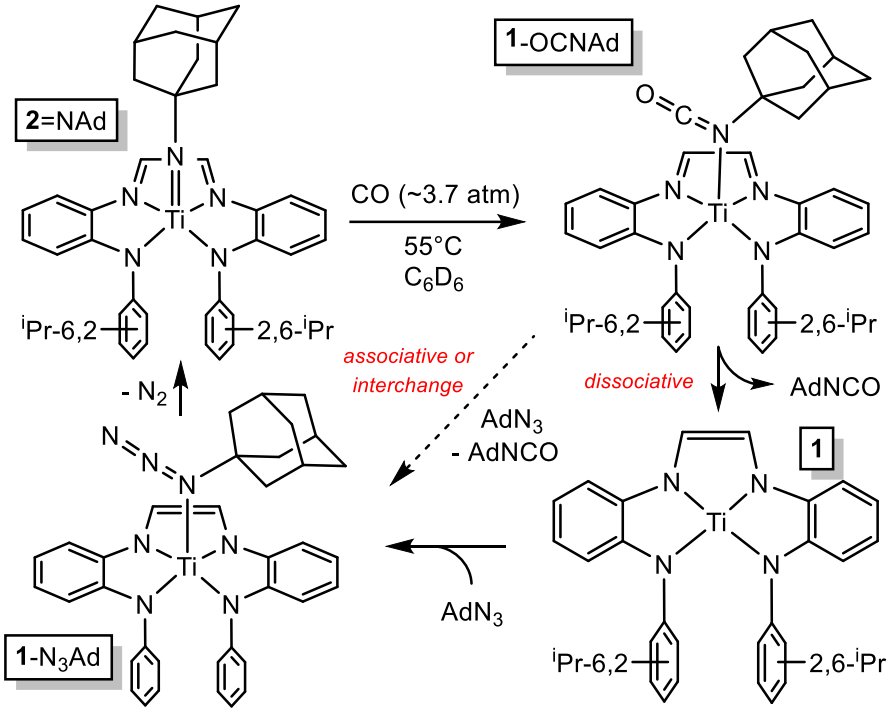

Scheme 2.5. Plausible mechanisms for the catalyzed conversion of AdN_3 + CO -> AdNCO + N_2 by the imide, (dadi)Ti=NAd (**2**=NAd).

carbonyl into the Ti-imide bond, conceivably *via* initial *cis*-binding of CO, forms an isocyanate adduct (**1**-OCNAd). Subsequent substitution by adamantylazide, either through an associative, interchange, or dissociative process releases product (AdNCO) to form a transient azide adduct (**1**-N_3Ad). Release of dinitrogen closes the catalytic cycle, regenerating **2**=NAd.

2.7.2. *Kinetic analysis of catalytic carbonylation*

P (atm)	T (K)	$\chi_g * 10^4$ (at 1 atm)	[CO] $*10^2$ (at P)
3.10	298.0(5)	6.59	2.31
3.21	308.0(5)	6.87	2.49
3.27	318.0(5)	7.12	2.63
3.34	328.0(5)	7.39	2.79
3.49	338.0(5)	7.73	3.05
3.60	348.0(5)	8.08	3.29

Table 2.1. Mole fraction solubility's (χ_g) of CO in benzene at 1 atm and specified temperature extrapolated from reference 36. Calculated [CO] (M) at the specified temperature and pressure.

Once the viability of carbonylation had been established, attention was turned to measuring the reaction kinetics under catalytic conditions. Two challenges, one chemical and one experimental in nature, were encountered when attempting to gather reliable rate data for the catalytic carbonylation of **2**=NAd. The first being catalyst decomposition, was handled by fitting the rate data, and will be discussed in detail in the next section. The second, experimental challenge, was ensuring that that diffusion of CO into solution was occurring at a faster rate than carbonylation. In this laboratory, a maximum limit of 5 atm CO can be charged into an NMR tube. Fortunately, it was found that by maximizing the surface area of solution exposed to CO gas, simply by maintaining the NMR tube in a horizontal position, CO gas was replenished fast enough to keep up with catalysis. This effectively produces a steady state concentration of CO, thus carbon monoxide concentrations can be calculated from Henry's Law[35] using the temperature dependent mole fraction solubility's (χ_g) extrapolated from reference 37. Table 1 lists χ_g values

with calculated CO concentrations under experimentally relevant conditions (a sample calculation for [CO] is detailed in the Experimental section).

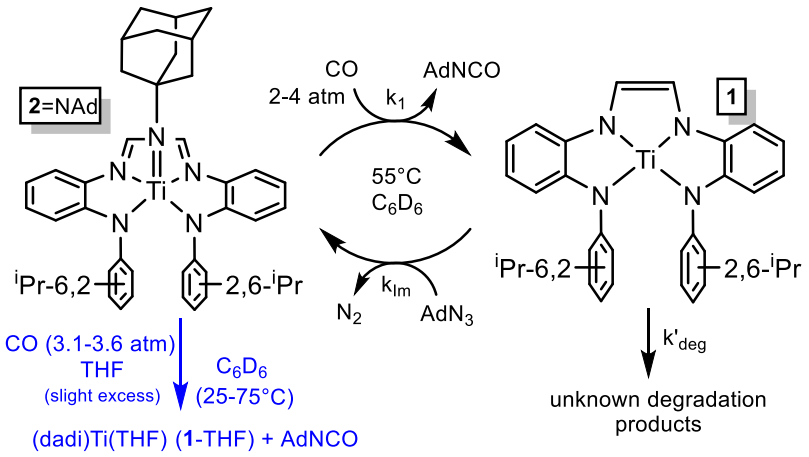

Scheme 2.6. Kinetic model for AdN_3 carbonylation catalysis by **2**=NAd (black) and stoichiometric study of imide carbonylation (blue).

$$\frac{d[\mathbf{2}\text{=NAd}]}{dt} = -k_1[\mathbf{2}\text{=NAd}] + k_{im}[AdN_3][\mathbf{1}] \qquad \text{(eq 1)}$$

$$\frac{d[\mathbf{1}]}{dt} = k_1[\mathbf{2}\text{=NAd}] - k'_{deg} - k_{im}[\mathbf{1}][AdN_3] \qquad \text{(eq 2)}$$

$$\frac{d[AdN_3]}{dt} = -k_{im}[\mathbf{1}][AdN_3] \qquad \text{(eq 3)}$$

Where:

$k_1 = k_{co}[CO]$

$k_{im} = 1000\ M^{-1}s^{-1}$

$k'_{deg} = k_{deg}[\mathbf{1}]$

Entry	**2**=NAd (M)	CO (M)[a]	T (°C)	k_{CO} x 10^3 ($M^{-1}s^{-1}$)	$\Delta G^{\ddagger}$ (kcal/mol)
1	0.047[b]	0.023	25.0(5)	1.25(6)	21.4(1)
2	0.048[b]	0.025	35.0(5)	1.83(8)	21.9(1)
3	0.047[b]	0.026	45.0(5)	3.58(15)	22.2(1)
4	0.047[b,c]	0.028	55.0(5)	5.44(42)	22.7(1)
5	0.047[b]	0.03	65.0(5)	7.95(86)	23.1(1)
6	0.047[b]	0.033	75.0(5)	14.0(11)	23.4(1)
7	0.047[c]	0.0105	55.0(5)	4.62(69)	22.8(1)
8	0.046[c]	0.023	55.0(5)	4.20(45)	22.8(1)
9	0.0063[d]	0.022	55.0(5)	3.13(24)	23.0(1)

Table 2.2. Kinetics of **2**=NAd carbonylation, stoichiometric and catalytic, in C_6D_6. [a]Calculated from Henry's Law and corrected for temperature dependence. [b]Rate constants obtained from an average of three trials; from a weighted Eyring plot: $\Delta H^{\ddagger}$ = 9.6(9) kcal/mol, $\Delta S^{\ddagger}$ = -39.9(28) eu, $\Delta G^{\ddagger}$(55°C) = 22.6(9) kcal/mol. An unweighted Eyring plot gives: $\Delta H^{\ddagger}$ = 9.3(4) kcal/mol, $\Delta S^{\ddagger}$ = -40.7(13) eu, $\Delta G^{\ddagger}$(55°C) = 22.6(6) kcal/mol. [c]To determine order in CO; k_{obs} = 4.85(55) x 10^{-5} s^{-1} at [CO] = 0.0105 M; k_{obs} = 9.67(95) x 10^{-5} s^{-1} at [CO] = 0.023 M; k_{obs} = 1.52(8) x 10^{-4} s^{-1} at [CO] = 0.028 M. [d]Catalytic rate obtained from fitting disappearance of [AdN_3] and [**2**=NAd] according to Scheme 5 (3 trials): p(CO) = 2.58 atm, total mol CO = 1.82 x 10^{-4}, [AdN_3] = 0.123 M, k_{deg} = 3.2(3) x 10^{-5} Ms^{-1}. See experimental section for details.

During catalysis, imide (dadi)Ti=NAd (**2**=NAd) is the only metal-containing species observed by ^{1}H NMR spectroscopy. As previously mentioned, the concentration of **2**=NAd diminishes over time, and the catalysis was modeled as a two-step process, with a degradation pathway to account for the loss of **2**=NAd (Scheme 2.6, black). In Figure 2.9 are two concentration versus time plots for [AdN_3] and [**2**=NAd], measured by ^{1}H NMR spectroscopy during catalytic carbonylation experiments. These data are representative of three independent trials, the latter of which are included in the experimental section. The use of eqs 1-3 resulted in satisfactory fits for the data collected under catalytic conditions. Based upon experimental observations, the formation of **2**=NAd from **1**-THF and AdN_3 is fast ($t_{1/2}$ ~ seconds) relative to carbonylation, therefore k_{im} was fixed at large, but arbitrary value of 1000 $M^{-1}s^{-1}$ for the data fitting. The concentration of CO in solution is ~3.5 times that of **2**=NAd, but the atmosphere holds ~60 fold

excess thereby replenishing CO from the gas phase rendering CO a pseudo-first order reagent. The phenomenological rate ($-d[AdN_3]/dt = k_{obs}$; $k_{obs} = k_{co}$[**2**=NAd][CO]) is zeroth-order because catalyst concentration does not change aside from decomposition. Thus, factoring out [CO] and [**2**=NAd] gives a second-order rate constant of 3.13(24) x 10^{-3} $M^{-1}s^{-1}$, translating to a free energy of activation of $\Delta G^{\ddagger}$(55°C) = 23.0(1) kcal/mol (Table 2.2, entry 9).

$$\frac{d[\mathbf{1}]}{dt} = k_1[\mathbf{2}\text{=NAd}] - k_{deg}[\mathbf{1}] - k_{im}[\mathbf{1}][AdN_3] = 0 \qquad \text{(eq 4)}$$

Rearrangement of eq 4 gives eq 5:

$$[\mathbf{1}] = \left(\frac{k_1[\mathbf{2}\text{=NAd}]}{(k_{im}[AdN_3] + k_{deg})} \right) \qquad \text{(eq 5)}$$

Substitution of [**1**] into eq 1 gives eq 6:

$$\frac{d[\mathbf{2}\text{=NAd}]}{dt} = -k_1[\mathbf{2}\text{=NAd}] + k_{im}[AdN_3] \times \left(\frac{k_1[\mathbf{2}\text{=NAd}]}{(k_{im}[AdN_3] + k_{deg})} \right) \qquad \text{(eq 6)}$$

As previously discussed, time dependent concentration plots obtained using ^{1}H NMR spectroscopy for catalytic runs were fitted to a set of differential equations (eqs 1,2,3) describing the mechanistic model shown in Scheme 2.6 (black). The resting state of the catalyst is **2**=NAd, and it was empirically determined that the rate of decomposition had an *apparent* zero-order dependence on titanium (either in the form of **2**=NAd or the putative species **1**). To understand this counterintuitive result, a closer look at the differential equations used to describe the process of degradation is required.

Decomposition is post-rate limiting and under non-equilibrium conditions, hence the steady-state approximation can be used to describe the concentration of (dadi)Ti (**1**), as shown in eq 4. Note that the degradation of

catalyst should have a dependence on the concentration of **1**, hence the phenomenological rate constant ($k`_{deg}$) contains the term [**1**]. Solving for [**1**] and substituting into eq 1 gives an expression that describes the loss of catalyst (**2**=NAd) over time (eq 6) that contains a first order dependence on [**1**]. Thus, the relevant expressions describing the concentrations of AdN_3, intermediate **1**, and **2**=NAd are eq's 3, 4, and 6, respectively.

Modeling of time dependent concentration plots using eqs 3,4, and 6 are in agreement with the experimental data, as shown in Figure 2.10. The linear decrease in catalyst concentration shown in Figure 2.10.b is replicated with this model. Moreover the curvature in the adamantyl azide concentration versus time (Figure 2.10.a), due to catalyst degradation, is also well modeled.

On possible explanation for the apparent zeroth order degradation of catalyst comes when the concentrations of [**2**=NAd] and [AdN_3] *decrease at the same rate*. In this situation, the ratio [**2**=NAd]/[AdN_3] becomes constant, and [**1**] becomes a product of terms that are also constant (*i.e.*, k_{co}, k_{im}, [CO]). This situation would result in a degradation rate constant ($k`_{deg}$), with an *apparent* zeroth-order dependence on titanium, as described in eq 2. It should be noted that the zeroth- and first-order degradation processes cannot be

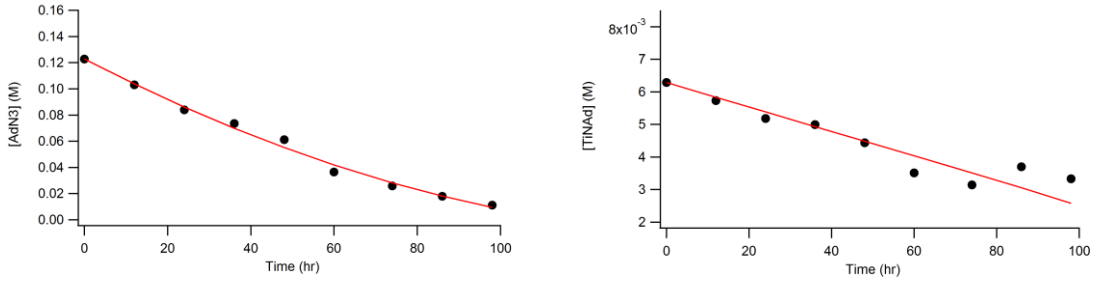

Figure 2.9. Experimentally measured concentrations (black dots) and fitted data (red line) for catalytic carbonylation. Plots of [AdN_3] vs time (left) and [Ti(dadi)NAd] vs time (right). P_{CO} = 2.58 atm, [CO] = 0.022 M, [Ti(dadi)NAd]$_o$ = 0.0063 M, [AdN_3]$_o$ = 0.12 M, T = 298 K.

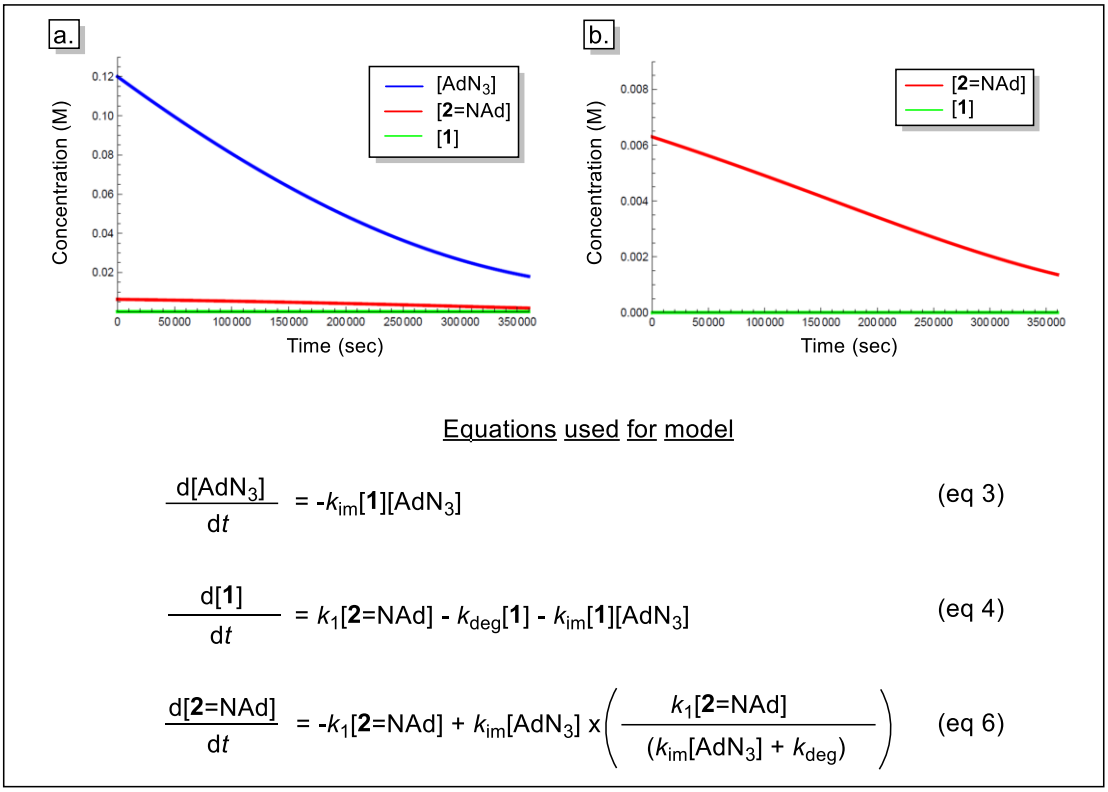

Figure 2.10. Model of time dependent concentrations for catalytic carbonylation. (a) Non-linear decrease in [AdN_3] due to catalyst degradation. (b) Apparent zeroth order, linear decrease in [**2**=NAd] matching experimentally observed data.

distinguished, however, the more critical k_{co} values obtained during catalysis are still taken to accurately represent the carbonylation the **2**=NAd as they are consistent with calculations and stoichiometric carbonylation experiments (*vide infra*).

2.7.3. *Kinetic and Eyring analyses of stoichiometric carbonylation*

A stoichiometric study supported carbonylation as the rate-determining elementary step during catalysis, as shown in Scheme 2.5. Treatment of **2**=NAd with an excess of CO (3.1-3.6 atm) in the presence of 1 equiv THF, at temperatures ranging from 25-70 ^{o}C, gave AdNCO, and **1**-THF (Table 2.2, entries 1-6). Additionally, a first-order dependence on [CO] was established (Table 2.2, entries 4,7,8; -d[**2**=NAd]/dt = k_{co}[**2**=NAd][CO]).

Activation parameters for the carbonylation of **2**=NAd were obtained through an Eyring analysis of the second-order rate constants (Table 2.2, entries 1-6, Figure 2.11). The calculated $\Delta G^{\ddagger}$ at 55 °C of 22.6(9) kcal/mol is consistent with that obtained during catalysis, lending credence to the claim of carbonylation as the rate determining step. The enthalpy of activation of $\Delta H^{\ddagger}$ = 9.6(9) kcal/mol, is a modest value that reflects the balance between C=N bond-formation and Ti=N bond-breaking that occurs in the transition state. The large and negative entropy of activation ($\Delta S^{\ddagger}$ = -39.8(28) eu) is consistent with a second order process, providing further evidence for carbonylation as the rate determining step.

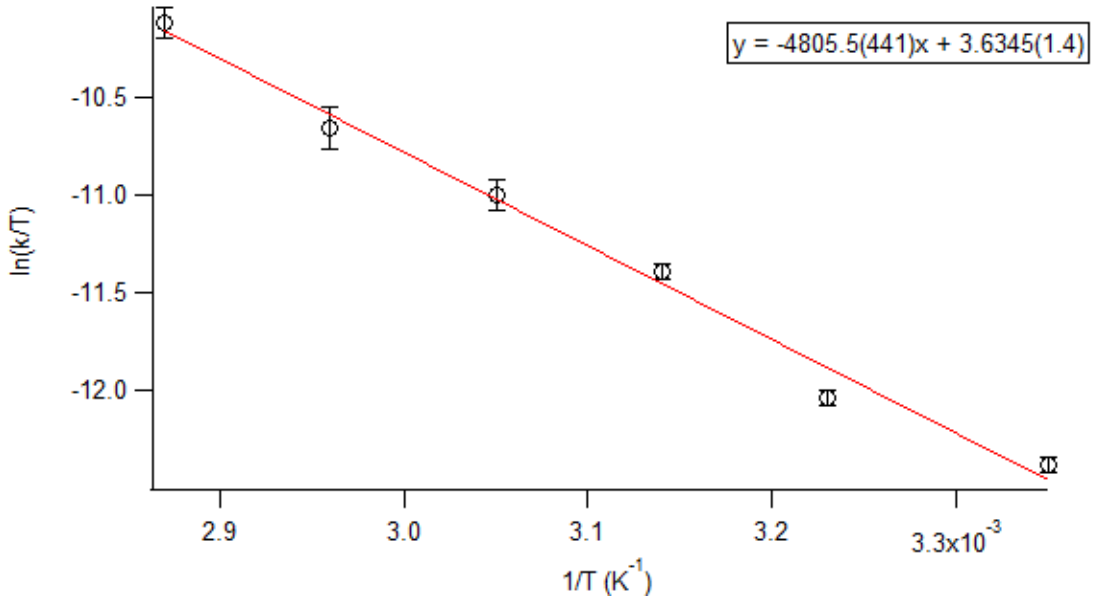

Figure 2.11. Eyring plot for carbonylation. Experimentally determined rate constants (black circles) and linear regression weighted by standard deviation of each data point (red line).

2.8. Calculated carbonylation mechanism

2.8.1. *Free energy profile of AdN_3 carbonylation*

Figure 2.10 depicts the calculated free energy profile for the carbonylation of AdN_3 to AdNCO + N_2, catalyzed by **2**=NAd. The overall reaction is exergonic by -72.9 kcal/mol. In terms of free energy, carbon nitrogen double-bond formation represents the driving force for catalysis, whereby formation of the C=N bond in AdNCO is enthalpically favored by -72.2 kcal/mol over the corresponding azide N=N bond. A calculated $\Delta G^{\ddagger}_{calc}$ = 20.9 kcal/mol (298.15 K) is found to agree fairly well with experiment ($\Delta G^{\ddagger}_{exp}$ = 21.5 kcal/mol at 298.15 K). The minor discrepancy is distributed between the two enthalpic and entropic terms ($\Delta H^{\ddagger}_{calc}$ = 8.0 kcal/mol, $\Delta S^{\ddagger}_{calc}$ = -43.3 eu),

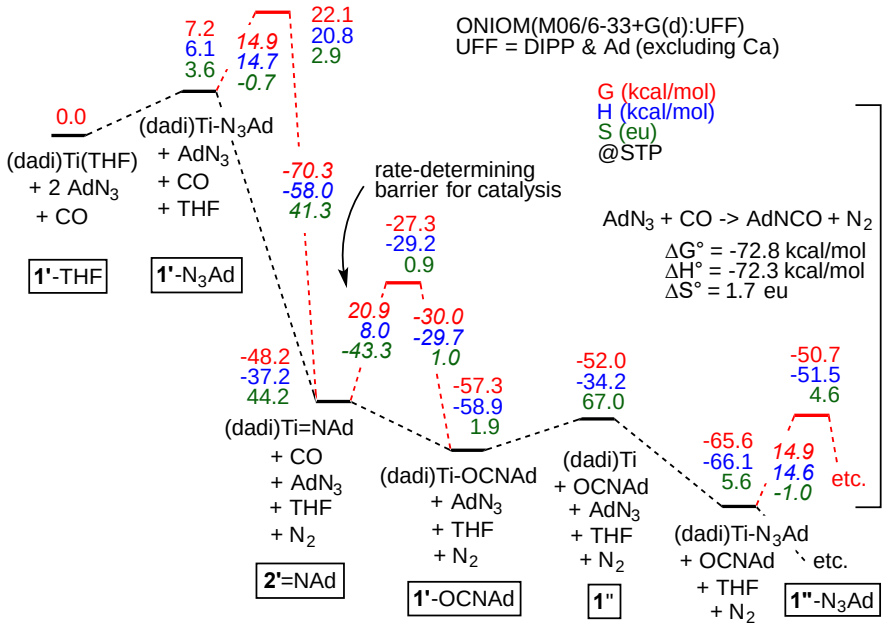

Figure 2.12. Calculations are of Scheme 2.5, with transition states (primes indicate calculated states; activation energies *italicized*) pertaining to N_2 loss from bound azide, (dadi)Ti(N_3Ad) (1-N_3Ad) and carbonylation of (dadi)Ti=NAd (2=NAd). Association/dissociation transition states are not included. Small inconsistencies are due to round-off errors. Calculated **1**'-L and **1**"-L compounds have $(dadi)^{4-}$ configurations, **2**'=NAd has a $(dadi)^{2-}$ structure, and **1**" is computed as $[(dadi)^{3-\downarrow}]Ti(III)^{\uparrow}$.

with the calculated entropy of activation being similar to that for the microscopic reverse of N_2 extrusion from (dadi)Ti(N_3Ad) (**1**-N_3Ad) ($\Delta S^{\ddagger}_{calc}$ = -42.3 eu).

The reaction of **2**=NAd and CO to form (dadi)Ti (**1**) and AdNCO is slightly favorable by ΔG_{calc} = -3.8 kcal/mol, and unfavorable enthalpically by ΔH_{calc} = 3.0 kcal/mol. With a calculated bond dissociation enthalpy (BDE_{calc}) for AdN=CO of only 81 kcal/mol, and a titanium–imide bond estimated to be (BDE_{calc}) ~ 84 kcal/mol, carbonylation has modest thermodynamic impetus.

Formation of **1**-N_3Ad from binding of AdN_3 to (dadi)Ti is favored by -13.6 kcal/mol. This leads to the next highest transition state, occurring during the loss of N_2 from **1**-N_3Ad, at $\Delta G^{\ddagger}_{calc}$ = 14.9 kcal/mol. Significant thermodynamic influence is imparted by the loss of N_2 to form **2**=NAd, which is favorable by -55.4 kcal/mol. It is worth noting that associative or interchange transition states could not be located for AdN_3 displacement of isocyanate from **1**-OCNAd.

OAT from the isocyanate produced during catalysis, to afford **2**=O and AdNC, is calculated to be slightly favorable ($\Delta G°_{calc}$ = -1.1 kcal/mol). The released isocyanide (AdNC) would be expected to scavenge any (dad)Ti (**1**) to generate (dadi)Ti(CNAd) ($\Delta G°_{calc}$ = -22.1 kcal/mol). (dadi)Ti=O (**2**=O) is not observed during the carbonylation of **2**=NAd, likely due to a barrier of OAT that is high compared to dinitrogen loss from (dadi)Ti-N_3Ad (**1**-N_3Ad) to (dadi)Ti=NAd (**2**=NAd), which is exergonic by $\Delta G°_{calcd}$ = -69.0 kcal/mol. Furthermore, no IR spectral evidence for isocyanide formation is observed at the end of catalytic runs. Since all adduct formations are expected to be rapid and reversible, OAT does not appear to be competitive.

2.8.2. *Calculated transition state of imide carbonylation*

Figure 2.13 illustrates the transition state (TS) for the carbonylation of (dadi)Ti=NAd (**2**=NAd) found *via* DFT calculations. The CO attacks the imide

at an angle consistent with its lone pair interacting with an unoccupied d_{xz}/d_{yz} orbital, and the new CN bond is formed through a N-pπ -> CO-π* interaction. The computed TS appears early in the reaction coordinate, even though there is considerable lengthening of the d(CO) to 1.17 Å. The d(TiN) of 1.79 Å is only 0.11 Å longer than the calculated d(TiN), and 0.085 Å longer than d(TiN) found in the crystal structure of **2**=NAd. Moreover, the d(NC) is long at 1.69 Å, the TiNC(Ad) angle is still large at 162.5°, and the accompanying NCO angle is 120.3°, which is significantly bent from the 175° in the κ^1-Ti-N-OCNAd adduct that is the initial intermediate of carbonylation.

Mindiola[36] and Cummins[37] have reported carbonylations of early metal nitrides suggesting that binding of the π-acid to the metal center is important, and that the interaction may also induce reduction of the metal by the nitride. Although the d(Ti-C) of 1.79 Å in the computed TS indicates an interaction with titanium, the ligand metrics conform to the $(dadi)^{2-}$ formulation. The $Ti\text{-}N_{am}$ distances of 2.12 and 2.14 Å are significantly shortener than the $d(TiN_{im})$ bond lengths of 2.23 and 2.24 Å. Furthermore, CN_{im} distances of 1.30 and 1.29 Å, accompanied by a CC distance of 1.43 Å in the ligand backbone do not indicate reduction of the ligand. In a late TS, the ligand metrics would be expected to more closely resemble a $(dadi)^{4-}$ core, and display similar Ti-N distances for all four N-donors.

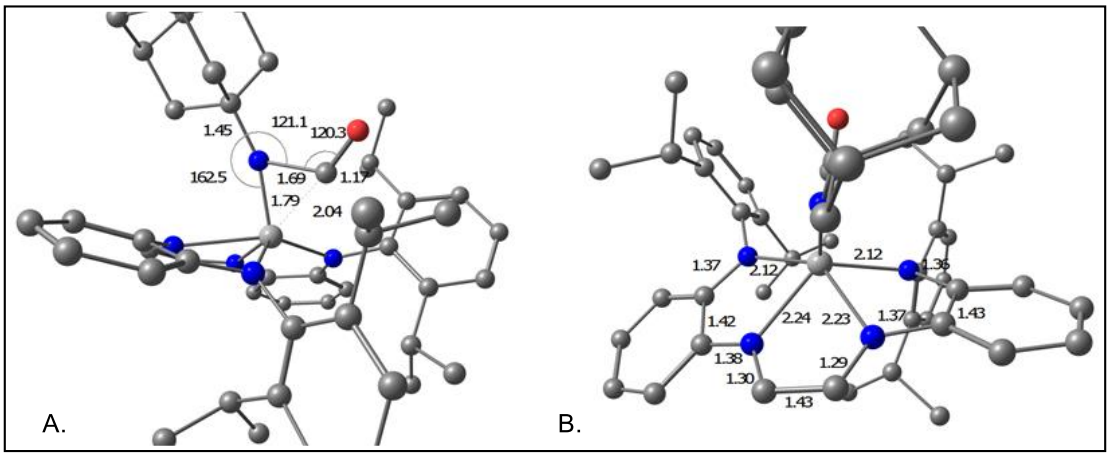

Figure 2.13. Views of the computed transition state for carbonyl addition to the imide of (dadi)Ti=NAd (**2**=NAd): A. metrics (distances (Å), angles (°)) of the imide-carbonyl fragment; B. distances of the core and dadi ligand.

2.9. RNI manifested in (dadi)TiL$_n$ (n = 1, L = THF, PMe$_2$Ph; n = 2, L = CNMe) and (dadi)Ti=X (X = NAd, O)

The (dadi)^n RNI plays a critical role in the transfer of the imido in (dadi)Ti=NAd (**2**=NAd) to CO. During catalytic carbonylation, the (dadi)^n ligand stabilizes transient (dadi)Ti (**1**) as [(dadi)$^{3-\uparrow}$]Ti(III)$^{\downarrow}$, (dadi)Ti-L (**1**-L) *via* (dadi)$^{4-}$, and **2**=NAd through (dadi)$^{2-}$ by acting as an electronic buffer and maintaining the titanium in its favorable higher oxidation states. The electronic structures of **1**-PMe$_2$Ph and **2**=O, serve as useful analogues for a potential carbonyl species and **2**=NAd. Carbon monoxide, a potent π-acid towards titanium, is less oxidizing to the metal center than the (dadi)$^{4-}$ ligand containing a conjugated 4n+2 π-electron configuration. As shown in Figure 2.5, any backbonding interaction with CO would need to stabilize a dπ-orbital by about 3 ev in order to depopulate the NCCN π-bonding orbital, and render the dadi dianionic. In contrast, the ligand is less oxidizing than a nitrene (i.e., NAd), and it resides in its dianionic 20 π-electron (4n) form. As the truncated MO diagram for **2**=O indicates (Figure 2.8), the LUMO of the system is the NCCN

π-orbital at -3.41 eV, which has been depopulated in favor of the imide π-bonding orbitals of low energy.

With the titanium-dadi system, carbodiimide formation was envisioned to be possible, similar to Heyduk's zirconium examples.[12] Unfortunately, attempts to catalyze this transformation failed, as treatment of (dadi)Ti=NAd with CNMe afforded only a trace amount of MeNCNAd and (dadi)Ti$(CNMe)_2$ (**1**-$(CNMe)_2$). In contrast to CO, the strongly sigma-donating CNMe imparts too much stability on the highly electropositive Ti^{IV} center, as exposure of (**1**-$(CNMe)_2$) to AdN_3 was also ineffective.

OAT from (dadi)Ti=O (**2**=O) was tested with a variety of substrates (olefins, CO, etc.), but only transfer to PMe_3, resulting in green (dadi)Ti-$OPMe_3$ (**1**-$OPMe_3$), was observed. The phosphine oxide adduct was independently prepared from (dadi)Ti(THF) (**1**-THF) and 1 equiv of $Me_3P(O)$ (Scheme 2.4). Attack by PMe_3 on (dadi)TiO (**2**=O) to form the adduct (dadi)Ti$OPMe_3$ (**1**-$OPMe_3$) is relatively slow, presumably due to known orbital symmetry constraints for OAT.[38] The reaction is calculated to be favorable by $\Delta G°_{calc}$ = -22.5 kcal/mol, presumably due to strong P=O bond formation. In addition, the phosphine oxide complex (**1**-$OPMe_3$) is favored over the THF adduct (**1**-THF) by $\Delta G°_{calcd}$ = -17.2 kcal/mol.

Conclusions:

Structural and computational investigations show that $(dadi)^n$ is capable of binding as a $(dadi)^{4-}$ tetraanion in $[dadi^{4-}]Ti^{IV}L_x$ (**1**-L_x; L_x = THF, PMe_2Ph, $(CNMe)_2$) and as a dianion in $[dadi^{2-}]Ti^{IV}X$ (**2**=X; X = O, NAd). The ability of the dadi ligand to distribute charge throughout its π-system maintains the titanium in its favorable high-oxidation state. Computational studies into the electronic

structure of [dadi^{4-}]Ti^{IV}L (**1**-L; L = THF, PMe_2Ph) revealed a HOMO that is well placed energetically for catalysis. The $(dadi)^{4-}$ state is stable enough as a 22 π-electron (4n+2) system to prevent binding/oxidation by CO, but still allows oxidation by a nitrene (AdN). The redox non-innocence (RNI) of dadi^n renders CO binding to (dadi)Ti (**1**) essentially devoid of π-backbonding, and uncompetitive with THF adduct formation by $\Delta G°_{calc}$ = 7.7 kcal/mol. As a consequence, the RNI $(dadi)^n$ ligand permits this unusual carbonylation catalysis with titanium.

*Experimental***:**

A. General Considerations

All manipulations were performed using either glovebox or high vacuum line techniques. All glassware was oven dried. THF and diethyl ether were distilled under nitrogen from purple sodium benzophenone ketyl and vacuum transferred from the same prior to use. Hydrocarbon solvents were treated in the same manner with the addition of 1-2 mL/L tetraglyme. Benzene-d_6 was dried over sodium, vacuum transferred and stored over activated 4Å molecular sieves. THF-d_8 was dried over sodium and stored over purple sodium benzophenone ketyl. Hexamethyldisilazane was purchased from Oakwood Chemicals then dried and stored over activated 4Å molecular sieves. Dimethylphenylphosphine was purchased from Strem Chemicals Inc., degassed and stored in a dry box before use. Nitrous oxide, ferrocene, and 1-azidoadamantane were purchased from Sigma-Aldrich Chemical Company and used as received. N, N'-di-2-(2,6-diisopropylphenylamine)-phenylglyoxaldiimine (DadiH_2) was prepared following literature procedures.[22]

NMR spectra were acquired using Mercury 300 MHz, INOVA 400 MHz, or Bruker AV III HD 500 MHz (equipped with a 5 mm BBO Prodigy cryoprobe) spectrometers. Assignments of carbon chemical shifts were determined from HSQCAD and gHMBCAD spectra collected on an INOVA 600 MHz NMR spectrometer. Reaction monitoring for kinetic analysis was performed using an INOVA 600 MHz spectrometer. Chemical shifts are reported relative to benzene-d6 (^{1}H δ 7.16; ^{13}C{^{1}H} δ 128.06). NMR spectra were processed using MNova 11.0. Infrared spectra were recorded on a 20 Nicolet Avatar 370 DTGX spectrophotometer interfaced to an IBM PC (OMNIC software). Fitting of

kinetic data was performed using Igor Pro 6. Heating of NMR tubes to 25, 35, and 45 ^{o}C was done using a Hewlett Packard 5890 Series II gas chromatograph oven. Heating of NMR tubes to 55, 65, and 75 ^{o}C was done using an oil bath equipped with a Thermo Scientific AC200 immersion circulator.

B. Procedures

1. *Sodium bis(trimethylsilyl)amide:* This is a modified literature procedure.[39] To a 300 mL round bottom flask charged with NaH (4.21 g, 175.5 mmol) and toluene (150 mL) was added hexamethyldisilazane (40mL, 190.8 mmol) via syringe under argon purge. After heating to reflux for 48 hours, the reaction mixture was concentrated to *ca.* 35 mL and filtered. The filter cake was then washed with toluene (2x) then stripped of all volatiles, then washed again with pentane (3x). Following removal of all volatiles NaHMDS was obtained as a white voluminous powder (16.990 g, 92.5 mmol, 48 %). ^{1}H NMR (C_6D_6, 300MHz, 295K): δ 0.12 (s, 18H).

2. *Titanium-dichloride-bis(tetramethylethylenediamine):* This is a modified literature procedure.[23] In a dry box under a N_2 atmosphere, a 100 mL round bottom flask was charged with $TiCl_3(THF)_3$ (5.00 g, 13.6 mmol) and freshly chopped lithium metal (321 mg, 46.2 mmol). The reaction flask was then assembled onto a large swivel frit with a 100 mL receiving flask. The swivel frit apparatus was degassed then put under an argon atmosphere. Under a strong argon purge, the lithium metal was cut as much as possible using a sharpened spatula. The swivel-frit apparatus was degassed and THF (65 mL) then TMEDA (12 mL, 80.0 mmol) were vac. transferred to the reaction flask. The reaction mixture was allowed to warm to room temperature

and stirred for 43 hours. The swivel-frit apparatus was degassed, and the reaction mixture filtered. The filter-cake was washed until no purple solid remained on the fritted filter. The reaction mixture was then concentrated to *ca*. 30 mL and cooled to -78 ^{o}C while stirring for 30 min. The entire frit apparatus was then cooled to -78 ^{o}C and the reaction mixture was filtered and washed once with the remaining solvent. All volatiles were removed by vacuum and $TiCl_2(TMEDA)_2$ was collected as a purple crystalline solid (2.952 g, 62 %).

3. *Bis(tetrahydrofuran-2-yl)sodium(III) (((1E,1'E)-ethane-1,2-diylidenebis(azanylylidene))bis(2,1-phenylene))bis((2,6-diisopropylphenyl)amide)*, **(dadi)Na_2**. To a 100 mL round bottom flask charged with dadiH_2 (2.0 g, 3.58 mmol) and NaHMDS (1.313 g, 7.16 mmol) was added 40 mL freshly distilled THF at – 78 ^{o}C. The reaction was allowed to warm to room temperature over the course of 30 minutes then the reaction volume was concentrated to *ca.* 15 mL. The blue solution was cooled to -78 ^{o}C then 40 mL of freshly distilled pentane was added resulting in blue precipitate which was filtered. After removal of all volatiles, Na_2dadi$(THF)_4$ was collected as a blue crystalline solid (2.994 g, 3.36 mmol, 94 %). *Na_2dadi$(THF)_4$* was quenched with a mixture of C_6D_6 and saturated $NH_4Cl_{(aq)}$ to determine the amount of THF in the product. ^{1}H NMR (300 MHz, THF-d_8) δ 1.04 (dd, *J* = 10.9, 6.9 Hz, 24H), 3.39 (hept, *J* = 7.3, 6.9 Hz, 4H), 5.58 (t, J = 7.0 Hz, 2H), 5.67 (d, *J* = 8.4 Hz, 2H), 6.35 (t, J = 7.4 Hz, 2H), 6.72 (t, J = 7.7 Hz, 2H), 6.87 (d, *J* = 7.7 Hz, 2H), 6.94 (d, *J* = 7.4 Hz, 2H), 8.32 (s, 2H). ^{13}C NMR (126 MHz, THF-d_8) δ 24.55, 25.20, 26.55, 68.39, 106.49, 116.53, 117.16, 120.55, 123.57, 129.58, 135.33, 143.42, 148.39, 154.45, 158.47.

4. *Titanium N, N'-di-2-(2,6-diisopropylphenylamide)-phenylglyoxaldiimine-tetrahydrofuran*, **(dadi)Ti(THF)** (**1**-THF). To a 100 mL round bottom flask, cooled to -78 ^{o}C and charged with Na_2dadi$(THF)_4$ (1.479 g, 1.66 mmol) and $TiCl_2$(TMEDA) (584 mg, 1.66 mmol) was added ca. 75 mL freshly distilled THF. The reaction mixture was warmed to -20 ^{o}C and stirred for 4 hours. The resulting green solution was stripped of volatiles, triturated with THF (3x, 20 mL). 30 mL of cyclohexane was added and the reaction was filtered. The filter cake was washed until the filtrate was colorless. The resulting mixture was cooled to 10 ^{o}C for 30 minutes then filtered. After all volatiles were removed, Ti(dadi)THF was collected as an olive green powder with 0.66 eq. of residual cyclohexane (597 mg, 48 %). *Varying amounts of cyclohexane were present in the isolated product, ranging from 0.50–1.3 eq. per titanium. ^{1}H NMR (C_6D_6, 400MHz, 295K): δ 0.57 (d, *J* = 6.6 Hz, 6H) , 0.94 (d, *J* = 6.4 Hz, 6H) , 1.06 (d, *J* = 5.9 Hz, 12H) , 1.25 – 1.15 (m, 4H) , 1.40 (s, 4H), 2.48 – 2.29 (m, 2H), 3.50 (p, J= 6.5 Hz, 2H) , 3.89 (t, J= 6.5 Hz, 4H) , 5.78 (d, *J* = 7.8 Hz, 2H) , 6.48 (dd, *J* = 7.7, 0.9 Hz, 2H) , 6.69 – 6.57 (m, 4H) , 6.81 (t, *J* = 7.5 Hz, 2H) , 7.01 (d, *J* = 6.2 Hz, 2H), 7.14 – 7.06 (m, 6H). ^{13}C{^{1}H} NMR (C_6D_6, 126 MHz, 295K) δ 22.92, 23.54, 24.67, 25.12, 25.67, 26.87, 28.98, 74.42, 105.98, 113.76, 120.41, 123.28, 123.52, 125.27, 126.45, 127.75, 141.77, 143.50, 143.82, 146.25, 151.78.

5. *Titanium N, N'-di-2-(2,6-diisopropylphenylamide)-phenylglyoxaldiimine-dimethylphenyphosphine*, **(dadi)TiPMe$_2$Ph** (**1**-PMe$_2$Ph). To a 100 mL round bottom flask, cooled to -78 ^{o}C and charged with Na_2dadi (1.000 g, 8.78 mmol) and $TiCl_2$(TMEDA) (584 mg, 1.66 mmol) was added *ca.* 75 mL freshly distilled THF. The reaction mixture was warmed to -20 ^{o}C and stirred for 2 hours. The resulting green solution was stripped of volatiles,

triturated with THF (3x, ca. 20 mL). 25 mL of freshly distilled benzene was added and the reaction mixture was warmed to 23 ^{o}C. Next, a solution of PMe_2Ph in 0.7 mL of benzene was added via syringe under an argon purge. The resulting red solution was stirred for 1 hour. The benzene was then removed in *vacuo* and 30 mL of freshly distilled hexanes was added to the reaction flask. The mixture was filtered and the filter cake was washed until colorless. The filtered solution was concentrated to ca. 15 mL total volume, cooled to -78 ^{o}C and filtered. After all volatiles were removed, Ti(dadi)PMe_2Ph was collected as a maroon solid (706 mg, 0.95 mmol, 57%). A single crystal suitable for X-Ray diffraction was acquired by slow diffusion of hexanes into a concentrated Et_2O solution. ^{1}H NMR (C_6D_6, 500 MHz, 295K) δ 0.40 (d, *J* = 6.8 Hz, 6H, Me), 0.83 (d, *J* = 6.7 Hz, 6H, Me), 1.03-1.06 (m, 12H, Me), 1.21 (d, *J* = 7.8 Hz, 6H), 2.07 (sept, *J* = 6.9 Hz, 2H), 3.74 (sept, *J* = 6.8 Hz, 2H), 5.81 (dd, *J* = 8.0, 1.3 Hz, 2H), 6.41 (dd, *J* = 7.8, 1.3 Hz, 2H), 6.60 (td, *J* = 7.7, 1.3 Hz, 2H), 6.62 (s, 2H), 6.79 (td, *J* = 7.5, 1.3 Hz, 2H), 6.90 – 7.01 (m, 5H), 7.08 (t, *J* = 7.7 Hz, 2H), 7.15 – 7.18 (m, 2H), 7.21 – 7.28 (m, 2H). ^{1}H{^{31}P} NMR (C_6D_6, 400 MHz, 295 K) ^{1}H NMR δ 0.40 (d, *J* = 6.8 Hz, 6H), 0.83 (d, *J* = 6.6 Hz, 6H), 1.03-1.06 (m, 12H), 1.20 (s, 6H), 2.07 (p, *J* = 6.8 Hz, 2H), 3.74 (p, *J* = 6.7 Hz, 2H), 5.81 (dd, *J* = 7.9, 1.3 Hz, 2H), 6.41 (dd, *J* = 7.8, 1.3 Hz, 2H), 6.55 – 6.64 (m, 4H), 6.79 (td, *J* = 7.5, 1.3 Hz, 2H), 6.89 – 7.03 (m, 5H), 7.08 (t, *J* = 7.6 Hz, 2H), 7.12 – 7.20 (m, 2H), 7.25 (d, *J* = 7.4 Hz, 2H). ^{31}P NMR (C_6D_6, 202 MHz, 295K) δ -6.40 (s). ^{13}C{^{1}H} NMR (C_6D_6, 126 MHz, 295K) δ 10.68 (P-CH_3,d, J_{PC} = 19.1 Hz), 23.42 (^{i}Pr-CH_3), 24.38 (^{i}Pr-CH_3), 25.08 (^{i}Pr-CH_3), 26.26 (^{i}Pr-CH_3), 29.21 (^{i}Pr-CH), 29.60 (^{i}Pr-CH), 107.16 (Ar-CH), 115.36 (Ar-CH), 120.70 (Ar-CH), 123.74 ($^{2,6\text{-}iPr}$Ar-CH), 124.07 (Ar-CH), 125.81 ($^{2,6\text{-}iPr}$Ar-CH), 126.50 ($^{2,6\text{-}iPr}$Ar-CH), 128.92 (Ar-CN), 129.04 (d, J_{PC}=9.3 Hz, P-Ar-CH), 130.19 (d, J_{PC}=

1.4 Hz, P-Ar-CH), 130.83 (d, J_{PC}= 11.8 Hz, P-Ar-CH), 133.72 (d, J_{PC}= 31.5 Hz, P-Ar-C) 142.10 (d, J_{PC}= 1.1 Hz, Ar-CN), 143.75 ($^{2,6\text{-iPr}}$Ar-C), 143.84 ($^{2,6\text{-iPr}}$Ar-C), 147.86 ($^{2,6\text{-iPr}}$Ar-CN), 153.30 (Ar-CN).

6. *Titanium N, N'-di-2-(2,6-diisopropylphenylamide)-phenylglyoxaldiimine-1-imidoadamantane*, **(dadi)Ti=NAd** (**2**=NAd). To a 50 mL round bottom flask charged with Ti(dadi)THF·^{c}Hex$_{(0.89)}$ (317 mg,0.42 mmol) and C_6H_6 (1.9 mL) was added a solution of 1-azidoadamantane (74 mg, 0.42 mmol) in 1.1 mL of C_6H_6. Effervescence and an immediate color change to red were observed. The reaction solution was stirred for 15 minutes at room temperature then attached to a swivel frit. The crude mixture was triturated with hexanes (5x, 15 mL). The red solid was taken up in hexanes (*ca.* 30 mL), cooled to -78 ^{o}C and filtered. The red filter cake was washed two times with hexanes and then all volatiles were removed by vacuum. Ti(dadi)NAd was collected as a maroon red powder (236 mg, 0.31 mmol, 74 %). ^{1}H NMR (C_6D_6, 400 MHz, 295K) δ 0.87 (d, *J* = 6.8 Hz, 6H), 1.10 (d, *J* = 4.9 Hz, 6H), 1.11 (d, *J* = 5.2 Hz, 6H), 1.39 (d, *J* = 6.6 Hz, 6H), 1.50 (q, *J* = 12.3 Hz, 6H), 1.93 (s, 3H), 1.99 (s, 6H), 3.19 (p, *J* = 6.8 Hz, 2H), 4.15 (sept, *J* = 6.8 Hz, 2H), 5.71 (d, *J* = 8.4 Hz, 2H), 6.07 (t, *J* = 7.4 Hz, 2H), 6.30 (s, 2H), 6.42 (d, *J* = 8.1 Hz, 2H), 6.46 (t, *J* = 7.7 Hz, 2H), 7.07 – 7.14 (m, 3H), 7.17 (td, *J* = 8.4, 7.9, 2.0 Hz, 3H). ^{13}C{^{1}H} NMR (C_6D_6, 126 MHz, 295K) δ 23.93, 24.18, 24.42, 26.51, 29.15, 29.44, 30.32, 36.88, 45.42, 72.71, 115.73, 116.54, 118.55, 124.68, 124.92, 125.60, 133.46, 134.34, 141.04, 144.82, 146.03, 146.06, 164.10.

7. *Titanium N, N'-di-2-(2,6-diisopropylphenylamide)-phenylglyoxaldiimine-oxide*, **(dadi)Ti=O** (**2**=O). A 50 mL round bottom flask attached to a small swivel frit was charged with Ti(dadi)THF·^{c}Hex$_{(1.3)}$ (202 mg,

0.256 mmol). To this flask was added *ca.* 20 mL of freshly distilled benzene. Upon thawing and warming to room temperature, the reaction apparatus was placed under 1 atmosphere of $N_2O_{(g)}$ and purged for 60 seconds while stirring vigorously, then the needle valve was closed. The reaction was stirred at room temperature for 35 minutes, after which the volatiles were pumped away and the reaction solution was concentrated to approximately 1 mL. The resulting mixture was filtered and the filter-cake was washed with benzene (2x) and the remaining volatiles were removed in *vacuo*. 10 mL of pentane was added to the reaction apparatus, the filter-cake was then washed with pentane (3x), followed by removal of the solvent by vacuum. Ti(dadi)O was collected as a lime green powder (115 mg, 0.185 mmol, 70%). A single crystal suitable for X-Ray diffraction was acquired from a concentrated benzene solution of Ti(dadi)O layered with pentane. ^{1}H NMR ^{1}H NMR (C_6D_6, 400 MHz, 295K) δ 0.82 (d, *J* = 6.8 Hz, 6H), 1.06 (d, *J* = 6.8 Hz, 6H), 1.12 (d, *J* = 6.6 Hz, 6H), 1.28 (d, *J* = 6.8 Hz, 6H), 3.04 (p, *J* = 6.8 Hz, 2H), 4.54 (p, *J* = 6.8 Hz, 2H), 5.86 (d, *J* = 8.3 Hz, 2H), 6.16 (ddd, *J* = 8.2, 6.9, 1.2 Hz, 2H), 6.54 – 6.62 (m, 4H), 6.66 (s, 2H), 7.10 (dd, *J* = 7.5, 1.4 Hz, 2H), 7.20 (d, *J* = 7.6 Hz, 2H), 7.25 (dd, *J* = 7.7, 1.4 Hz, 2H).^{13}C{^{1}H} NMR (C_6D_6, 126 MHz, 295K) δ 23.14, 23.53, 24.20, 25.27, 28.86, 28.97, 116.75, 116.92, 117.90, 124.07, 125.26, 126.34, 132.91, 133.51, 143.24, 143.51, 144.84, 147.06.

8. *Titanium N, N'-di-2-(2,6-diisopropylphenylamide)-phenylglyoxaldiimine-bis(methylisocyanide)*, **(dadi)Ti(CNMe)$_2$** (**1**-(CNMe)$_2$). To a 50 mL round bottom flask charged with Ti(dadi)THF·^{c}Hex$_{(0.74)}$ (194 mg, 0.261 mmol) was distilled C_6H_6 (*ca.* 15 mL). An excess of CNMe (*ca.* 8 equivalents) was then condensed into the reaction flask at -78 ^{o}C. Upon thawing an immediate color change to blood red was observed. The reaction

was stirred for 16 hours then all volatiles were removed in *vacuo* yielding Ti(dadi)$(CNMe)_2$ as a dark red powder (149 mg, 0.216 mmol, 83%). A single crystal suitable for X-Ray diffraction was acquired by diffusion of pentane into a concentrated benzene solution of Ti(dadi)$(CNMe)_2$. ^{1}H NMR (C_6D_6, 300 MHz, 295K) δ 0.79 (d, *J* = 6.8 Hz, 12H), 1.19 (d, *J* = 6.6 Hz, 12H), 2.22 (s, 6H), 3.12 (p, *J* = 6.6 Hz, 4H), 5.79 (dd, *J* = 7.7, 1.5 Hz, 2H), 6.16 (s, 2H), 6.25 (dd, *J* = 7.5, 1.6 Hz, 2H), 6.52 (td, *J* = 7.5, 1.5 Hz, 2H), 6.59 (td, *J* = 7.4, 1.5 Hz, 2H), 7.02 – 7.12 (m, 6H). ^{13}C NMR (C_6D_6, 126 MHz, 295K) δ 23.70 (^{i}Pr-CH_3), 25.49 (^{i}Pr-CH_3), 28.50 (CN-CH_3), 29.45 (^{i}Pr-CH), 105.25 (Ar-CH), 112.88 (Ar-CH), 117.48 (Ar-CH), 124.42 (Ar-CH), 124.73 ($^{2,6\text{-iPr}}$Ar-CH), 125.53 (im-CH), 125.56 ($^{2,6\text{-iPr}}$Ar-CH), 140.58 (Ar-CN), 144.55 ($^{2,6\text{-iPr}}$Ar-C), 146.69 ($^{2,6\text{-iPr}}$Ar-C), 157.61 (Ar-CN), 164.50 (Ti-CNMe). IR (nujol mull, cm^{-1}) 570.89, 615.14, 674.98, 684.25, 710.54, 734.10, 758.48, 793.57, 833.90, 840.32, 868.63, 893.97, 898.85, 939.17, 943.46, 1036.95, 1054.92, 1100.83, 1113.56, 1170.92, 1269.29, 1318.23, 1359.08, 1379.90, 1587.47, 2166.19, 2199.25 (CN), 2222.95, 2642.73, 2704.96, 2719.69, 2751.81, 2932.03, 3056.35.

9. *Titanium N, N'-di-2-(2,6-diisopropylphenylamide)-phenylglyoxaldiimine-trimethylphosphineoxide*, **(dadi)Ti-$OPMe_3$** (**1**-$OPMe_3$). To a 25 mL round bottom flask charged with Ti(dadi)O (111 mg, 0.179 mmol) and equipped with a 109 mL gas bulb was distilled C_6H_6 (10 mL). PMe_3 (15 cm Hg, 0.895 mmol) was frozen into the reaction flask then the gas bulb was sealed. Once thawed, the reaction mixture was stirred at room temperature for 72 hours. The volatiles were removed under vacuum yielding Ti(dadi)$OPMe_3$ as a rifle-green crystalline solid (101 mg, 0.106 mmol, 81 %) ^{1}H NMR (400 MHz, Benzene-d_6) ^{1}H NMR (C_6D_6, 400 MHz, 295K) δ 0.69 (d, J_{PH} = 13.0 Hz, 9H), 0.73 (d, *J* = 6.6 Hz, 6H), 0.92 (d, *J* = 6.8 Hz, 6H), 1.10 (d, *J*

= 6.7 Hz, 12H), 2.57 – 2.68 (m, 2H), 3.40 (sept, *J* = 6.6 Hz, 2H), 5.78 (dd, *J* = 7.9, 1.3 Hz, 2H), 6.53 (dd, *J* = 7.7, 1.4 Hz, 2H), 6.66 (td, *J* = 7.6, 1.4 Hz, 2H), 6.81 (td, *J* = 7.5, 1.3 Hz, 2H), 6.82 (s, 2H), 7.11 (dd, *J* = 16.9, 7.3 Hz, 6H). $^{1}H\{^{31}P\}$ NMR (C_6D_6, 400 MHz, 295K) δ 0.69 (s, 9H), 0.73 (d, *J* = 6.6 Hz, 6H), 0.92 (d, *J* = 6.8 Hz, 6H), 1.10 (d, *J* = 6.7 Hz, 12H), 2.57 – 2.68 (m, 2H), 3.40 (sept, *J* = 6.6 Hz, 2H), 5.78 (dd, *J* = 7.9, 1.3 Hz, 2H), 6.53 (dd, *J* = 7.7, 1.4 Hz, 2H), 6.66 (td, *J* = 7.6, 1.4 Hz, 2H), 6.81 (td, *J* = 7.5, 1.3 Hz, 2H), 6.82 (s, 2H), 7.11 (dd, *J* = 16.9, 7.3 Hz, 6H). $^{31}P\{^{1}H\}$ NMR (C_6D_6, 202 MHz, 295K) δ 70.88. $^{13}C\{^{1}H\}$ NMR (C_6D_6, 126 MHz, 295K) δ 15.76 ($OP(CH_3)_3$, d, J_{PC} = 69.3 Hz), 23.97 (^{i}Pr-CH_3), 25.20 (^{i}Pr-CH_3), 25.71 (^{i}Pr-CH_3), 29.21 (^{i}Pr-CH), 105.81 (Ar-CH), 114.04 (Ar-CH), 119.51 (Ar-CH), 122.69 (Ar-CH), 124.01 ($^{2,6\text{-iPr}}$Ar-CH), 125.50 ($^{2,6\text{-iPr}}$Ar-CH), 126.38 (im-CH), 126.40 (im-CH), 128.59 ($^{2,6\text{-iPr}}$Ar-CH), 142.51 (Ar-CN), 144.24 ($^{2,6\text{-iPr}}$Ar-C), 147.79 ($^{2,6\text{-iPr}}$Ar-C), 151.70 (Ar-CN).

C. Procedure for Monitoring Carbonylation Reactions

The volumes of each NMR tube, sealed onto 14/20 ground glass joints and their designated needle valve adapter were determined by filling with water and measuring the mass. The tubes and needle valves were dried in an oven then charged with 0.5 mL of a stock solution of C_6D_6 containing 0.046 M Ti(dadi)NAd, *ca.* 0.40 M ferrocene, and 0.048 M THF in the dry box. These were then moved to the vacuum line on needle valve adapters. The NMR tubes were degassed with three freeze-pump-thaw cycles. 760 mm Hg of $CO_{(g)}$ was measured using a mercury monometer after being passed through a -78 ^{o}C trap. The needle valve was then closed and the tubes were cooled to 77 K with liquid nitrogen and flame-sealed with a CH_4/O_2 torch. The remaining gas in the headspace of the needle valve and 14/20 ground glass joint was

measured using a Teopler pump. Each reaction was performed in triplicate at each temperature.

NMR tubes for catalytic carbonylation experiments were performed in the same fashion only with 600 mm Hg of $CO_{(g)}$ and using a stock solution containing $[Ti(dadi)NAd]_o$ = 0.0063 M, $[AdN_3]_o$ = 0.12 M, and *ca.* 0.005 M ferrocene.

D. Carbonylation Rate Analysis

Time dependent concentration plots obtained using ^{1}H NMR spectroscopy for catalytic runs were fit to a set of differential equations (eq. 10-12) describing the mechanistic model shown below (Scheme 2.7). Time dependent concentration plots obtained using ^{1}H NMR spectroscopy for stoichiometric runs were linearized then fitted in Microsoft Excel using linear regression. The Eyring plot was fitted in Igor Pro 6 using linear regression weighted by the standard deviation of each point. The standard deviation of each data point was determined using propagation of error calculations (*cf.* Appendix A).[40] Carbon monoxide concentrations were calculated using the temperature dependent mole fraction solubility's (χ_g) extrapolated from reference 36 (Table 2.1).[35]

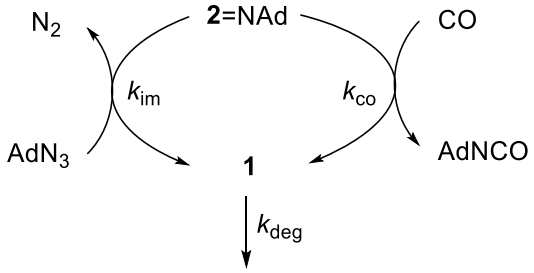

Scheme 2.7. Mechanistic model for catalytic carbonylation

$$\frac{d[\mathbf{2}{=}NAd]}{dt} = -k_1[\mathbf{2}{=}NAd] + k_{im}[AdN_3][\mathbf{1}] \quad \text{(eq 1)}$$

$$\frac{d[\mathbf{1}]}{dt} = k_1[\mathbf{2}{=}NAd] - k'_{deg} - k_{im}[\mathbf{1}][AdN_3] \quad \text{(eq 2)}$$

$$\frac{d[AdN_3]}{dt} = -k_{im}[\mathbf{1}][AdN_3] \quad \text{(eq 3)}$$

Where:

$k_1 = k_{co}[CO]$

$k_{im} = 1000\ M^{-1}s^{-1}$

$k'_{deg} = k_{deg}[\mathbf{1}]$

Sample calculation of [CO] (M) at 3.1 atm and 298 K

Henry's Law: [35]

$P_g = \chi_g/H_T$ (eq 7)

Where: P_g = partial pressure, χ_g = mole fraction solubility of gas dissolved, H_T = Henry's law constant at temperature T.

Mole fraction solubility of gas dissolved is:

$\chi_g = \eta_g/(\eta_g + \eta_s)$ (eq 8)

Where: η_g = moles of gas and η_s= moles of solvent.

Henry's law constant at 298 K, and 1 atm:

$H_{298K} = (1 \pm 0.1\ atm)/(6.59x10^{-4} \pm 1.0\ x10^{-5}) = 1.\ 52x10^3 \pm 38\ atm$

Mole fraction solubility of CO at the partial pressure in the reaction vessel (NMR tube):

$\chi_g = P/H_{298K} = (3.10 \pm 0.1\ atm/1.52x10^3 \pm 38\ atm) = 2.04x10^{-3} \pm 1.2x10^{-4}$

Using eq 14 gives the moles of CO in 0.5 mL of C_6H_6:

$2.04x10^{-3} \pm 1.2x10^{-4} = \eta_{CO}/(\eta_{CO} + 5.61x10^{-3} \pm 1.3x10^{-5}$ mol $C_6H_6)$

$\eta_{CO} = 1.155x10^{-5} \pm 2.2x10^{-6}$ moles

Therefore:

$[CO] = (1.155x10^{-5} \pm 2.2x10^{-6}$ moles CO$)/(0.0005 \pm 1.1x10^{-7}$ L $C_6H_6) = 2.31x$

$10^{-2} \pm 4.4x10^{-3}$ M

Run	k_{co} x 10^3 ($M^{-1}s^{-1}$)	k'_{deg} x 10^5 (Ms^{-1})
1	3.48(21)	3.70(62)
2	3.32(11)	2.38(30)
3	2.60(60)	3.53(31)
Avg.	3.13(24)	3.20(25)

Table 2.3. Rate constants obtained from fits of experimental data for catalytic carbonylations.

Run	k_{co} x 10^3 (M^{-1} s^{-1}); 298 K	k_{co} x 10^3 (M^{-1} s^{-1}); 308 K	k_{co} x 10^3 (M^{-1} s^{-1}); 318 K	k_{co} x 10^3 (M^{-1} s^{-1}); 328 K	k_{co} x 10^3 (M^{-1} s^{-1}); 338 K	k_{co} x 10^3 (M^{-1} s^{-1}); 348 K
1	1.24	1.82	3.65	5.31	8.55	13.2
2	1.25	1.80	3.59	5.14	7.25	15.4
3	1.26	1.88	3.51	5.85	8.04	13.5
Ave	1.25	1.83	3.58	5.44	7.95	14.0
σ	0.055	0.080	0.15	0.42	0.86	1.10

Table 2. 4. Rate constants obtained from stoichiometric carbonylation reactions.

Run	k_{obs} x 10^5 (s^{-1}) [a]	k_{obs} x 10^5(s^{-1}) [b]	k_{obs} x 10^5(s^{-1}) [c]
1	4.07	10.2	14.9
2	5.18	8.34	14.4
3	5.29	1.05	16.4
Ave	4.85	9.67	15.2
σ	0.55	0.948	1.04

Table 2.5. Observed rate constants for carbonylation. [a]P_{CO} = 1.26 atm, [CO] = 0.0105 M, $[TiNAd]_o$ = 0.047 M, $[THF]_o$ = 0.048 M, T = 328 K. [b]P_{CO} = 2.73 atm, [CO] = 0.023 M, $[TiNAd]_o$ = 0.046 M, T = 328 K. [c]P_{CO} = 3.34 atm, [CO] = 0.028 M, $[TiNAd]_o$ = 0.047 M, T = 328 K.

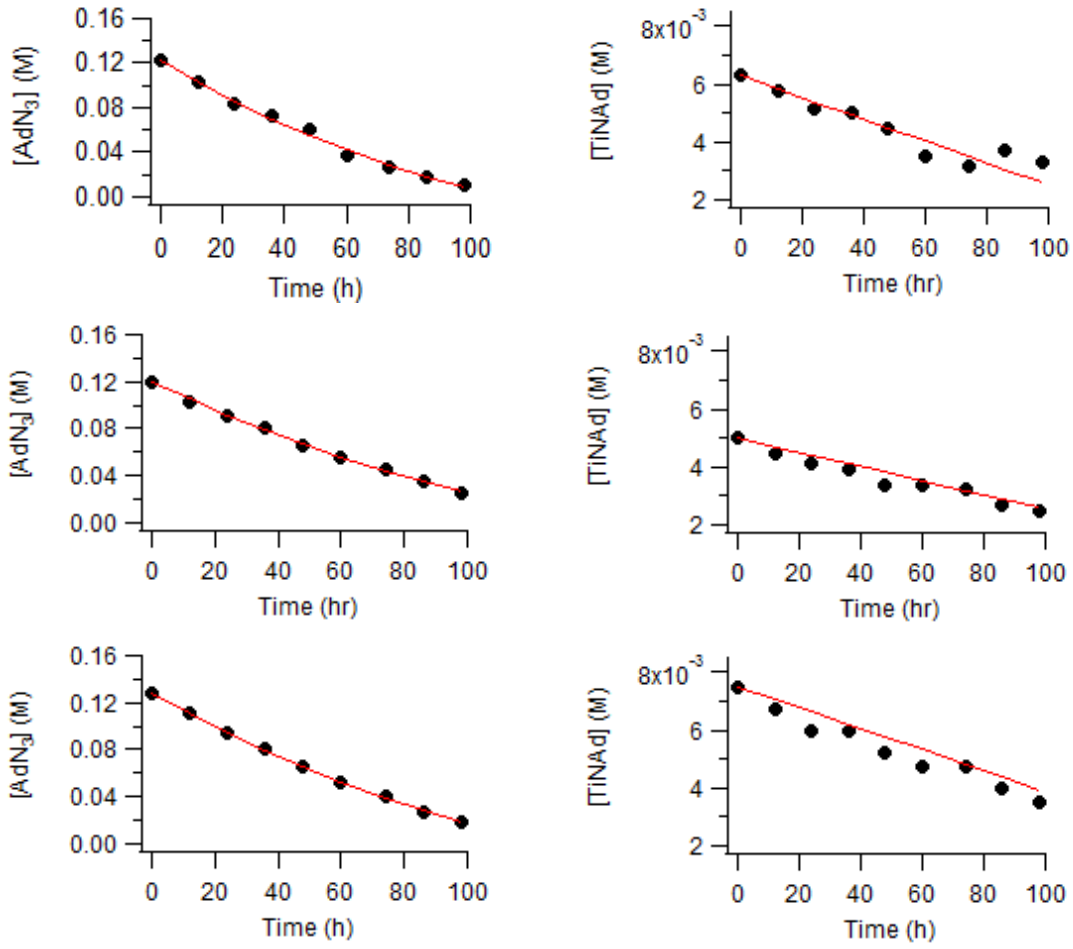

Figure 2.14. Experimentally measured concentrations (black dots) and fitted data (red line) for catalytic carbonylation. Plots of $[AdN_3]$ vs time (left) and [Ti(dadi)NAd] vs time (right). Run 1 (top), run 2 (middle), and run 3 (bottom). P_{CO} = 2.58 atm, [CO] = 0.022 M, $[Ti(dadi)NAd]_o$ = 0.0063 M, $[AdN_3]_o$ = 0.12 M, T = 298 K.

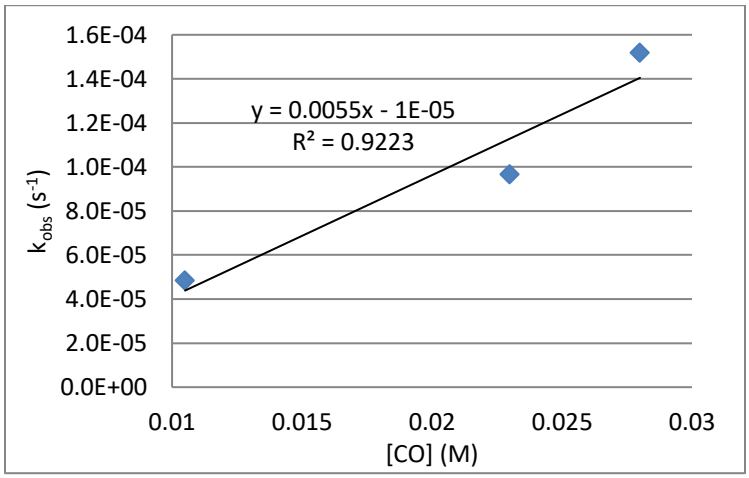

Figure 2.15. Plot of observed rate constant (k_{obs}) versus CO concentration. Experimentally determined observed rate constants (blue diamonds) and linear regression (black line) showing first order dependence on CO.

E. Modeling of kinetic data

Modeling of time dependent concentrations of [**2**=NAd], [AdN3], and [1] were performed in Mathematica 12.0 using eq's 3,4, and 6 described in the main text.

F. Computations

All simulations employed the Gaussian09[41] package. Geometries were optimized, and their energy Hessians computed to confirm them as either minima or transition states, at the ONIOM[42] (M06/6-311+G(d):UFF)[43,44] level of theory. Ultrafine integration grids were employed. The 2,6-$^{i}Pr_2$-Ar substituents were included in the UFF partition, and the remainder of the complex modeled with M06/6-311+G(d). For organic substrates, the alpha C of the 1-adamantyl substituent was included in the QM partition while the remainder was in the MM partition. Reported free energies for the transition metal complexes assume 1 atm and 298.15 K, except where noted, and were determined using unscaled vibrational frequencies.

Energies

M06/6-311+G(d) Calculated Enthalpies (H) and Free Energies (G), both in Hartrees, at 298.15 K and 1 atm. Spin states other than singlet are denoted by a superscripted prefix numeral.

Compound	**H**	**G**
N_2	-109.4816	-109.5033
CO	-113.2775	-113.3000
CO_2	-188.5437	-188.5679
N_2O	-184.6080	-184.6292
AdNC	-132.3482	-132.3884
AdN_3	-203.7020	-203.7446
AdNCO	-207.6132	-207.6572
THF	-232.2161	-232.2507
PMe_3	-460.8852	-460.9221
$OPMe_3$	-536.1287	-536.1678
Ti(dadi) (**1**)	-1607.9530	-1608.0612
^{3}Ti(dadi)	-1607.9520	-1608.0609
TiO(dadi) (**2**=O)	-1683.2248	-1683.3317
Ti(dadi)(NAd) (**2**=NAd)	-1702.2934	-1702.4125
Ti(dadi)(CO)	-1721.2720	-1721.3821
Ti(dadi)(κ^1-N-AdNCO) (**1**-OCNAd)	-1815.6056	-1815.7268
Ti(dadi)(κ^1-O-$OPMe_3$) (**1**-$OPMe_3$)	-2144.1662	-2144.2896
Ti(dadi)(THF) (**1**-THF)	-1840.2298	-1840.3451
Ti(dadi)(κ^1-N-AdN_3) (**1**-N_3Ad)	-1811.7060	-1811.8274
Ti(dadi)(κ^1-O-CO_2)	-1796.5198	-1796.6326
Ti(dadi)(CNAd)	-1740.3603	-1740.4848
TiO(dadi)(CNAd)	-1815.5943	-1815.6977

Calculated geometries

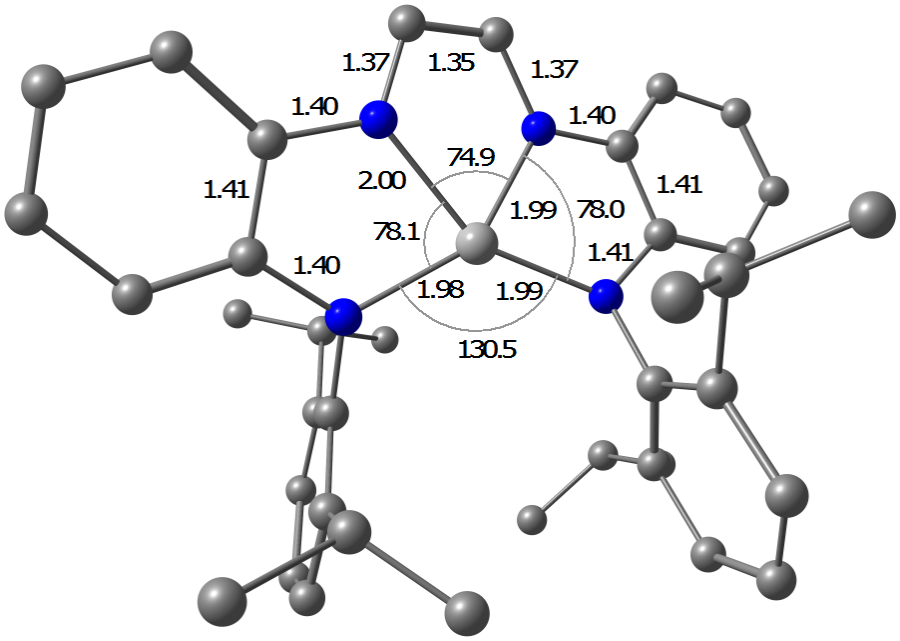

Figure 2.16. ONIOM(M06/6-311+G(d):UFF) optimized singlet state of (dadi)Ti (**1**). Gray = C; blue = N; light gray = Ti. Hydrogen atoms omitted from the figure for clarity. Bond lengths in Å. Bond angles in (°).

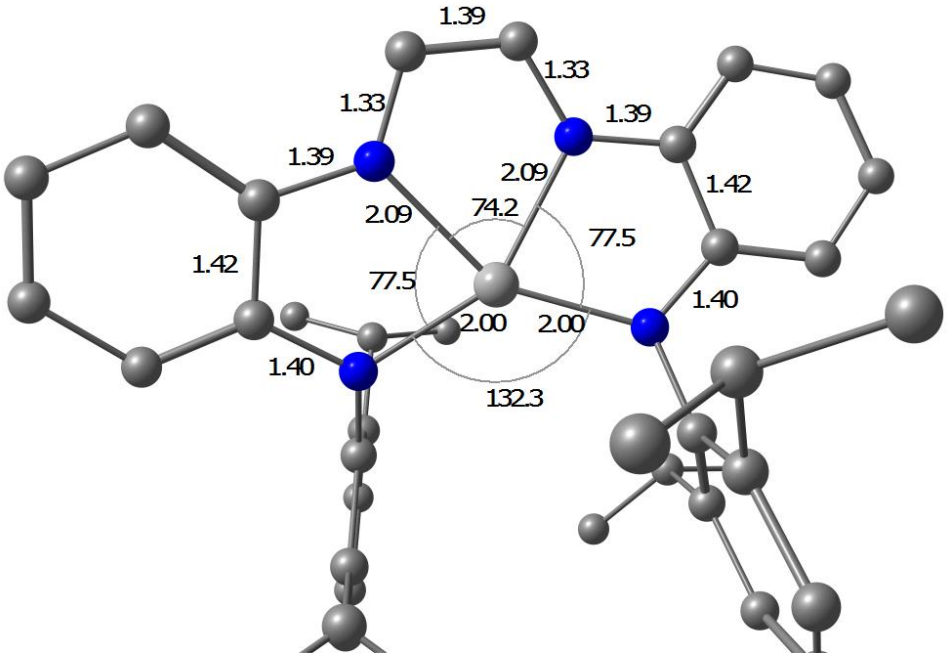

Figure 2.17. ONIOM(M06/6-311+G(d):UFF) optimized triplet state of (dadi)Ti (^{3}**1**). Gray = C; blue = N; light gray = Ti. Hydrogen atoms omitted from the figure for clarity. Bond lengths in Å. Bond angles in (°).

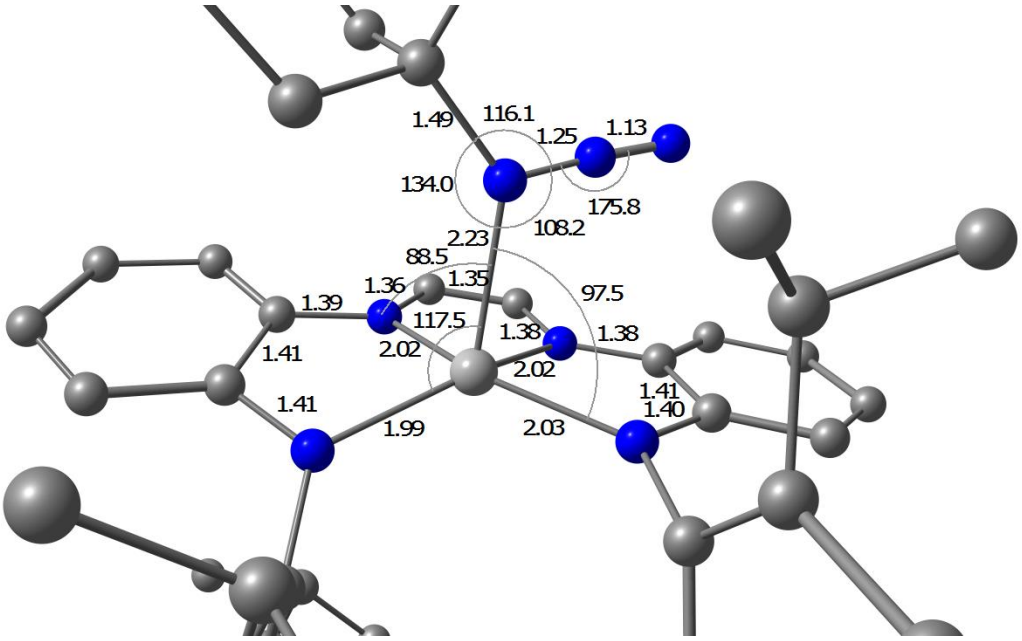

Figure 2.18. ONIOM(M06/6-311+G(d):UFF) optimized singlet ground state of (dadi)Ti(κ^1-N-N_3Ad). Gray = C; blue = N; light gray = Ti. Hydrogen atoms omitted from the figure for clarity. Bond lengths in Å. Bond angles in (°).

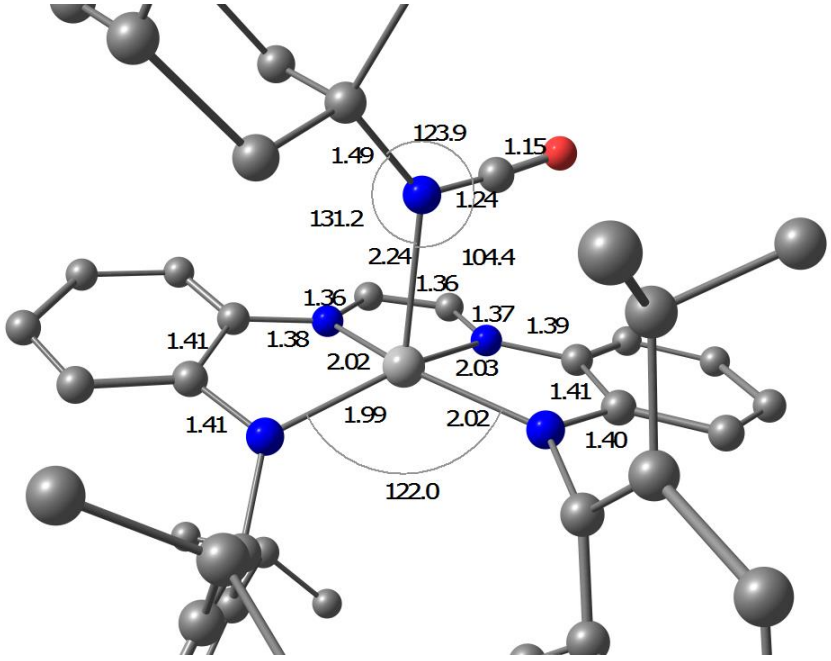

Figure 2.19. ONIOM(M06/6-311+G(d):UFF) optimized singlet ground state of (dadi)Ti(k1-AdNCO) (1-OCNAd). Gray = C; blue = N; O = red; light gray = Ti. Hydrogen atoms omitted from the figure for clarity. Bond lengths in Å. Bond angles in (°).

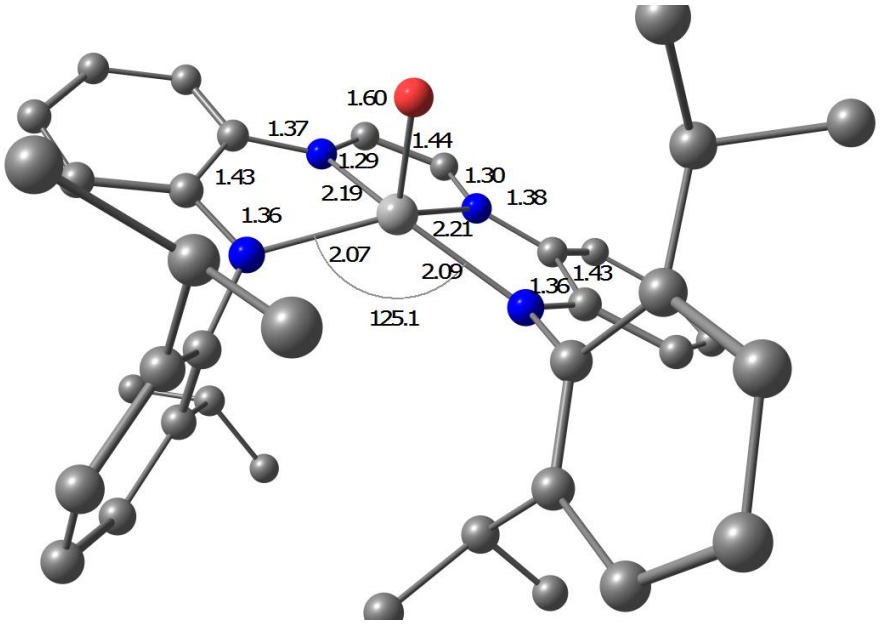

Figure 2.20. ONIOM(M06/6-311+G(d):UFF) optimized singlet ground state of (dadi)Ti=O (**2**=O). Gray = C; blue = N; O = red; light gray = Ti. Hydrogen atoms omitted from the figure for clarity. Bond lengths in Å. Bond angles in (°).

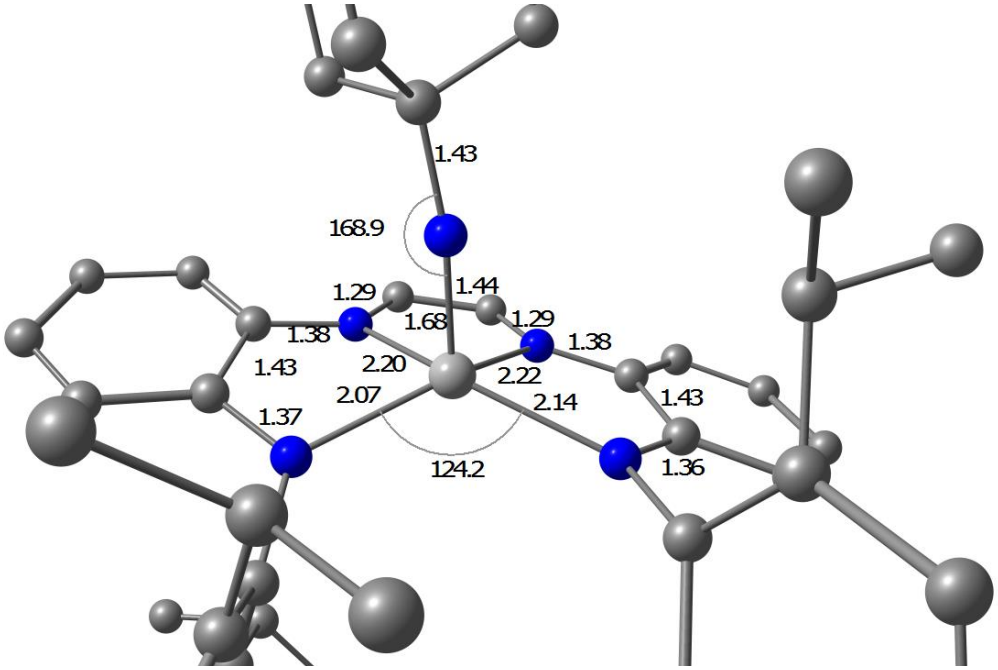

Figure 2.21. ONIOM(M06/6-311+G(d):UFF) optimized singlet ground state of (dadi)Ti=NAd (**2**=NAd). Gray = C; blue = N; light gray = Ti. Hydrogen atoms omitted from the figure for clarity. Bond lengths in Å. Bond angles in (°).

References:

(1) Budzelaar, P. H. M. *Eur. J. Inorg. Chem.* **2011**, *2012* (3), 530–534.

(2) Caulton, K. G. *Eur. J. Inorg. Chem. 2012* (3), 435–443.

(3) Sébastien, B.; Etienne, D.; Marine, D. M.; Louis, F.; Max, M.; Virginie, M. *Eur. J. Inorg. Chem.* **2012**, *2012* (3), 376–389.

(4) Wojciech, I. D.; van der Vlugt Jarl, I.; Reek, J. N. H.; de Bruin, B. *Angew. Chemie Int. Ed.* **2011**, *50* (15), 3356–3358.

(5) De Bruin, B.; Hetterscheid, D. G. H.; Koekkoek, A. J. J.; Grützmacher, H. *Prog. Inorg. Chem. Progress in Inorganic Chemistry*. April 2008.

(6) Ray, K.; Petrenko, T.; Wieghardt, K.; Neese, F. *Dalt. Trans.* **2007**, No. 16, 1552–1566.

(7) Emilia, E.; Daniel, R. *Eur. J. Inorg. Chem.* **2005**, *2005* (15), 2957–2971.

(8) Pierpont, C. G. *Coord. Chem. Rev.* **2001**, *216–217*, 99–125.

(9) Williams, V. A.; Wolczanski, P. T.; Sutter, J.; Meyer, K.; Lobkovsky, E. B.; Cundari, T. R. *Inorg. Chem.* **2014**, *53* (9), 4459–4474.

(10) Chirik, P. J. *Inorg. Chem.* **2011**, *50* (20), 9737–9740.

(11) Chirik, P. J.; Wieghardt, K. *Science (80-.).* **2010**, *327* (5967), 794–795.

(12) Nguyen, A. I.; Zarkesh, R. A.; Lacy, D. C.; Thorson, M. K.; Heyduk, A. F. *Chem. Sci.* **2011**, *2* (1), 166–169.

(13) Zarkesh, R. A.; Heyduk, A. F. *Organometallics*. **2011**, *30* (18), 4890–4898.

(14) Blackmore, K. J.; Lal, N.; Ziller, J. W.; Heyduk, A. F. *J. Am. Chem. Soc.* **2008**, *130* (9), 2728–2729.

(15) Lu, F.; Zarkesh, A. R.; Heyduk, F. A. *Eur. J. Inorg. Chem.* **2012**, *2012* (3), 467–470.

(16) Zarkesh, R. A.; Ziller, J. W.; Heyduk, A. F. *Angew. Chem. Int. Ed. Engl.* **2008**, *47* (25), 4715–4718.

(17) Carter, S. M.; Sia, A.; Shaw, M. J.; Heyduk, A. F. *J. Am. Chem. Soc.* **2008**, *130* (18), 5838–5839.

(18) Blackmore, K. J.; Ziller, J. W.; Heyduk, A. F. *Inorg. Chem.* **2005**, *44* (16), 5559–5561.

(19) Heins, S. P.; Wolczanski, P. T.; Cundari, T. R.; MacMillan, S. N. *Chem.*

Sci. **2017**, *8* (5), 3410–3418.

(20) Luca, O. R.; Crabtree, R. H. *Chem. Soc. Rev.* **2013**, *42* (4), 1440–1459.

(21) Heyduk, A. F.; Zarkesh, R. A.; Nguyen, A. I. *Inorg. Chem.* **2011**, *50* (20), 9849–9863.

(22) Heins, S. P.; Morris, W. D.; Wolczanski, P. T.; Lobkovsky, E. B.; Cundari, T. R. *Angew. Chemie Int. Ed. 54* (48), 14407–14411.

(23) Edema, J. J. H.; Duchateau, R.; Gambarotta, S.; Hynes, R.; Gabe, E. *Inorg. Chem.* **1991**, *30* (2), 154–156.

(24) Frazier, B. A.; Wolczanski, P. T.; Keresztes, I.; DeBeer, S.; Lobkovsky, E. B.; Pierpont, A. W.; Cundari, T. R. *Inorg. Chem.* **2012**, *51* (15), 8177–8186.

(25) Frazier, B. A.; Williams, V. A.; Wolczanski, P. T.; Bart, S. C.; Meyer, K.; Cundari, T. R.; Lobkovsky, E. B. *Inorg. Chem.* **2013**, *52* (6), 3295–3312.

(26) Addison, A. W.; Rao, T. N.; Reedijk, J.; van Rijn, J.; Verschoor, G. C. *J. Chem. Soc., Dalt. Trans.* **1984**, No. 7, 1349–1356.

(27) Stowasser, R.; Hoffmann, R. *J. Am. Chem. Soc.* **1999**, *121* (14), 3414–3420.

(28) Cavaliere, V. N.; Crestani, M. G.; Pinter, B.; Pink, M.; Chen, C.-H.; Baik, M.-H.; Mindiola, D. J. *J. Am. Chem. Soc.* **2011**, *133* (28), 10700–10703.

(29) Bing, L.; Spaniol, T. P.; Horrillo-Martínez, P.; Hultzsch, K. C.; Okuda, J. *Eur. J. Inorg. Chem.* **2009**, *2009* (3), 429–434.

(30) Clark, K. M.; Ziller, J. W.; Heyduk, A. F. *Inorg. Chem.* **2010**, *49* (5), 2222–2231.

(31) Christian, L.; Robert, C.; Laure, V. *Eur. J. Inorg. Chem.* **2006**, *2006* (22), 4503–4518.

(32) Lorber, C.; Vendier, L. *Organometallics*. **2008**, *27* (12), 2774–2783.

(33) Stuart, D. R.; Friedrich, A.; Willman, A., D.; Mountford, P.; Radius, U. *Chem. – A Eur. J.* **2003**, *9* (15), 3634–3654.

(34) Wilson, P. J.; Blake, A. J.; Mountford, P.; Schröder, M. *J. Organomet.Chem.* **2000**, *600* (1), 71–83.

(35) Fogg, P. G. T.; Gerrard, W. *Solubility of Gases in Liquids*, 3rd ed.; John Wiley & Sons: Chichester, 1991.

(36) Tran, B. L.; Pink, M.; Gao, X.; Park, H.; Mindiola, D. J. *J. Am. Chem. Soc.* **2010**, *132* (5), 1458–1459.

(37) Cozzolino, A. F.; Silvia, J. S.; Lopez, N.; Cummins, C. C. *Dalt. Trans.* **2014**, *43* (12), 4639–4652.

(38) Veige, A. S.; Slaughter, L. M.; Lobkovsky, E. B.; Wolczanski, P. T.; Matsunaga, N.; Decker, S. A.; Cundari, T. R. *Inorg. Chem.* **2003**, *42* (20), 6204–6224.

(39) Eppinger, J.; Herdtweck, E.; Anwander, R. *Polyhedron*. **1998**, *17* (7), 1195–1201.

(40) Taylor, J. R. *An Introduction to Error Analysis: The Study of Uncertainties in Physical Measurements*, 2nd ed.; University Science Books: Sausalito, 1997.

(41) Gaussian 09, Revision D.01, M. J. Frisch, G. W. Trucks, H. B. Schlegel, G. E. Scuseria, M. A. Robb, J. R. Cheeseman, G. Scalmani, V. Barone, B. Mennucci, G. A. Petersson, H. Nakatsuji, M. Caricato, X. Li, H. P. Hratchian, A. F. Izmaylov, J. Bloino, G. Zheng, J. L. Sonnenberg, J. M. Hada, M. Ehara, K. Toyota, R. Fukuda, J. Hasegawa, M. Ishida, T. Nakajima, Y. Honda, O. Kitao, H. Nakai, T. Vreven, J. A. Montgomery, Jr., J. E. Peralta, F. Ogliaro, M. Bearpark, J. J. Heyd, E. Brothers, K. N. Kudin, V. N. Staroverov, R. Kobayashi, J. Normand, K. Raghavachari, A. Rendell, J. C. Burant, S. S. Iyengar, J. Tomasi, M. Cossi, N. Rega, J. M. Millam, M. Klene, J. E. Knox, J. B. Cross, V. Bakken, C. Adamo, J. Jaramillo, R. Gomperts, R. E. Stratmann, O. Yazyev, A. J. Austin, R. Cammi, C. Pomelli, J. W. Ochterski, R. L. Martin, K. Morokuma, V. G. Zakrzewski, G. A. Voth, P. Salvador, J. J. Dannenberg, S. Dapprich, A. D. Daniels, Ö. Farkas, J. B. Foresman, J. V. Ortiz, J. Cioslowski, D. J. Fox, Gaussian, Inc., Wallingford CT, 2009.

(42) Svensson, M.; Humbel, S.; Froese, R. D. J.; Matsubara, T.; Sieber, S.; Morokuma, K. *J. Phys. Chem.* **1996**, *100* (50), 19357–19363.

(43) Zhao, Y.; Truhlar, D. G. *Theor. Chem. Acc.* **2008**, *120* (1), 215–241.

(44) Casewit, C. J.; Colwell, K. S.; Rappe, A. K. *J. Am. Chem. Soc.* **1992**, *114* (25), 10046–10053.

CHAPTER 3

Probing Redox Non-Innocence with {(dadi)^{n}Ti(L/X)}^{n} Complexes, and a Stepwise Carbene Insertion into a CC Bond

Introduction:

The (dadi)^n chelate, ((dadi)^n = [{-CH=N(1,2-C_6H_4)NH(2,6-^{i}Pr$_2$-C_6H_3)}$_2$]^n (n = 0 to -4)), has been introduced as a redox non-innocent (RNI) ligand (*cf.* Chapter 1,2).[1,2] In an effort to generate reactive metal imidos, the reactivity of (dadi)M (M = Cr(THF), Fe) with organic azides was explored, where the RNI of the dadi ligand played a major role in the ensuing chemistry. Treatment of chromium and iron dadi complexes (dadi)M (M = Cr(THF), Fe) with alkyl- and aryl-azides did not result in isolable metal imidos. The nitrene (RN, R = adamantyl, 2,6-^{i}Pr$_2$-C_6H_3) produced from N_2 loss is not oxidizing enough to generate stable, higher oxidation states of the (dadi) ligand. Moreover the metal centers do not deviate from their preferred charge states of (Cr ~ +2.6, Fe +2)[3] and as a consequence, products derived from reactive imidyls were obtained.

According to calculations, the ground state of (dadi)Ti (**1**) is best ascribed as {(dadi)$^{3-}$}$^{\downarrow}$Ti(III)$^{\uparrow}$, but coordination of even weak donors such as THF, induces reduction to the (dadi)$^{4-}$ state. In contrast to the chromium and iron systems, the AdN (Ad = adamantyl) nitrene generated from AdN_3 is able to oxidize the dadi ligand from its -4 to -2 state. Starting from the (dadi)$^{4-}$ tetraanion, 2-electron redox cycles are supported, hence (dadi)Ti=X (X = O, NAd) can be isolated, which also exhibit group transfer capabilities (*cf*. Chapter 2).

Given the successes in generating multiply bonded titanium species (**2**=O, **2**=NAd) through oxidation, it was surmised that the generation of titanium alkylidenes would be feasible. (dadi)Ti(THF) (**1**-THF) is best decribed as a d^0 Ti(IV) center chelated by a tetraanionic $(dadi)^{4-}$ ligand. Common routes to access d^0-metal akylidenes includes promoting α-abstraction or α-deprotonation from metal-alkyls lacking β-hydrogens.[4–12] The use of the dadi ligand permits a divergence from these sometimes limiting methodologies. The RNI of the dadi ligand supports reactivity by maintaining the titanium center in favorable, higher oxidation states between +3 and +4, while storing electrons in the dadi π-type orbitals.

Reactivity studies were conducted to probe if (dadi)Ti (**1**) would support 2-electron oxidations to afford alkylidenes, similar to the formation of **2**=X (X = O, NAd). Through these studies, it was found that a titanium alkylidene is unlikely to be stable, as indicated by calculations, and instead direct carbene

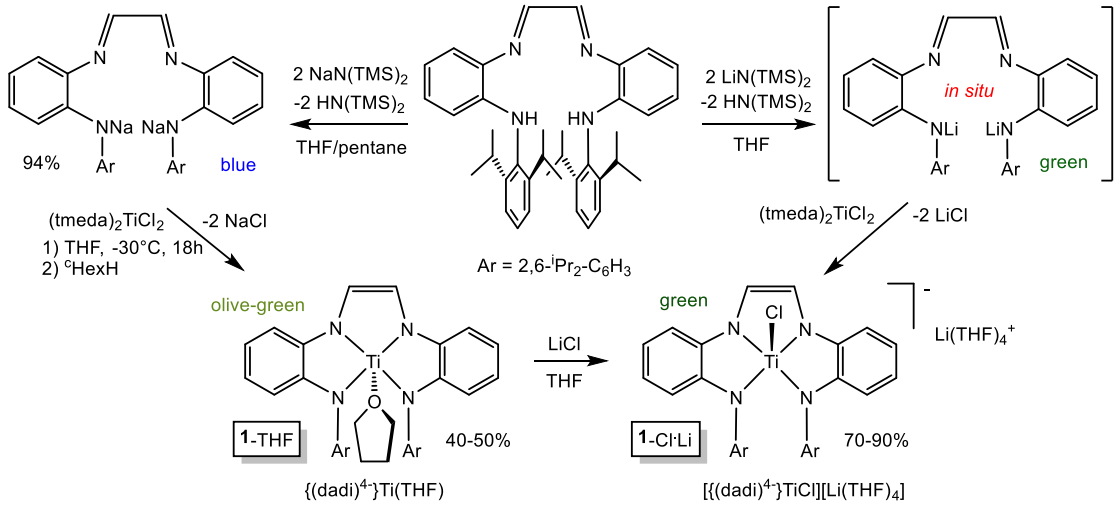

Scheme 3.1. Metatheses of $(tmeda)_2TiCl_2$ with $(dadi)M_2$ afforded different adducts depending on M.

transfer to the ligand occurs, yielding cycloproponated {PhC_3H_3(-NC_6H_4-2-$NAr)_2$}Ti(THF) (**3**, Ar = 2,6-$^{i}Pr_2$-C_6H_3). In addition, the dadi RNI was investigated through the synthesis of adducts $[(dadi)Ti(L/X)]^n$ (**1**-L, n = 0, N_2CPh_2; n = -1, X =Cl^-, N_3^-, O^iPr^-, CH_3^-, $^{neo}Pe^-$, $CH{=}CH_2^-$, $CCPh^-$, $CCTMS^-$, $H(D)^-$). Intimate Li^+ cation binding was also discovered, which manifests J_{LiC} for **1**-C_2Ph·Li and J_{LiH} for **1**-H·Li. This dadi-cation interaction was also studied with *via* DOSY diffusion experiments with **1**-H·Li, and X-ray crystallography for **1**-CH_3·Li.

Results and Discussion:

1.1. Adducts of (dadi)Ti (1)

*1.1.1. $[(dadi)Ti(L/X)]^n$ (X = Cl, n = -1, **1**-Cl·Li; L = THF, n = 0, **1**-THF)*

Initial attempts to generate (dadi)Ti (**1**) were conducted through *in situ* generation of Li_2(dadi), followed by addition of $(TMEDA)_2TiCl_2$,[13] as illustrated in Scheme 3.1. Incomplete metathesis resulted in the formation of the chloride adduct, [(dadi)TiCl][$Li(THF)_4$] (**1**-Cl·Li), that was isolated in ~90% yield as a black lustrous solid. Removal of the chloride anion from **1**-Cl·Li via repeated recrystallizations failed. Hence, a less soluble byproduct from metathesis, such as NaCl, was reasoned to be a route that would yield a chloride free adduct. Deprotonation of $dadiH_2$ ($dadiH_2$ = {-CH=N(1,2-C_6H_4)NH(2,6-$^{i}Pr_2$-C_6H_3)}$_2$) with 2 equiv sodium hexamethyldisilazide (NaHMDS) in THF generated $(dadi)Na_2$ as a vibrant blue crystalline solid upon precipitation with pentane (Scheme 3.1). Treatment of $(dadi)Na_2$ with $(TMEDA)_2TiCl_2$[13] in THF, at -30 ^{o}C for ~18 h, yielded (dadi)Ti(THF) (**1**-THF) as an olive-green microcrystalline solid.[2] Compared to the chloride, THF proved to be much

more labile, thus **1**-THF was used exclusively for subsequent reactivity studies.

1.1.2. Electronic structure of [(dadi)Ti(THF)] (1-THF)

Figure 3.1 portrays the truncated molecular orbital (MO) diagram for **1**-THF which resembles that of (dadi)Ti(PMe_2Ph) **1**-PMe_2Ph (*cf*. Chapter 2). The ligand field contains orbitals that are largely *3*d in character and are separated

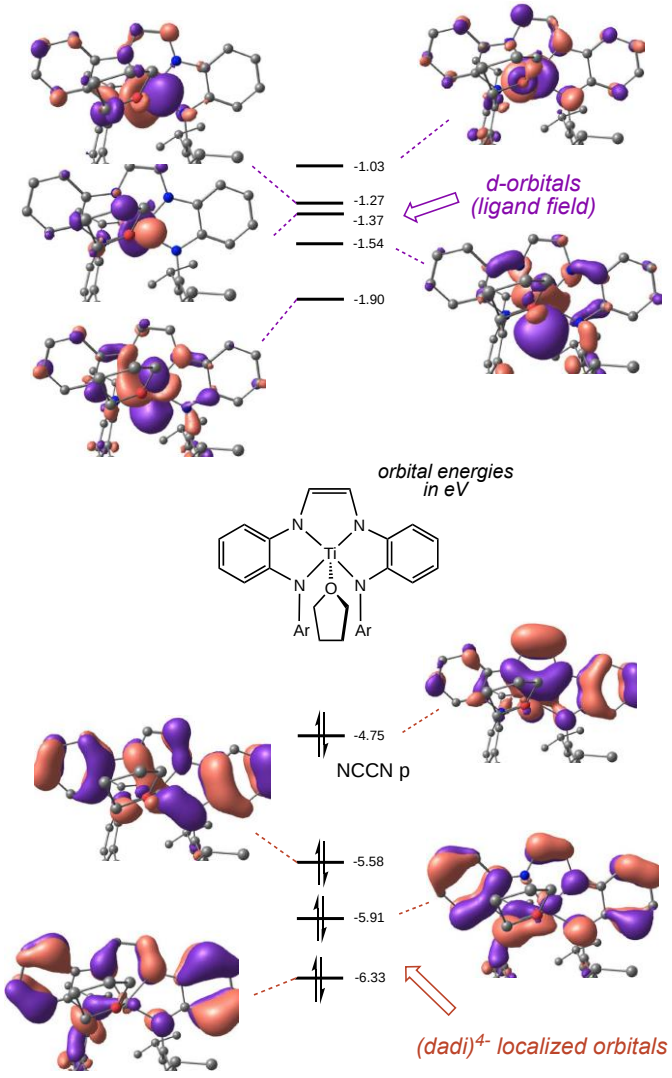

Figure 3.1. Truncated molecular orbital diagram of (dadi)Ti(THF) (**1**-THF), showing empty d-orbitals, and the four highest occupied $(dadi)^{4-}$ molecular orbitals.

from the rest of the dadi based orbitals. The calculated HOMO/LUMO gap of 2.85 eV in **1**-THF is similar to that for **1**-PMe_2Ph (2.96 eV). The LUMO appears to be a 3d-orbital of roughly xy-character, but the remaining unoccupied 3d-orbitals spanning 0.51 eV are difficult to assign, reflecting the low symmetry of the system. The HOMO, an orbital with backbone carbon-carbon double bond and diamide character, is 0.83 eV above the HOMO-1, an orbital that has significant density on the dadi aryl-rings. Overall, the MO diagram is consistent with the $(dadi)^{4-}$ formulation, where the HOMO is an NCCN π-orbital that is clearly double bond in character.

*1.1.3. [(dadi)Ti(L/X)]^n (**1**-L, n = 0, N_2CPh_2; n = -1, X = N_3^-, O^iPr^-, CH_3^-, $^{neo}Pe^-$, $CH{=}CH_2^-$, $CCPh^-$, $CCTMS^-$, $H(D)^-$)*

Displacement of the labile solvent molecule from (dadi)Ti(THF) (**1**-THF) permitted the preparation of a series of [(dadi)Ti(L/X)]^n (**1**-L, n = 0, -1) adducts. Scheme 3.2 illustrates the adducts, which were synthesized in THF in 40-90% yields as given. ^{1}H NMR spectroscopy serves as a diagnostic tool for the 5-coordinate environment at titanium, by virtue of observing four independent isopropyl-methyl groups. As previously discussed (*cf.* Chapter 2), the 2,6-^{i}Pr$_2$-C_6H_3 groups are roughly perpendicular to the basal plane of the dadi ligand, as defined by the four N-donors. Hence, the 2,6-^{i}Pr$_2$-C_6H_3 aryl groups are approximately aligned face-to-face, and rotation around the *ipso*-carbon is severely restricted by sterics upon coordination to a metal. This renders the isopropyl-methyls diastereotopic, which are observed as two doublets if two mirror planes are present, and four doublets when one mirror plane is present in the ^{1}H NMR spectrum. The latter is the case for 5-coordinate adducts, although the isopropyl-methyl doublets are often overlapping. When comparing the ^{1}H NMR chemical shifts of **1**-THF and **2**=X (X = O, NAd),

particularly the sp^2 backbone imine protons, the $(dadi)^{4-}$ and $(dadi)^{2-}$ redox forms of the ligand could not be distinguished *via* ^{1}H NMR spectroscopy (*cf*. Chapter 2). As expected, there is no significant difference in the ^{1}H NMR chemical shifts of the adducts, thus structural information is required to confidently asses the redox form of the dadi ligand.

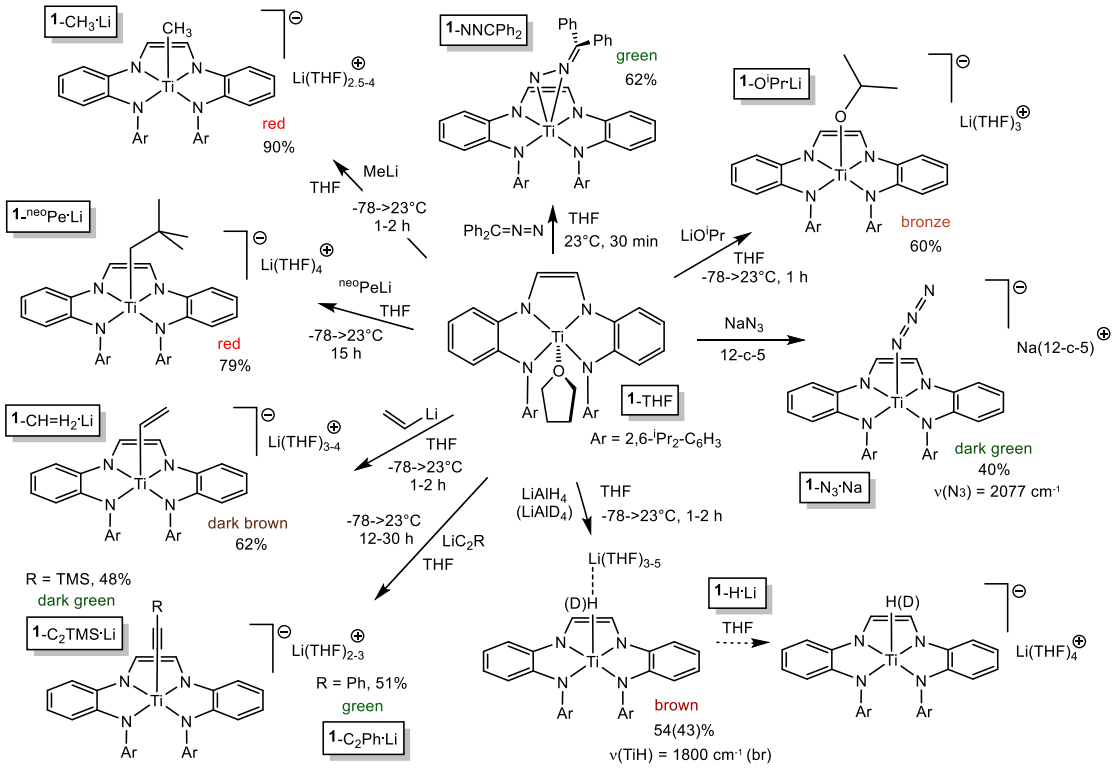

Scheme 3.2. Various adducts prepared from (dadi)Ti(THF) (**1**-THF) and suitable reagents in THF; precipitation or crystallization was from pentane in most cases. Ar = 2,6-iPr_2-C_6H_3.

1.1.4. Spectroscopic features of [(dadi)Ti(L/X)]^n

Treatment of **1**-THF with $Ph_2C{=}N{=}N$ failed to elicit the generation of N_2 and the diphenylalkylidene complex. As depicted in Scheme 3.2, the simple adduct (dadi)Ti(N=N=CPh_2) (**1**-NNCPh_2) was formed instead, which was isolated as a green solid in 62% yield. Calculations suggest that **1**-NNCPh_2 is

best described as an η^2-N_2CPh_2 adduct. Unfortunately, a variety of thermal and photochemical attempts to trigger dinitrogen loss from **1**-$NNCPh_2$ failed. Treatment of **1**-THF with sodium azide and 12-crown-5 formed the adduct [(dadi)Ti(N_3)]Na(12-crown-5) (**1**-N_3·Na), as indicated by a $\nu(N_3)$ at 2077 cm^{-1} in the IR spectrum. Additionally, its structure was corroborated by X-Ray crystallography (*vide infra*). Similarly, attempts to thermally or photochemically induce dinitrogen loss with hopes of generating the nitride anion [{(dadi)$^{2-}$}$Ti^{IV}N]^-$ were unsuccessful. The bronze-colored isopropoxide adduct [(dadi)Ti(O^iPr)][Li$(THF)_4$] (**1**-O^iPr·Li), is tentatively assigned as an ion pair in solution, due to the observation of four THF molecules that persist in benzene-d_6 solution.

As the X-ray crystal structure and some NMR spectra indicate (*vide infra*), the main group counterion can become an integral part of the dadi complex *via* binding to X^-, or through complexation to the $C_2N_2^{2-}$ fragment of the dadi^{4-} backbone. Hydrocarbyl derivatives display shifted ^{1}H and $^{13}C\{^1H\}$ NMR resonances upon complexation, accompanied by a color change from green to red/red-brown. The ^{1}H NMR spectrum of (dadi)Ti(CH_3)·Li$(THF)_2$ (**1**-CH_3·Li) manifests a singlet at δ 0.79 ppm for the methyl ligand. The $^{13}C\{^1H\}$ NMR spectrum of **1**-CH_3·Li displays a resonance at δ 36.07 ppm that is assigned to the Ti-CH_3 moiety. Normal ^{1}H NMR spectral shifts for the ^{neo}Pe group in (dadi)Ti(^{neo}Pe)·Li$(THF)_{2.4}$ (**1**-^{neo}Pe·Li) are observed at δ 1.21 (CH_2) and δ 0.89 (Me_3) ppm. In contrast, the $^{13}C\{^1H\}$ resonances are shifted considerably ($TiCH_2$, δ 86.83; C_β, δ 39.94; $(CH_3)_3$, δ 34.8) revealing structural ambiguities regarding the coordination mode of main group counterion.

The ^{1}H NMR spectrum of the vinyl derivative (**1**-$CH{=}CH_2$·Li) exhibits a non first-order ABX splitting pattern for the Ti-$CH{=}CH_2$ unit. Extraction of the

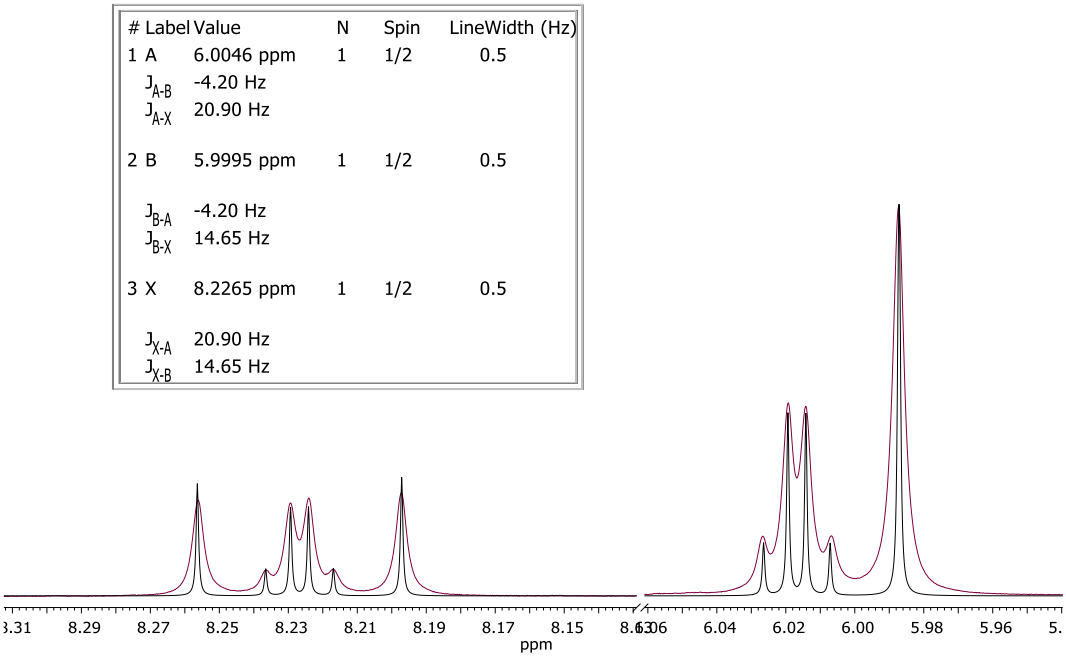

Figure 3.2. Simulated ^{1}H NMR spectrum of vinylic resonances (black) overlaid with experimental ^{1}H NMR spectrum of vinylic resonances (purple) for [(dadi)TiC$_2$H$_3$]Li(THF)$_{2.5}$ (**1**-CH=CH$_2$·Li); C$_6$D$_6$, 600 MHz, 295K. A = β–CH, B = β-CH, X = α-CH.

coupling constants required simulation of the vinyl resonances. Figure 3.2 displays the simulated spectrum overlaid with the experimentally observed vinyl resonances. The result of the spin simulation gave the following parameters: δ 8.2265, C$_\alpha$H, J_{trans} = 20.90 Hz; J_{cis} = 14.65 Hz; δ 6.0046, C$_\beta$H*H*, J_{trans} = 20.90 Hz, J_{gem} = -4.20 Hz; C$_\beta$*H*H at δ 5.9995, J_{cis} = 14.65 Hz, J_{gem} = -4.20 Hz. While no lithium-carbon coupling is observed in the vinyl derivative, the ^{13}C{^{1}H} NMR spectrum of [(dadi)TiCCPh][Li(THF)$_2$] (**1**-CCPh·Li) displays a quartet at δ 138.72 ppm with a J_{CLi} of 6.8 Hz, suggesting a significant C$_\alpha$-Li interaction in benzene-d_6. Curiously, no coupling was observed for C$_\beta$ (δ 142.69 ppm), nor was any lithium-carbon coupling observed in the trimethylsilylacetylide congener, [(dadi)TiCCSiMe$_3$][Li(THF)$_2$] (**1**-CCTMS·Li).

The C_α-shift for the latter (δ 162.27 ppm in benzene-d_6) is at considerably lower field than the phenylacetyllide derivative, suggesting that there is no significant lithium-carbon interaction in **1**-CCTMS·Li, or that it is fluxional on the NMR time-scale.

*1.1.5. Spectroscopic and dynamic solution behavior of (dadi)TiHLi (**1**-H·Li)*

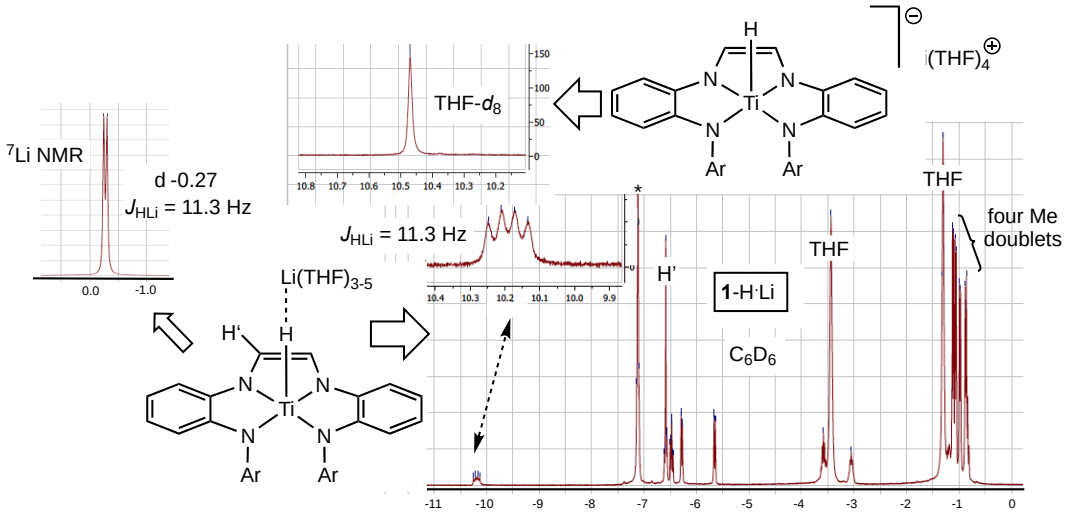

Figure 3.3. The hydride anion, [(dadi)TiH][Li(THF)$_3$] (**1**-H·Li), showing J_{HLi} coupling in C_6D_6 (^{1}H and ^{7}Li NMR) that is lost in THF-d_8 (insets upper left). The four Me doublets indicate 5-coordination, and the remaining unlabeled resonances are aryl or Me_2CH signals.

The hydride anion, [(dadi)TiH][Li(THF)$_x$] (**1**-H·Li, x = 3-5) exhibits a quartet at δ 10.22 ppm (J_{HLi} = 11.3 Hz, ^{7}Li (I = 3/2, 92.5-96%)) in the ^{1}H NMR spectrum (Figure 3.3), which is assigned to the hydride resonance. Initially, this assignment was tentative, and despite the resonance integration corresponding to only 1 proton, additional experiments were required to distinguish between **1**-H·Li and a potential η^1-AlH_4 complex. Hence, the ^{7}Li NMR spectrum was taken in benzene-d_6, revealing a clear doublet with the requisite 11.3 Hz coupling, which collapses to a singlet in the ^{7}Li{^{1}H} NMR

spectrum. In THF-d_8, the hydride resonance appears as a broad ($\Delta\nu_{1/2}$ ~ 4 Hz) singlet at δ 10.47 ppm, which was absent in the ^{1}H NMR spectrum of the corresponding deuteride (**1**-D·Li). The IR spectrum of **1**-H·Li displays an absorption at 1800 cm^{-1} (ν(TiH)). Unfortunately, no clear ν(TiD) is observed for

	^{1}H (δ) C_6D_6	D(cm^2/s) (x 10^6)	^{1}H (δ) THF-d_8	D(cm^2/s) (x 10^6)	^{7}Li (δ)	D(cm^2/s) (x 10^6)
	0.9	4.13(3)	0.84	5.00(3)	-0.27 (C_6D_6)	5.2(1)
	1.01	4.04(3)	3.21	5.2(1)	-0.49 (THF-d_8)	5.5(4)
	1.09	4.11(3)	5.18	4.9(2)		
	1.14	4.10(3)	6.05	5.0(2)		
	1.32[c]	8.9(9) 67%	6.18	4.9(2)		
		4.6(9) 33%	6.24	4.9(2)		
	3.08	4.0(1)	6.44	4.9(2)		
	3.45[c]	8.7(6) 73%	6.89	4.85(4)		
		4.5(9) 27%	10.46	4.9(3)		
	3.61	4.5(1)				
	5.68	4.1(1)				
	6.31	4.10(6)				
	6.5	4.1(1)				
	6.63	4.10(3)				
	10.22	4.1(2)				
Ave.	4.1(2) [d]			5.0(5)		

Table 3.1. [a]Diffusion coefficients were measured using double pulsed gradient stimulated spin-echo (DPGSE) experiments with convection compensation using the DgscsteSL_cc or Dbppste_cc pulse sequence as provided in VnmrJ 3.2 at 295 K. The ^{7}Li signal in C_6D_6 was ^{1}H-decoupled. The following parameter values were used: ^{1}H nucleus, δ = 0.0018 sec, Δ = 0.1244 sec; ^{7}Li nucleus, δ = 0.004 sec, Δ = 0.0987 sec. Gradient strength was varied from 2.1 to 58.6 Gauss/cm in 24 linear increments. [b]D was determined from plots of $\ln(I/I_o)$, the integrated intensities, vs $\delta^2\gamma^2(\Delta-\delta/3)G^2$, where the constants have their usual definitions; see experimental section for the relevant equations and details. Igor Pro was used for the fits and the reported errors. [c]Deviation from linear behavior was observed, indicating free and bound THF in C_6D_6 prompting bi-exponential decay fits. [d]THF (bi-exponentially determined D's) not included.

the deuteride, although subtle changes in the fingerprint region are observed near the 1270 cm^{-1}, as would be expected for **1**-D·Li.

The coupling observed between the lithium and hydride nuclei in benzene-d_6 suggests the lithium-hydride bond in [(dadi)TiH][Li(THF)$_2$] (**1**-H·Li) has significant covalency in solution. When dissolved in THF-d_8, the coupling is disrupted, prompting several possible explanations: 1) the rate of intermolecular lithium exchange is fast on the NMR time scale, effectively decoupling the hydride and lithium resonances; 2) the lithium is solvated by THF, but exists as a tight ion-pair; and 3) THF completely solvates the lithium separating it from the [(dadi)TiH]$^-$ anion.

The many resonances attributable to (dadi)^n permit significant redundancy in the measurement of diffusion coefficients by the gradient method (Figure 3.4), and these are listed along with average diffusion coefficients in Table 3.1. It should be noted that the uncertainties for the ^{7}Li resonances were approximated from the baseline noise across the spectra. In benzene-d_6, the linearization of the data corresponding to the THF resonances revealed significant curvature, suggesting the presence of two types of THF species in solution. The satisfactory fits using a bi-exponential decay function are consistent with free (~ 67%, D = 8.7(6) x 10^{-6} cm^2/sec) and bound (~ 33%, D = 4.6(9) x 10^{-6} cm^2/sec) THF molecules diffusing in solution.

As shown in Table 3.1, the ^{7}Li diffusion coefficients of 5.2(1) x 10^{-6} and 5.5(4) x 10^{-6} cm^2/sec in benzene-d_6 and THF-d_8, respectively, do not differ significantly, suggesting the lithium is associated with the dadi complex in either solvent. Furthermore, the average diffusion coefficients for the dadi ligand of 4.1(2) x 10^{-6} and 5.0(5) x 10^{-6} cm^2/sec in benzene-d_6 and THF-d_8, respectively, are on the same order of magnitude as those observed for the lithium, providing further evidence that it is associated with the dadi complex in THF solution. These observations are inconsistent with a fully solvated and

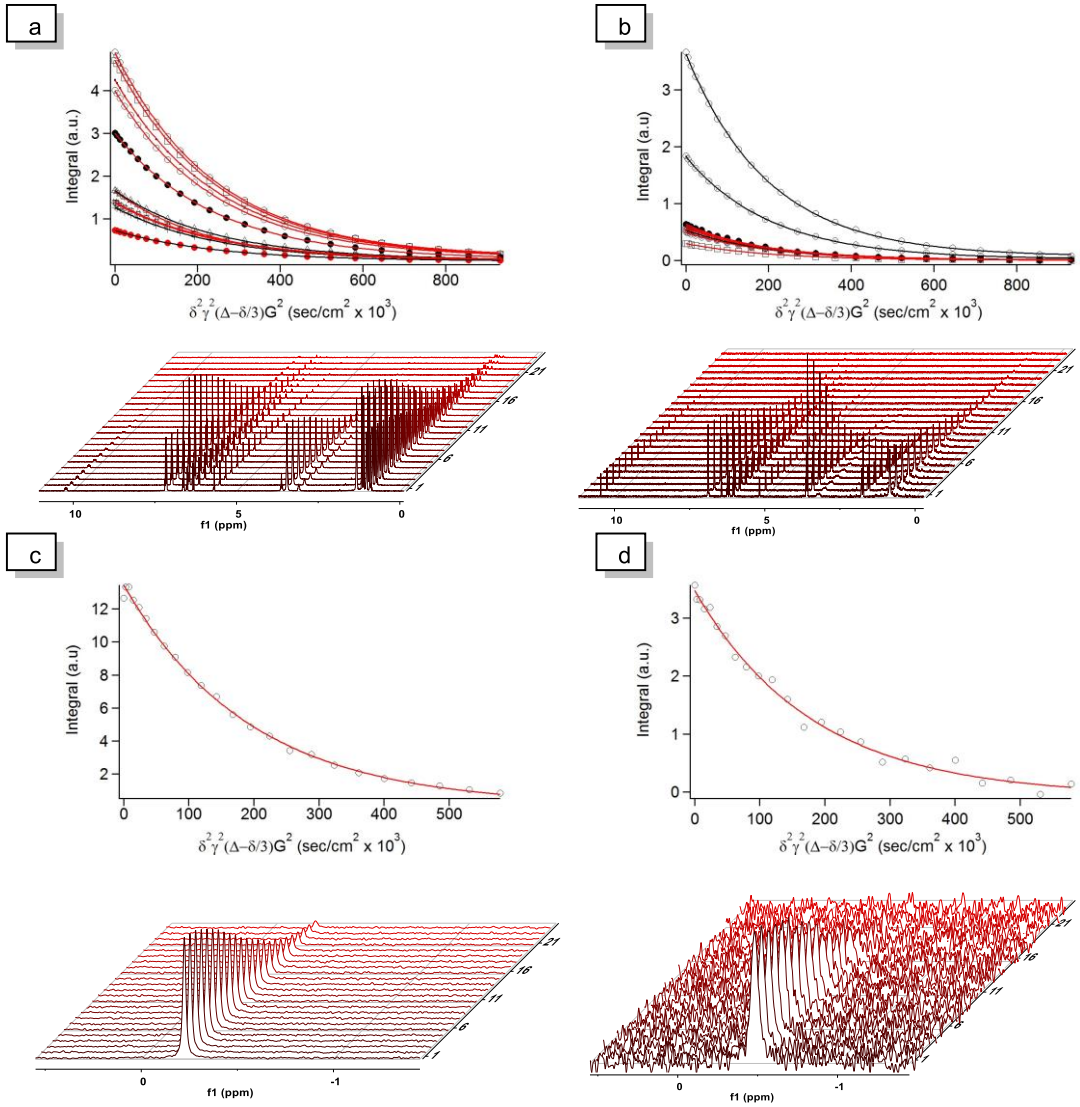

Figure 3.4. [a] Integrations of ligand ^{1}H resonances versus $\delta^2\gamma^2(\Delta-\delta/3)G^2$ with corresponding fits (solid lines), and stacked spectra in C_6D_6, 295 K, 500 MHz. [b] Integrations of ligand ^{1}H resonances versus $\delta^2\gamma^2(\Delta-\delta/3)G^2$ with corresponding fits (solid lines), and stacked spectra in THF-d_8, 295 K, 500 MHz. [c] Integrations of ligand ^{7}Li resonance versus $\delta^2\gamma^2(\Delta-\delta/3)G^2$ with corresponding fit (solid line) and stacked spectra in C_6D_6, 295 K, 194 MHz. [d] Integrations of ligand ^{7}Li resonance versus $\delta^2\gamma^2(\Delta-\delta/3)G^2$ with corresponding fit (solid lines) and stacked spectra in THF-d_8, 295 K, 194 MHz.

separated $Li^+(THF)_n$ cation, but are consistent with a tight ion pair, or integral HLi bonding in THF, but with fast exchange. It is also possible that this exchange is occurring in benzene-d_6 but the rate is slow on the NMR time

scale (*i.e.*, < ~ $1/J_{LiH}$ = 0.1 sec), preserving coupling between the hydride and lithium resonances.

*1.1.6. Structure of [(dadi)Ti(N_3)]Na(12-crown-5) (**1**-N_3·Na)*

Figure 3.5 portrays the solid state structure of [(dadi)Ti(N_3)]Na(15-crown-5) (**1**-N_3·Na), revealing a pseudo square pyramidal coordination geometry around titanium and a sodium counterion chelated by a crown ether and two THF molecules. Despite the asymmetric unit containing four molecules of **1**-N_3·Na, which are each accompanied by disordered THF and

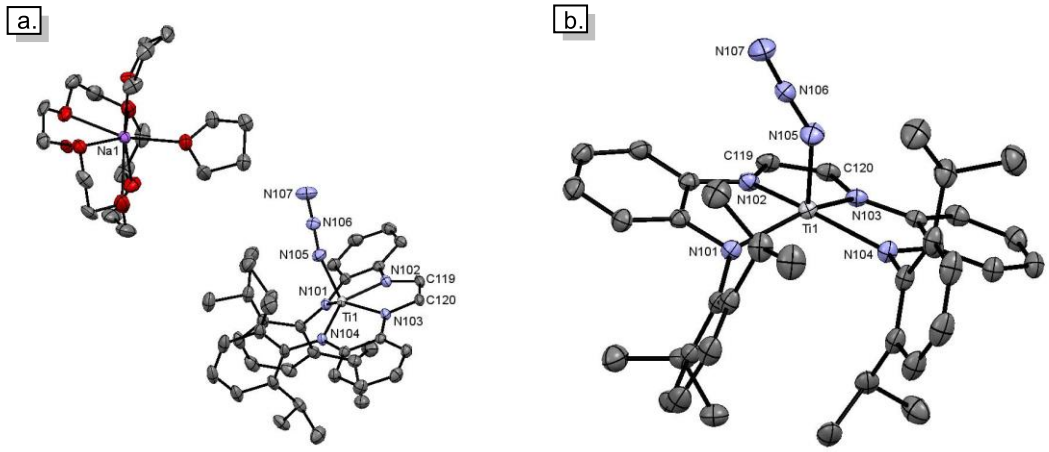

Figure 3.5. Molecular structure of **1**-N_3·Na. (a.) One molecule from the asymmetric unit with counterion; (b.) core view of one molecule from the asymmetric unit. Hydrogens along with disordered 12-crown-5 and THF molecules omitted for clarity. Table 3.2 contains selected average distances, while its average core angles (°) are: $N_{\alpha\text{-Azide}}$-Ti-N_{am}, 103.33(6); $N_{\alpha\text{-Azide}}$-Ti-$N_{am'}$, 102.72(6); $N_{\alpha\text{-Azide}}$-Ti-N_{im}, 99.06(6); $N_{\alpha\text{-Azide}}$-Ti-$N_{im'}$, 108.84(6); N_{am}-Ti-$N_{am'}$, 119.22(5); N_{am}-Ti-N_{im}, 77.53(5); $N_{am'}$-Ti-$N_{im'}$, 77.74(5); N_{im}-Ti-$N_{im'}$, 73.21(5); N_{am}-Ti-$N_{im'}$, 140.65(5); $N_{am'}$-Ti-N_{im}, 146.41(5).

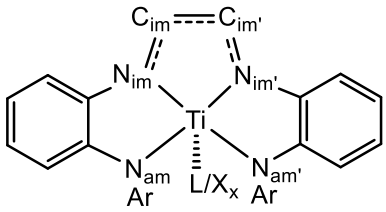

cmpd	TiN_{im}	TiN_{am}	$C_{im}C_{im}$	$C_{im}N_{im}$	C^1N_{am}	C^1C^2	C^2N_{im}	TiL/X
1-N_3·Na (ave)[a]	2.031(1)	2.017(1)	1.350(2)	1.384(2)	1.402(2)	1.419(2)	1.389(2)	1.983(2)
	2.027(1)	2.017(1)		1.383(2)	1.402(2)	1.149(2)	1.389(2)	
1-CH_3·Li[b]	2.021(2)	2.002(2)	1.348(2)	1.383(2)	1.414(2)	1.398(2)	1.397(2)	2.133(2)
	2.060(2)	2.020(2)		1.393(2)	1.407(2)	1.416(2)	1.400(2)	
	2.016(2)	2.014(2)	1.349(2)	1.385(2)	1.407(2)	1.415(2)	1.394(2)	2.131(2)
	2.056(2)	2.016(2)		1.392(2)	1.404(2)	1.419(2)	1.403(2)	
1-PMe_2Ph[c]	2.019(2)	2.003(2)	1.338(3)	1.379(3)	1.411(3)	1.413(3)	1.396(3)	2.605(2)
	2.033(2)	2.009(2)		1.381(3)	1.406(3)	1.408(3)	1.396(3)	
1-$(CNMe)_2$[c]	2.033(2)	2.064(2)	1.350(3)	1.373(2)	1.396(2)	1.418(3)	1.403(2)	2.236(2)
	2.035(2)	2.068(2)		1.371(2)	1.395(2)	1.423(2)	1.401(2)	2.248(2)
1-Cl·Li[d]	1.999(4)	2.008(4)	1.343(7)	1.371(6)	1.402(6)	1.411(6)	1.391(6)	2.310(2)
	2.044(4)	2.018(4)		1.382(6)	1.422(5)	1.413(6)	1.392(6)	
1-L_x (ave)[e]	2.031(22)	2.021(22)	1.346(3)	1.381(3)	1.406(3)	1.392(3)	1.396(3)	
2=NAd[b]	2.172(5)	2.122(5)	1.436(8)	1.297(8)	1.373(7)	1.413(8)	1.389(8)	1.702(5)
	2.193(5)	2.084(5)		1.293(7)	1.384(8)	1.425(8)	1.402(7)	
	2.166(5)	2.074(5)	1.428(9)	1.303(8)	1.374(7)	1.420(8)	1.386(8)	1.702(5)
	2.200(5)	2.121(5)		1.300(8)	1.375(7)	1.418(8)	1.376(8)	
2=O[c]	2.160(2)	2.054(2)	1.433(2)	1.297(2)	1.377(2)	1.419(2)	1.395(2)	1.636(2)
	2.194(2)	2.064(2)		1.301(2)	1.375(2)	1.418(2)	1.388(2)	
2=X (ave)[f]	2.181(17)	2.087(29)	1.432(4)	1.299(4)	1.376(4)	1.419(4)	1.389(9)	

Table 3.2. [a]Average of four molecules in asymmetric unit. [b]Two molecules per asymmetric unit. [c]Ref.[2]. [d]Ref. 14 [e]Average of all {(dadi)$^{4-}$}TiL_x (1-L_x) distances. [f]Average of all {(dadi)$^{2-}$}Ti=X (**2**=X) distances.

15-crown-5 molecules, the data set was satisfactorily refined in the triclinic *P-1* space group. The core metric parameters around the titanium are listed in Table 3.2 and data refinement details are included in Table 3.3.

The four Ti-N distances (2.023(1) Å ave) are consistent with four amide donors and the $(dadi)^{4-}$ formulation. Examination of the metrics within the NCCN backbone reveals single CN bonds (d(CN) = 1.384(2) Å (ave)) accompanied by a double CC bond (d(CC) = 1.350(2) Å (ave)), which is in line with the $(dadi)^{4-}$ redox state and an ene-diamide backbone. As seen with other five-coordinate $(dadi)^{n}Ti(L/X)$ complexes, the titanium center sits out of the basal plane by ~0.463 Å, and the angle between the two aryl amides is contracted compared to six-coordinate $(dadi)^{n}Ti(L/X)_2$ complexes (*cf.* Chapter 2, 4) to 119.223(5)°. The titanium-azide angle differs by 13° across the four molecules in the asymmetric unit, ($\angle Ti\text{-}N_{\alpha}\text{-}N_{\beta}$ = 140.13(9)°, 145.15(9)°, 148.23(9)°, 153.23(9)°). The $N_{\alpha\text{-azide}}$ ($N_{\alpha\text{-azide}}$ = N(105,205,305,405)) atom is canted toward the aryl-amide nitrogen (N(101,201,304,401)) that sits below the plane of the three other N-donors, hence the difference in titanium-azide angles is likely to be steric in origin. The rest of the ligand metrics do not deviate significantly, and relevant core angles are listed in Figure 3.5.

*1.1.7. Structure of [(dadi)TiCH$_3$][Li(THF)$_2$] (**1**-CH$_3$·Li)*

Attempts to obtain X-ray quality crystals of most adducts of (dadi)Ti (**1**) often resulted in the formation of thin plates or crystals with severe twinning issues. Fortunately, repeated efforts led to a successful crystal structure determination of [(dadi)TiCH$_3$][Li(THF)$_2$] (**1**-CH$_3$·Li), which has two molecules in the asymmetric unit. Figure 3.6 portrays the methyl adduct, and selected

refinement details with comparative metric parameters are listed in Tables 3.2 and 3.3, respectively.

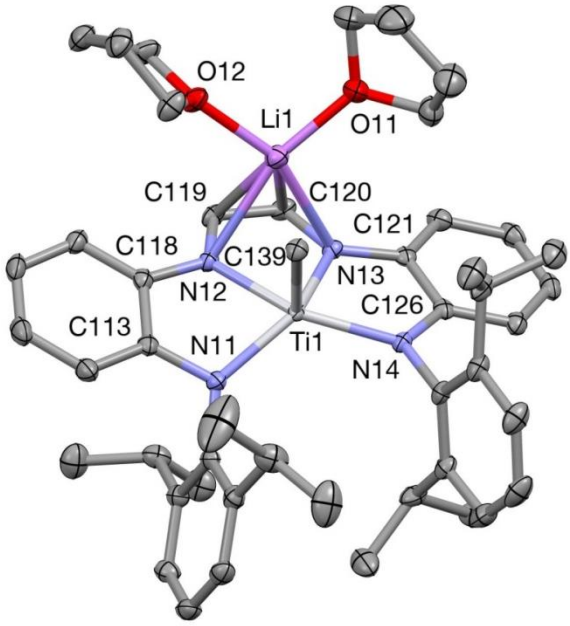

Figure 3.6. A view of one of the two molecules of [(dadi)TiCH$_3$][Li(THF)$_2$] (**1**-CH$_3$·Li) in the asymmetric unit. Table 3.2 contains selected average distances, while its core angles (°) are: C-Ti-N(11,21), 97.03(5), 96.58(5); C-Ti-N(14,24), 103.33(5), 102.31(5); C-Ti-N(12,22), 94.73(5), 94.81(5); C-Ti-N(13,23), 110.03(5), 105.88(5); N(11,21)-Ti-N(12,22), 79.10(4), 78.74(4); N(11,21)-Ti-N(13,23), 141.73(4), 144.67(4); N(11,21)-Ti-N(14,24), 123.94(4), 125.41(4); N(12,22)-Ti-N(13,23), 72.35(4), 72.60(4); N(12,22)-Ti-N(14,24), 147.70(4), 147.60(4); N(13,23)-Ti-N(14,24), 76.35(4), 76.33(4).

1-CH$_3$·Li is a pseudo-square pyramidal species exhibiting additional coordination of the main group counterion to the ene-diamide backbone of the dadi ligand. The coordination environment of the lithium is capped with two additional THF molecules displaying typical lithium-oxygen interactions (d(Li-O) = 1.934(17) Å (ave)). As with the other 5-coordinate (dadi)Ti(L/X)^n complexes (*cf.* Chapter 2, *vide infra*), the titanium is out of the N$_4$-plane by ~0.363 Å (ave) resulting in C$_{Me}$-Ti-N angles that are >90°. The methyl group is tilted away from the arylamides (∠C$_{Me}$-Ti-N = 105.4(34)° (ave)), and canted toward the ene-diamide (∠C$_{Me}$-Ti-N = 95.8(12)° (ave)) backbone. The ene-

diamide bite angle of ∠N(12,22)-Ti-N(13,23) = 72.48(18)° (ave), and opposing aryl-amide angle of ∠N(11,21)-Ti-N(14,24) = 127.7(32)° (ave) do not differ significantly compared to 1-N_3·Na. Moreover, the ene-amide/arylamide bite angles (∠N(11,21)-Ti-N(12,22) = 79.9(3)° (ave); ∠N(13,23)-Ti-N(14,24) = 76.34(2)° (ave)) are consistent with those observed in 1-N_3·Na.

	1-N_3·Na[a]	**1**-CH_3·Li	**3**[b]	**4**[c]
formula	$C_{56}H_{80}N_7O_7NaTi$	$C_{47}H_{63}N_4O_2LiTi$	$C_{59}H_{82}N_4OTi$	$C_{62}H_{70}N_6OTi$
formula wt	1034.16	770.85	911.18	963.14
space group	P-1	$P2_1/c$	P-1	$P2_1/n$
Z	8	8	2	4
a, Å	17.56594(7)	24.7609(3)	13.2345(3)	17.40700(10)
b, Å	18.96752(6)	14.7825(2)	14.2250(3)	14.19110(10)
c, Å	35.94505(12	25.4230(3)	15.1880(3)	21.8908(2)
α, deg	94.9017(3)	90	88.071(2)	90
β, deg	97.4404	111.750(2)	80.073(2)	102.9310(10)
γ, deg	109.1952(3)	90	70.364(2)	90
V, $Å^3$	11109.88(7)	8643.1(2)	2651.80(10)	5270.43(7)
ρ_{calc}, $g \cdot cm^{-3}$	1.237	1.185	1.141	1.214
μ, mm^{-1}	1.834	0.239	0.204	1.735
temp, K	100.00(10)	100.01(11)	100.01(10)	100.00(10)
λ (Å)	1.54184	0.71073	0.71073	0.71073
R indices [$I > 2\sigma(I)$][d,e]	R_1 = 0.0460	R_1 = 0.0361	R_1 = 0.0385	R_1 = 0.0375
	wR_2 = 0.1273	wR_2 = 0.0954	wR_2 = 0.1025	wR_2 = 0.1020
R indices (all data)[d,e]	R_1 = 0.0483	R_1 = 0.0415	R_1 = 0.0445	R_1 = 0.0416
	wR_2 = 0.1294	wR_2 = 0.0985	wR_2 = 0.1059	wR_2 = 0.1048
GOF[f]	1.028	1.059	1.075	1.067

Table 3.3. [a]Contains disordered THF and 15-crown-5 molecules. [b]Contains two pentane molecules of crystallization. [c]Contains one Et_2O molecule of crystallization. [d]$R_1 = \Sigma||F_o| - |F_c||/\Sigma|F_o|$. [e]$wR_2 = [\Sigma w(|F_o| - |F_c|)^2/\Sigma wF_o^2]^{1/2}$. [f]*GOF* (all data) = $[\Sigma w(|F_o| - |F_c|)^2/(n - p)]^{1/2}$, *n* = number of independent reflections, *p* = number of parameters.

The titanium-carbon distance of 2.1318(16) Å (ave) is close to the sum of the covalent radii (2.08 Å).[15] The core d(Ti-N_{am}) distance of of 2.012(8) Å

(ave), accompanied by d(Ti-N_{im}) distances of 2.019(4) and 2.058(3) Å (ave), both support the tetranionic $(dadi)^{4-}$ ligand formulation. In the ligand backbone, the average CN_{imine} distance is 1.388(5) Å, and the average CC bond length is 1.3487(6) Å, which are consistent with C-N single and CC double bonds, respectively. The lithium appears to be weakly bound to the ene-diamide backbone, as indicated by Li-$N_{im/im`}$ and Li-$C_{im/im`}$ distances of 2.417(36) Å (ave) and 2.387(36) Å, respectively. The two distinct molecules of **1**-CH_3·Li possess different d(C_{Me}-Li) distances at 2.625(3) and 2.421(3) Å, which are greater than the sum of their respective covalent radii (~ 2.00 Å),[15] but well within the sum of their van der Waals radii (~3.5 Å).[16]

1.1.8. Lithium-dadi interactions

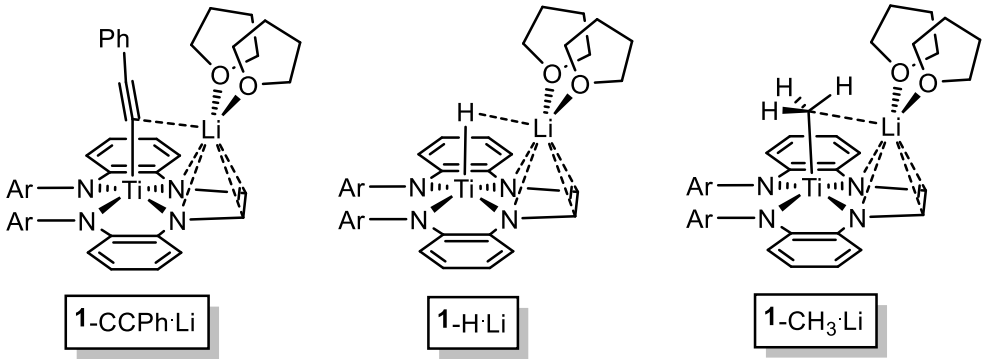

Figure 3.7. Plausible structures of complexes exhibiting $J_{Li(C/H)}$ based on the crystal structure of [(dadi)$TiCH_3$][Li$(THF)_2$] (**1**-CH_3·Li).

Evidence of intimate lithium bonding in solution, for [(dadi)TiCCPh][Li$(THF)_2$] (**1**-CCPh·Li), comes from the observation of J_{LiC} (6.9 Hz) in the $^{13}C\{^1H\}$ NMR spectrum. The aforementioned gradient diffusion experiments in conjunction with the observed lithium-hydride coupling support the contention that the main group conterion may be directly bound in [(dadi)TiH][Li$(THF)_{3\text{-}5}$] (**1**-H·Li) when in solution. Based upon the solid state

structure of [(dadi)TiCH$_3$][Li(THF)$_2$] (**1**-CH$_3$·Li), which clearly shows lithium bound to the dadi ligand, potential structures of these species are shown in Figure 3.7. It is interesting that the alkyl complexes [(dadi)TiR][Li(THF)$_2$] (**1**-R·Li, R = Me, ^{neo}Pe) do not manifest lithium-carbon coupling, and it may be that the *sp*^{3} and *sp*^{2} (*e.g.,* [(dadi)TiCH=CH$_2$][Li(THF)$_2$] (**1**-CH=CH$_2$·Li) constituents lack the orbital overlap for significant interaction. The modest CH$_3$···Li contact is supported by the crystal structure of **1**-CH$_3$·Li, and the *s*- and *sp*-interactions in the hydride (**1**-H·Li) and phenylacetylide (**1**-CCPh·Li) complexes, respectively, may allow enough orbital overlap for $J_{Li(C/H)}$ to be observed.

1.2. Cyclopropanation of dadi^{4-}

*1.2.1. Synthesis of {PhC$_3$H$_3$-2,3-NC$_6$H$_4$-2-Ar)}Ti(THF) (**3**)*

The successful synthesis of titanium imido complex (dadi)Ti=NAd (**2**=NAd) from treating **1**-THF with AdN$_3$ suggested that titanium alkylidenes could similarly be formed. The initial attempts to form alkylidene species included protonation of **1**-CH=CH$_2$·Li and hydride abstraction from **1**-CH$_3$·Li, both of which failed to form the desired (dadi)Ti=CHR (R = Me, H) complexes. Thus, a more conventional route *via* diazoalkanes was attempted. As depicted in Scheme 3.2, treatment of **1**-THF with diphenyldiazomethane resulted in the formation of the aforementioned adduct (**1**-NNCPh$_2$), prompting a switch to the more reactive PhHCN$_2$ alkylidene precursor. Addition of PhHCN$_2$ to a THF solution of **1**-THF at -78 °C generated a red complex with a cyclopropanated backbone, PhC$_3$H$_3$-(NC$_6$H$_4$-2-NAr)$_2$}Ti(THF) (**3**, Ar = 2,6-^{i}Pr$_2$-C$_6$H$_3$), in 70% yield. The ^{1}H NMR spectrum of **3** indicated assimilation of PhHCN$_2$, and retention of one molecule of THF. The observed mirror plane, indicative of a 5-

coordinate titanium center, with the loss of the imine singlet of **1**-THF and the appearance of a triplet (δ 3.12 ppm) and a doublet (δ 3.90 ppm) integrating to one and two protons, respectively, are consistent with cyclopropanation of the backbone olefin and coordination of THF to the titanium center.

An attempt using variable temperature (VT) ^{1}H NMR spectroscopy was made to detect possible intermediates *en route* to (**3**), such as a $PhCN_2$ adduct, or a (dadi)Ti=CHPh species. Between -100 and -80 °C, broad and unchanging resonances were observed in THF-d_8. Upon warming to -65 °C, broad resonances were still observed, but ~60% conversion to the product PhC_3H_3-$(NC_6H_4$-2-$NAr)_2\}$Ti(THF) (**3**) was apparent. Further warming to -55 °C revealed total conversion to one dominant isomer (>95%). From these VT ^{1}H NMR experiments, the barrier to form (**3**) was approximated to be ~15 kcal/mol.

*1.2.2. Structure of PhC_3H_3-$(NC_6H_4$-2-$NAr)_2\}$Ti(THF) (**3**)*

As Figure 3.8 reveals, the $(CH)_2N_2$ backbone of the $(dadi)^{4-}$ ligand has indeed been cyclopropanated, yielding PhC_3H_3-$(NC_6H_4$-2-$NAr)_2\}$Ti(THF) (**3**), consistent with that observed by ^{1}H NMR spectroscopy. The major isomer is that in which the phenyl group is oriented toward the titanium core, with the proton originating from the “carbene” directed away. The titanium-nitrogen distances of 2.003(16) Å (ave) are consistent with four amide donors. The titanium is slightly out of the basal plane by ~0.3 Å, as the O-Ti-N angles are all greater than 90°. The THF is oriented away from the aryl-amides (O-Ti-N(1,2) = 104.94(4), 100.32(4)), likely a consequence of sterics. The usual arylamide-titanium-arylamide angle of 120.63(4)° is observed, along with phenylene-diamide bite angles of 78.85(4)° and 77.78(4)°, which are

accompanied by the “diimine” bite angle of 75.72(4)°. The distances and angles are appropriate within the cyclopropane unit, along with standard metric parameters for a tetraamide chelate.

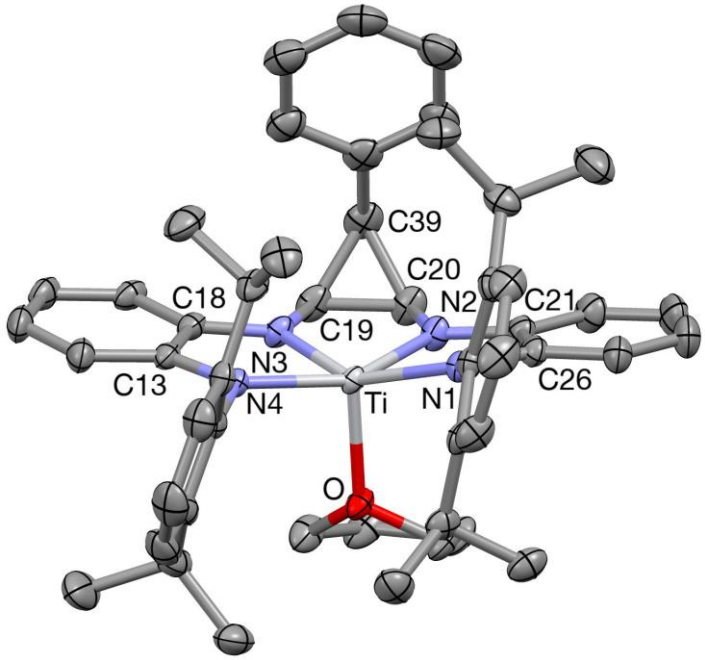

Figure 3.8. A molecular view of {PhC_3H_3(-NC_6H_4-2-Ar)$_2$}Ti(THF) (**3**, Ar = 2,6-^{i}Pr$_2$-C_6H_3). Selected interatomic distances (Å) and angles (°): Ti-O, 2.0796(9); Ti-N1, 2.0228(10); Ti-N2, 1.9892(11); Ti-N3, 1.9915(10); Ti-N4, 2.0089(10); N3-C19, 1.4364(17); N2-C20, 1.4292(17); C19-C20, 1.495(2); C19-C39, 1.518(2); C20-C39, 1.518(2); O-Ti-N1, 104.94(4); O-Ti-N2, 93.64(4); O-Ti-N3, 96.83(4); O-Ti-N4, 100.32(4); N1-Ti-N2, 78.85(4); N1-Ti-N3, 147.35(5); N1-Ti-N4, 120.63(4); N2-Ti-N3, 75.72(4); N2-Ti-N4, 151.29(4); N3-Ti-N4, 77.78(4).

*1.2.3. Synthesis of {PhC(CNC$_6$H$_4$-2-NAr)$_2$}Ti(η^2-HNNCPh$_2$) (**4**)*

The strained cyclopropane ring of (**3**) can be envisioned as a moiety capable of storing electrons in a redox non-innocent fashion, *via* a reversible ring-opening/closing process. Attempts were made to probe the ability of the cyclopropanated dadi to act as a RNI ligand through reversible CC bond formation. First, the thermal stability of (**3**) was tested by heating a solution of (**3**) in benzene-d_6 to 55 °C, which resulted in a mixture of products that

unfortunately could not be identified. Loss of the diagnostic cyclopropane triplet and doublet resonances in the ^{1}H NMR spectrum suggested that ring-opening or isomerization was occurring. Treatment of (**3**) with potential oxidants such as AdN_3 and adamantyl diazirine[17] gave complex mixtures of products that were unidentifiable, but the ^{1}H NMR spectra of the crude reaction mixtures indicated the integrity of the cyclopropane ring had been lost. The presence of the β-H on the cyclopropane ring in (**3**) was thought to be problematic for a reversible ring-opening/closing cycle, as transfer of the hydrogen to substrate or β-H elimination would generate a nacnac backbone, which is predicted to be irreversible.

Treatment of (**3**) with diphenyl diazomethane led to the formation of one major product (>90%), exhibiting spectroscopic features consistent with nacnac formation in the product {PhC(CNC$_6$H$_4$-2-NAr)$_2$}Ti(η^2-HNNCPh$_2$) (**4**). The IR spectrum of (**4**) indicated the presence of an NH group (ν(NH) = 3303 cm^{-1}), and the ^{1}H NMR spectrum revealed the loss of a cyclopropane hydrogen, and a product that was dissymmetric. These results suggest that transfer of the cyclopropane β-H may hinder reversible RNI behavior, but provide a model to how C-C bond formation could be utilized in a redox non-innocent fashion. Current synthetic efforts are focused on synthesizing an analog of (**3**) with two alkyl substituents in the β-position of the cyclopropane ring.

*1.2.4. Structure of {PhC(CNC$_6$H$_4$-2-NAr)$_2$}Ti(η^2-HNNCPh$_2$) (**4**)*

Figure 3.9 illustrates the structure of {PhC(CNC$_6$H$_4$-2-NAr)$_2$}Ti(η^2-HNNCPh$_2$) (**4**), containing a nacnac backbone as predicted by the ^{1}H NMR spectrum of (**4**). The η^2-HNNCPh$_2$ group is angled across the face of the

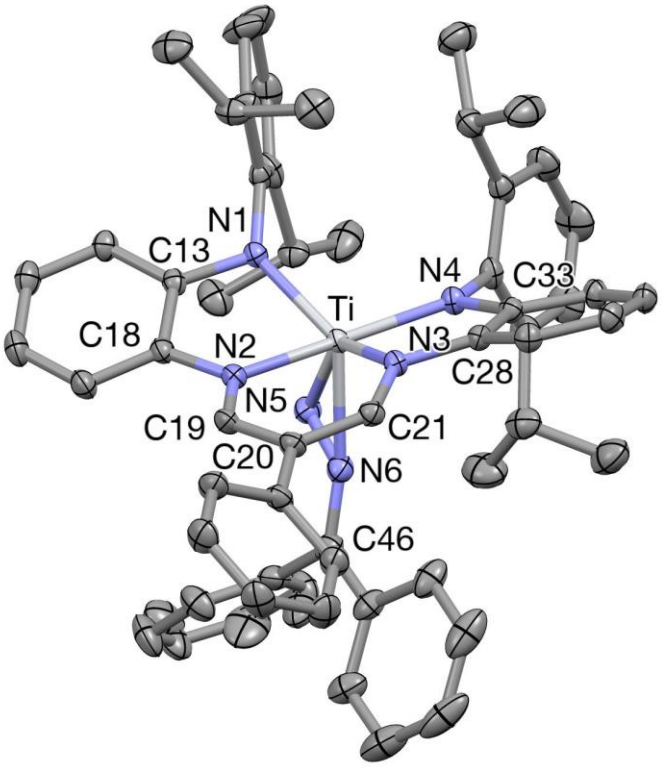

Figure 3.9. A molecular view of {PhC(CNC$_6$H$_4$-2-NAr)$_2$}Ti(η^2-HNNCPh$_2$) (**4**, Ar = 2,6-^{i}Pr$_2$-C$_6$H$_3$). Selected interatomic distances (Å) and angles (°): Ti-N1, 2.0023(12); Ti-N2, 2.1316(12); Ti-N3, 2.1389(12); Ti-N4, 2.0115(12); Ti-N5, 1.9243(13); Ti-N6, 2.1899(13); N2-C19, 1.3288(18); C19-C20, 1.389(2); C20-C21, 1.393(2); N3-C21, 1.3322(18); N1-Ti-N2, 78.00(5); N1-Ti-N3, 129.24(5); N1-Ti-N4, 111.13(5); N1-Ti-N5, 92.67(5); N1-Ti-N6, 126.72(5); N2-Ti-N3, 79.83(4); N2-Ti-N4, 156.03(5); N2-Ti-N5, 92.95(5); N2-Ti-N6, 85.43(5); N3-Ti-N4, 77.42(4); N3-Ti-N5, 133.64(5); N3-Ti-N6, 95.96(5); N4-Ti-N5, 108.23(5); N4-Ti-N6, 104.32(5); N5-Ti-N6, 37.68(5).

nacnac-diarylamide titanium core causing the asymmetry in the product that is evident in the ^{1}H NMR spectrum. The titanium-arylamide distances (d(Ti-N1) = 2.0023(12) Å, d(Ti-N4) = 2.0115(12) Å) are consistent with anionic nitrogens. Complex (**4**) contains titanium-nitrogen distances in the backbone which are elongated to 2.1316(12) Å and 2.1389(12) Å, compared to the tetraanionic cyclopropanated dadi starting material (**3**). The N-N distance of d(N5-N6) = 1.352(2) Å is consistent with an N-N single bond, while the d(N6-C46) = 1.301(2) Å bond length is in agreement with a C=N double bond.[18] In

conjunction, the d(Ti-N5) = 1.9243(13) Å and d(Ti-N6) = 2.1899(13) Å lengths are both in line with anionic and neutral N-donors, respectively.

*1.2.5. Calculated structure of (dadi)TiC(H)Ph (**2**-C(H)Ph)*

Two discrete redox forms of $(dadi)^{n}$ (n = -2, -4) are clearly evident upon examination of the metric parameters listen in Table 3.2. In order to oxidize the tetraanionic $(dadi)^{4-}$ to the dianionic $(dadi)^{2-}$, the ligand must be a potent oxidant such as AdN generated *via* N_2 loss. As previously mentioned (*cf*. Chapter 2), even ligands capable of significant backbonding interactions such as CO and CNMe, do not have the oxidizing power to render the dadi a dianion.

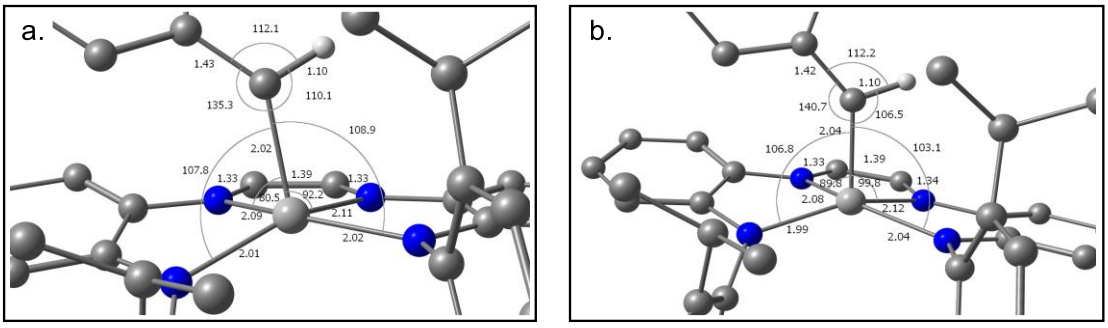

Figure 3.10. DFT (ONIOM(M06/6+311+G(d):UFF) calculations of (dadi)TiC(H)Ph (**2**-C(H)Ph). Geometries of unrestricted singlet (0.0 kcal/mol, **a.**), and unrestricted triplet (3.4 kcal/mol, **b.**).

It also apparent that a carbene fragment (RR'C:) is not capable of fully oxidizing to the $(dadi)^{2-}$ state, hence attempts to generate (dadi)Ti=CR(R') have failed. Calculations on a benzylidene portray it as a diradical species best considered $(dadi^{\uparrow})^{3-}Ti^{IV}(C{\cdot}(H)Ph)$ (**2**-C·HPh) (Figure 3.12). The calculated geometries, illustrated in Figure 3.10, show the singlet $d(CN_{im})$ to be 1.33 Å, and d(CC) = 1.39 Å, distances that are between those found in the $(dadi)^{4-}$ and $(dadi)^{2-}$ forms. These ligand metrics suggest that unpaired spin density on

(dadi$^{\uparrow}$)$^{3-}$ is likely to be antiferromagnetically coupled to a radical benzylidene anion (Ph(H)C:$^{\downarrow}$)$^{1-}$, consistent with the d(TiC) distance of 2.02 Å. The triplet species (Figure 3.10), with (dadi$^{\uparrow}$)$^{3-}$ ferromagnetically coupled to (Ph(H)C:$^{\uparrow}$)$^{1-}$ sits only 3.4 kcal/mol above the singlet.

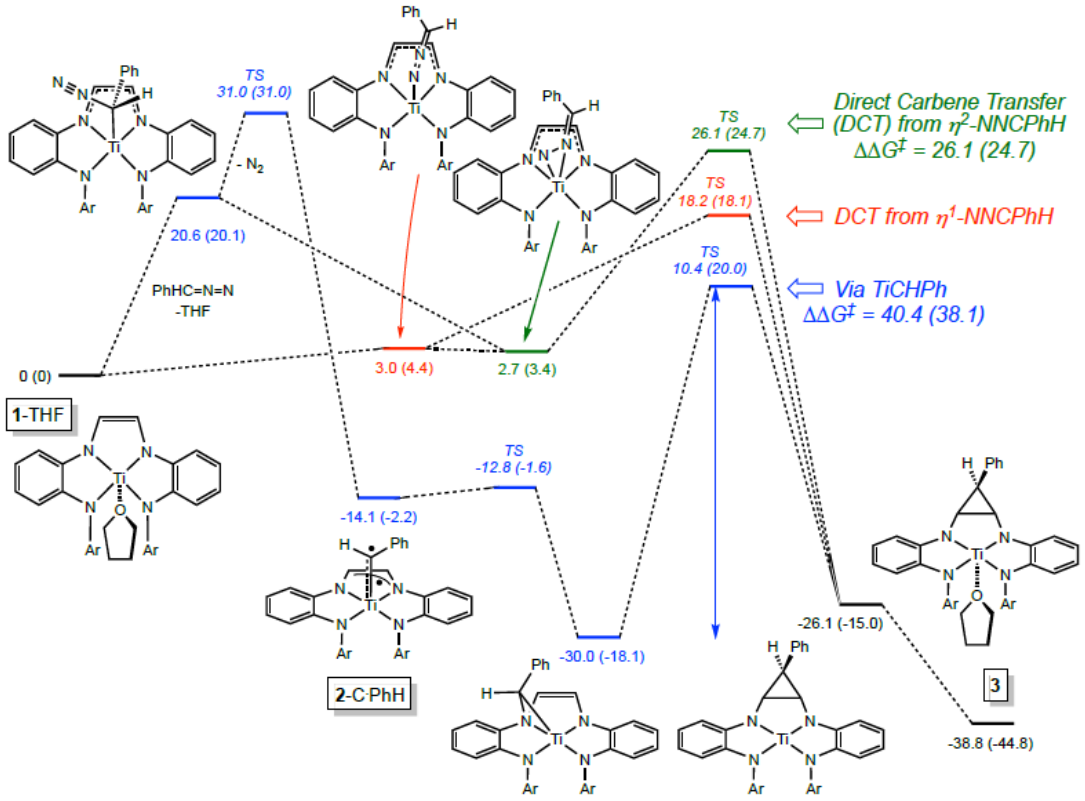

Figure 3.11. Computed intermediates (ΔG° (ΔH°)) relative to (dadi)Ti(THF) (**1**): in two plausible cyclopropanation mechanisms. A *Direct Carbene Transfer* to the dadi backbone possesses a lower barrier than one involving the intermediacy of (dadi)TiC(H)Ph. The product with opposite cyclopropane stereochemistry actually has a lower free energy of -40.7 kcal/mol (ΔH° = -44.0 kcal/mol).

*1.2.6. Calculated mechanism of the cyclopropanation of (dadi)Ti(THF) (**1**-THF)*

The mechanism of the dadi cyclopropanation was assumed to involve a benzylidene intermediate, but calculations indicate otherwise. Figure 3.11 depicts three plausible cyclopropanation mechanisms involving an

intermediate (dadi)TiC(H)Ph species, or “direct carbene transfer” pathways. The latter pathway, involves binding of the diazo substrate to titanium, which is slightly unfavorable for both the η^1- (3.0 kcal/mol) and η^2-NNCHPh (2.5 kcal/mol) species. The formation of (**1**-$NNCPh_2$) suggests adduct formation with $N_2C(H)Ph$ is reasonable. The intermediate diazo adduct can deliver the Ph(H)C: fragment directly to the dadi ligand with a barrier of $\Delta G^{\ddagger}_{calc}$ = 18.2 kcal/mol ($\Delta H^{\ddagger}_{calc}$ = 18.1 kcal/mol), which is in decent agreement with the crude experimental barrier of ~15 kcal/mol. Direct carbene transfer from an η^2-NNCPhH adduct has a barrier of $\Delta G^{\ddagger}_{calc}$ = 26.2 kcal/mol, which is incommensurate with that measured experimentally. It should be noted that the calculated 1,3-dipolar addition mechanism,[19] without the involvement of titanium, is calculated to have a barrier of $\Delta G^{\ddagger}_{calc}$ = 50.4 kcal/mol ($\Delta H^{\ddagger}_{calc}$ = 53.7 kcal/mol).

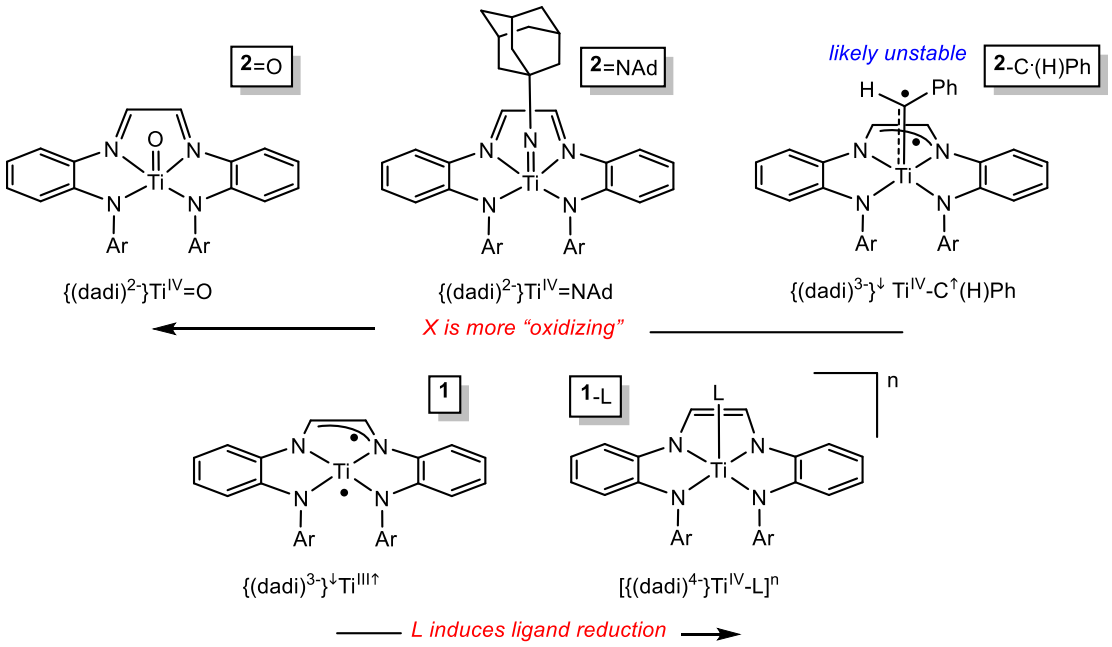

Figure 3.12. Progressively more oxidizing X, O > NAd > CHPh, and the dadi redox consequences compared to calculated $\{(dadi)^{3-}\}^{\downarrow}Ti^{III\uparrow}$ (**1**) and adducts $[\{(dadi)^{4-}\}Ti^{IV}\text{-}L]^n$ (**1**-L).

As illustrated in Figure 3.11, the transfer of Ph(H)C: to titanium is more favorable ($\Delta G° = -14.1$ kcal/mol), but a considerable barrier is found ($\Delta G^{‡} =$ 31.0 kcal/mol) for dinitrogen loss from an unfavorable η^1-C-N_2CPhH adduct at 20.6 kcal/mol, leading to the formation of $(dadi^{\uparrow})^{3-}Ti^{IV}(C^{\cdot}(H)Ph)$ (**2**-$C^{\cdot}$(H)Ph). More importantly, the titanaziridine generated from (**2**-$C^{\cdot}$(H)Ph), *via* attack at the imine nitrogen, is considerably stable at $\Delta G° = -30.0$ kcal/mol. The barrier for cyclopropanation from the titanaziridine, which is a two-step process, is quite substantial at $\Delta G^{‡} = 40.4$ kcal/mol ($\Delta H^{‡} = 38.1$ kcal/mol). The titanaziridine represents a free energy sink in the system, but it is not observed experimentally, possibly due to unfavorable sterics of the 2,6-iPr_2-C_6H_3 groups that prevent the formation of (**2**-$C^{\cdot}$(H)Ph). Given the intermediacy of the η^1-NNCHPh adduct, the PhHC fragment is ideally positioned above the dadi backbone for transfer. A mechanism that proceeds through the benzylidene radical $(dadi^{\uparrow})^{3-}Ti^{IV}(C^{\cdot}(H)Ph)$ (**2**-$C^{\cdot}$(H)Ph) is unlikely to be operative.

Conclusions:

This study of $[(dadi)Ti(X/L)]^n$ (**1**-L, n = 0, N_2CPh_2; n = -1, X = Cl^-, N_3^-, O^iPr^-, CH_3^-, $^{neo}Pe^-$, $CH{=}CH_2^-$, $CCPh^-$, $CCTMS^-$, $H(D)^-$) complexes clearly indicate these species are supported by the tetranionic $(dadi)^{4-}$ redox state of the ligand. Previous calculations on (dadi)Ti (**1**), a species that has not been isolated or observed spectroscopically, suggest that it is best described as $\{(dadi)^{3-}\}^{\downarrow}Ti^{III\,\uparrow}$, with the electron on titanium AF-coupled to an unpaired spin on the $dadi^{3-}$ ligand (Figure 3.12). The donation of any L to **1**, even weak donors such as THF, induces transfer of another electron, hence all (dadi)TiL (**1**-L) complexes are $\{(dadi)^{4-}\}Ti^{IV}$-L (Figure 3.12). As the tetranion, the $(dadi)^{4-}$ ligand electrostatically stabilizes the titanium in its preferred higher charge

state, while additional stability may be imparted by the conjugated 22 π-electron $(dadi)^{4-}$ π-system.

It is interesting that the titanium remains in a formally +4 oxidation state, and pulling electrons from $(dadi)^{4-}$ to generate $(dadi)^{2-}$ requires potent oxidants such as a nitrenes (RN) or oxo groups. It appears that a carbene (RR`C:) fragment does not fall in the category of a potent enough oxidant to generate a $(dadi)^{2-}$ ligand. This affects the chemistry, and in the case of phenyldiazomethane, a carbene precursor, cyclopropanation occurs *via* lower energy pathways. Thus, it may not be possible to form a stable (dadi)Ti=C(R')R complex, although they may be generated transiently with the use of less sterically demanding carbene precursors. The cyclopropanation of the dadi ligand does open a new avenue for ligand redox non-innocence through reversible CC bond formation, prompting further synthetic studies.

*Experimental***:**

A. General Considerations

All manipulations were performed using either glovebox or high vacuum line techniques. All glassware was oven dried. THF and diethyl ether were distilled under nitrogen from purple sodium benzophenone ketyl and vacuum transferred from the same prior to use. Hydrocarbon solvents were treated in the same manner with the addition of 1-2 mL/L tetraglyme. Benzene-d_6 was dried over sodium, vacuum transferred and stored over activated 4Å molecular sieves. THF-d_8 was dried over sodium and stored over purple sodium benzophenone ketyl. Methyl lithium (1.6 M in hexanes), lithium isopropoxide, and lithium aluminum hydride were purchased from Sigma-Aldrich and used as received. Sodium hydride (60 wt% in mineral oil) was purchased from Sigma-Aldrich, washed with hexanes to remove mineral oil, and stored in the glove box until use. Lithium aluminum deuteride was purchased from Acros Organics and used as received. Sodium azide was purchased from TCI Chemicals and used as received. Vinyl lithium,[20] lithium phenylacetylide,[21] lithium trimethylsilyacetylide,[22] neopentyl lithium,[12] diphenyldiazomethane,[23] benzaldehyde tosylhydrazone,[24] and sodium benzaldehyde tosylhyadrazide[24] were made according to literature procedures. N, N'-di-2-(2,6-diisopropylphenylamine)-phenylglyoxaldiimine (dadiH_2),[1] (dadi)$Na_2(THF)_4$,[2] and (dadi)Ti$(THF)^2$ were prepared following literature procedures.

NMR spectra were acquired using Mercury 300 MHz, INOVA 400 MHz, or Bruker AV III HD 500 MHz (equipped with a 5 mm BBO Prodigy cryoprobe) spectrometers. Assignments of carbon chemical shifts were determined from HSQCAD and gHMBCAD spectra collected on an INOVA 600 MHz NMR

spectrometer. Chemical shifts are reported relative to benzene-d_6 (^{1}H δ 7.16; ^{13}C{^{1}H} δ 128.06). NMR spectra were processed using MNova 12.0. Infrared spectra were recorded on a 20 Nicolet Avatar 370 DTGX spectrophotometer interfaced to an IBM PC (OMNIC software).

B. Procedures

1. *Phenyldiazomethane (Ph(H)CN_2). Caution! Diazo compounds are presumed to be highly toxic and potentially explosive.* All manipulations should be carried out in a fume hood. Although in numerous preparations, and explosion was never observed, all pyrolyses were carried out behind a safety shield. Leather welding gloves and a face shield were worn when manipulating the vacuum pyrolysis apparatus once phenyldiazomethane has been generated.

This is a modified literature procedure.[25,26] Sodium benzaldehyde tosylhydrazide (753 mg, 2.5 mmol) was placed in an oven-dried 100 mL round bottom flask and attached to a short path distillation head equipped with a vacuum tubing adapter and a 50 mL Schlenk receiving flask containing 15 mL of dry pentane. The pentane in the receiving flask was degassed by freeze-pump-thaw cycles (3x). The flask containing sodium benzaldehyde tosylhydrazide was heated using an oil bath to 70 ^{o}C for 2 hours under vacuum (0.1 mtorr); the receiving flask was kept at -78 ^{o}C. The Schlenk receiving flask was then placed under argon and warmed to -50 ^{o}C to dissolve the phenyldiazomethane. The resulting red solution (15 mL, 0.13 M, 77%) was titrated according to the method described by Redina.[27] Solutions of phenyldiazomethane were stored in a nitrogen filled glove box at -35 ^{o}C in an amber vial or at -80 ^{o}C under argon protected from light.

2. *[(dadi)TiCl][Li(THF)$_4$] (**1**-Cl·Li).* ***a.*** To a 50 mL round bottom flask charged with $TiCl_2(TMEDA)_2$ was added freshly distilled THF (10 mL) at -78 ^oC. To a separate 50 mL round bottom flask charged with $DadiH_2$ (500 mg, 0.89 mmol) and LiHMDS (299 mg, 1.79 mmol) was added freshly distilled THF (ca. 10 mL) at -78 ^oC then stirred for 30 minutes. The resulting dark green solution of $(dadi)Li_2$ was transferred to the flask containing $TiCl_2(TMEDA)_2$ via syringe. The reaction mixture was then allowed to warm slowly to 23 °C and stirred for 24 h. All volatiles were stripped, the reaction mixture was triturated with THF (3 x 20 mL), and taken up in C_6H_6 and filtered. All volatiles were then removed by vacuum and the crude product was collected as a black lustrous solid (90%). The crude mixture was purified by fractional crystallization from a concentrated THF solution layered with pentane yielding the product as a black (very dark green) crystalline solid (78 mg, 10 %) with 4 equivalents of THF.

b. To a round bottom flask charged with $(dadi)Ti(THF)^cHex_{0.45}$ (100 mg, 0.14 mmol) and LiCl (6 mg, 0.14 mmol was added freshly distilled THF (10 mL). The reaction solution was stirred at room temperature for 24 hrs. The reaction solution was then concentrated to 5 mL, cooled to -78 ^oC and 40 mL of freshly distilled pentane was added while stirring. The cold bath was removed and the reaction mixture was allowed to warm to room temperature, filtered, and washed (3x). The product was collected as a dark green micro-crystalline solid (79 mg, 70 %) with 1.5 equivalents of THF. Spectral signatures were identical to those of the product obtained by method A. ^1H NMR (600 MHz, THF-d_8): δ δ 0.63 (bs, 6H, CH_3), 0.67 (bs, 6H, CH_3), 0.72 (d, J = 6.8 Hz, 6H, CH_3), 0.87 (d, J = 6.7 Hz, 6H, CH_3), 1.74 – 1.83 (m, 6H, THF-CH_2), 3.01 (sept, J = 6.6 Hz, 2H, ^{i}Pr-CH), 3.07 (bs, 2H, $_i$Pr-CH), 3.59 – 3.64

(m, 6H, THF-CH_2), 5.27 (d, *J* = 7.9 Hz, 2H, Ar-CH), 6.17 – 6.24 (bt, *J* = 6.3 Hz, 2H, Ar-CH), 6.33 (d, *J* = 6.9 Hz, 2H, Ar-CH), 6.37 (t, *J* = 7.1 Hz, 2H, Ar-CH), 6.71 (bs, 2H, Im-CH), 6.90 (m, 6H). ^{13}C NMR (126 MHz, THF-d_8): δ 24.12 (CH_3), 24.41 (CH_3), 25.43 (CH_3), 26.54 (THF-CH_2), 26.59 (CH_3), 29.23 (^{i}Pr-CH), 29.50 (^{i}Pr-CH), 68.39(THF-CH_2), 104.95 (Ar-CH), 113.47 (Ar-CH), 118.20 (Ar-CH), 120.45 (Ar-CH), 124.51 ($^{2,6\text{-iPr}}$Ar-CH), 124.75 ($^{2,6\text{-iPr}}$Ar-CH), 124.85 (Im-CH), 125.75 ($^{2,6\text{-iPr}}$Ar-CH), 143.98 (Ar-CN), 144.72 ($^{2,6\text{-iPr}}$Ar-C), 146.54 ($^{2,6\text{-iPr}}$Ar-C), 149.66 ($^{2,6\text{-iPr}}$Ar-CN), 151.89 (Ar-CN). Anal. Calc'd for $C_{44}H_{56}LiN_4O_{1.5}Ti$: C, 69.98; H, 7.47; N, 7.42. Found: C, 69.31; H 7.45; N 6.77.

3. *[(dadi)TiCH$_3$][Li(THF)$_2$] (**1**-CH$_3$Li).* To a 100 mL round bottom flask charged with [(dadi)Ti(THF)](^{c}Hex)$_{0.8}$ (500 mg, 0.67 mmol) was added THF (15 mL) by vacuum transfer. The resulting solution was cooled to -78 ^{o}C and a solution of CH_3Li (0.44 mL, 1.68 M in Et_2O) was added dropwise *via* syringe under an argon purge. The resulting maroon solution was allowed to warm to 23 °C over 30 min. The reaction solution was cooled to -78 ^{o}C and pentane (*ca.* 40 mL) was slowly added by vacuum transfer. The resulting suspension was warmed to 0 ^{o}C, filtered and the maroon filtercake was washed once with the reaction solvent. All volatiles were removed by vacuum and the product was collected as maroon powder (518 mg, 0.61 mmol, 90 %). Single crystals were grown by slow evaporation of a pentane solution at room temperature. ^{1}H NMR (600 MHz, Benzene-d_6): δ 0.72 (s, 3H, Ti-CH_3), 0.93 (bd, *J* = 4.7 Hz, 6H, CH_3), 1.02 (d, *J* = 4.2 Hz, 6H, CH_3), 1.05 (d, *J* = 6.8 Hz, 6H, CH_3), 1.20 (d, *J* = 6.8 Hz, 6H, CH_3), 1.27 – 1.36 (m, 14.6 H, THF-CH_2), 3.26 (m, 2H, ^{i}Pr-CH), 3.35–3.44 (m, 16.6H, ^{i}Pr-CH and THF-CH_2), 5.80 (d, *J* = 7.7 Hz, 2H, Ar-CH), 6.47 (dd, *J* = 7.7, 0.8 Hz, 2H, Ar-CH), 6.62 (t, *J* = 7.6 Hz, 2H, Ar-CH), 6.73 (td, J = 7.5, 0.8 Hz, 2H), 6.77 (s, 2H, Im-CH), 7.17 – 7.21 (m, 6H, $^{2,6\text{-iPr}}$Ar-CH). ^{13}C

NMR (126 MHz, Benzene-d_6): δ 23.81 (CH_3), 24.16 (CH_3), 25.24 (CH_3), 25.61 (THF-CH_2), 25.99 (CH_3), 29.07 (^{i}Pr-CH), 29.36 (^{i}Pr-CH), 36.07 (Ti-CH_3), 68.31 (THF-CH_2), 106.76 (Ar-CH), 114.33 (Ar-CH), 118.40 (Ar-CH), 121.55 (Im-CH), 121.98 (Ar-CH), 124.33 ($^{2,6\text{-iPr}}$Ar-CH), 125.29 ($^{2,6\text{-iPr}}$Ar-CH), 126.33 ($^{2,6\text{-iPr}}$Ar-CH), 142.06 (Ar-CN), 144.58 ($^{2,6\text{-iPr}}$Ar-C), 144.98 ($^{2,6\text{-iPr}}$Ar-C), 147.37 ($^{2,6\text{-iPr}}$Ar-CN), 152.67 (Ar-CN). Anal. Calc'd for $C_{53.8}H_{76.6}LiN_4O_{3.7}Ti$: C, 72.33; H, 8.64; N, 6.27 Found: C, 71.77; H, 8.59; N, 5.96.

4. *[(dadi)TiCCPh][Li(THF)$_2$] (**1**-CCPh·Li).* To a 50 mL round bottom flask charged with [(dadi)Ti(THF)](^{c}Hex)$_{0.8}$ (137 mg, 0.18 mmol) and PhC_2Li (20 mg, 0.18 mmol) was added THF (*ca*. 10 mL) by vacuum transfer at -78 °C. The reaction was allowed to warm slowly to 23 °C, then stirred for 36 h. All volatiles were removed by vacuum and pentane was added (10 mL). The resulting brown mixture was filtered and the filter cake was washed until colorless (3x) whereupon a crystalline solid began to form in the filtrate. This solid was filtered and the pentane was removed by vacuum yielding the product as a green microcrystalline solid (81 mg, 51%). ^{1}H NMR (599 MHz, Benzene-d_6): δ 0.98 (d, *J* = 6.7 Hz, 6H, CH_3), 1.03 (d, *J* = 6.7 Hz, 6H, CH_3), 1.14 (d, *J* = 6.8 Hz, 6H, CH_3), 1.23 (d, *J* = 6.7 Hz, 6H, CH_3), 1.27 (m, 8H, THF-CH_2), 3.31 (bp, 5.9 Hz, 2H, ^{i}Pr-CH), 3.45 (m, 8H, THF-CH_2), 3.54 – 3.67 (sept, *J* = 6.8, 2H, ^{i}Pr-CH), 5.75 (dd, *J* = 7.9, 1.4 Hz, 2H, Ar-CH), 6.36 (dd, *J* = 7.7, 1.4 Hz, 2H, Ar-CH), 6.58 (td, *J* = 7.6, 1.4 Hz, 2H, Ar-CH), 6.65 (s, 2H, Im-CH), 6.68 (td, *J* = 7.5, 1.3 Hz, 2H, Ar-CH), 6.85 – 6.90 (m, 1H, *para*-Ar-CH), 6.90 – 6.96 (m, 2H, *meta*-Ar-CH), 7.13 – 7.18 (m, 4H, $^{2,6\text{-iPr}}$Ar-CH), 7.18 – 7.24 (m, 4H,$^{2,6\text{-iPr}}$Ar-CH and *ortho*-Ar-CH).^{13}C NMR (126 MHz, Benzene-d_6): δ 23.98 (CH_3), 24.02 (CH_3), 25.05 (CH_3), 25.43 (THF-CH_2), 26.11 (CH_3), 29.34 (^{i}Pr-CH), 30.04 (^{i}Pr-CH), 68.74 (THF-OCH_2), 106.32 (Ar-CH), 114.06 (Ar-CH),

118.66 (Ar-CH), 122.83 (Ar-CH), 124.20 (Im-CH), 124.38 ($^{2,6\text{-iPr}}$Ar-CH), 125.12 ($^{2,6\text{-iPr}}$Ar-CH), 125.17 (Ar-C), 126.40 ($^{2,6\text{-iPr}}$Ar-CH), 127.31 (*para*-Ar-CH), 128.43 (*meta*-Ar-CH), 130.36 (*ortho*-Ar-CH), 138.72 (q, J_{CLi} = 6.8 Hz,Ti-**C**-CAr), 142.26 (Ar-CN), 142.69 TiC-**C**-Ar, 144.00 ($^{2,6\text{-iPr}}$Ar-C), 144.64 ($^{2,6\text{-iPr}}$Ar-C), 147.05 ($^{2,6\text{-iPr}}$Ar-CN), 153.50 (Ar-CN). Anal. Calc'd for $C_{54}H_{65}LiN_4O_2Ti$: C, 75.69, H, 7.65; N, 6.54 Found: C, 76.61; H, 7.67; N, 6.46.

5. *[(dadi)TiCCTMS][Li(THF)$_2$] (**1**-CCTMS·Li).* To a 50 mL round bottom flask charged with [(dadi)Ti(THF)](^{c}Hex)$_{2.1}$ (100 mg, 0.12 mmol) and Me_3SiC_2Li (12 mg, 0.12 mmol) was added THF (*ca*. 10 mL) by vacuum transfer at -78 ^{o}C. The reaction was allowed to warm slowly to 23 °C over the course of 1 h, then concentrated to ~3 mL. The green solution was cooled to -78 ^{o}C and 20 mL of freshly distilled pentane was added resulting in dark green precipitate which was filtered at -78 ^{o}C. After removal of all volatiles the product was collected as a dark green crystalline solid (50 mg, 48 %). ^{1}H NMR (500 MHz, Benzene-d_6): δ 0.04 (s, 9H, $SiMe_3$), 1.00 (d, *J* = 6.7 Hz, 12H, CH_3), 1.11 (d, *J* = 6.8 Hz, 6H, CH_3), 1.19 (d, *J* = 6.7 Hz, 6H, CH_3), 1.35 (bs, 8H, THF-CH_2), 3.12 (sept, *J* = 6.7 Hz, 2H, ^{i}Pr-CH), 3.48 (bs, 8H, THF-OCH_2), 3.55 (sept, *J* = 6.8 Hz, 2H, ^{i}Pr-CH), 5.71 (dd, *J* = 7.9, 1.4 Hz, 2H, Ar-CH), 6.33 (dd, *J* = 7.7, 1.1 Hz, 2H, Ar-CH), 6.55 (td, *J* = 7.9, 1.4 Hz, 2H, Ar-CH), 6.60 (s, 2H, Im-CH), 6.65 (td, *J* = 7.5, 1.2 Hz, 2H, Ar-CH), 7.10 – 7.24 (m, 6H, $^{2,6\text{-iPr}}$Ar-CH).^{13}C NMR (126 MHz, C_6D_6) δ 0.65 (Si-CH_3), 23.99 (CH_3), 24.49 (CH_3), 25.09 (CH_3), 25.51 (THF-CH_2), 26.08 (CH_3), 29.38 (^{i}Pr-CH), 29.43 (^{i}Pr-CH), 68.67 (THF-OCH_2), 106.25 (Ar-CH), 114.05 (Ar-CH), 118.79 (Ar-CH), 122.97 (Ar-CH), 124.32 (Im-CH), 124.45 ($^{2,6\text{-iPr}}$Ar-CH), 125.16 ($^{2,6\text{-iPr}}$Ar-CH), 126.44 ($^{2,6\text{-iPr}}$Ar-CH), 142.14 (Ar-CN), 144.00 ($^{2,6\text{-iPr}}$Ar-C), 144.51 ($^{2,6\text{-iPr}}$Ar-C), 146.29 (Ti-C-**C**-

TMS), 147.03 ($^{2,6\text{-iPr}}$Ar-CN), 153.46 (Ar-CN), 162.27 (Ti-**C**-CTMS). Anal. Calc'd for $C_{51}H_{69}N4O_2Ti$: C, 71.81; H, 8.15; N, 6.57. Found: C, 71.55; H 8.10; N 6.76.

6. *[(dadi)TiC_2H_3]Li(THF)$_{2.5}$ (**1**-CH=CH_2·Li).* To a 50 mL round bottom flask charged with [(dadi)Ti(THF)](^{c}Hex)$_{0.4}$ (330 mg, 0.46 mmol) and vinyl lithium (16 mg, 0.47 mmol) was added THF (*ca*. 15 mL) by vacuum transfer at -78 °C. The reaction was allowed to stir for 30 min at -78 °C then allowed to warm slowly to 23 °C over the course of ~1 h. The resulting red solution was concentrated to 10 mL, and cooled to -78 °C with stirring stopped. The cold reaction solution was then layered with 35 mL pentane and allowed to warm slowly to 23 °C over the course of 2 h. The crystalline precipitate that formed was filtered and washed twice. After removal of all volatiles the product was collected as a very dark burgundy crystalline solid (247 mg, 0.28 mmol, 60 %).^{1}H NMR (600 MHz, Benzene-d_6, vinyl ABX spin system is simulated): δ 0.94 (d, *J* = 6.7 Hz, 6H, CH_3), 0.98 (d, *J* = 6.7 Hz, 6H, CH_3), 1.10 (d, *J* = 6.8 Hz, 6H, CH_3), 1.14 (d, *J* = 6.7 Hz, 6H, CH_3), 1.27 (m, *J* = 6.4 Hz, 9H,THF-CH_2), 3.03 (sept, *J* = 6.7, 2H, ^{i}Pr-CH), 3.28 (m, *J* = 6.1 Hz, 9H, THF-CH_2), 3.53 (sept, *J* = 6.7 Hz, 2H, ^{i}Pr-CH_2), 5.79 (d, *J* = 7.7 Hz, 2H, Ar-CH), 5.9995 (bs, 1H,Ti-CHCHH_B, J_{BA} = -4.20, J_{BA} = 14.65), 6.0046 (1H, Ti-CHCH_AH, J_{AB} = -4.20, J_{AX} = 20.90), 6.42 (d, *J* = 7.5 Hz, 2H, Ar-CH), 6.61 (t, *J* = 7.5 Hz, 2H, Ar-CH), 6.64 (s, 2H, Im-CH), 6.72 (t, *J* = 7.1 Hz, 2H, Ar-CH), 7.13-7.15 (m, *J* = 7.5 Hz, 4H,$^{2,6\text{-iPr}}$Ar-CH), 7.20 (dd, *J* = 7.0, 2.1 Hz, 2H,$^{2,6\text{-iPr}}$Ar-CH), 8.2265 (1H, Ti-C$H_X$$CH_2$, J_{AX} = 20.90, J_{BX} = 14.65). ^{13}C NMR (126 MHz, Benzene-d_6): δ 23.92 (CH_3), 23.98 (CH_3), 25.07 (CH_3), 25.41 (THF-CH_2), 25.81 (CH_3), 29.29 (^{i}Pr-CH), 29.53 (^{i}Pr-CH), 68.26 (THF-CH_2), 106.46 (Ar-CH), 113.98 (Ar-CH), 118.56 (Ar-CH), 122.41 (Im-CH), 122.48 (Ar-CH), 123.73 (Vinyl-CH_2), 124.31 ($^{2,6\text{-iPr}}$Ar-CH), 125.33 ($^{2,6\text{-iPr}}$Ar-CH), 126.23 ($^{2,6\text{-iPr}}$Ar-CH), 141.93 (Ar-CN),

144.27 ($^{2,6\text{-iPr}}$Ar-C), 144.67 ($^{2,6\text{-iPr}}$Ar-C), 147.22 ($^{2,6\text{-iPr}}$Ar-CN), 153.14 (Ar-CN), 189.03 (Vinyl-CH). Anal. Calc'd for $C_{50}H_{67}LiN_4O_{2.5}Ti$: C,73.33; H,8.25; N, 6.84. Found: C, 73.33; H, 8.07; N, 6.94.

7. *(dadi)Ti(^{neo}Pe)·Li(THF)$_{2.4}$ (**1**-^{neo}Pe·Li)*. To a 50 mL round bottom flask charged with [(dadi)Ti(THF)](^{c}Hex)$_{1.7}$ (200 mg, 0.24 mmol) and ^{neo}PenLi (19 mg, 0.24 mmol was added THF (*ca*. 10 mL) by vacuum transfer at -78 ^{o}C . The reaction solution was stirred and allowed to warm to 23 °C over the course of *ca.* 16 h. The resulting red solution was concentrated to 5 mL and 25 mL of freshly distilled hexanes was added at -78 ^{o}C. The red crystalline precipitate was warmed to 0 ^{o}C and filtered. After removal of all volatiles the product was collected as a red crystalline precipitate (201 mg, 0.19 mmol, 79 %).^{1}H NMR (600 MHz, THF-d_8): δ 0.59 (bs, 6H, CH_3), 0.65 (d, J = 6.8 Hz, 6H, CH_3), 0.73 (bs, 6H, CH_3), 0.89 (s, 9H, ^{neo}Pen-CH_3), 0.92 (d, J = 6.6 Hz, 6H), 1.21 (s, 2H, ^{neo}Pen-CH_2), 1.75 – 1.81 (m, 10H, THF-CH_2), 2.97 (sept, J = 6.8 Hz, 2H, ^{i}Pr-CH), 3.24 (bs, 2H, ^{i}Pr-CH), 3.59 – 3.64 (m, 10H, THF-CH_2), 5.26 (d, J = 7.3 Hz, 2H, Ar-CH), 6.08 (t, J = 7.3 Hz, 2H, Ar-CH), 6.28 (t, J = 7.2 Hz, 2H, Ar-CH), 6.33 (d, J = 7.2 Hz, 2H, Ar-CH), 6.59 (s, 2H, Im-CH), 6.81 – 6.93 (m, 6H, $^{2,6\text{-iPr}}$Ar-CH). ^{13}C NMR (126 MHz, THF-d_8): δ 24.25 (CH_3), 24.36 (CH_3), 25.45 (CH_3), 26.52 (CH_3), 26.55 (THF-CH_2), 29.14 (^{i}Pr-CH), 29.26 (^{i}Pr-CH), 34.80 (^{neo}Pen-CH_3), 39.94 (^{neo}Pen-C), 68.39 (THF-OCH_2), 86.83 (^{neo}Pen-CH_2), 104.69 (Ar-CH), 113.09 (Ar-CH), 117.25 (Ar-CH), 118.49 (Ar-CH), 121.37 (Im-CH), 124.03 ($^{2,6\text{-iPr}}$Ar-CH), 124.66 ($^{2,6\text{-iPr}}$Ar-CH), 124.80 ($^{2,6\text{-iPr}}$Ar-CH), 144.33 (Ar-CN), 145.02 ($^{2,6\text{-iPr}}$Ar-C), 146.28 ($^{2,6\text{-iPr}}$Ar-C), 150.87 ($^{2,6\text{-iPr}}$Ar-CN) 152.60. Anal. Calc'd for $C_{52.6}H_{74.2}N_4O_{2.4}Ti$: C, 73.82; H, 8.74; N, 6.55. Found: C, 72.14; H 8.74; N 5.99.

8. *[(dadi)TiH][Li(THF)$_2$] (**1**-H·Li).* To a 50 mL round bottom flask charged with [(dadi)Ti(THF)](^{c}Hex)$_{0.6}$ (96 mg, 0.13 mmol) and $LiAlH_4$ (6 mg, 0.16 mmol) was added THF (5 mL) by vacuum transfer at -78 ^{o}C . The reaction solution was stirred at -78 °C for 70 min, then 35 mL of freshly distilled pentane was added slowly while the reaction mixture was vigorously stirred. The -78 ^{o}C bath was then removed and the resulting suspension was allowed to warm to 23 °C while maintaining vigorous stirring. The precipitate was filtered and washed (2x) with the THF/pentane mixture. After removal of all volatiles the product was collected as a brown powder (64 mg, 0.71 mmol, 54 %). ^{1}H NMR (600 MHz, Benzene-d_6): δ 0.90 (d, J = 6.6 Hz, 6H, CH_3), 1.01 (d, J = 6.7 Hz, 6H, CH_3), 1.09 (d, J = 6.7 Hz, 6H, CH_3), 1.14 (d, J = 6.7 Hz, 6H, CH_3), 1.32 (bs, 12H, THF-CH_2), 3.08 (bp, J = 6.5 Hz, 2H, ^{i}Pr-CH), 3.45 (bs, 12H, THF-CH_2), 3.61 (sept, J = 6.7 Hz, 2H, ^{i}Pr-CH), 5.68 (d, J = 7.7 Hz, 2H, Ar-CH), 6.31 (d, J = 7.5 Hz, 2H, Ar-CH), 6.50 (t, J = 7.5 Hz, 2H, Ar-CH), 6.61 (t, J= 7.0 Hz, 2H, Ar-CH) 6.62 (s, 2H, Im-CH), 7.05 – 7.26 (m, 6H, $^{2,6\text{-iPr}}$Ar-CH), 10.22 (d, J = 11.3 Hz, 1H, Ti-H). ^{1}H NMR (300 MHz, THF-d_8): δ 0.61 (bs, 6H, CH_3), 0.74 (bs, 6H, CH_3), 0.84 (d, J= 6.1 Hz, 12 H, CH_3), 1.77 (m, 14 H, THF-CH_2), 3.21 (bs, 4H, ^{i}Pr-CH), 3.62 (m, 14 H, THF-CH_2), 5.17 (d, J= 7.6 Hz, 2H, Ar-CH), 6.04 (t, J = 7.3 Hz, 2H, Ar-CH), 6.24 (t, J = 7.3 Hz, 2H, Ar-CH), 6.43 (s, 2H, Im-CH), 6.89 (bs, 6H, $^{2,6\text{-iPr}}$Ar-CH), 10.47 (s, 1H, Ti-H). ^{7}Li NMR (194 Hz Benzene-d_6) -0.27 (d, $J_{H\text{-}Li}$ = 11.3 Hz). ^{7}Li NMR (194 Hz THF-d_8) -0.49 (s).^{13}C NMR (126 MHz, Benzene-d_6): δ 23.54 (CH_3), 23.97 (CH_3), 25.07 (CH_3), 25.52 (CH_3), 25.56 (THF-CH_2), 29.25 (^{i}Pr-CH), 29.28 (^{i}Pr-CH), 68.52 (THF-CH_2), 105.92 (Ar-CH), 112.94 (Ar-CH), 118.64 (Ar-CH), 122.10 (Ar-CH), 122.86 (Im-CH), 124.35($^{2,6\text{-iPr}}$Ar-CH), 124.96($^{2,6\text{-iPr}}$Ar-CH), 126.36($^{2,6\text{-iPr}}$Ar-CH), 142.77 (Ar-CN), 144.02 ($^{2,6\text{-iPr}}$Ar-C), 144.77 ($^{2,6\text{-iPr}}$Ar-C), 145.28($^{2,6\text{-iPr}}$Ar-CN), 153.52(Ar-

CN). Anal. Calc'd for $C_{50}H_{69}LiN_4O_3Ti$: C,72.45; H,8.39; N, 6.76. Found: C, 72.85; H, 8.30; N, 7.20.

9. *[(dadi)TiN_3]Na(12-crown-5) (**1**-N_3·Na).* A scintillation vial was charged with [(dadi)Ti(THF)](^{c}Hex)$_{0.8}$ (103 mg, 0.14 mmol),NaN_3 (9 mg, 0.14 mmol), THF (10 mL) and 12-crown-5 (31 mg, 0.14 mmol), then stirred for 16 h at 23 °C. After removal of all volatiles the resulting green solid was taken up in *ca.* 5 mL of THF, filtered, then layered with hexanes to crystallize at room temperature over 48 h. The mother liquor was decanted and the product was collected as a dark green crystalline solid (62 mg, $5.6x10^{-5}$ mol, 40%). Single crystals were grown from a THF-d_8 solution layered with with hexanes. ^{1}H NMR (500 MHz, THF-d_8): δ 0.68 (bs, 12H, CH_3), 0.76 (d, J = 6.8 Hz, 6H, (CH_3), 0.89 (d, J = 6.7 Hz, 6H, CH_3), 2.91 (bs, 2H, ^{i}Pr-CH), 3.04 (sept, J = 6.5 Hz, 2H, iPr-CH),3.63, (s, 20H, 12c5-CH_2) 5.21 (d, J = 7.6 Hz, 2H, (Ar-CH), 6.17 (m, 2H, Ar-CH), 6.34 (m, 4H), 6.66 (s, 2H), 6.90 (bs, 6H). ^{13}C NMR (126 MHz, THF-d_8): δ 23.67, 24.03, 25.39, 26.24, 29.08, 29.72, 69.65, 105.11, 112.91, 118.07, 120.11, 123.97, 124.37, 124.55, 125.71, 143.81, 144.89, 146.20, 148.65, 151.79. Anal. Calc'd for $C_{48}H_{64}N_7NaO_5Ti$: C, 64.78; H, 7.25; N, 11.02. Found: C, 64.98; H 7.46; N 9.79.

10. *[(dadi)Ti(O^{i}Pr)][Li(THF)$_4$] (**1**-O^{i}Pr·Li).* To a 50 mL round bottom flask charged with (dadi)Ti(THF)^{c}Hex$_{0.55}$ (**1**-THF) (110 mg, 0.15 mmol) and LiO^{i}Pr (12 mg, 0.182 mmol) was added freshly distilled THF (10 mL) at -78 ^{o}C. The reaction was allowed to warm to 23 °C over the course of 1 h then cooled back to -78 ^{o}C and 35 mL of freshly distilled pentane was added while maintaining vigorous stirring. The reaction mixture was allowed to warm slowly to room temperature over the course of 1 h then filtered. After removal of all volatiles the product was collected was a bronze microcrystalline solid (87 mg,

60%). ^{1}H NMR (600MHz, THF-d_8): δ δ 0.63 (bs, 12H, CH_3), 0.73 (d, J = 6.8 Hz, 6H, CH_3), 0.84 (d, J = 6.7 Hz, 6H, CH_3), 0.94 (d, J = 6.1 Hz, 6H, OCH(**CH_3**)$_2$), 1.78 (m, 12H, THF-CH_2), 2.99 (sept, J = 6.9 Hz, 2H, ^{i}Pr-CH), 3.38 (bs, 2H, ^{i}Pr-CH), 3.60 – 3.64 (m, 12H, THF-CH_2), 4.51 (sept, J = 6.1 Hz, 1H, O-**CH**(CH_3)), 5.17 (d, J = 5.8 Hz, 2H, Ar-CH), 6.06 (t, J = 7.2 Hz, 2H, Ar-CH), 6.24 (t, J = 7.0 Hz, 1H, Ar-CH), 6.36 (d, J = 7.4 Hz, 2H, Ar-CH), 6.68 (s, 2H, Im-CH), 6.80 – 6.93 (m, 6H, $^{2,6\text{-iPr}}$Ar-CH). ^{13}C NMR (126 MHz, THF-d_8): δ 24.14 (CH_3), 24.26 (CH_3), 25.62 (CH_3), 26.43 (THF-CH_2), 26.52 (CH_3), 27.52 (OCH(**CH_3**)$_2$), 28.53 (^{i}Pr-CH), 28.71 (^{i}Pr-CH), 68.30 (THF-CH_2), 76.57 (O**CH**(CH_3)$_2$), 104.59 (Ar-CH), 112.15 (Ar-CH), 116.14 (Ar-CH), 117.74 (Ar-CH), 119.95 (Im-CH), 124.11 ($^{2,6\text{-iPr}}$Ar-CH), 124.22 ($^{2,6\text{-iPr}}$Ar-CH), 124.78 ($^{2,6\text{-iPr}}$Ar-CH), 143.85 (Ar-CN), 145.72 ($^{2,6\text{-iPr}}$Ar-C), 147.22 ($^{2,6\text{-iPr}}$Ar-C), 149.85 ($^{2,6\text{-iPr}}$Ar-CN), 151.18 (Ar-CN). Anal. Calc'd for $C_{53}H_{75}LiN_4O_4Ti$: C, 71.72; H, 8.52; N, 6.32. Found: C, 70.76; H, 8.59; N, 6.24.

11. *(dadi)Ti(η^2-N,N-N_2CPh_2) (**1**-N_2CPh_2).* To a 25 mL round bottom flask charged with (dadi)Ti(THF)^{c}Hex$_{0.55}$ (200 mg, 0.28 mmol) and C_6H_6 (4 mL) was added a solution of diphenyldiazomethane (56 mg, 0.29 mmol) at 23 °C. The solution was stirred for 30 min then all volatiles were removed. The crude reaction mixture was taken up in pentane (15 mL), filtered and washed (3x). The product was collected as a green powder (137 mg, 62%). ^{1}H NMR (600 MHz, Benzene-d_6): δ 0.97 (bs, 12H, CH_3), 1.27 (s, 12H, CH_3), 3.20 (bs, 2H, ^{i}Pr-CH), 3.91 (bs, 2H, ^{i}Pr-CH), 5.75 (d, J = 8.4 Hz, 2H, Ar-CH), 6.19-6.20 (m, 4H, Im-CH and Ar-CH), 6.36 (d, J = 7.9 Hz, 2H, Ar-CH), 6.56 (t, J = 7.6 Hz, 2H, Ar-CH), 6.96 (t, J = 7.3 Hz, 4H, N_2C-Ar-**CH**), 7.01 (t, J = 7.5 Hz, 4H, N_2C-Ar-**CH**), 7.16 (bs, 6H, $^{2,6\text{-iPr}}$Ar-CH), 7.44 (d, J = 7.6 Hz, 4H, N_2C-Ar-**CH**). ^{13}C NMR (126 MHz, Benzene-d_6): δ 23.78 (CH_3), 24.81 (^{i}Pr), 25.76 (^{i}Pr), 29.60

(^{i}Pr), 114.93 (Ar-CH), 116.79 (Ar-CH), 117.26 (Ar-CH), 124.91 ($^{2,6\text{-}iPr}$Ar-CH), 126.38 ($^{2,6\text{-}iPr}$Ar-CH), 127.06 (N_2C-Ar-**CH**), 128.30 (N2C-Ar-**CH**), 128.68 (N_2C-Ar-**CH**), 133.17 (Ar-CH), 134.99 (Ar-CN), 139.01 (N_2C-Ar-**C**), 141.29 (Im-CH), 144.89 ($^{2,6\text{-}iPr}$Ar-C), 145.27 ($^{2,6\text{-}iPr}$Ar-CN), 146.31 ($^{2,6\text{-}iPr}$Ar-C), 161.81 (Ar-CN), not observed (N_2**C**-Ph_2). IR neat film ν(N=N) = 2020, 2040 cm^{-1}. Anal. Calc'd for $C_{51}H_{54}N_6Ti$: C, 76.68; H, 6.81; N, 10.52. Found: C, 76.60; H 6.66; N 10.38.

12. *[(dadi)Ti(N_3)]Na(12-crown-5) (**1**-N_3·Na)***.** A scintillation vial was charged with [(dadi)Ti(THF)](^{c}Hex)$_{0.8}$ (103 mg, 0.14 mmol),NaN_3 (9 mg, 0.14 mmol), THF (10 mL) and 12-crown-5 (31 mg, 0.14 mmol) then stirred for 16 hours at room temperature. After removal of all volatiles the resulting green solid was taken up in *ca.* 5 mL of THF, filtered then layered with hexanes to crystallize at room temperature over 48 hours. The mother liquor was decanted and the product was collected as a dark green crystalline solid (62 mg, 5.6*10-5 mol, 40%). Single crystals were grown from a THF-$_{d8}$ solution layered with hexanes. ^{1}H NMR (500 MHz, THF-d_8) δ 0.68 (bs, 12H, CH_3), 0.76 (d, J = 6.8 Hz, 6H, (CH_3), 0.89 (d, J = 6.7 Hz, 6H, CH_3), 2.91 (bs, 2H, ^{i}Pr-CH), 3.04 (sept, J = 6.5 Hz, 2H, iPr-CH),3.63, (s, 20H, 12c5-CH_2) 5.21 (d, J = 7.6 Hz, 2H, (Ar-CH), 6.17 (m, 2H, Ar-CH), 6.34 (m, 4H), 6.66 (s, 2H), 6.90 (bs, 6H). ^{13}C NMR (126 MHz, THF-d_8) δ 23.67, 24.03, 25.39, 26.24, 29.08, 29.72, 69.65, 105.11, 112.91, 118.07, 120.11, 123.97, 124.37, 124.55, 125.71, 143.81, 144.89, 146.20, 148.65, 151.79. Anal. Calc'd for $C_{48}H_{64}N_7NaO_5Ti$: C, 64.78; H, 7.25; N, 11.02. Found: C, 64.98; H 7.46; N 9.79. IR nujol mull ν(N_3) = 2077 cm^{-1}.

13. *{PhC_3H_3(-NC_6H_4-2-Ar)$_2$}Ti(THF) (**3**, Ar = 2,6-$^{i}Pr_2$-C_6H_3).* To a 100 mL round bottom flask charged with [(dadi)Ti(THF)](^{c}Hex)$_{0.5}$ (300 mg, 0.42 mmol) was added 75 mL THF at -78 °C. A solution of $PhCHN_2$ (3.4 mL, 0.13 M

in pentane, 0.44 mmol) was added dropwise *via* syringe, and the reaction mixture was stirred for 8 h at -78 ^{o}C. The mixture was then allowed to warm slowly to 23 °C and stirred for an additional 12 h. After removal of the volatiles, the red residue was triturated with hexanes (1 x 20 mL), then taken up in hexanes (20 mL). The reaction mixture was filtered and the filter cake was washed until colorless. The filtrate was cooled to -78 ^{o}C and filtered. After removal of all volatiles the product was collected as a red brown powder (225 mg,0.29 mmol, 70%). ^{1}H NMR (400 MHz, Benzene-d_6): δ δ 0.64 (d, J = 6.7 Hz, 6H, CH_3), 0.78 (d, J = 6.7 Hz, 6H, CH_3), 0.79 (d, J = 6.8 Hz, 6H, CH_3), 1.05 (d, J = 6.7 Hz, 6H, CH_3), 1.08-1.12 (m, 4H, THF-CH_2) 2.12 (sept, J = 6.6 Hz, 2H, ^{i}Pr-CH), 2.86 (sept, J = 6.9 Hz, 2H, ^{i}Pr-CH), 3.12 (t, J = 7.0 Hz, 1H, ^{c}Pr-CH), 3.62 – 3.69 (m, 4H, THF-CH_2), 3.90 (d, J = 7.0 Hz, 2H, ^{c}Pr-CH), 5.62 (dd, J = 7.9, 1.1 Hz, 2H, Ar-CH), 6.55 – 6.61 (m, 2H, Ar-CH), 6.72 (dd, J = 7.8, 1.2 Hz, 2H, Ar-CH), 6.95 (td, J = 7.5, 1.2 Hz, 2H, Ar-CH), 7.00 – 7.14 (m, 9H, ^{c}Pr-Ar-CH and $^{2,6\text{-iPr}}$Ar-CH), 7.58 – 7.62 (m, 2H, ^{c}Pr-Ar-CH).^{13}C NMR (126 MHz, Benzene-d_6): δ 23.60 (CH_3), 24.32 (CH_3), 24.76 (THF-CH_2), 24.88 (CH_3), 26.38 (CH_3), 29.02 (^{i}Pr-CH), 29.30 (^{i}Pr-CH), 43.99 (^{c}Pr-C-Ar), 49.68 (^{c}Pr-C-N), 76.81 (THF-CH_2), 106.42 (Ar-CH), 113.86 (Ar-CH), 120.05 (Ar-CH), 121.51 (Ar-CH), 123.92 ($^{2,6\text{-iPr}}$Ar-CH), 125.63 ($^{2,6\text{-iPr}}$Ar-CH), 126.53 ($^{2,6\text{-iPr}}$Ar-CH), 127.45 (^{c}Pr-Ar-**C**H), 128.35 (^{c}Pr-Ar-**C**H), 131.40(^{c}Pr-Ar-**C**H), 135.66 (^{c}Pr-Ar-**C**), 143.36 ($^{2,6\text{-iPr}}$Ar-C), 143.95 ($^{2,6\text{-iPr}}$Ar-C), 146.33 (Ar-CN), 146.52 (Ar-CN), 146.77 ($^{2,6\text{-iPr}}$Ar-CN). Anal. Calc'd for $C_{49}H_{57}N_4OTi$: C, 76.84; H, 7.50; N, 7.32. Found: C, 75.55: H, 8.03; N, 6.67.

14. *{PhC(CNC$_6$H$_4$-2-NAr)$_2$}Ti(η^2-HNNCPh$_2$) (**4**, Ar = 2,6-^{i}Pr$_2$-C$_6$H$_3$).* To a 25 mL round bottom flask charged with (^{cPr}dadi)Ti(THF) (100 mg, 0.13 mmol) and C_6H_6 (10 mL) was added Ph_2CN_2 (25 mg, 0.13 mmol) in C_6H_6 (3 mL). The

solution was stirred for 4 h at 23 °C. After removal of all volatiles the product was collected as a red solid (104 mg, 90 %). Single crystals were grown by slow evaporation of a concentrated Et_2O solution at -35 °C. ^{1}H NMR (600 MHz, benzene-d_6): δ 0.54 (d, *J* = 6.8 Hz, 3H, CH_3), 0.65 (d, *J* = 6.7 Hz, 3H, CH_3), 0.75 (d, *J* = 6.9 Hz, 3H, CH_3), 0.87 (d, *J* = 6.7 Hz, 3H, CH_3), 0.99 (d, *J* = 6.8 Hz, 3H, CH_3), 1.03 (d, *J* = 6.7 Hz, 3H, CH_3), 1.04 (d, *J* = 6.6 Hz, 3H, CH_3), 1.24 (d, *J* = 6.9 Hz, 3H, CH_3), 3.01 (sept, *J* = 6.7 Hz, 1H, ^{i}Pr-CH), 3.26 (p, *J* = 6.8 Hz, 1H, ^{i}Pr-CH), 3.31 (p, *J* = 6.8 Hz, 1H, ^{i}Pr-CH), 3.38 (sept, *J* = 6.8 Hz, 1H, ^{i}Pr-CH), 5.52 (dd, *J* = 8.0, 1.2 Hz, 1H, Ar-CH), 5.94 (dd, *J* = 8.3, 1.4 Hz, 1H, Ar-CH), 6.64 (ddd, *J* = 8.4, 7.3, 1.2 Hz, 1H, Ar-CH), 6.68 – 6.74 (m, 3H, Ar-CH), 6.78 (ddd, *J* = 8.3, 7.2, 1.3 Hz, 1H, Ar-CH), 6.80 – 6.84 (m, 6H, Ar-CH), 6.87 – 6.94 (m, 3H, Ar-CH), 6.98 (d, *J* = 7.6 Hz, 1H, Ar-CH), 7.05 – 7.25 (m, 12H, Ar-CH), 7.40 (dd, *J* = 7.9, 1.7 Hz, 1H, Ar-CH), 8.52 (s, 1H, nacnac-CH), 8.63 (s, 1H, nacnac-CH), 8.68 (s, 1H, NH). ^{13}C NMR (126 MHz, benzene-d_6): δ 23.23 (coincident CH_3,CH_3), 24.02 (CH_3), 24.36 (CH_3), 24.97 (CH_3), 25.17 (CH_3), 26.28 (CH_3), 26.87 (CH_3), 27.17 (^{i}Pr-CH), 28.58 (^{i}Pr-CH), 28.95 (^{i}Pr-CH), 29.77 (^{i}Pr-CH), 112.22 (Ar-CH), 114.13 (Ar-CH), 115.66 (Ar-CH), 115.72 (Ar-CH), 117.47 (**Ar-C**-nacnac), 120.75 (Ar-CH), 122.03 (Ar-CH), 124.52 ($^{2,6\text{-dipp}}$Ar-CH), 124.77 ($^{2,6\text{-dipp}}$Ar-CH), 124.92 (Ar-CH), 125.67 (coincident Ar-CH,$^{2,6\text{-dipp}}$Ar-CH), 125.85 ($^{2,6\text{-dipp}}$Ar-CH), 125.88(Ar-CH), 127.19 ($^{2,6\text{-dipp}}$Ar-CH), 127.22 (Ar-CH), 127.49 ($^{2,6\text{-dipp}}$Ar-CH), 128.29 (Ar-CH), 128.35 (Ar-CH), 128.59 (Ar-CH), 128.84 (Ar-CH), 129.08 (Ar-CH), 129.38 (Ar-CH), 129.51 (Ar-CH), 134.14 (Ar-C), 137.49 (Ar-CN), 137.57 (Ar-C), 140.42 (nacnac-C), 142.85 (HNN=**C**Ph_2), 143.09 (Ar-CN), 144.24 ($^{2,6\text{-dipp}}$Ar-C), 144.42 ($^{2,6\text{-dipp}}$Ar-C), 144.69 ($^{2,6\text{-dipp}}$Ar-C), 144.81 ($^{2,6\text{-dipp}}$Ar-C), 146.87 (Ar-CN), 148.06 ($^{2,6\text{-dipp}}$Ar-CN), 149.24 (Ar-CN), 149.58 (nacnac-CH), 149.93 ($^{2,6\text{-dipp}}$Ar-CN),

153.68 (nacnac-CH). Anal. Calc'd for $C_{58}H_{60}N_6Ti$: C, 78.36; H, 6.8; N, 9.45. Found: C, 78.50; H 7.38; N 8.69. IR neat film ν(NH) = 3303 cm^{-1}. Anal. Calc'd for $C_{58}H_{60}N_6Ti$: C, 78.36; H, 6.80; N, 9.45. Found: C, 77.88; H 6.99; N 9.20.

C. **Variable Temperature NMR of (dadi)Ti(THF) (1) + $PhHCN_2$.**

An NMR tube sealed onto a 14/20 ground glass joint was charged with (dadi)Ti(THF)·(^{c}HexH)$_{0.5}$ (**1**) (10 mg, 0.014 mmol) and 0.4 mL THF-d_8. The solution was frozen by dipping the tube in LN_2 (covering only 2/3 of the solution to avoid freezing Ar) and 100 µL of a 0.14 M solution of $PhHCN_2$ in pentane was added via syringe under counterflow. The tube was then evacuated and flame sealed. The NMR tube was warmed to -100 °C with a toluene/LN_2 bath, quickly mixed and placed in an NMR probe pre-cooled to -100 °C. The probe was warmed in 5 °C increments up to -25 °C while monitoring by ^{1}H NMR spectroscopy.

D. X-ray Crystal Structures

Upon isolation, the crystals were covered in polyisobutenes and placed under a 173 K N_2 stream on the goniometer head of a Siemens P4 SMART CCD area detector (graphite-monochromated MoKα radiation, λ = 0.71073 Å). The structures were solved by direct methods (SHELXS). All non-hydrogen atoms were refined anisotropically unless stated, and hydrogen atoms were treated as idealized contributions (Riding model).

*[(dadi)TiCH_3][Li(THF)$_2$] (**1**-CH_3·Li).* A red block (0.22 x 0.21 x 0.13 mm) was obtained from pentane. A total of 92,971 reflections were collected with 18,851 determined to be symmetry independent (R_{int} = 0.0264), and 16,643 were greater than 2σ(I). A semi-empirical absorption correction from

equivalents was applied, and the refinement utilized $w^{-1} = \sigma^2(F_o^2) + (0.0484p)^2 + 4.3137p$, where $p = ((F_o^2 + 2F_c^2)/3)$.

*[(dadi)TiN$_3$]Na(12-crown-5) (**1**-N$_3$·Na).* A green needle (0.237 x 0.195 x 0.124 mm) was obtained from THF-*d*$_8$ layered with hexanes. A total of 497,250 reflections were collected with 43,737 determined to be symmetry independent (R_{int} = 0.0354), and 40,931 were greater than 2σ(I). A semi-empirical absorption correction was applied, and the refinement utilized utilized $w^{-1} = \sigma^2(F_o^2) + (0.0778p)^2 + 4.9882p$, where $p = ((F_o^2 + 2F_c^2)/3)$.

*{PhC$_3$H$_3$(-NC$_6$H$_4$-2-Ar)$_2$}Ti(THF) (**3**, Ar = 2,6-^{i}Pr$_2$-C$_6$H$_3$).* A red block (0.44 x 0.25 x 0.12 mm) was obtained from benzene. A total of 58,697 reflections were collected with 11,697 determined to be symmetry independent (R_{int} = 0.0332), and 10,228 were greater than 2σ(I). A semi-empirical absorption correction from equivalents was applied, and the refinement utilized $w^{-1} = \sigma^2(F_o^2) + (0.0502p)^2 + 0.9574p$, where $p = ((F_o^2 + 2F_c^2)/3)$.

*{PhC(CNC$_6$H$_4$-2-NAr)$_2$}Ti(η^2-HNNCPh$_2$) (**4**, Ar = 2,6-^{i}Pr$_2$-C$_6$H$_3$).* A red block (0.15 x 0.12 x 0.3 mm) was obtained from ether. A total of 53,934 reflections were collected with 9,998 determined to be symmetry independent (R_{int} = 0.0332), and 9,038 were greater than 2σ(I). A semi-empirical absorption correction from equivalents was applied, and the refinement utilized $w^{-1} = \sigma^2(F_o^2) + (0.0550p)^2 + 1.7563p$, where $p = ((F_o^2 + 2F_c^2)/3)$.

E. ^{1}H and ^{7}Li DOSY Experiments

Two solutions of **1**-H·Li (10 mg, 490 μL C_6D_6, 22 mM) and (12 mg, 487 μL THF-d_8, 27 mM) were prepared in a scintillation vial then filtered through glass-wool into J-Young NMR tubes. The diffusion coefficients were measured using double pulsed gradient stimulated spin-echo (DPGSE) experiments with convection compensation using the DgscsteSL_cc or Dbppste_cc pulse sequence as provided in VnmrJ 3.2 at 295 K. The ^{7}Li signal in C_6D_6 was ^{1}H-decoupled. The following parameter values were used: ^{1}H nucleus, δ = 0.0018 sec, Δ = 0.1244 sec; ^{7}Li nucleus, δ = 0.004 sec, Δ = 0.0987 sec. Gradient strength was varied from 2.1 to 58.6 Gauss/cm in 24 linear increments.

The raw data was analyzed in MestReNova (v12.0.0-20080) using eq 1 and fitted in IGOR Pro v6.3.7.2. During the fit, each data point was weighted with the standard deviation of the baseline in the corresponding spectrum. The errors reported were obtained directly from the fits in IGOR Pro and represent 3 standard deviations. A plot of $\ln(I/I_o)$ vs $\delta^2\gamma^2(\Delta-\delta/3)G^2$ (Fig. 21) showed deviation from linear behavior indicating free and bound THF species in C_6D_6. Therefore, the data for the THF resonances in C_6D_6 were fitted using a bi-exponential decay (eq 2).

$$I(G') = e^{[-(\gamma G'\delta)^2 * \left(\Delta - \frac{\delta}{3}\right) * D]} \qquad (eq\ 1)$$

$$I(G') = Ae^{[-(\gamma G'\delta)^2 * \left(\Delta - \frac{\delta}{3}\right) * D_1]} + Be^{[-(\gamma G'\delta)^2 * \left(\Delta - \frac{\delta}{3}\right) * D_2]} \qquad (eq\ 2)$$

Where:
I = Peak integral
G' = Strength of the pulse field gradient (Gauss/cm)

G' = G x k (k = 0.0021 that is the probe-specific, calibrated, conversion factor from DAC units of gradient strength to Gauss/cm generated at the coil.)
γ = Gyromagnetic ratio of observed nucleus (26753.2205 $Gauss^{-1}sec^{-1}$ for ^{1}H and 10396.2 $Gauss^{-1}sec^{-1}$ for ^{7}Li)
δ = Pulse field gradient length (sec)
Δ = Diffusion delay (sec)
D = Diffusion coefficient (cm^2/sec)
A = pre-exponential factor representing the relative amount of species with diffusion coefficient D_1
B = pre-exponential factor representing the relative amount of species with diffusion coefficient D_2

F. Calculations.

Density functional theory, within the Gaussian 09 code,[28] was used for all calculations described herein. The ONIOM[29] methodology was utilized to carry out hybrid quantum/molecular mechanics (QM/MM) simulations. Full experimental ligands were modeled with the Dipp substituents on the dadi ligand placed within the MM partition (UFF force field)[30] and the remainder of the system modeled at the M06[31]/6-311+G(d) level of theory. All systems – singlet and otherwise – were modeled with unrestricted Kohn-Sham techniques and the guess=mix option in Gaussian. All geometries were optimized sans symmetry or structural constraint. For all species – minima and transition states – the singlet ground state was predicted to be lowest in energy, to possess the correct number of imaginary frequencies, and to have near zero spin densities (as calculated by Mulliken population analyses), the latter thus indicating closed-shell singlet solutions. Enthalpies and free energies are reported in kcal/mol and assumed 1 atm and 298.15 K.

Table 3. 4. ONIOM(M06/6-311+G(d)/:UFF) Derived Enthalpies (H) and Free Energies (G) for Species Investigated. uDFT = unrestricted DFT. H_{rel} and G_{rel} are the computed relative (to Ti(dadi)(THF) + N_2 + $PhCHN_2$) enthalpies and free energies in kcal/mol @ 298.15 K and 1 atm; Mult = multiplicity.

file	Stoich (Mult)	H(a.u.)	H_{rel} (kcal/mol)	G (a.u.)	G_{rel} (kcal/mol)	Comments
n2	N2	-109.4816		-109.5033		dinitrogen
thf	C4H8O	-232.2161		-232.2507		THF adduct
phchn2	C7H6N2	-379.4817		-379.5222		T ~ 1 eV higher
ti	C38H44N4Ti	-1607.9523	38.5	-1608.0602	21.5	Ti(dadi)
ti-us	C38H44N4Ti	-1607.9523	38.5	-1608.0602	21.5	uDFT for singlet Ti(dadi)
ti-t	C38H44N4Ti(3)	-1607.9354	49.1	-1608.0442	31.5	T Ti(dadi)
tin2	C38H44N6Ti	-1717.4605	-16.7	-1717.5709	-4.7	Ti(N2)(dadi)
tithf	C42H52N4OTi	-1840.2298	0	-1840.3451	0	Ti(dadi)(THF)
tithf-us	C42H52N4OTi	-1840.2298	0	-1840.3451	0	uDFT of S Ti(dadi)THF
tithf-t	C42H52N4OTi(3)	-1840.2091	13	-1840.3271	11.3	T Ti(dadi)(THF)
ti=chph-b	C45H50N4Ti	-1878.0148	-0.6	-1878.1318	-11.6	Ti(=CHPh)(dadi)
ti=chph-b-us	C45H50N4Ti	-1878.0156	-1.1	-1878.1325	-12.1	uDFT for singlet Ti(=CHPh)(dadi)
ti=chph-b-us-conf2	C45H50N4Ti	-1878.0173	-2.2	-1878.1356	-14.1	flip-flop H and Ph of Ti(=CHPh)(dadi), uDFT
ti=chph-b-t	C45H50N4Ti(3)	-1878.0089	3.1	-1878.1271	-8.7	T Ti(=CHPh)(dadi)
ts1	C45H50N4Ti	-1878.0124	0.9	-1878.1284	-9.5	TS1, collapse of terminal carbene to 3-membered TiNC ring, T~20 kcal/nol higher
ts1-conf2	C45H50N4Ti	-1878.0164	-1.6	-1878.1337	-12.8	TS1, flip-flop H and Ph
ts1-us	C49H58N4OTi	-1878.0126	0.8	-1878.1285	-9.6	uDFT of TS1
ts1-t	C45H50N4Ti(3)	-1877.9734	25.3	-1878.0937	12.3	T of TS1
ti=chph	C45H50N4Ti	-1878.0426	-18.1	-1878.1594	-29	3-membered TiNC ring
ti=chph-conf2	C45H50N4Ti	-1878.0426	-18.1	-1878.161	-30	3-membered TiNC ring, flip-flop H and Ph
ti=chph-us-conf2	C45H50N4Ti	-1878.0426	-18.1	-1878.161	-30	uDFT of 3-membered TiNC ring, flip-flop H and Ph
ti=chph-t	C45H50N4Ti(3)	-1878.0082	3.5	-1878.1285	-9.6	T of ti=chph

tinc-t	C45H50 N4Ti(3)	-1878.0011	8	-1878.1214	-5.1	T version of 3-membered TiNC ring
ts3	C45H50 N4Ti	*-1877.973*	25.6	-1878.0903	14.4	TS3, conversion of 3-membered TiNC ring to cPr product (w./o THF)
ts3-us	C45H50 N4Ti	-1877.9819	20	-1878.0967	10.4	uDFT TS3
ticpr-b	C45H50 N4Ti	-1877.9687	28.3	-1878.0892	15.1	3-membered CCN ring
ticpr-b-t	C45H50 N4Ti(3)	-1877.9852	17.9	-1878.1077	3.5	T 3-membered CCN ring
ticpr-wo-thf	C45H50 N4Ti	-1878.0377	-15	-1878.1548	-26.1	product w/o THF
ticpr-wo-thf-us	C45H50 N4Ti	-1878.0377	-15	-1878.1548	-26.1	uDFT of S product w/o THF
ticpr-wo-thf-conf2	C45H50 N4Ti	-1878.0308	-10.7	-1878.1539	-25.5	product w/o THF, H & Ph flip-flopped
ticpr-wo-thf-t	C45H50 N4Ti(3)	-1877.9966	10.8	-1878.1149	-1	T of product w/o THF, H & Ph flip-flopped
13ts-wo-THF	C45H50 N6Ti	-1987.4099	53.7	-1987.5363	50.4	1,3-dipolar addition TS
13-wo-THF	C45H50 N6Ti	-1987.4712	15.2	-1987.5941	14.1	intermediate generated by 1,3-dipolar addn
k1N	C45H50 N6Ti	-1987.4883	4.4	-1987.6118	3	k1-N-phenyldiazomethane complex
eta2NN	C45H50 N6Ti	-1987.49	3.4	-1987.6123	2.7	eta2-NN-phenyl diazomethane complex
eta2NN-conf2	C45H50 N6Ti	-1987.4977	-1.5	-1987.6206	-2.5	eta2-NN-phenyl diazomethane complex, flip-flop H and Ph
eta2NN-conf2-us	C45H50 N6Ti	-1987.4977	-1.5	-1987.6206	-2.5	uDFT of eta2-NN-phenyl diazomethane complex, flip-flop H and Ph
k1C	C45H50 N6Ti	-1987.4633	20.1	-1987.5837	20.6	k1-C-phenyldiazomethane complex
ts4	C45H50 N6Ti	-1987.4551	25.3	-1987.5747	26.3	TS4, TS to form product (w/o THF) direct from eta-2-NNCHPh
ts4-b	C45H50 N6Ti	-1987.4551	25.3	-1987.5747	26.3	TS4 but w/ CalcFC
ts4-b-us	C45H50 N6Ti	-1987.4551	25.3	-1987.5747	26.3	uDFT of TS4
ts4-b-conf2	C45H50 N6Ti	-1987.4557	24.9	-1987.5745	26.4	TS4 w/flip-flop of H and Ph
ts4-b-conf2-us	C45H50 N6Ti	-1987.4561	24.7	-1987.575	26.1	uDFT of above
ts5	C45H50 N6Ti	-1987.4461	31	-1987.5672	31	Nuc attack @ C of PhCHN2 to elim N2 & make carbene
ticpr-wo-thf-n2	C45H50 N6Ti	-1987.5368	-26	-1987.6579	-25.9	Ti(cPr-dadi)(N2)
ticpr	C49H58 N4OTi	-2110.3012	-44.8	-2110.4258	-38.8	CHPh adds to C=C of dadi, from xtal
ticpr-conf2	C49H58 N4OTi	-2110.2999	-44	-2110.4288	-40.7	flip-flop H and Ph from the xtal
ticpr-conf2	C49H58 N4OTi	-2110.2999	-44	-2110.4288	-40.7	uDFT of flip-flop H and Ph from the xtal

ticpr-t	C49H58 N4OTi(3)	-2110.2634	-21.1	-2110.3919	-17.5	T of xtal
ticpr-b-thf	C49H58 N4OTi	-2110.2522	-14	-2110.3807	-10.5	T of 3-membered CCN ring

References:

(1) Heins, S. P.; Morris, W. D.; Wolczanski, P. T.; Lobkovsky, E. B.; Cundari, T. R. *Angew. Chemie Int. Ed. 54* (48), 14407–14411.

(2) Heins, S. P.; Wolczanski, P. T.; Cundari, T. R.; MacMillan, S. N. *Chem. Sci.* **2017**, *8* (5), 3410–3418.

(3) Wolczanski, P. T. *Organometallics*. **2017**, *36* (3), 622–631.

(4) Clark, D. N.; Schrock, R. R. *J. Am. Chem. Soc.* **1978**, *100* (21), 6774–6776.

(5) Fellmann, J. D.; Rupprecht, G. A.; Wood, C. D.; Schrock, R. R. *J. Am. Chem. Soc.* **1978**, *100* (18), 5964–5966.

(6) Gerald, F.; R., S. R. *Prog. Inorg. Chem.* In *Progress in Inorganic Chemistry*; Wiley-Blackwell, 2007; pp 1–74.

(7) Rupprecht, G. A.; Messerle, L. W.; Fellmann, J. D.; Schrock, R. R. *J. Am. Chem. Soc.* **1980**, *102* (20), 6236–6244.

(8) Schrock, R. R.; Sharp, P. R. *J. Am. Chem. Soc.* **1978**, *100* (8), 2389–2399.

(9) Schrock, R. R. *Acc. Chem. Res.* **1979**, *12* (3), 98–104.

(10) Schrock, R. R. *Acc. Chem. Res.* **1990**, *23* (5), 158–165.

(11) Schrock, R. R. *J. Organomet. Chem.* **1986**, *300* (1), 249–262.

(12) Schrock, R. R.; Fellmann, J. D. *J. Am. Chem. Soc.* **1978**, *100* (11), 3359–3370.

(13) Edema, J. J. H.; Duchateau, R.; Gambarotta, S.; Hynes, R.; Gabe, E. *Inorg. Chem.* **1991**, *30* (2), 154–156.

(14) Heins, S. P.; Morris, W. D.; Cundari, T. R.; MacMillan, S. N.; Lobkovsky, E. B.; Livezey, N.; Wolczanski, P. T. *Organometallics*. **2018**, *In Press*.

(15) Sanderson, R. T. *J. Am. Chem. Soc.* **1983**, *105* (8), 2259–2261.

(16) Bondi, A. *J. Phys. Chem.* **1964**, *68* (3), 441–451.

(17) Hare, S. R.; Orman, M.; Dewan, F.; Dalchand, E.; Buzard, C.; Ahmed, S.; Tolentino, J. C.; Sethi, U.; Terlizzi, K.; Houferak, C.; et al. *J. Org. Chem.* **2015**, *80* (10), 5049–5065.

(18) Allen, F. H.; Kennard, O.; Watson, D. G.; Brammer, L.; Orpen, A. G.; Taylor, R. *J. Chem. Soc. Perkin Trans. 2*. **1987**, No. 12, S1–S19.

(19) Branchadell, V.; Muray, E.; Oliva, A.; Ortuño, R. M.; Rodríguez-García, C. *J. Phys. Chem. A*. **1998**, *102* (49), 10106–10112.

(20) Bartlett, P. A.; Meadows, J. D.; Ottow, E. *J. Am. Chem. Soc.* **1984**, *106* (18), 5304–5311.

(21) Michael, S.; Michał, B.; J., N. A.; Tobias, F.; M., L. R.; Nattamai, B.; A., G. J. *Angew. Chemie Int. Ed.* **2011**, *50* (29), 6647–6651.

(22) Fabian, R.; Kai, A.; Dirk, H.; Anke, S.; Haijun, J.; Perdita, A.; Uwe, R.; Torsten, B. *Chem. – A Eur. J.* **2017**, *23* (33), 7891–7895.

(23) Otte, D. A. L.; Woerpel, K. A. *Org. Lett.* **2015**, *17* (15), 3906–3909.

(24) McMahon, R. J.; Abelt, C. J.; Chapman, O. L.; Johnson, J. W.; Kreil, C. L.; LeRoux, J. P.; Mooring, A. M.; West, P. R. *J. Am. Chem. Soc.* **1987**, *109* (8), 2456–2469.

(25) Lévesque, É.; Goudreau, S. R.; Charette, A. B. *Org. Lett.* **2014**, *16* (5), 1490–1493.

(26) Creary, X. *Org. Synth.* **1986**, *64*, 207–216.

(27) Rendina, V. L.; Kingsbury, J. S. *J. Org. Chem.* **2012**, *77* (2), 1181–1185.

(28) Gaussian 09, Revision D.01, M. J. Frisch, G. W. Trucks, H. B. Schlegel, G. E. Scuseria, M. A. Robb, J. R. Cheeseman, G. Scalmani, V. Barone, B. Mennucci, G. A. Petersson, H. Nakatsuji, M. Caricato, X. Li, H. P. Hratchian, A. F. Izmaylov, J. Bloino, G. Zheng, J. L. Sonnenberg, J. M. Hada, M. Ehara, K. Toyota, R. Fukuda, J. Hasegawa, M. Ishida, T. Nakajima, Y. Honda, O. Kitao, H. Nakai, T. Vreven, J. A. Montgomery, Jr., J. E. Peralta, F. Ogliaro, M. Bearpark, J. J. Heyd, E. Brothers, K. N. Kudin, V. N. Staroverov, R. Kobayashi, J. Normand, K. Raghavachari, A. Rendell, J. C. Burant, S. S. Iyengar, J. Tomasi, M. Cossi, N. Rega, J. M. Millam, M. Klene, J. E. Knox, J. B. Cross, V. Bakken, C. Adamo, J. Jaramillo, R. Gomperts, R. E. Stratmann, O. Yazyev, A. J. Austin, R. Cammi, C. Pomelli, J. W. Ochterski, R. L. Martin, K. Morokuma, V. G. Zakrzewski, G. A. Voth, P. Salvador, J. J. Dannenberg, S. Dapprich, A. D. Daniels, Ö. Farkas, J. B. Foresman, J. V. Ortiz, J. Cioslowski, D. J. Fox, Gaussian, Inc., Wallingford CT, 2009.

(29) Dapprich, S.; Komáromi, I.; Byun, K. S.; Morokuma, K.; Frisch, M. J. *J. Mol. Struct. THEOCHEM*. **1999**, *461–462*, 1–21.

(30) Casewit, C. J.; Colwell, K. S.; Rappe, A. K. *J. Am. Chem. Soc.* **1992**, *114* (25), 10046–10053.

(31) Zhao, Y.; Truhlar, D. G. *Theor. Chem. Acc.* **2008**, *120* (1), 215–241.

CHAPTER 4

Oxidative Additions to (dadi^{4-})Ti(THF)

Introduction:

Pyridine diimine and α-diimine ligands have shown to be useful chelates for Fe catalyzed C-C bond formation.[1–3] Redox non-innocence (RNI) was not invoked in early examples of iron catalyzed diene coupling[3] but it is likely operative. Examples out of the Heyduk and Abu-Omar laboratories showed *o*-phenylenediamide[4] and α-diimine[5] ligands can act as electron reservoirs permitting oxidative addition to formally d^0 metal centers. C-C bond forming reactions *via* reductive elimination from Zr(IV) complexes is facilitated by the use of the RNI 2,4-di-*tert*-butyl-6-*tert*-butylamidophenolate (ap^{2-}) ligand.[6] Furthermore, the requirement that a metal ion have accessible M^{n+} and $M^{(n+2)+}$ oxidation states for oxidative addition[7] can be circumvented with the RNI ap^{2-} ligand which can be oxidized to an imino-semiquinone diradical, enabling oxidative addition to the formally d^0 $Zr^{IV}(ap)_2(THF)_2$ complex.[8] A primary goal of this laboratory has been to find solid experimental evidence of similar radical character in the tetradentate diamide-dimine chelate ($[\{\text{-CH=N(1,2-}C_6H_4\text{)NH(2,6-}^{i}Pr_2\text{-}C_6H_3\text{)}\}_2]^n$ = $(dadi)^n$ (n = -0 to -4)) with titanium.

Reactivity studies revealed alkylation of the ligand backbone of (dadi^{4-})Ti(THF) (**1**-THF, dadi = $[\{\text{-CH=N(1,2-}C_6H_4\text{)NH(2,6-}^{i}Pr_2\text{-}C_6H_3\text{)}\}_2]^n$). These reactions represent a divergence from the two-electron processes discussed previously (*cf.* Chapters 1-3). Isolated products that are likely a result of direct oxidative additions or polar oxidative additions between alkyl halides and **1**-THF highlight the versatility of the dadi ligand as well as its redox non-innocence. Additionally, the formation of complexes (dadi-Bz)TiX (**5**-X, dadi-Bz

= (C_6H_5-CH_2)-C[=N(1,2-C_6H_4)NAr]-[CH_2-N(1,2-C_6H_4)NAr], Ar = 2,6-$^{i}Pr_2$-C_6H_3,X = Cl, Br) and (dadi-CH_3)TiBr (**6**-Br, dadi-CH_3 = CH_3-C[=N(1,2-C_6H_4)NAr]-[CH_2-N(1,2-C_6H_4)NAr], Ar = 2,6-$^{i}Pr_2$-C_6H_3) provides mechanistic insight into the formation of titanium dimer [(^{C}Hex-dadi)Ti(NHAd)]$_2$ (**9**, ^{c}Hex-dadi = 2,5-(C=N(1,2-C_6H_4)NAr)-1,4-(CH-N(1,2-C_6H_4)NAr)cyclohexane, Ar = 2,6-$^{i}Pr_2$-C_6H_3, Ad = adamantyl).

Results and Discussion:

4.1. Synthesis of (dadi-R)TiX (5-Cl, R = Bz, X = Cl; 5-Br, R = Bz, X = Br; 6-Br, R = Me, X = Br)

*4.1.1. (dadi-Bz)TiX (**5**-X, X = Cl, Br)*

Treatment of **1**-THF with BzX (X = Cl, Br) in C_6H_6 afforded brown crystalline products that precipitated from solution. ^{1}H NMR spectroscopy revealed the presence of a benzyl group in the product and a disappearance of symmetry in the ligand. Curiously, two sets of diastereotopic protons exhibiting strong geminal coupling (J_{HH} = 24-25 Hz) were observed in the ^{1}H NMR sprectra of **5**-Cl and **5**-Br, accompanied by the loss of the typical diimine hydrogen singlet. Based upon the ^{1}H NMR spectra of the products, it was hypothesized that a rearrangement of the protons within the diimine backbone had occurred. Single crystals of **5**-Cl obtained from a concentrated THF solution layered with pentane permitted X-ray diffraction experiments. This structural study revealed installation of the benzyl moiety on the diimine carbon and a 1,2-hydrogen migration generating an adjacent sp^3 carbon center.

4.1.2. (dadi-Me)TiBr

Initial attempts to synthesize a methyl derivative of **5**-X (X = Cl, Br) were unsuccessful. No reaction was observed between **1**-THF and methyl iodide at room temperature. Attempts to initiate the reaction by addition of 10

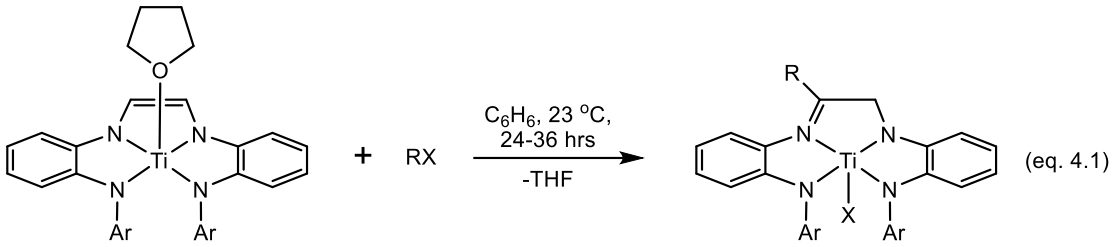

1-THF
Ar = 2,6-^{i}Pr-C_6H_3

5-Cl, R = Benzyl, X = Cl, 54%
5-Br, R = Benzyl, X = Br, 73%
6-Br, R = Me, X = Br, 69%
6-Cl, R = Me, X = Cl, 1H NMR only, (not isolated)

(eq. 4.1)

mol % benzyl chloride only resulted in formation of **5-**Cl with the remaining 90% of **1**-THF left unreacted. It should be noted that heating **1**-THF with methyl iodide was not attempted. Treating a C_6D_6 solution of **1-**THF with methyl bromide at 23 °C for 10 days resulted in only 50 % conversion to the desired product **6**-Br. However, heating the reaction to 55 °C resulted in complete conversion after approximately 1.5 days.

4.1.3. Synthesis of (dadi)TiX$_2$ (X = Cl, Br, I)

(dadi)$TiCl_2$ (**1**-Cl_2) was targeted during the early reactivity studies of **1**-THF but reactions with various chlorine atom sources were fraught with inseparable side products and low yields. The first attempt to synthesize **1**-Cl_2 utilized two equiv. of N-chlorosuccinamide (NCS) as a chlorine atom source, and gave promising results. The ^{1}H NMR spectrum of the crude reaction mixture revealed a product with C_2 symmetry, as would be expected for the

dichloride **1**-Cl_2. However, the bi-products from NCS could only be removed after repeated crystallizations and impurities of unknown origin still remained in the final product. Treatment of **1**-THF with CCl_4 gave similar results but with more side products derived from the dadi ligand.

The preparation of pure **1**-Cl_2 was achieved by treating **1**-THF with 2.1 equivalents of hexachloropropene in the presence of 10 mol% azobisisobutyronitrile (AIBN) as a radical initiator. Unfortunately, the 12 % yield of **1**-Cl_2 as a green crystalline solid after recrystallization from toluene was not synthetically practical. Finally, the use of 1 equiv. of $SnCl_4(THF)_2$ proved to be an effective chlorine atom source and **1**-Cl_2 was obtained in 56% yield after precipitation from a THF solution with diethyl ether (Scheme 4.2). Oxidation of **1**-THF by tin(IV) reagents proved to be a general route to access the bromide and iodide derivatives where green **1**-Br_2 and brown **1**-I_2 were obtained in 46% and 58% yields, respectively (eq. 4.2).

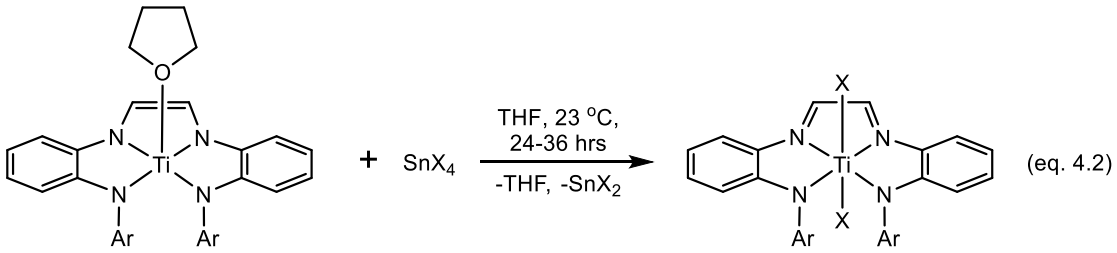

1-THF
Ar = 2,6-^{i}Pr-C_6H_3

1-Cl_2, 56%
1-Br_2, 48%
1-I_2, 58%

4.2. Crystal structures of 1-Br_2 and 5-Cl_2

*4.2.1. (dadi)$TiBr_2$ (**1**-Br_2)*

The structure of **1**-Br_2 shown in Figure 4.1 depicts a pseudo octahedral titanium center chelated by a dadi^{2-} ligand with the two bromines occupying the apical positions. The d(C=N) distances of 1.312(3) and 1.316(3) Å in the

backbone indicate double bond character and the d(C-C) distance of 1.416(3) Å is appropriate for a single bond,[9] demonstrating the dadi^{2-} oxidation state of the ligand. In corroboration, d(Ti-N_{amide}) distances of 2.0052(18) Å and 2.0063(19) Å, compared to the elongated d(Ti-N_{imine}) distances of 2.1352(19) Å and 2.1131(18) Å are in line with the dadi^{2-} formalism. The d(Ti-N) distances in **1**-Br_2 are the shortest of the structurally characterized complexes containing a dadi^{2-} ligand, likely a consequence of the titanium essentially positioned in the plane of the four N-donors. The two N_{amide}-Ti-N_{imine} angles differ by only 0.14^o (N1-Ti-N2 = 78.12(8)^o; N3-Ti-N4 = 77.98(7)^o) whereas the angle between the two amides and the titanium of 131.51(8)^o is larger relative to the

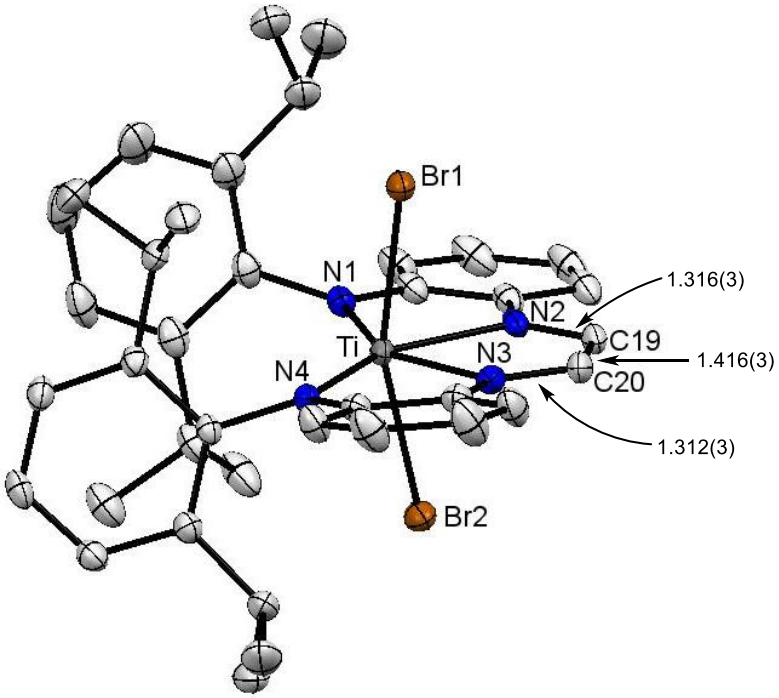

Figure 4.1. Crystal structure of **1**-Br_2 and bond lengths of the diimine ligand backbone (Å). Hydrogen atoms have been omitted for clarity.

two other structurally characterized (dadi^{2-})TiX complexes (X = NAd, O; N_{amide}-Ti-N_{amide} = 123.75(2)^{o}, 124.02(5)^{o}).[10] The titanium center in six-coordinate (dadi^{4-})Ti(CNMe)$_2$ (**1**-($CNMe_2$))[10] is also in-plane with the tetradentate chelate and shows similar angles around N-donors of the dadi ligand despite it existing as a tetraanion. Regardless of the ligand redox state, when the titanium center is 5-coordinate the metal can extend out of the plane of the ligand, but coordination of a sixth ligand forces the titanium into the chelate plane, and subsequently the angles between the N-donors and the titanium become wider.

*4.2.2. (dadi-Bz)TiCl (**5**-Cl)*

Shown in Figure 4.2 is the structure of (dadi-Bz)TiCl (**5**-Cl, (dadi-Bz) = (C_6H_5-CH_2)-[C(=N(1,2-C_6H_4)NAr)]-[CH_2-N(1,2-C_6H_4)NAr], Ar = 2,6-$^{i}Pr_2$-C_6H_3) revealing its 5-coordinate Ti(IV) center chelated by the tetradentate dadi-Bz ligand. The benzyl modified dadi ligand is trianionic with 3 amide nitrogens and one imine nitrogen. Nearly identical d(Ti-N_{amide}) distances of 1.9848(18), 1.9785(18), and 1.9790(18) Å compared to the elongated d(Ti-N_{imine}) distance of 2.1584(18) Å support the tris-amide formulation for the ligand. Furthermore, the metrics of the ligand backbone are consistent with imine and amide nitrogens (d(N2-C19) = 1.291(3) Å, d(N3-C20) = 1.445(3) Å, d(C19-C20) = 1.479(3) Å). The Ti is out of the plane of the four N-donors by ~0.458 Å, and as a result, the angle between the 2,6-^{i}Pr-C_3H_6 amides (∠N1-Ti-N4 = 121.02(7)°) and Ti is contracted compared to the six-coordinate (dadi)TiL_2/X_2 (L = CNMe; X = Br) complexes. The angle between the two aryl amides is consistent with other 5-coordinate [(dadi)TiL/X]^{n} complexes (n = -1, X = CH_3, N_3, Cl; n = 0, X = NAd, O, L = PMe_2Ph).

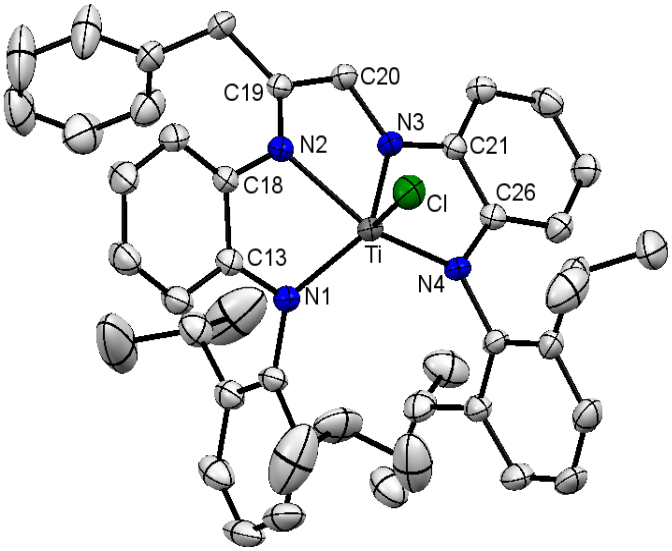

Figure 4.2. Molecular structure of **5**-Cl. Hydrogens atoms have been omitted for clarity.

4.3. Thermolysis of (dadi)$TiCl_2$ (1-Cl_2)

*4.3.1. Synthesis of (DaIm)$TiCl_2$ ((DaIm) = N^1-Ar-N^2-((1-Ar-1-benzo[d]imidazol-2-yl)methyl)benzene-1,2-diamide; Ar = 2,6-^{i}Pr-C_6H_3)) (**8**)*

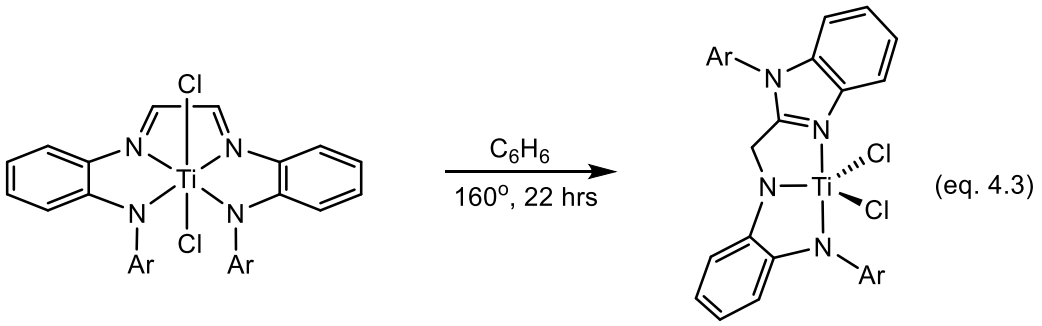

1-Cl_2
Ar = 2,6-^{i}Pr-C_6H_3

8, 80%

(eq. 4.3)

While testing the thermal stability of **1**-Cl_2 an interesting ligand rearrangement was discovered yielding (DaIm)$TiCl_2$ (**8**, (DaIm) = N^1-Ar-N^2-((1-Ar-1-benzo[*d*]imidazol-2-yl)methyl)benzene-1,2-diamide; Ar = 2,6-^{i}Pr-C_6H_3) in 80% yield (eq 4.3). ^{1}H and ^{13}C NMR spectra of the product were puzzling at

first. The ^{1}HNMR spectrum of **8** shows four independent ^{i}Pr-CH_3 groups and an apparent shift of the signature diimine singlet from δ = 7.60 ppm to δ = 4.88 ppm. In addition, a quaternary carbon is observed at δ = 160.09 ppm in the $^{13}C\{^{1}H\}$ NMR spectrum that showed an HSQC correlation to the singlet at δ = 4.88 ppm.

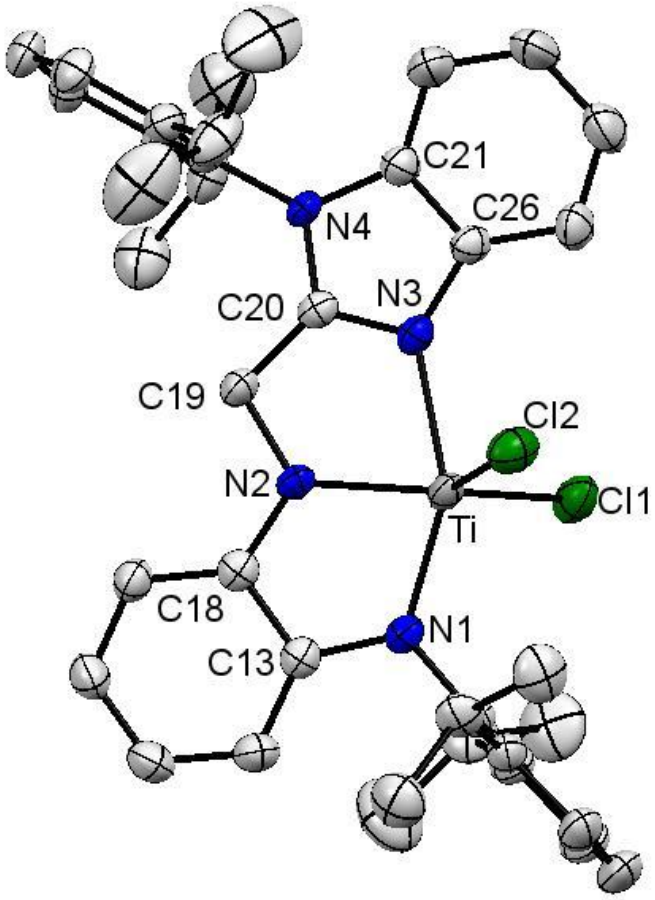

Figure 4.3. Molecular structure of **8**. Hydrogen atoms have been omitted for clarity.

It was initially hypothesized that the product was generated by transfer of both chlorides to the ligand backbone accompanied by a 1,2-hydrogen shift, the latter of which was also observed with complexes **5**-X and **6**-X (X = Cl,Br).

Incommensurate with the chemical shift of the quaternary carbon at δ 160.09 ppm (tentatively assigned to the backbone carbon with two chlorides) are the carbon chemical shifts of dichloromethane and carbon tetrachloride of δ 53.46 and 96.44 ppm, respectively. Thus, single crystals of **8** obtained by slow evaporation of a concentrated pentane solution were subjected to X-ray diffraction experiments. The structure of **8** (Figure 4.3) revealed a benzimidazole moiety, resulting from nucleophilic attack of the 2,6-^{i}Pr-C_6H_3 amide on the diimine carbon. En route to the final product, a 1,2-hydrogen shift also occurs, explaining the up-field shift of the "diimine" hydrogen singlet and appearance of the quaternary carbon at δ 160.09 ppm observed in the $^{13}C\{^{1}H\}$ NMR sprectrum of **8**. The oxidized dadi^{2-} can be construed as electrophilic compared to the dadi^{4-} form, making it susceptible to attack by nucleophiles such as the 2,6-^{i}Pr-C_6H_3 aryl amides.

*4.3.2 Crystal structure of (DaIm)$TiCl_2$ (**8**)*

The molecular structure of **8** consists of a distorted trigonal bipyramidal (τ_5 = 0.27)[11] titanium center (∠Cl1-Ti-Cl2 = 107.69(4)°; ∠Cl2-Ti-N2 = 115.11(8)°; ∠N2-Ti-Cl1 = 135.58(8)°) with two chloride ligands and an amide occupying the base of the bipyramid (d(Ti-Cl1) = 2.2579(11) Å; d(Ti-Cl2) = 2.2519(10) Å ; d(Ti-N2) = 1.978(2) Å). In the two axial positions are an amide nitrogen (d(Ti-N1) = 1.955(2) Å) and a neutral imine nitrogen (d(Ti-N3) = 2.138(2) Å) of the benzimidazole ring. The carbon-nitrogen distances of d(N3-C20) = 1.322(3) Å and d(N4-C20) = 1.352 Å confirm the benzimidazol formulation.[8] Validation of the methylene assignment made from HSQC and ^{1}H NMR experiments are carbon nitrogen distances of d(N2-C19) = 1.458(3) Å

and d(C19-C20) = 1.463(4) Å, consistent with N(sp^3)-C(sp^3) and C(sp^3)-C(sp^2) single bonds.[9]

4.4. Mechanism of alkyl halide additions forming (dadi-R)TiX (5-Cl, R = Bz, X = Cl; 5-Br, R = Bz, X = Br; 6-Br, R = Me, X = Br; 6-Cl, R = Me, X = Cl)

4.4.1. General

The mechanism for the addition of alkyl halides to **1**-THF producing complexes **5**-X and **6**-X (X = Cl, Br) was initially believed to proceed through a radical chain or ion-pair/oxidative addition mechanism. Consistent with both mechanisms is the qualitative reactivity trend of Bz >> Me and Br > Cl. The half-life of the benzyl halide additions are approximated to be on the order of seconds, but the reactions proceed too quickly to be measured by ^{1}H NMR spectroscopy at 23 ^{o}C. The half-life for the addition of methyl bromide to **1**-THF is 1 h and *ca.* 28 h for methyl chloride. During the attempts to measure the rates for the addition of MeX (X = Br, Cl) it was found that the reaction was sporadic. For example, when monitoring the addition of methyl chloride to **1**-THF, 2 of 6 trials produced only trace amount of **6**-Cl from the same batch of starting materials. Moreover, a similar situation was encountered when monitoring the addition of methyl bromide. Thus quantitative kinetic data for the alkyl halide addition to **1**-THF is not available at this time.

4.4.2. Radical chain mechanism

The sporadic nature of the alkyl halide additions seemed to hint at the possibility of a radical chain process. To test this, **1**-THF was treated with two different “radical clocks”, 1-bromomethylcyclopropane and 1-bromo-1-hexene. Cyclopropylcarbinyl ring opening proceeds with a rate constant of 1.3 x 10^8

s^{-1} (310 K) and ring closing of 1-hexenyl radical occurs with a rate constant of 1.0×10^5 s^{-1} (298 K),[12] both of which are expected to be faster than trapping by a (dadi)TiL/X_n (n = 0,1) species. ^{1}H NMR spectroscopic analysis of the crude reaction mixture of **1**-THF and 1 equiv 1-bromomethylcyclopropane revealed new cyclopropyl resonances but no new vinylic resonances. Similar analysis of the reaction mixture from treating **1**-THF with 1 equiv 1-bromo-1-hexene revealed a product containing only vinylic resonances and no apparent cyclopentyl species. These data suggest that radicals are unlikely to be involved in the mechanism to form complexes (dadi-R)TiX (R = Bz, Me; X = Cl, Br).

4.4.3. Oxidative addition/migratory insertion and polar oxidative addition

Alternative mechanisms to form complexes (dadi-R)TiX (R = Bz, Me; X = Cl, Br) involve a standard oxidative addition (OA), followed by migratory insertion (MI) and a 1,2-H shift (Scheme 4.1). The dadi ligand may be flexible enough to allow the *cis*-addition, and the electrophilicity of the diimine backbone is enhanced as the dianion ($dadi^{2-}$) making the backbone susceptible migratory insertion events.

The (dadi)Ti(THF) (**1**-THF) complex can also be viewed as an enediamide nucleophile when in its tetraanionic form ($dadi^{4-}$). Hence, another mechanistic possibility leading to alkyl halide addition involves nucleophilic attack of the enediamide backbone as a polar oxidative addition pathway. This may proceed as a chain process initiated by reduction of **1**-THF to a $[(dadi)Ti-X]^-$ anion such as the known $[(dadi)TiCl]Li(THF)_4$, followed by alkylation of the backbone to generate halide anion. Propagation would proceed by coordination of X^- to titanium and enediamide attack at alkyl halide. The 1,2 H-

shift would either occur after backbone alkylation or previous to nucleophilic attack.

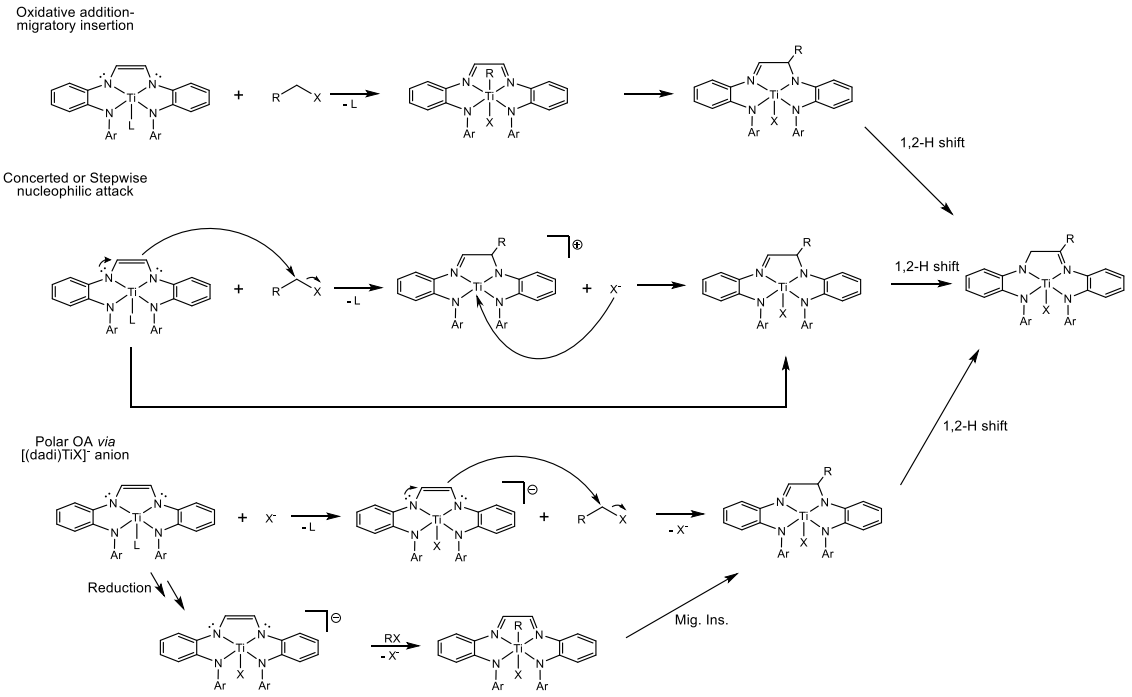

Scheme 4.1. Possible mechanisms for alkyl halide addition to **1**-THF.

To probe the viability of the polar oxidative addition mechanism, [(dadi)TiCl]Li(THF)$_4$ was treated with benzyl chloride in C_6D_6 at 23 ^oC leading to an immediate color change from dark green to orange-brown. ^1H NMR spectroscopic analysis showed complete conversion to a new species after 12 minutes, tentatively assigned as the alkylation product that precedes the 1,2-H shift (**5`**-Cl, eq 4.4).

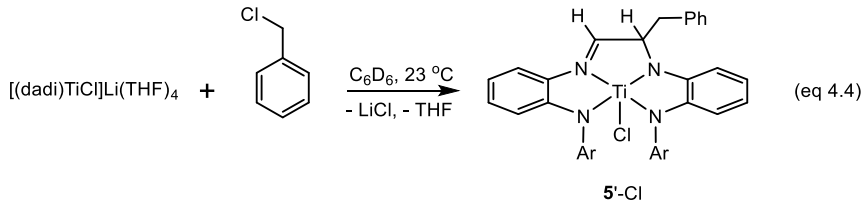

5'-Cl

After characterization of complex **5**`-Cl by 2D-NMR spectroscopy, the sample was heated to 55 ^{o}C for 2 h, which did not induce the 1-2-H shift. This suggests that the 1,2-H shift is likely to occur prior or alkylation of the dadi backbone, although other pathways such as a base assisted 1,2-H shift ,or those shown in Scheme 4.1 cannot be ruled out at this time.

*4.4.2. Synthesis and Structure of [(^{C}Hex-dadi)Ti(NHAd)]$_2$ (**9**, ^{c}Hex-dadi = 2,5-(C=N(1,2-C$_6$H$_4$)NAr)-1,4-(CH-N(1,2-C$_6$H$_4$)NAr)cyclohexane, Ar = 2,6-^{i}Pr$_2$-C$_6$H$_3$, Ad = adamantyl).*

The chance discovery of titanium dimer [(^{C}Hex-dadi)Ti(NHAd)]$_2$ (**9**) is an intriguing example of the intricate processes displayed by dadi-related complexes. The opening reactivity studies of Cr-, Fe-, and Ti-dadi complexes focused on the formation of metal imidos with the hopes of aziridinating alkenes. As previously discussed (*cf.* Chapter 1), intramolecular aziridination of the dadi ligand occurs when (dadi)Fe and (dadi)Cr(THF) complexes are treated with organic azides. Following these studies, research efforts were focused on (dadi)TiNAd (**2**=NAd) and the possibility of reactivity derived from iminyl chararacter in the Ti=NAd bond.

To assess the possibility of aziridination, **2**=NAd was treated with 2 equiv ethylene in the presence of 0.5 eqiv PMe$_2$Ph, and heated to 55 ^{o}C in C$_6$D$_6$ (eq. 4.4). No direct reaction between **2**=NAd and ethylene was observed, but the disappearance of **2**=NAd and the formation of a small amount of red-brown crystals was noted after approximately 3-4 weeks. Upon removal from the 55 ^{o}C oil bath, and sitting at room temperature for 1 week, more crystals had formed. These harvested crystals were subjected to X-ray diffraction experiments with the hopes of attaining a structure of the starting imido

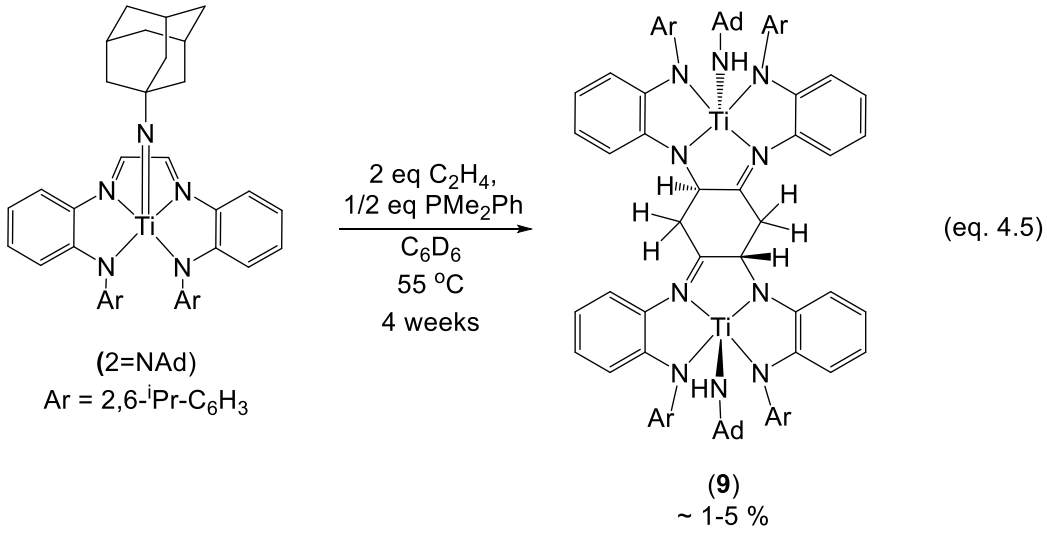

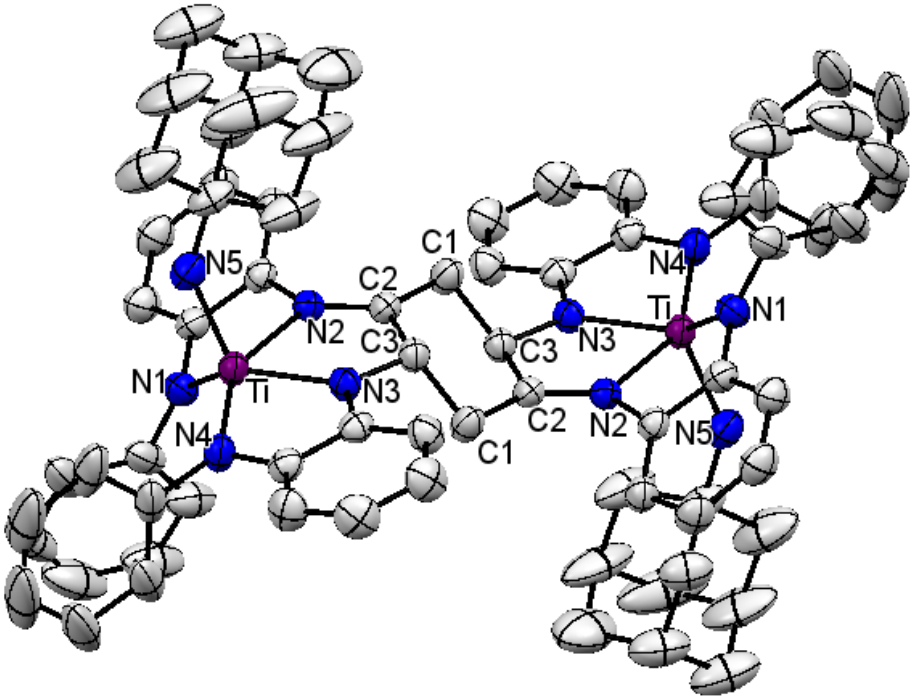

Figure 4.4. Molecular structure of [(^{C}Hex-dadi)Ti(NHAd)]$_2$ (**9**). ^{i}Pr groups, hydrogens, and disordered adamantyl atoms are omitted for clarity.

2=NAd. Surprisingly, complex **9** (eq. 4.5) was revealed containing two (dadi)Ti(HNAd) centers linked together with bridging methylenes forming a 1,4-diamido-2,5-diimino-cyclohexyl moiety. The significantly bent angle of Ti-

N_{amide}-C_{Ad} (∠Ti1-N5-C49 = 140.6(2)°) and Ti-N_{amide} distance (d(Ti-N5) = 1.887(3) Å) are uncharacteristic of a metal imido, providing evidence for the

Selected Bond Distances (Å)		Selected Bond Angles (°)	
Ti-N1	1.995(3)	N1-Ti-N2	76.59(9)
Ti-N2	2.142(2)	N2-Ti-N3	73.41(9)
Ti-N3	1.980(2)	N3-Ti-N4	78.5(1)
Ti-N4	2.006(3)	N1-Ti-N4	116.8(1)
N2-C2	1.282(3)	Ti-N5-C40	140.6(2)
N3-C3	1.441(3)	N2-C2-C1	128.7(2)
Ti-N5	1.887(3)	C2-C1-C3	110.7(2)
C2-C1	1.498(4)	C3-C2-C1	117.7(2)
C1-C3	1.552(3)	N2-C2-C3	113.4(2)
		N3-C3-C2	108.4(2)

Table 4. 1. Selected interatomic distances and bond angles for [(^{C}Hex-dadi)Ti(NHAd)]$_2$ (**9**).

imide to amide conversion. Furthermore, the disparity between the two carbon-nitrogen bond distances in the dadi NCCN backbone (d(N3-C3) = 1.441(3) Å and d(N2-C2) = 1.282(3) Å) indicates single and double bonds. By considering the stoichiometry of **9**, it is conceivable that the cyclohexyl methylenes originate from 1 molecule of ethylene and the hydrogen lost from the backbone was transferred to the imido nitrogen to furnish the final amide. Reactivity studies were conducted to elucidate the mechanism of the formation of **9**. A complete list of reaction conditions and control experiments are listed in Table 4.2.

First, to unveil the origin of the cyclohexyl methylenes, the synthesis of **9** was conducted using D_4- and ^{13}C-labeled ethylenes (Table 4.2 entries 10-14). Unfortunately, isotopic incorporation into **9** was not observed in either case, indicating that ethylene is not the source of the cycohexyl methylenes found in the product. Ethylene does appear to be a critical component for the

Entry	Ethylene [a]	Solvent	T (°C)	PR_3	Additive	**9**
1	C_2H_4	C_6D_6	55	PMe_2Ph	-	Y
2	C_2H_4	C_6D_6	55	PMe_2Ph	-	Y
3	C_2H_4	THF-D_8	55	PMe_2Ph	-	N
4	C_2H_4	C_6D_6	55	PMe_2Ph[b]	-	N
5	C_2H_4	C_6D_6	55	-	-	N
6	-	C_6D_6	55	PMe_2Ph	-	N
7	C_2H_4	C_6D_6	105	PMe_2Ph	-	N
8[c]	1 atm C_2H_4	C_6D_6	55	PMe_2Ph	-	Y
9[c]	5 atm C_2H_4	C_6D_6	55	PMe_2Ph	-	Y
10	C_2D_4	C_6D_6	55	PMe_2Ph	-	Y
11	C_2D_4	THF-D_8	55	PMe_2Ph	-	N
12	$C_2H_2(D)_2$	C_6D_6	55	PMe_2Ph	-	Y
13	$^{13}C_2H_4$	THF-D_8	55	PMe_2Ph	-	N
14	$^{13}C_2H_4$	C_6D_6	55	PMe_2Ph	-	Y
15	C_2H_4	C_6D_6	55	$P(CD_3)_2Ph$	-	N
16	C_2H_4	C_6D_6	55	$P(CH_3)(^{13}CH_3)Ph$	-	N
17	C_2H_4	C_6D_6	55	10 eqiv $P(CH_3)(^{13}CH_3)Ph$	-	N
18	C_2H_4	C_6D_6	55	$P(^{13}CH_3)_2Ph$	1 mol% AIBN	N
19	C_2H_4	C_6D_6	55	$P(^{13}CH_3)_2Ph$	2 mol% $(O)PMe_2Ph$	N
20	C_2H_4	C_6D_6	55	$P(CH_3)(^{13}CH_3)Ph$	1 mol% AIBN	N
21	C_2H_4	C_6D_6	55	0.25 eqiv PMe_2Ph	0.25 equiv $P(^{13}CH_3)_2Ph$	N
22	C_2H_4	C_6D_6	55	PMe_2Ph	6 mol% benzoylperoxide	Y
23	C_2H_4	C_6D_6	55	PMe_2Ph	1 mol% AIBN	Y
24	-	C_6D_6	55	PMe_2Ph	Ph_2PCl	N
25	C_2H_4	C_6D_6	55	PMe_2Ph	Ph_2PCl	N
26	C_2H_4	C_6D_6	55	PMe_2Ph	12 mol % PMe_3	N
27	C_2H_4	C_6D_6	55	PMe_2Ph	12 mol % PMe_3	N
28	-	C_6D_6	55	PMe_2Ph	1 eqiv stilbene	N
29[d]	-	C_6D_6	75	-	1.1 equiv toluene	N
30	-	C_6D_6	55	-	0.5 equiv CHD	N
31	-	C_6D_6	55	PMe_3	0.5 equiv CHD	N
32[e]	-	C_6D_6	55	-	-	N

Table 4.2. Control experiments attempting to synthesize **9**. [a] 2 eqiv unless stated otherwise. [b] New commercial sample. [c] No discernable change in rate of starting material decay. [d] No reaction after 7 days. [e] No decomposition after 28 days.

synthesis of **9**. When **2**=NAd was subjected to the same reaction conditions without ethylene, the formation of **9** is not observed (entry 6).

Attention was then turned to the dimethylphenylphosphine as the source of the cyclohexyl methylenes. **9** is not formed in the absence of PMe_2Ph (entry 5), hinting at its role in the reaction. The use of $P(CD_3)_2Ph$ did not result in product formation either (entry 15). Originally, this was taken to mean that a hydrogen atom abstraction may be an initial step in the formation of **9**, and if a large kinetic isotope effect is at play, then the rate of dimer formation could be outcompeted by simultaneous reactions occurring in solution. Experiments using $P(CD_3)(CH_3)Ph$ and $P(^{13}CH_3)_2Ph$ (entries 16-20) were conducted with the hopes that **9** would be formed with partial deuterium or ^{13}C incorporation but did not form **9**. Lastly, a control experiment was conducted using a freshly purchased sample of PMe_2Ph, which also did not yield the dimer **9** (entry 4). This led to the conclusion that a small impurity (albeit unknown) present in the original bottle of PMe_2Ph may be initiating the formation of **9**, since independently synthesized phosphines and newly purchased commercial samples of phosphine did not yield the desired product. The active impurity was reasoned to be dimethylphenylphosphine oxide, which is present in the bottle of PMe_2Ph (*ca.* 2%) that yields **9**. Thus, $OP(Me)_2Ph$ (2 mol%) was added to reaction mixture using $P(^{13}CH_3)_2Ph$ labeled phosphine. This did not result in the formation of dimer **9**, suggesting that $OP(Me)_2Ph$ is not the active product forming reagent or reaction initiator. Only one bottle of PMe_2Ph leads to product formation and one possible explanation is that a radical reaction is occurring, which is initiated by an impurity or lack an inhibitor.

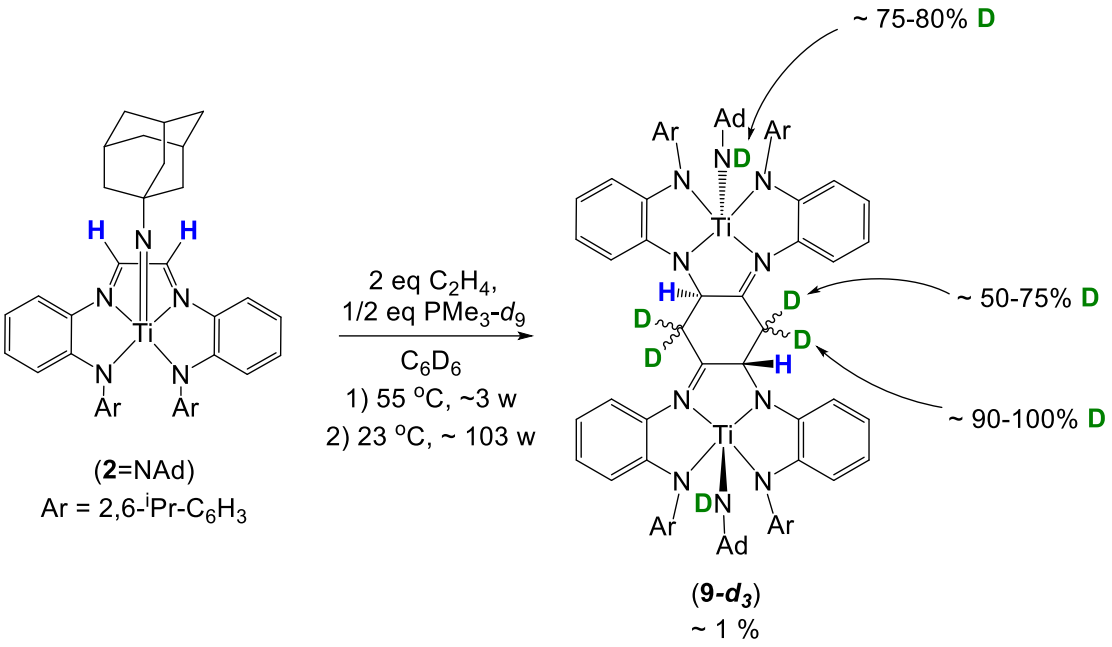

Scheme 4.2. Synthesis of **9**-d_6 and corresponding amounts of deuterium incorporation detected by ^{1}H NMR spectroscopic analysis.

When **2**=NAd was treated with ethylene and 0.5 eqiv PMe_3-d_9 in C_6D_6, and heated for the prescribed 3 weeks, the formation of crystalline solid was not observed (Scheme 4.2). After allowing the reaction mixture to sit undisturbed for ~103 weeks at room temperature, an extremely small amount of crystalline solid had formed in the bottom of the reaction vessel. These crystals (~ <1 mg) were carefully harvested and taken up in THF-d_8. After sonication for 30 minutes, the clear solution turned a faint orange, indicating dissolution of the crystals. Upon ^{1}H NMR spectroscopic analysis, the product was revealed to be **9**-d_6 (Scheme 4.2). As illustrated in Figure 4.7, complex **9**-d_6 contains ~75-80% deuterium incorporation into the adamantyl-amide nitrogen, ~90-100% deuterium incorporation into one methylene position, and ~50-75% deuterium incorporation into the other methylene position of the cyclohexyl diimine ring. This provides critical evidence that the alkyl phosphine serves as the methylene source for complex **9**/**9**-d_6.

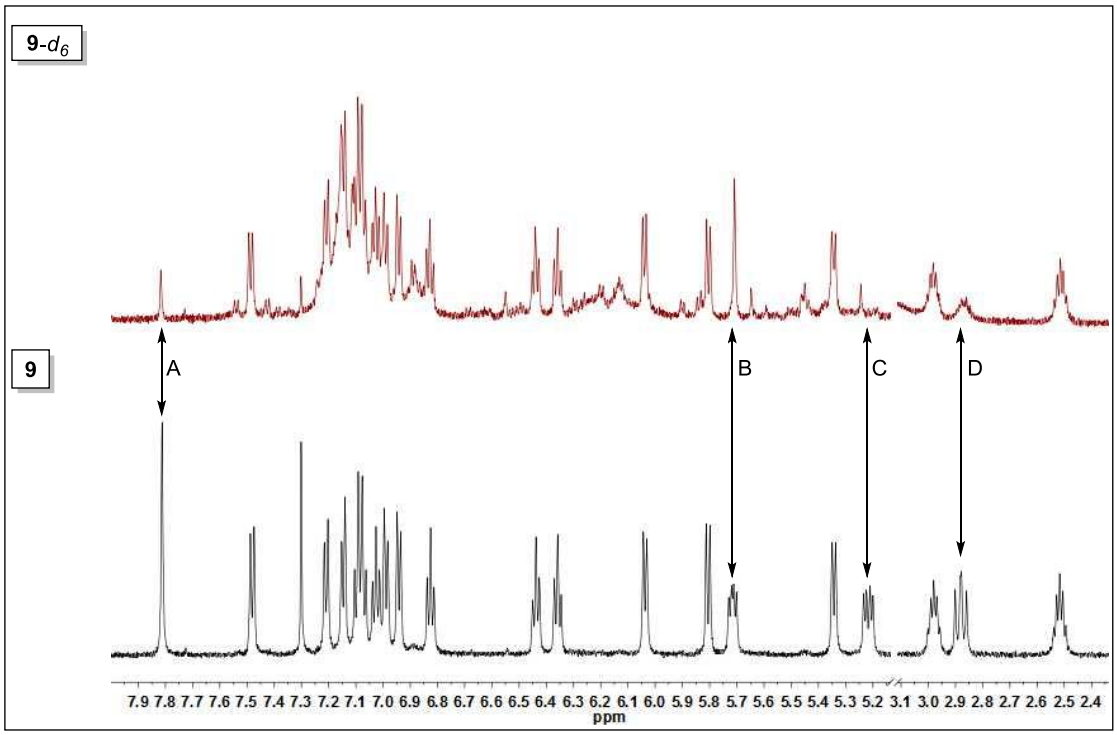

Figure 4.5. Stacked ^{1}H NMR spectra of **9** (bottom) synthesized from PMe_2Ph and **9**-d_6 (top) synthesized from PMe_3-d_9; THF-d_8, 600MHz, 298 K. A) Adamantyl amide nitrogen with ~75-80% deuterium incorporation into **9**-d_6. B) Imine-CH that has no deuterium incorporation and has collapsed into a singlet in **9**-d_6. C) Methylene-CH with ~90-100% deuterium incorporation in **9**-d_6. D) Methylene-CH with ~50-75% deuterium incorporation into **9**-d_6. All other δ and J_{HH} values are within 0.01 ppm and 0.5 Hz, respectively, for both complexes.

Isotope incorporation at the adamantyl amide nitrogen suggests that a hydrogen/deuterium abstraction step may occur, potentially *via* an imidyl species that initiates a radical chain mechanism (Scheme 4.3). Scheme 4.3 illustrates a hydrogen atom abstraction step involving **2**=NAd and PMe_2Ph to generate (dadi^{3-})$^{\uparrow}$Ti(NHAd) and a ($^{\bullet}CH_2$)PMePh radical. Propagation involves attack of the phosphine radical at the ligand backbone of **2**=NAd to create an imidyl intermediate. Hydrogen atom abstraction from PMe_2Ph would regenerate the propagating ($^{\bullet}CH_2$)PMePh radical. Thus, PMe_2Ph serves as the H atom source for the imide to amide conversion, producing (dadi'-P)Ti(NHAd) as the key intermediate.

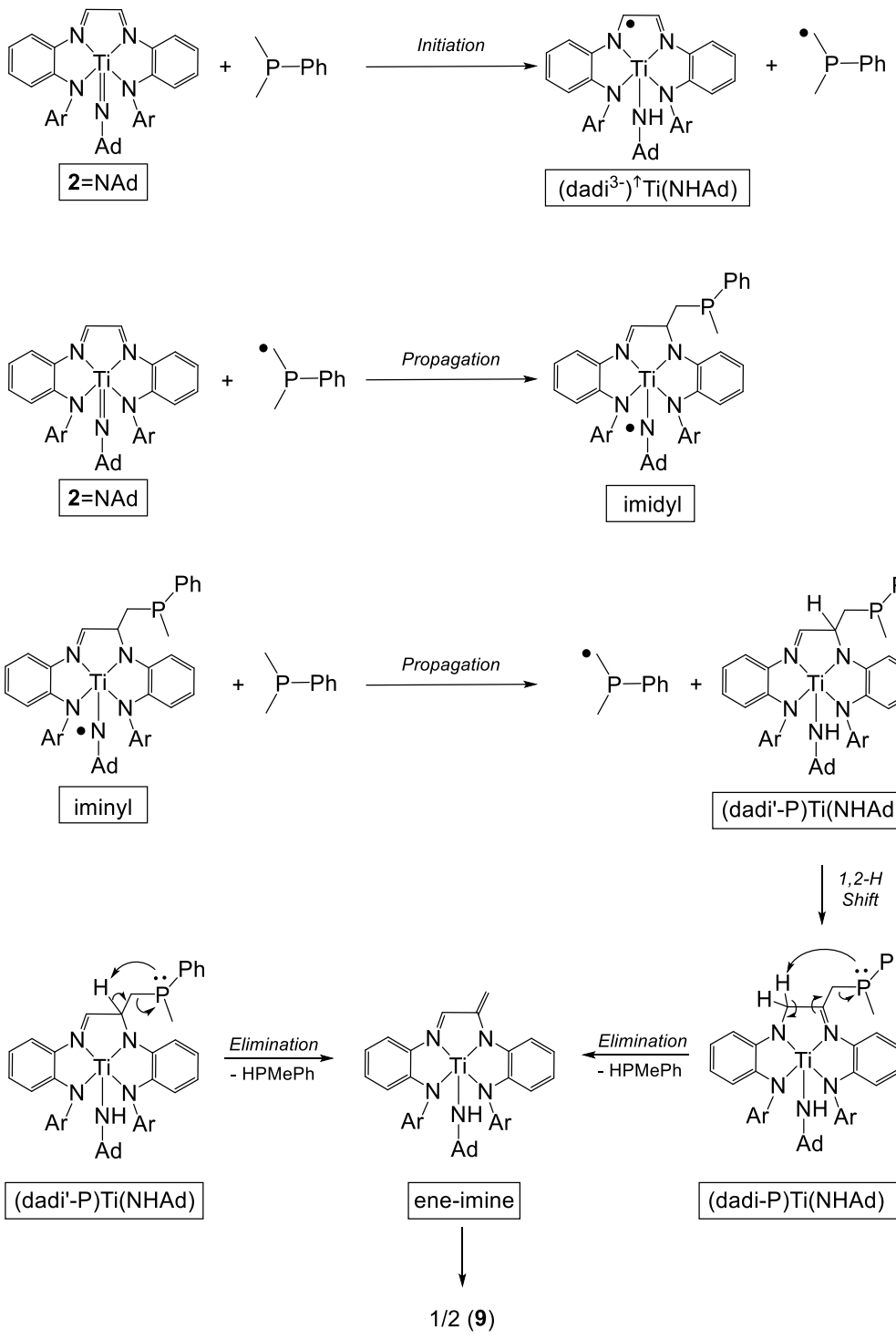

Scheme 4.3. Proposed mechanism leading to the formation of [(^{C}Hex-dadi)Ti(NHAd)]$_2$ (**9**). Ad = adamantyl. Ar = 2,6-^{i}Pr-C_6H_3.

Imidyls are known to undergo hydrogen atom abstractions during hydroamination reactions[13] lending credence to this claim. (dadi'-P)Ti(NHAd) is postulated to undergo either a 1,2 hydrogen shift (similar that observed for compounds **5**-X and **6**-X (X = Cl, Br)) to give (dadi-P)Ti(NHAd), which then eliminates HPMePh, or to directly eliminate HPMePh to give the ene-imine intermeditate. Cyclization of two ene-imines would furnish the final product **9**. Lastly, ethylene may be necessary to scavenge reactive side products such as HPMePh, or to generate imidyl character *via* coordination to the titanium center.

*4.2.3. Synthesis of (dadi-CH_2PPh_2)TiCl (**7**, (dadi-CH_2PPh_2) = ($(C_6H_5)_2P$-CH_2)-[C(=N(1,2-C_6H_4)NAr)]-[CH_2-N(1,2-C_6H_4)NAr], Ar = 2,6-$^iPr_2$-C_6H_3)*

The proposed mechanism in Scheme 4.3 has guided the current efforts to provide concrete evidence for the involvement of (dadi-P)Ti(NHAd) and the ene-imine intermediate to form **9**. Hence, the synthesis of a (dadi-P)TiX (P = CH_2PPh_2, X = Cl) complex was targeted to test the possibility that elimination of HPR_2 could generate an ene-imine capable of cyclization. A strategy analogous to the synthesis **5**-X and **6**-X (X = Cl, Br) was employed to install a ($–CH_2PR_2$) moiety on the backbone with an X type ligand at titanium. It was envisioned that chloromethyldiphenyl phosphine would be able to undergo a radical addition giving the ($–CH_2PPh_2$) group on the backbone with a chloride ligand on titanium.

Initial attempts to synthesize chloromethyldiphenyl phosphine involved deprotonation of diphenylphosphine with ^{n}BuLi in THF, followed by addition of the *in situ* generated phosphide to neat dichloromethane at -78 ^{o}C. This resulted in an 8:2 mixture of chloromethyldiphenyl phosphine and

bis(diphenylphosphino)methane which could not be separated. Chloromethyldiphenyl phosphine was instead synthesized following the method of Lanhaus et. al. (eq. 4.6).[13] This method uses the phase transfer catalyst $^{n}Bu_4NCl$ with KOH as a mild way of generating diphenyl phosphide, which then undergoes nucleophilic attack at methylene chloride to give the desired chloromethyldiphenyl phosphine as an air and thermally sensitive colorless oil in 45% yield. Samples chloromethyldiphenyl phosphine decompose to an unknown insoluble solid, but toluene solutions can be stored at -35 ^{o}C for weeks without any noticeable decomposition.

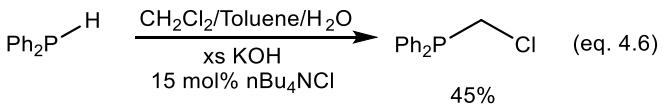

(eq. 4.6)

Treatment of **1**-THF with chloromethyldiphenyl phosphine at room temperature in C_6H_6, gave the desired product (dadi-CH_2PPh_2)TiCl (**7**, (dadi-CH_2PPh_2) = ((C_6H_5)$_2$P-CH_2)-[C(=N(1,2-C_6H_4)NAr)]-[CH_2-N(1,2-C_6H_4)NAr], Ar = 2,6-$^{i}Pr_2$-C_6H_3) as a brown powder in 59% yield (eq. 4.7). The ^{1}H NMR spectrum of **7** is similar the complexes **5**-X and **6**-X (X = Cl, Br) with one notable exception: the diastereotopic methylene protons adjacent to the phosphine show the usual doublet pattern (J_{HH} = 12.2 Hz), but only one of the protons is coupled to the phosphorous (J_{HP} = 1.2 Hz).

*4.2.4. Thermolysis of (dadi-CH_2PPh_2)TiCl (**7**, (dadi-CH_2PPh_2) = ((C_6H_5)$_2$P-CH_2)-[C(=N(1,2-C_6H_4)NAr)]-[CH_2-N(1,2-C_6H_4)NAr], Ar = 2,6-$^{i}Pr_2$-C_6H_3)*

With the hopes of eliminating diphenyl phosphine to give an ene-imine (Scheme 4.3) capable of dimerization, (dadi-CH_2PPh_2)TiCl (**7**) was heated to

55 °C in C_6D_6 for one week. The reaction was monitored by ^1H NMR spectroscopy and the decay of **7** in solution appears to be first order. This suggests that an intermolecular deprotonation is not occurring. Unfortunately, the only isolated product from the reaction, which crystallized upon standing at room temperature for 1 week, was complex **6**-Cl. It should be noted that **6**-Cl a minor product and that the identity(s) of the other species generated from the thermolysis of **7** are currently unknown.

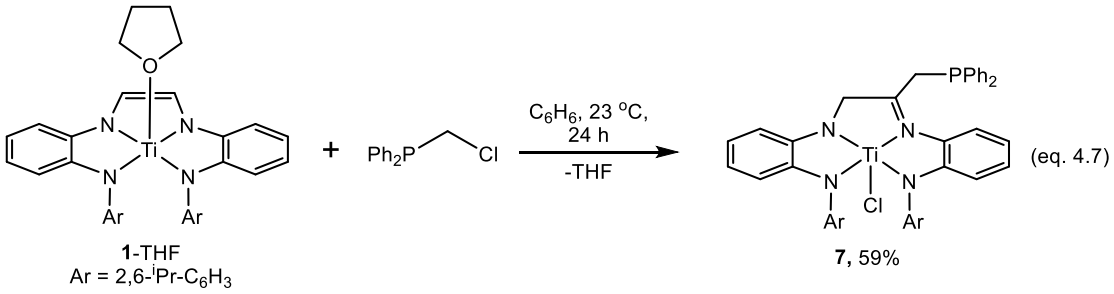

*4.2.5. Structure of (dadi-CH_3)TiCl (**6**-Cl,* dadi-CH_3 = (CH_3-CH_2)-C[=N(1,2-C_6H_4)NAr]-[CH_2-N(1,2-C_6H_4)NAr], Ar = 2,6-^{i}Pr$_2$-C_6H_3)

The crystal structure of **6**-Cl is illustrated in Figure 4.6, and relevant parameters are listed in Table 4.3. The methyl modified dadi ligand, similar to (dadi-Bz)Ti-Cl (**5**-Cl), is trianionic consisting of one neutral N_{imine} (d(Ti-N3) = 2.154(1) Å) and three anionic N_{amide} donors (d(Ti-N_{amide}) = 1.976(1) Å (ave)) occupying the equatorial plane. Moreover, the metrics of the NCCN backbone are consistent with imine (d(N3-C20 = 1.288(2) Å) and amide (d(N2-C19) = 1.451(2) Å) nitrogens. The titanium sits out of the plane of the four N-donors by ~0.482 Å resulting in a contracted angle between the 2,6-^{i}Pr-C_6H_3 amides (∠N1-Ti-N4 = 118.68(5)°).

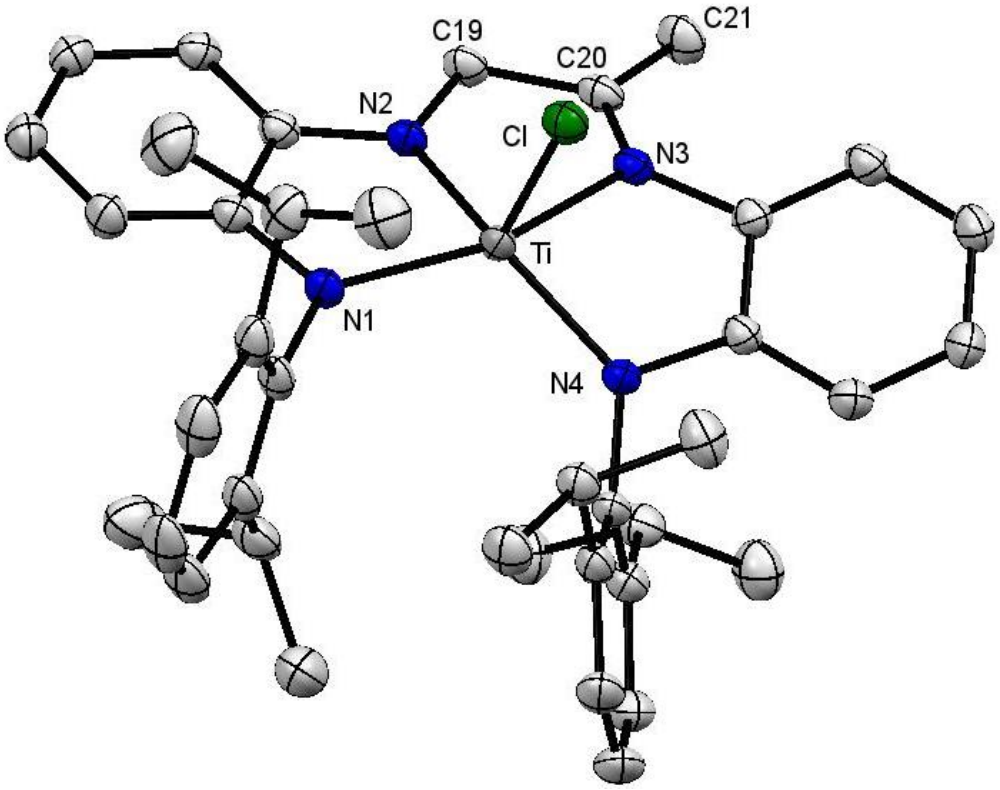

Figure 4.6. Molecular structure of (dadi-CH_3)TiCl (**6**-Cl). Hydrogens omitted for clarity.

Selected Bond Distances (Å)		Selected Bond Angles (°)	
Ti-N1	1.980(1)	N1-Ti-N2	78.99(5)
Ti-N2	1.975(1)	N2-Ti-N3	73.14(5)
Ti-N3	2.154(1)	N3-Ti-N4	76.50(5)
Ti-N4	1.973(1)	N4-Ti-N1	118.68(5)
Ti-Cl	2.2804(4)	N1-Ti-Cl	106.34(4)
N2-C19	1.451(2)	N2-Ti-Cl	108.73(4)
N3-C20	1.288(2)	N3-Ti-Cl	92.07(4)
C19-C20	1.487(2)	N4-Ti-Cl	105.54(4)
C20-C21	1.496(2)	N2-C19-C20	108.1(1)
		C19-C20-N3	113.6(1)
		N3-C20-C21	127.6(1)
		C19-C20-C21	118.8(1)

Table 4.3. Selected interatomic distances and bond angles for (dadi-CH_3)TiCl (**6**-Cl).

*4.2.6. Synthesis of (DaIm)Ti=NAd(OPMe$_2$Ph) (**10**, (DaIm) = N^1-Ar-N^2-((1-Ar-1-benzo[d]imidazol-2-yl)methyl)benzene-1,2-diamide; Ad = adamantyl; Ar = 2,6-^{i}Pr-C$_6$H$_3$)*

While testing the reactivity of **2**=NAd, a ligand rearrangement similar to the thermolysis of **1**-Cl$_2$ was discovered, yielding (DaIm)Ti=NAd(OPMe$_2$Ph) (**10**, (DaIm) = N^1-Ar-N^2-((1-Ar-1-benzo[*d*]imidazol-2-yl)methyl)benzene-1,2-diamide; Ad = adamantyl; Ar = 2,6-^{i}Pr-C$_6$H$_3$) in 67% yield. As depicted in eq 4.8, the rearrangement to **10** is chemically induced by dimethylphenylphoshine oxide. A 1,2-hydrogen shift giving the final product parallels that observed during the thermolysis of **1**-Cl$_2$. The mild conditions to generate **10** stand in contrast to the relatively harsh thermal conditions (160 °C) required to induce the same reaction for **1**-Cl$_2$. It should be noted that treatment of **2**=NAd with other Lewis bases such as phosphines (PMe$_3$, PMe$_2$Ph) and isocyanides (CNMe, 2,6-dimethylphenylisocyanide) does not induce the ligand rearrangement. It is interesting that treatment with a mild Lewis base (OPMe$_2$Ph) causes the arylamide ligand to become labile, and nucleophilically attack at the imine carbon of the (dadi)$^{2-}$ backbone. As previously mentioned, the dianionic form of the dadi ligand with a diimine backbone, renders it electrophilic and susceptible to nucleophiles.

The ^{1}H NMR spectrum of **10** in THF-*d*$_8$ displays broad resonances, and free (O)PMe$_2$Ph is observed in the ^{31}P NMR spectrum. This suggests exchange with THF-*d*$_8$ and indicates that the phosphine oxide may be labile. Compared to the (dadi)Ti=NAd (**2**=NAd) starting material, complex **10** now has an open coordination site upon dissociation of (O)PMe$_2$Ph, adjacent to the titanium-imido double bond. The possibility of CH activation is currently being explored.

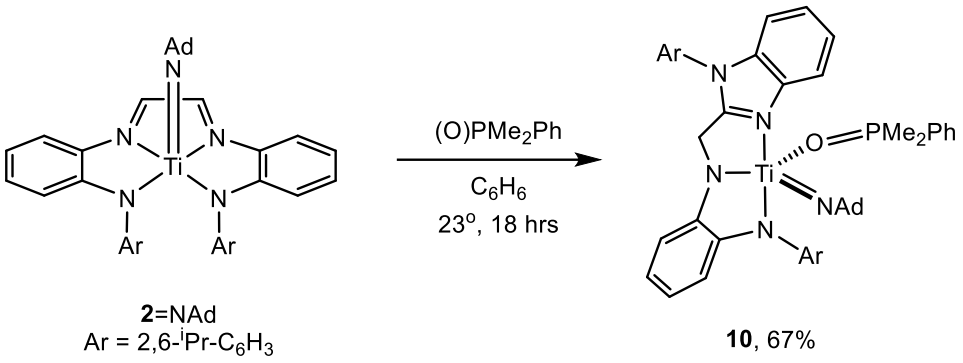

2=NAd
Ar = 2,6-^{i}Pr-C_6H_3

10, 67%

(eq. 4.8)

*4.2.6. Strucuture of (DaIm)Ti=NAd(OPMe$_2$Ph) (**10**, (DaIm) = N^1-Ar-N^2-((1-Ar-1-benzo[d]imidazol-2-yl)methyl)benzene-1,2-diamide; Ad = adamantyl; Ar = 2,6-^{i}Pr-C_6H_3)*

Complex **10** crystallized as a non-merohedral twin, but the data set was able be refined in the *P-1* space group. Figure 4.8 illustrates the molecular structure of (DaIm)Ti=NAd(OPMe$_2$Ph) (**10**), revealing the distorted square pyramidal coordination geometry (τ_5 = 0.15)[11] around the titanium center. The axial site of the square pyramid is occupied by the imido nitrogen with a d(Ti-N_{imido}) distance of 1.723(2) Å, which is slightly longer (0.023 Å) than that found in (dadi)Ti=NAd (**2**=NAd). Compared to the titanium-imido angle in **2**=NAd (169.4(4)°), that for **10** is less (∠Ti-N5-C39 = 157.7(2)°), although the bond metrics are in line with Ti^{IV}-imido species.[14] At the base of the square pyramid are the aryl-amide, phenylene-amide, and imidazole nitrogens, where the latter two are derived from the original (dadi)$^{2-}$ backbone. The d(Ti-N1) and d(Ti-N2) bond lengths of 2.091(3) Å and 2.042(2) Å, respectively, are consistent with anionic nitrogens, while the titanium-$N_{imidazole}$ distance of 2.222(2) Å is in line with a neutral donor. The bond lengths in the benzimidazole ring are normal (d(N3-C20) = 1.328(4) Å; d(N4-C20) = 1.362(3) Å), and are similar to those found in (DaIm)$TiCl_2$ (**8**). The d(C19-C20) distance

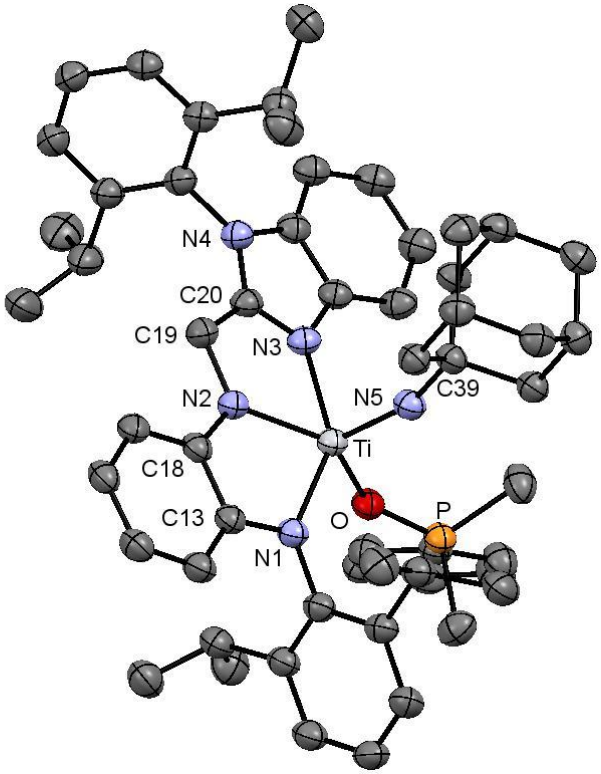

Figure 4.7. Molecular view of (DaIm)Ti=NAd(OPMe$_2$Ph) (**10**). Hydrogen atoms removed for clarity.

Selected Bond Distances (Å)		Selected Bond Angles (°)	
Ti-N1	2.091(3)	Ti-N5-C39	157.7(2)
Ti-N2	2.042(2)	O-Ti-N5	107.9(1)
Ti-N3	2.222(2)	O-Ti-N2	137.60(9)
Ti-N5	1.723(2)	N1-Ti-N5	109.8(1)
N3-C20	1.328(4)	N2-Ti-N5	114.1(1)
N4-C20	1.362(3)	N3-Ti-N5	96.0(1)
C20-C19	1.483(5)	Ti-O-P	138.4(1)
N2-C19	1.438(3)		
N2-C18	1.373(4)		
C18-C13	1.429(3)		
N1-C13	1.388(4)		
Ti-O	2.035(2)		
O-P	1.514(2)		

Table 4.4. Selected interatomic distances and angles for (DaIm)Ti=NAd(OPMe$_2$Ph) (**10**).

of 1.483(5) Å is consistent with an C_{sp3}-C_{sp2} single bond[9] and the angles around planar C20 of the benzimidazole sum to 359.95(3) °, providing further evidence for the 1,2-hydrogen shift indicated by ^{1}H NMR spectroscopy. The remaining angles and distances are listed in Table 4.4, and do not deviate significantly from those found in complex **8**.

Conclusions:

While the exact mechanism to form dimer [(^{C}Hex-dadi)Ti(NHAd)]$_2$ (**9**) has not been fully elucidated, it seems likely that radical processes are involved. Even though the thermolysis of (dadi-CH_2PPh_2)TiCl (**7**) did not yield the dimer (**9**) *via* elimination of phosphine, the formation of complex (dadi-CH_3)TiCl (**6**-Cl) does suggest that an alkyl phosphine, once bonded to the dadi ligand backbone, can act as a methyl/methylene source. It may be that the diphenyl substituted phosphine is not basic enough to deprotonate the adjacent imine to induce the elimination. Thus, current efforts are focused on appending a more basic phosphine with an alkyl substituent in place of one of the phenyl groups. Secondly, the role of the imido nitrogen may be important in proton or hydrogen atom transfer *en route* to dimer **9**, therefore substitution of the chloride, with an amide ligand in complex **7**, is being explored through metathetical routes.

The reactivity studies presented herein showcase the nucleophilic and electrophilic nature of the dadi^{4-} and dadi^{2-} redox states, respectively. The mechanism of (dadi)Ti(THF) (**1**-THF) alkylation does not appear to involve a radical chain mechanism based upon radical clock experiments. Hence, oxidative addition/migratory insertion or direct backbone alkylation *via* enediamide nucleophilic attack represent viable mechanisms leading to

(dadi-R)TiX (R = Bz, Me; X = Cl, Br) complexes. The synthesis of dihalides **1**-X_2, (X = Cl, Br, I), in conjunction with the studies presented in Chapters 2 and 3, provide clear evidence for the $(dadi)^{2-}$ and $(dadi)^{4-}$ redox states. This chemistry highlights the diverse types of reactivity that can be achieved with a single, redox non-innocence ligand.

Experimental:

A. General Considerations

All manipulations were performed using either glovebox or high vacuum line techniques. All glassware was oven dried. THF and diethyl ether were distilled under nitrogen from purple sodium benzophenone ketyl and vacuum transferred from the same prior to use. Hydrocarbon solvents were treated in the same manner with the addition of 1-2 mL/L tetraglyme. Benzene-d_6 was dried over sodium, vacuum transferred and stored over activated 4Å molecular sieves. THF-d_8 was dried over sodium and stored over purple sodium benzophenone ketyl. Benzyl chloride and benzyl bromide were purchased from Sigma-Aldrich and distilled under vacuum before use. Methyl bromide was purchased from Union Carbide and used as received. $SnCl_4$, $SnBr_4$, SnI_4 were all purchased from Sigma-Aldrich and used as received. Dimethylphenyl phosphine was purchased from Strem Chemicals and degassed before use. Ethylene was purchased from Matheson and used as received. N,N'-di-2-(2,6-diisopropylphenylamine)-phenylglyoxaldiimine (dadiH_2),[15] (dadi)$Na_2(THF)_4$,[10] and (dadi)Ti(THF)[10] were prepared following literature procedures.

NMR spectra were acquired using Mercury 300 MHz, INOVA 400 MHz, or Bruker AV III HD 500 MHz (equipped with a 5 mm BBO Prodigy cryoprobe) spectrometers. Chemical shifts are reported relative to benzene-d_6 (^{1}H δ 7.16; ^{13}C{^{1}H} δ 128.06) or THF-d_8 (1H 3.58; ^{13}C{^{1}H} 67.57). Due to the low solubility of **9**, a 1D-^{13}C NMR spectrum could not be attained; hence all ^{13}C NMR chemical shifts were indirectly detected *via* HSQC- and HMBC-2D NMR spectroscopy obtained using a Bruker AV III HD 800 MHz NMR spectrometer equipped with a 5mm TCI cryoprobe. NMR spectra were processed using

MNova 12.0. Infrared spectra were recorded on a 20 Nicolet Avatar 370 DTGX spectrophotometer interfaced to an IBM PC (OMNIC software).

B. Procedures

1. (dadi)$TiCl_2$ ($1\text{-}Cl_2$): To a 50 mL round bottom flask charged with (dadi)Ti(THF)$^{C}Hex_{0.4}$ (200 mg, 0.28 mmol) and $SnCl_4(THF)_2$ (114 mg, 0.28 mmol) was added 25 mL of freshly distilled THF at -78 ^{o}C. The reaction mixture was allowed to warm slowly to room temperature and stirred for 60 hrs. The green solution was filtered then concentrated to a total volume of 10 mL. The reaction solution was cooled to -78 ^{o}C and freshly distilled Et_2O was added while maintaining vigorous stirring. The reaction mixture was allowed to warm to room temperature, stirred for 8 hours, filtered then washed (2x). After removal of all volatiles (dadi)$TiCl_2$ was collected as a green microcrystalline solid (107 mg, 56%). ^{1}H NMR (500 MHz, Benzene-d_6) δ 0.98 (d, J = 6.7 Hz, 12H, CH_3), 1.07 (d, J = 6.6 Hz, 12H, CH_3), 3.56 (bs, 4H, ^{i}Pr-CH), 6.05 (d, J = 8.5 Hz, 2H, Ar-CH), 6.65 (t, J = 7.6 Hz, 2H, Ar-CH), 6.79 (t, J = 8.1 Hz, 2H, Ar-CH), 7.04 (d, J = 8.3 Hz, 2H, Ar-CH), 7.16 – 7.25 (m, 6H, $^{2,6\text{-dipp}}$Ar-CH), 7.60 (s, 2H, Im-CH). ^{13}C NMR (126 MHz, Benzene-d_6) δ 24.16 (CH_3), 25.53 (CH_3), 29.55 (^{i}Pr-CH), 115.51 (Ar-CH), 117.58 (Ar-CH), 124.04 (Ar-CH), 125.48 (Ar-CH), 129.13 (Ar), 131.70 (Ar), 134.18 (Ar), 139.16 (Ar), 144.00 (Ar-CN), 144.95 (Ar-CN), 155.85 (Ar-CN). Anal. Calc'd for $C_{38}H_{44}Cl_2N_4Ti$: C, 67.56; H, 6.57; N, 8.29. Found: C, 68.07; H, 6.59; N, 7.36.

2. (dadi)$TiBr_2$ ($1\text{-}Br_2$): To a 50 mL round bottom flask charged with (dadi)Ti(THF)$^{C}Hex_{0.4}$ (200 mg, 0.28 mmol) and $SnBr_4$ (123 mg, 0.28 mmol) was added 25 mL of freshly distilled THF at -78 ^{o}C. The reaction mixture was allowed to warm slowly to room temperature and stirred for 20 hrs. The green

solution was filtered then concentrated to a total volume of 10 mL. The reaction solution was cooled to -78 ^{o}C and freshly distilled Et_2O was added while maintaining vigorous stirring. The reaction mixture was allowed to warm to room temperature, filtered then washed (2x). After removal of all volatiles (dadi)$TiBr_2$ was collected as a green microcrystalline solid (99 mg, 46%). Crystals suitable for X-Ray diffraction were obtained by the slow evaporation of a concentrated benzene solution layered with pentane at 23 °C. ^{1}H NMR (500 MHz, Benzene-d_6) δ 0.96 (d, *J* = 6.6 Hz, 12H, CH_3), 1.04 (d, *J* = 6.5 Hz, 12H, CH_3), 3.59 (sept, *J* = 6.6 Hz, 4H), 6.06 (d, *J* = 8.6 Hz, 2H, Ar-CH), 6.65 (t, *J* = 7.7 Hz, 2H, Ar-CH), 6.76 (t, *J* = 7.8 Hz, 2H, Ar-CH), 7.09 (d, *J* = 8.4 Hz, 2H, Ar-CH), 7.16 (m, 6H, $^{2,6\text{-dipp}}$Ar-CH), 7.66 (s, 2H, Im-CH). ^{13}C NMR (126 MHz, Benzene-d_6) δ 24.45 (CH_3), 25.87 (CH_3), 29.92 (^{i}Pr-CH), 115.17 (Ar), 117.96 (Ar), 124.84 (Ar), 125.58 (Ar), 129.23 (Ar), 131.58 (Ar), 135.47 (Ar), 140.05 (x Ar), 144.43 (Ar-CN), 144.58 (Ar-CN), 155.27 (Ar-CN).

3. (dadi)TiI_2 (1-I_2): To a 50 mL round bottom flask charged with (dadi)Ti(THF)^{C}$Hex_{1.7}$ (200 mg, 0.24 mmol) and SnI_4 (152 mg, 0.24 mmol) was added 25 mL of freshly distilled THF at -78 ^{o}C. The reaction mixture was allowed to warm slowly to room temperature and stirred for 20 hrs. After removal of all volatiles, the brown residue was taken up in toluene (10 mL) and filtered. The reaction was cooled to -78 ^{o}C and filtered. After removal of all volatiles (dadi)TiI_2 was collected as a brown powder (123 mg, 58%). ^{1}H NMR (500 MHz, Benzene-d_6) δ 0.99 (d, *J* = 6.6 Hz, 12H, CH_3), 1.05 (d, *J* = 6.5 Hz, 12H, CH_3), 3.61 (sept, *J* = 6.6 Hz, 4H, ^{i}Pr-CH), 6.10 – 6.16 (dd, *J* = 8.5, 1.4 Hz, 2H, Ar-CH), 6.70 (ddd, *J* = 8.2, 6.9, 1.4 Hz, 2H), 6.76 (ddd, *J* = 8.5, 6.9, 1.5 Hz, 2H), 7.15 – 7.18 (m, 6H, $^{2,6\text{-dipp}}$Ar-CH) ,7.20 (dd, *J* = 8.3, 1.4 Hz, 2H), 7.80 (s, 2H). ^{13}C NMR (126 MHz, Benzene-d_6) δ 24.53, 26.05, 30.01, 114.31,

118.02, 125.19, 125.20, 128.82, 130.93, 136.99, 141.55, 143.42, 144.54, 154.17.

4. (dadi-Bz)TiBr (5-Br): A solution of benzyl bromide (35 mg, 0.28 mmol) in C_6H_6 (1 mL) was added dropwise to a solution of (dadi)Ti(THF)^{C}Hex$_{1.3}$ (46 mg, 0.059 mmol) in C_6H_6 (4 mL) in a scintillation vial. The reaction was stirred for 36 hours, then filtered and washed with hexanes yielding (**5**-Br) as a brown crystalline solid (35 mg, 73%). ^{1}H NMR (600 MHz, THF-d_8) δ 0.31 (d, *J* = 6.6 Hz, 3H, CH_3), 0.43 (d, *J* = 6.7 Hz, 3H, CH_3), 0.45 (d, *J* = 6.7 Hz, 3H, CH_3), 0.75 (d, *J* = 6.6 Hz, 3H, CH_3), 0.87 (d, *J* = 6.8 Hz, 3H, CH_3), 1.10 (d, *J* = 6.8 Hz, 3H, CH_3), 1.23 (d, *J* = 6.5 Hz, 3H, CH_3), 2.39 (sept, *J* = 6.2 Hz, 1H, ^{i}Pr-CH), 2.80 (sept, *J* = 6.0 Hz, 1H, ^{i}Pr-CH), 3.22 (sept, *J* = 6.5 Hz, 1H, ^{i}Pr-CH), 4.13 (bs, 1H, ^{i}Pr-CH), 4.49 (d, *J* = 16.1 Hz, 1H, CH_2), 4.73 (d, *J* = 16.1 Hz, 1H, CH_2), 5.00 (d, *J* = 7.7 Hz, 1H, Ar-CH), 5.08 (d, *J* = 24.6 Hz, 1H, CH_2), 5.29 (d, *J* = 24.6 Hz, 2H, CH_2), 5.56 (d, *J* = 8.3 Hz, 1H, Ar-CH), 5.93 (d, *J* = 7.8 Hz, 1H, Ar-CH), 6.28 (t, *J* = 7.5 Hz, 1H, Ar-CH), 6.49 (t, *J* = 7.5 Hz, 1H, Ar-CH), 6.73 (t, *J* = 7.6 Hz, 1H, Ar-CH), 6.90 (t, *J* = 7.8 Hz, 1H, Ar-CH), 6.94 (d, *J* = 7.6 Hz, 1H, Ar-CH), 7.00 (d, *J* = 7.6 Hz, 1H, Ar-CH), 7.13 (q, *J* = 8.0 Hz, 2H), 7.19 (d, *J* = 7.4 Hz, 1H, Ar-CH), 7.23 (d, *J* = 7.5 Hz, 2H, Ar-CH), 7.37 – 7.46 (m, 6H, Ar-CH).^{13}C NMR (126 MHz, THF-d_8) δ 22.87 (CH_3), 23.35 (CH_3), 24.13 (CH_3), 24.46 (CH_3), 25.98 (CH_3), 26.05 (CH_3), 26.24 (CH_3), 26.59 (CH_3), 29.20 (^{i}Pr-CH), 29.71 (^{i}Pr-CH), 29.83 (^{i}Pr-CH), 32.54 (^{i}Pr-CH), 38.82 (N-CH_2), 69.35 (benzyl-CH_2), 106.64 (Ar-CH), 112.92 (Ar-CH), 116.31 (Ar-CH), 120.48 (Ar-CH), 121.71 (Ar-CH), 122.22 (Ar-CH), 124.24 (Ar-CH), 124.97 (Ar-CH), 125.14 (Ar-CH), 126.27 (Ar-CH), 126.51 (Ar-CH), 128.12 (Ar-CH), 128.55 (Ar-CH), 128.62 (Ar-CH), 129.97 (Ar-CH), 130.24 (Ar-CH), 130.27 (Ar-CH), 133.69 (Ar-CN), 136.38 (Ar-CN), 143.26 (Ar-C), 143.75 (Ar-C), 144.05

(Ar-C), 145.49 (Ar-C), 146.08 (Ar-CH), 146.41 (Ar-C), 146.43 (Ar-CN), 148.71 (Ar-CN), 155.35 (Ar-CN), 180.68 ($N=C_{im}$).

5. (dadi-Bz)TiCl (5-Cl): A solution of benzyl chloride (35 mg, 0.28 mmol) in C_6H_6 (3 mL) was added dropwise to a solution of (dadi)Ti(THF)^{C}Hex$_{0.5}$ (200 mg, 0.28 mmol) in C_6H_6 (13 mL) in a scintillation vial. The reaction was stirred for 24 hours, then filtered and washed with hexanes yielding (**5**-Cl) as a brown crystalline solid (110 mg, 54%). Single crystals suitable for X-ray diffraction were obtained from a concentrated THF solution layered with pentane. ^{1}H NMR (300 MHz, THF-d_8) δ 0.32 (d, J = 6.7 Hz, 3H), 0.45 (d, J = 6.8 Hz, 3H), 0.47 (d, J = 6.5 Hz, 3H), 0.75 (d, J = 6.6 Hz, 3H), 0.88 (d, J = 6.8 Hz, 3H), 1.06 (d, J = 6.8 Hz, 3H), 1.11 (d, J = 6.9 Hz, 3H), 1.21 (d, J = 6.7 Hz, 3H), 2.43 (sept, J = 6.6 Hz, 1H), 2.76 (sept, J = 6.6 Hz, 1H), 3.21 (sept, J = 6.8 Hz, 1H), 4.01 (m, 6.7 Hz, 1H), 4.50 (d, J = 16.2 Hz, 1H), 4.73 (d, J = 16.2 Hz, 1H), 4.97 (d, J = 7.9 Hz, 1H), 5.07 (d, J = 24.6 Hz, 1H, Ar-CH), 5.30 (d, J = 24.6 Hz, 1H), 5.52 (dd, J = 8.3, 1.3 Hz, 1H, Ar-CH), 5.91 (dd, J = 7.8, 1.3 Hz, 1H, Ar-H), 6.27 (t, J = 7.7 Hz, 1H, Ar-CH), 6.48 (td, J = 7.6, 1.3 Hz, 1H, Ar-CH), 6.72 (td, J = 7.6, 1.3 Hz, 1H, Ar-CH), 6.89 (ddd, J = 8.4, 7.5, 1.4 Hz, 1H, Ar-CH), 6.95 (dd, J = 7.7, 1.6 Hz, 1H, Ar-CH), 7.00 (dd, J = 7.6, 1.7 Hz, 1H, Ar-CH), 7.08 – 7.26 (m, 5H, Ar-CH), 7.33 – 7.50 (m, 6H, Ar-CH).

6. (dadi-CH_3)TiBr (6-Br): A thick walled glass bomb charged with (dadi)Ti(THF)CHex$_{0.7}$ (200 mg, 0.27 mmol) and C_6H_6 (2 mL) was degassed by freeze-pump-thaw cycles (3x). CH_3Br (1.8 cm Hg, 0.27 mmol) was transferred to the bomb using a 279 mL gas bulb. The reaction mixture was then heated to 55 ^{o}C for 73 hrs while stirring, filtered, then washed with hexanes yielding **4** as a brown crystalline solid (130 mg, 69%). ^{1}H NMR (599 MHz, THF-d_8) δ 0.43

(d, *J* = 5.8 Hz, 3H, CH_3), 0.46 (d, *J* = 6.7 Hz, 3H, CH_3), 0.57 (bs, 3H, , CH_3), 0.76 (d, *J* = 6.7 Hz, 3H, CH_3), 0.78 (d, *J* = 6.9 Hz, 3H, CH_3), 0.94 (bs, 3H, CH_3), 1.07 (d, *J* = 6.7 Hz, 6H, CH_3), 2.35 (p, *J* = 7.0 Hz, 1H, ^{i}Pr-CH), 2.82 (s, 3H, NC-CH_3), 2.86 (p, *J* = 6.5 Hz, 1H, ^{i}Pr-CH), 3.06 – 3.14 (m, 1H, ^{i}Pr-CH), 3.89 (s, 1H, ^{i}Pr-CH), 5.15 (d, *J* = 6.8 Hz, 1H, Ar-CH), 5.24 (d, *J* = 24.3 Hz, 1H, CH_2), 5.42 (d, *J* = 24.3 Hz, 1H, CH_2), 5.53 (dd, *J* = 8.3, 1.3 Hz, 1H, Ar-CH), 6.20 (d, *J* = 7.5 Hz, 1H, Ar-CH), 6.40 (t, *J* = 7.5 Hz, 1H, Ar-CH), 6.64 (t, *J* = 7.4 Hz, 1H, Ar-CH), 6.78 (td, *J* = 7.7, 1.3 Hz, 1H, Ar-CH), 6.90 (ddd, *J* = 8.4, 7.2, 1.4 Hz, 1H, Ar-CH), 6.96 (dd, *J* = 7.6, 1.6 Hz, 1H, $^{2,6\text{-dipp}}$Ar-CH), 7.04 (dd, *J* = 6.8, 2.5 Hz, 1H, $^{2,6\text{-dipp}}$Ar-CH), 7.09 – 7.19 (m, 4H,$^{2,6\text{-dipp}}$Ar-CH), 7.45 (d, *J* = 7.9 Hz, 1H, Ar-CH). ^{13}C NMR (150 MHz, THF-d_8) δ 18.46 (NC-CH_3), 22.42 (^{i}Pr-CH_3), 22.47 (^{i}Pr-CH_3), 22.50 (^{i}Pr-CH_3), 23.01 (^{i}Pr-CH_3), 23.45 (^{i}Pr-CH_3), 24.29 (^{i}Pr-CH_3), 25.11 (^{i}Pr-CH_3), 25.48, (^{i}Pr-CH_3), 28.52 (^{i}Pr-CH), 28.55 (^{i}Pr-CH), 28.79 (^{i}Pr-CH), 30.57 (^{i}Pr-CH),69.43 (CH_2), 105.72 (Ar-CH), 112.41 (Ar-CH), 115.20 (Ar-CH), 119.21 (Ar-CH), 120.57 (Ar-CH), 121.36 (Ar-CH), 123.01 (Ar-CH), 124.18 ($^{2,6\text{-dipp}}$Ar-CH), 124.22 ($^{2,6\text{-dipp}}$Ar-CH), 127.22 ($^{2,6\text{-dipp}}$Ar-CH), 128.59 (Ar-CH), 133.59 (Ar-CN), 141.91 ($^{2,6\text{-dipp}}$Ar-C), 143.15 ($^{2,6\text{-dipp}}$Ar-C), 144.23 ($^{2,6\text{-dipp}}$Ar-C), 145.29 ($^{2,6\text{-dipp}}$Ar-CN), 146.31 ($^{2,6\text{-dipp}}$Ar-C), 146.92 ($^{2,6\text{-dipp}}$Ar-CN), 154.94 9 (Ar-CN), 179.83 (N-**C-**CH_3). *Two quaternary Ar-CN carbon chemical shifts were not observed.

7. (dadi-CH_2PPh_2)TiCl (7): To a 50 mL round bottom flask charged (dadi)Ti(THF)^{C}$Hex_{0.58}$ (138 mg, 0.19 mmol) and C_6H_6 (5 mL) was added a solution of Ph_2PCH_2Cl (46 mg, 0.2 mmol) in toluene (1.5 mL). The reaction solution was stirred for 18 hours then attached to a small swivel frit apparatus. All volatiles were removed by vacuum then freshly distilled pentane was added (20 mL). The reaction mixture was filtered and washed (3x). After removal of

all volatiles, **6** was collected as a brown powder (94 mg, 59%). ^{1}H NMR (400 MHz, Benzene-d_6) δ 0.54 (d, J = 6.7 Hz, 3H, CH_3), 0.71 (d, J = 6.7 Hz, 3H, CH_3), 0.77 (d, J = 6.6 Hz, 3H, CH_3), 0.95 (d, J = 6.6 Hz, 3H, CH_3), 1.02 (d, J = 6.8 Hz, 3H, CH_3), 1.15 (d, J = 6.7 Hz, 3H, CH_3), 1.21 (d, J = 6.8 Hz, 3H, CH_3), 1.43 (d, J = 6.6 Hz, 3H, CH_3), 2.70 (p, J = 6.7 Hz, 1H, ^{i}Pr-CH), 3.01 (d, J = 12.1 Hz, 1H, CH_2-P), 3.09 (p, J = 6.6 Hz, 1H, ^{i}Pr-CH), 3.33 (dd, J_{HH} = 12.1, J_{PH} = 2.2 Hz, 1H, CH_2-P), 3.49 (p, J = 6.8 Hz, 1H, ^{i}Pr-CH), 4.19 (d, J = 24.1 Hz, 1H, CH_2), 4.24 – 4.32 (bs, 1H, ^{i}Pr-CH), 4.40 (d, J = 24.1 Hz, 1H, CH_2), 5.35 (d, J = 7.9 Hz, 1H, Ar-CH), 5.63 (d, J = 7.7 Hz, 1H, Ar-CH), 5.69 (d, J = 8.3 Hz, 1H, Ar-CH), 6.37 (d, J = 7.1 Hz, 1H, Ar-CH), 6.41 (d, J = 6.9 Hz, 1H, Ar-CH), 6.59 (t, J = 8.4 Hz, 1H, Ar-CH), 6.64 (t, J = 8.1 Hz, 1H, Ar-CH), 6.86 – 7.34 (m, 17H, Ar-CH). ^{1}H{^{31}P} NMR (400 MHz, Benzene-d_6) δ 0.54 (d, J = 6.7 Hz, 3H, CH_3), 0.71 (d, J = 6.7 Hz, 3H, CH_3), 0.77 (d, J = 6.6 Hz, 3H, CH_3), 0.95 (d, J = 6.6 Hz, 3H, CH_3), 1.02 (d, J = 6.8 Hz, 3H, CH_3), 1.15 (d, J = 6.7 Hz, 3H, CH_3), 1.21 (d, J = 6.8 Hz, 3H, CH_3), 1.43 (d, J = 6.6 Hz, 3H, CH_3), 2.70 (p, J = 6.7 Hz, 1H, ^{i}Pr-CH), 3.01 (d, J = 12.1 Hz, 1H, CH_2-P), 3.09 (p, J = 6.6 Hz, 1H, ^{i}Pr-CH), 3.33 (dd, J_{HH} = 12.1, 1H, CH_2-P), 3.49 (p, J = 6.8 Hz, 1H, ^{i}Pr-CH), 4.19 (d, J = 24.1 Hz, 1H, CH_2), 4.24 – 4.32 (bs, 1H, ^{i}Pr-CH), 4.40 (d, J = 24.1 Hz, 1H, CH_2), 5.35 (d, J = 7.9 Hz, 1H, Ar-CH), 5.63 (d, J = 7.7 Hz, 1H, Ar-CH), 5.69 (d, J = 8.3 Hz, 1H, Ar-CH), 6.37 (d, J = 7.1 Hz, 1H, Ar-CH), 6.41 (d, J = 6.9 Hz, 1H, Ar-CH), 6.59 (t, J = 8.4 Hz, 1H, Ar-CH), 6.64 (t, J = 8.1 Hz, 1H, Ar-CH), 6.86 – 7.34 (m, 17H, Ar-CH). ^{31}P NMR (162 MHz, Benzene-d_6) δ -12.32. ^{13}C NMR (126 MHz, Benzene-d_6) δ 22.92 (CH_3), 23.26 (CH_3), 24.23 (CH_3), 24.44 (CH_3), 25.17 (CH_3), 25.78 (CH_3), 25.94 (CH_3), 26.31 (CH_3), 28.83 (^{i}Pr-CH), 29.16 (^{i}Pr-CH), 29.38 (^{i}Pr-CH), 31.68 (^{i}Pr-CH), 33.59 (d, J_{PC} = 26.9 Hz, P-CH_2), 69.45 (d, J_{PC} = 4.8 Hz, N-CH_2), 105.83 (Ar-CH), 112.98 (Ar-CH),

115.84 (Ar-CH), 119.44 (Ar-CH), 121.01 (d, J_{PC} = 9.6 Hz, Ar-CH), 121.93 (Ar-CH), 123.65 (Ar-CH), 124.63 (Ar-CH), 124.93 (Ar-CH), 125.81 (Ar-CH), 125.91 (Ar-CH), 127.80 (Ar-CH), 128.20 (Ar-CH), 129.27 (d, J_{PC} = 6.2 Hz, Ar-CH), 129.45 (d, J_{PC} = 7.3 Hz), 129.69 (Ar-CH), 129.78 (Ar-CH), 130.38 (Ar-CH), 132.43 (d, J_{PC} = 18.9 Hz, Ar-CH), 132.92 (Ar-CN), 133.74 (d, J_{PC} = 21.2 Hz Ar-CH), 135.45 (d, J_{PC} = 16.3 Hz, P-C_{Ar}), 136.86 (d, J = 17.3 Hz, P-C_{Ar}), 142.84 ($^{2,6\text{-dipp}}$Ar-C), 142.97 (Ar-CN), 143.69 ($^{2,6\text{-dipp}}$Ar-C), 145.33 ($^{2,6\text{-dipp}}$Ar-C), 145.51 (Ar-CN), 145.80 ($^{2,6\text{-dipp}}$Ar-CN), 146.18 ($^{2,6\text{-dipp}}$Ar-C), 147.26 ($^{2,6\text{-dipp}}$Ar-CN), 154.97 (Ar-CN), 177.20 (d, J_{PC} = 6.4 Hz, N=**C**$_{im}$).

8. (diamide-benzimidazole)$TiCl_2$ (8): A thick walled glass bomb with a Teflon plug was charged with **1**-Cl_2 (210 mg, 0.31 mmol) and C_6H_6 (30 mL). The solution was heated to 160 ^{o}C for 22 hrs. After removal of all volatiles the product was obtained as a light yellow solid (168 mg, 80%). Single crystals suitable for X-ray diffraction were obtained by slow evaporation of a concentrated pentane solution. ^{1}H NMR (600 MHz, Benzene-d_6) δ 0.66 (d, J = 6.8 Hz, 6H, CH_3), 0.76 (d, J = 6.9 Hz, 6H, CH_3), 1.06 (d, J = 6.8 Hz, 6H, CH_3), 1.66 (d, J = 6.7 Hz, 6H, CH_3) , 2.12 (sept, J = 6.8 Hz, 2H, ^{i}Pr-CH), 4.09 (sept, J = 6.8 Hz, 2H, ^{i}Pr-CH), 4.88 (s, 2H, CH_2), 5.27 (dd, J = 7.9, 1.3 Hz, 1H, Ar-CH), 5.53 (dd, J = 7.8, 1.3 Hz, 1H, Ar-CH), 6.41 (td, J = 7.6, 1.3 Hz, 1H, Ar-CH), 6.47 (td, J = 7.6, 1.4 Hz, 1H, Ar-CH), 6.54 (d, J = 8.2 Hz, 1H, Ar-CH), 6.90 (t, J = 7.8 Hz, 1H, Ar-CH), 6.97 (d, J = 7.9 Hz, 1H, Ar-CH), 7.00 (d, J = 7.9 Hz, 2H, $^{2,6\text{-dipp}}$Ar-CH), 7.17 – 7.19 (m, 1H, $^{2,6\text{-dipp}}$Ar-CH), 7.34 (m, 3H, $^{2,6\text{-dipp}}$Ar-CH), 8.25 (d, J = 8.2 Hz, 1H, Ar-CH). ^{13}C NMR (126 MHz, Benzene-d_6) δ 23.65 (CH_3), 24.28 (CH_3), 24.59 (CH_3), 26.77 (CH_3), 28.92 (^{i}Pr-CH), 29.15 (^{i}Pr-CH), 53.30 (CH_2), 105.92 (Ar-CH), 110.53 (Ar-CH), 110.63 (Ar-CH), 120.65 (Ar-CH), 121.20 (Ar-CH), 124.22 (Ar-CH), 125.25 ($^{2,6\text{-dipp}}$Ar-CH), 125.33 ($^{2,6\text{-}}$

^{dipp}Ar-CH), 125.58 (Ar-CH), 125.63 (Ar-CH), 128.56 ($^{2,6\text{-dipp}}$Ar-C), 129.46 ($^{2,6\text{-dipp}}$Ar-CH), 131.85 ($^{2,6\text{-dipp}}$Ar-CH), 136.46 (Ar-CN), 139.62 (Ar-CN), 143.78 ($^{2,6\text{-dipp}}$Ar-C), 145.33 ($^{2,6\text{-dipp}}$Ar-CN), 147.45 (Ar-CN), 147.58 (Ar-CN), 147.63 (Ar-CN), 160.09 (N-$C_{imidazole}$-N).

9. [(dadi-CH_2)TiNHAd]$_2$ (9): An NMR tube sealed onto a 14/20 ground glass joint was charged with (**2**=Ad) (50 mg, 0.066 mmol), P(Me_2)Ph (4.7 μL, 0.033 mmol) and C_6D_6 (1.1 mL) then attached to a 15 mL gas bulb. The reaction solution was degassed by freeze-pump-thaw cycles (3x), C_2H_4 (16.4 cm Hg, 0.13 mmol) was frozen into the tube then flame sealed. The reaction was heated to 55 ^oC for 35 days, removed from the oil bath and allowed to stand at room temperature for 6 days. The tube was then opened inside the glove box, filtered and washed with C_6D_6 (1 mL). The identity of the crystals were confirmed to be complex **9** by checking the unit cell *via* X-ray crystallography. The remainder of the crystals (*ca*. 1-5 mg) were then collected, taken up into THF-d_8 (0.6 mL) and placed into a J. Young NMR tube, sonicated and periodically shaken until fully dissolved. ^{1}H NMR (600 MHz, THF-d_8) δ 0.30 (d, *J* = 6.9 Hz, 6H, CH_3), 0.57 (d, *J* = 6.7 Hz, 6H, CH_3), 0.59 (d, *J* = 6.4 Hz, 6H, CH_3), 0.89 (d, *J* = 5.8 Hz, 6H, CH_3), 1.01 (d, *J* = 6.6 Hz, 6H, CH_3), 1.11 (d, *J* = 6.8 Hz, 6H, CH_3), 1.13 (d, *J* = 6.7 Hz, 6H, CH_3), 1.17 (d, *J* = 6.4 Hz, 6H, CH_3), 1.43 – 1.55 (m, 24H, Ad-CH_2), 1.86 (s, 6H, Ad-CH), 2.52 (pent, *J* = 6.7 Hz, 2H, ^{i}Pr-CH), 2.88 (dd, *J* = 13.9, 9.4 Hz, 2H, ^{C}Hex-CH_2), 2.98 (pent, *J* = 6.7 Hz, 2H, ^{i}Pr-CH), 3.28 (pent, *J* = 6.7 Hz, 2H, ^{i}Pr-CH), 4.24 (pent, *J* = 6.5 Hz, 2H, ^{i}Pr-CH), 5.22 (dd, *J* = 13.9, 6.2 Hz, 2H, ^{C}Hex-CH_2), 5.34 (d, *J* = 7.9 Hz, 2H, Ar-CH), 5.72 (dd, *J* = 11.0, 6.2 Hz, 2H, (^{C}Hex-C(H)N), 5.81 (d, *J* = 8.3 Hz, 2H, Ar-CH), 6.04 (d, *J* = 7.6 Hz, 2H, Ar-CH), 6.36 (t, *J* = 7.5 Hz, 2H, Ar-CH), 6.44 (t, *J* = 7.4 Hz, 2H, Ar-CH), 6.83 (t, *J* = 7.6 Hz, 2H, Ar-

CH), 6.94 (d, *J* = 7.7 Hz, 2H, $^{2\text{-}6\text{-}dipp}$Ar-CH), 6.99 (d, *J* = 7.7 Hz, 2H, $^{2\text{-}6\text{-}dipp}$Ar-CH), 7.03 (t, *J* = 7.7 Hz, 2H, Ar-CH), 7.07 (d, *J* = 8.3 Hz, 2H, $^{2\text{-}6\text{-}dipp}$Ar-CH), 7.10 (d, *J* = 8.2 Hz, 2H, $^{2\text{-}6\text{-}dipp}$Ar-CH), 7.15 (d, *J* = 7.7 Hz, 2H, $^{2\text{-}6\text{-}dipp}$Ar-CH), 7.21 (d, *J* = 7.7 Hz, 2H, $^{2\text{-}6\text{-}dipp}$Ar-CH), 7.48 (d, *J* = 8.0 Hz, 2H, Ar-CH), 7.81 (s, 2H, NH). ^{13}C NMR (201 MHz, THF-d_8) δ 22.91 (CH_3), 23.52 (CH_3), 23.95 (CH_3), 24.61 (CH_3), 24.83 (CH_3), 25.38 (CH_3), 25.47 (CH_3), 26.18 (CH_3), 27.68 (^{i}Pr-CH), 29.27 (^{i}Pr-CH), 29.48 (^{i}Pr-CH), 31.08 (Ad-CH), 31.10 (^{i}Pr-CH), 36.18 (^{C}Hex-CH_2), 46.69 (Ad-CH_2), 47.29 (Ad-CH_2), 62.89 (Ad-CN), 73.26 (^{C}Hex-C(H)N), 107.53 (Ar-CH), 113.37 (Ar-CH), 118.24 (Ar-CH), 118.41 (Ar-CH), 119.50 (Ar-CH), 120.69 (Ar-CH), 121.26 (AR-CH), 124.42 ($^{2,6\text{-}dipp}$Ar-CH), 125.03 ($^{2,6\text{-}dipp}$Ar-CH, 2x), 126.25 ($^{2,6\text{-}dipp}$Ar-CH), 126.66 ($^{2,6\text{-}dipp}$Ar-CH), 127.02 ($^{2,6\text{-}dipp}$Ar-CH), 130.82 (Ar-CH), 133.06 (Ar-CN), 139.94 (Ar-CN), 143.80 ($^{2,6\text{-}dipp}$Ar-C), 144.54 ($^{2,6\text{-}dipp}$Ar-C), 145.56 ($^{2,6\text{-}dipp}$Ar-C), 146.56 ($^{2,6\text{-}dipp}$Ar-C), 147.88 ($^{2,6\text{-}dipp}$Ar-CN), 147.93 (Ar-CN), 148.69 ($^{2,6\text{-}dipp}$Ar-CN), 156.72 (Ar-CN), 174.17 (^{c}Hex-C_{im}=N).

10. [(dadi-CD_2)TiNDAd]$_2$ (9-*d_6*): An NMR tube sealed onto a 14/20 ground glass joint was charged with (**2**=Ad) (50 mg, 0.066 mmol) and C_6D_6 (0.668 mL) then attached to a 15 mL gas bulb. The reaction solution was degassed by freeze-pump-thaw cycles (3x), C_2H_4 (16.4 cm Hg, 0.13 mmol) and PMe_3-d_9 (4.1 cm Hg, 0.033 mmol) were sequentially frozen into the NMR tube which was then flame sealed. The reaction was heated to 55 ^{o}C for ~3 weeks, removed from the oil bath and allowed to stand at room temperature for ~103 weeks. The tube was then opened inside the glove box, filtered and washed with C_6D_6 (1 mL). The crystals (<1 mg) were collected, taken up into THF-d_8 (0.5 mL) and placed into a J. Young NMR tube. The suspension of crystals was sonicated for 30 minutes and periodically shaken to fully dissolve

the product. ^{1}H NMR spectroscopic analysis of **9**-*d*$_6$ is consistent with complex **9**.

11. (DaIm)Ti=NAd(OPMe$_2$Ph) (10). To a 50 mL round bottom flask charged with **2**=NAd (149 mg, 0.199 mmol) and C_6H_6 (10 mL) was added (O)PMe$_2$Ph (30 mg, 0.195 mmol). The reaction solution was stirred for 18 h and slowly changed color to green. The reaction solution was then stripped, and toluene was added (ca. 5 mL). The product was precipitated with pentane (ca. 15 mL) at -78 °C. The resulting suspension was warmed to 23 °C, filtered and washed (3x). After removal of all volatiles, complex **10** was collected as a green powder (120 mg, 67 %). Single crystals suitable for X-Ray diffraction were obtained from a concentrated toluene solution layered with pentane at 23 °C. ^{1}H NMR (400 MHz, Benzene-*d*$_6$) δ 0.63 (d, *J* = 6.8 Hz, 3H, CH_3), 0.67 (d, *J* = 6.7 Hz, 3H, CH_3), 0.73 (d, *J* = 13.1 Hz, 3H, P-CH_3), 0.86 (d, *J* = 6.7 Hz, 3H, CH_3), 0.97 (d, *J* = 6.8 Hz, 3H, CH_3), 1.14 (d, *J* = 6.8 Hz, 3H, CH_3), 1.31 (d, *J* = 6.8 Hz, 3H, CH_3), 1.49 (bs, 6H, Ad-CH_2), 1.58-1.61 (m, 6H, Ad-CH_2), 1.63 (d, *J* = 6.8 Hz, 3H, CH_3), 1.65 (d, *J* = 6.8 Hz, 3H, CH_3), 1.82 (d, *J* = 13.1 Hz, 3H, P-CH_3), 1.86 (bs, 3H, Ad-CH), 2.06 (p, *J* = 6.9 Hz, 1H, ^{i}Pr-CH), 2.71 (sept, *J* = 6.8 Hz 1H, ^{i}Pr-CH), 3.36 (sept, *J* = 6.5 Hz, 1H, ^{i}Pr-CH), 4.86 (d, *J* = 19.9 Hz, 1H, CH_2), 5.30 (d, *J* = 19.9 Hz, 1H, CH_2), 5.49 (sept, *J* = 6.8 Hz, 1H, Ar-CH), 6.27 (dd, *J* = 7.4, 1.5 Hz, 1H, Ar-CH), 6.34 (dd, *J* = 7.5, 1.5 Hz, 1H, Ar-CH), 6.63 (d, *J* = 8.1 Hz, 1H, Ar-CH), 6.77 – 7.06 (m, 8H, Ar-CH), 7.22 – 7.32 (m, 3H, Ar-CH), 7.42 – 7.52 (m, 4H, Ar-CH). ^{1}H{^{31}P} NMR (400 MHz, Benzene-*d*$_6$) δ 0.63 (d, *J* = 6.8 Hz, 3H, CH_3), 0.67 (d, *J* = 6.7 Hz, 3H, CH_3), 0.73 (s, 3H, P-CH_3), 0.86 (d, *J* = 6.9 Hz, 3H, CH_3), 0.97 (d, *J* = 6.8 Hz, 3H, CH_3), 1.14 (d, *J* = 6.8 Hz, 3H, CH_3), 1.31 (d, *J* = 6.8 Hz, 3H, CH_3), 1.49 (bs, 6H, Ad-CH_2), 1.58-1.61 (m, 6H, Ad-CH_2), 1.63 (d, *J* = 6.8 Hz, 3H, CH_3), 1.65 (d, *J* = 6.8 Hz, 3H,

CH_3), 1.82 (s, 3H, P-CH_3), 1.86 (bs, 3H, Ad-CH), 2.06 (p, J = 6.9 Hz, 1H, ^{i}Pr-CH), 2.71 (sept, J = 6.8 Hz 1H, ^{i}Pr-CH), 3.36 (sept, J = 6.5 Hz, 1H, ^{i}Pr-CH), 4.86 (d, J = 19.9 Hz, 1H, CH_2), 5.30 (d, J = 19.9 Hz, 1H, CH_2), 5.49 (sept, J = 6.8 Hz, 1H, Ar-CH), 6.27 (dd, J = 7.4, 1.5 Hz, 1H, Ar-CH), 6.34 (dd, J = 7.5, 1.5 Hz, 1H, Ar-CH), 6.63 (d, J = 8.1 Hz, 1H, Ar-CH), 6.77 – 7.06 (m, 8H, Ar-CH), 7.23-7.29 (m, 3H, Ar-CH), 7.45 – 7.51 (m, 4H, Ar-CH).^{13}C NMR (151 MHz, Benzene-d_6) δ 15.55 (d, J_{PC} = 74.5 Hz, P-CH_3), 15.93 (d, J_{PC} = 72 Hz, P-CH_3), 23.59 (CH_3), 24.05 (CH_3), 24.46 (CH_3), 24.84 (CH_3), 25.12 (CH_3), 25.22 (CH_3), 25.47 (CH_3), 26.91 (CH_3), 27.30 (^{i}Pr-CH), 27.78 (^{i}Pr-CH), 28.72 (^{i}Pr-CH), 29.02 (^{i}Pr-CH), 30.66 (Ad-CH_2), 37.18 (Ad-CH_2), 47.40 (Ad-CH), 49.69 (CH_2), 68.18 (Ad-CN), 104.27 (Ar-CH), 109.76 (Ar-CH), 111.04 (Ar-CH), 114.57 (Ar-CH), 115.85 (Ar-CH), 118.64 (Ar-CH), 122.77 (Ar-CH), 123.47 (Ar-CH), 123.50 ($^{2,6\text{-dipp}}$Ar-CH), 123.68 ($^{2,6\text{-dipp}}$Ar-CH), 124.84 ($^{2,6\text{-dipp}}$Ar-CH), 125.21 ($^{2,6\text{-dipp}}$Ar-CH), 125.24 ($^{2,6\text{-dipp}}$Ar-CH), 129.15 (d, J_{PC} = 12.3 Hz, P-Ar-CH), 130.43 (d, J_{PC} = 10.5 Hz, P-Ar-CH), 131.30 ($^{2,6\text{-dipp}}$Ar-CH), 131.31 (d, J_{PC} = 104 Hz, P-Ar-C), 132.84 (d, J_{PC} = 2.6 Hz, P-Ar-CH), 137.68 (Ar-CN), 141.25 ($^{2,6\text{-dipp}}$Ar-CN), 147.13 ($^{2,6\text{-dipp}}$Ar-C), 147.22 (Ar-CN, 2x), 147.46 ($^{2,6\text{-dipp}}$Ar-C), 147.66 ($^{2,6\text{-dipp}}$Ar-C), 147.71 ($^{2,6\text{-dipp}}$Ar-C), 150.74 (Ar-CN), 151.81 ($^{2,6\text{-dipp}}$Ar-CN), 162.41 (N-$C_{imidazole}$-N). ^{31}P NMR (162 MHz, Benzene-d_6) δ 52.85.

C. NMR Tube Scale Reactions

12. Bromomethyl cyclopropane radical clock. To a solution of (dadi)Ti(THF)^{C}Hex$_{1.0}$ (15 mg, 1.96 x 10^{-5} mol) in benzene-d_6 (0.5 mL) was added bromomethyl cyclopropane (2.1 μL, 2.16 x 10^{-5} mol). The reaction solution was transferred to an NMR tube attached to a 14/20 ground glass joint. The tube was then flame sealed, heated to 55 ^{o}C, and monitored by ^{1}H

NMR spectroscopy. The reaction was complete after 5 h and the major product observed contained cyclopropyl resonances but the no new vinylic resonances. The crystalline precipitate was harvested and analyzed by ^{1}H NMR spectroscopy, and contained no vinylic resonances.

13. 6-bromo-1-hexene radical clock. To a solution of (dadi)Ti(THF)^{C}Hex$_{1.0}$ (15 mg, 1.96 x 10^{-5} mol) in benzene-*d*$_6$ (0.5 mL) was added 6-bromo-1-hexene (2.9 μL, 2.16 x 10^{-5} mol). The reaction solution was transferred to an NMR tube attached to a 14/20 ground glass joint. The tube was then flame sealed, heated to 55 ^{o}C, and monitored by ^{1}H NMR spectroscopy. The reaction was complete after 96 h, and the major product contained only vinylic resonances.

14. Formation of 5`-Cl.** To a solution of [(dadi)TiCl]Li(THF)$_4$ (10 mg, 1.96 x $10^{-5}$ mol) in benzene-*d*$_6$ (0.5 mL) was added benzyl chloride (12.3 μL, 1.07 x $10^{-4}$ mol). The reaction mixture was added to a J. Young NMR tube, and assayed by NMR spectroscopy. Complete conversion to **5`-Cl was immediately noted (first time point = 12 minutes). The product was not isolated but characterized in the crude reaction mixture by ^{1}H, HSQCAD, gHMBCAD, and gCOSY NMR spectroscopy. ^{1}H NMR (600 MHz, Benzene-*d*$_6$) δ 0.74 (bs, 3H, ^{i}Pr-CH$_3$), 0.80 (d, *J* = 6.8 Hz, 3H, ^{i}Pr-CH$_3$), 0.94 (bs,, 3H, ^{i}Pr-CH$_3$), 0.95 (d, *J* = 6.9 Hz, 3H, ^{i}Pr-CH$_3$), (0.96, bs, 3H, ^{i}Pr-CH$_3$), 0.97 (d, *J* = 6.8 Hz, 3H, ^{i}Pr-CH$_3$), 1.24 (bs, 3H, ^{i}Pr-CH$_3$), 1.29 (d, *J* = 6.7 Hz, 3H, ^{i}Pr-CH$_3$), 2.55 (pent, *J* = 6.0 Hz, 1H, ^{i}Pr-CH), 3.14 (bs, 1H, ^{i}Pr-CH), 3.14 (dd, *J* = 10.6, 13.8 Hz, 1H, Bn-CH$_2$), 3.24 (sept, *J* = 6.8 Hz, 1H, ^{i}Pr-CH), 3.66 (dd, *J* = 5.1, 13.8, 1H, Bn-CH$_2$), 3.82 (bs, 1H, ^{i}Pr-CH), 4.79 (dd, *J* = 5.1, 10.6 Hz, 1H, N-C(**H**)-Bn), 5.72 (d, *J* = 8.3 Hz, 1H, Ar-CH), 5.80 (bd, *J* = 6.7 Hz, 1H, Ar-CH), 6.43 (bs, 1H, Ar-CH), 6.45 (t, *J* = 7.6 Hz, 1H, Ar-CH), 6.56 (d, *J* = 7.6 Hz, 1H, Ar-CH), 6.69 (bs, 1H,

Ar-CH), 6.70 (t, *J* = 7.5 Hz, 1H, Ar-CH), 6.81 (m, 2H, Bn-CH), 6.94 (t, *J* = 7.6 Hz, 1H, Ar-CH), 7.07-7.21 (m, 9H, $^{2,6\text{-dipp}}$Ar-CH and Bn-CH), 8.2 (s, Im-CH). ^{13}C NMR (202 MHz, Benzene-d_6, indirect detection *via* HSQCAD and gHMBCAD correlation spectroscopy) δ 23.28 (^{i}Pr-CH_3), 23.44 (^{i}Pr-CH_3), 23.91 (^{i}Pr-CH_3), 24.52 (^{i}Pr-CH_3), 24.59 (^{i}Pr-CH_3), 25.60 (^{i}Pr-CH_3), 26.04 (^{i}Pr-CH_3), 26.15 (^{i}Pr-CH_3), 28.51 (^{i}Pr-CH), 29.27 (^{i}Pr-CH), 29.81 (^{i}Pr-CH), 30.20 (^{i}Pr-CH), 40.14 (Bn-CH_2), 75.40 (N-**C**(H)-Bn), 107.66 (Ar-CH), 114.84 (Ar-CH), 115.38 (Ar-CH), 116.71 (Ar-CH), 119.65 (Ar-CH), 122.87 (Ar-CH), 123.53 (Ar-CH), 124.76 ($^{2,6\text{-dipp}}$Ar-CH), 124.84 ($^{2,6\text{-dipp}}$Ar-CH), 125.30 ($^{2,6\text{-dipp}}$Ar-CH), 126.00 ($^{2,6\text{-dipp}}$Ar-CH), 126.09 ($^{2,6\text{-dipp}}$Ar-CH), 127.09 (Bn-CH), 128.04 ($^{2,6\text{-dipp}}$Ar-CH), 129.09 (Bn-CH), 129.41 (Bn-CH), 130.70 (Ar-CN), 130.72 (Ar-CH), 133.47 (Ar-CN), 141.91 (Ar-CN), 142.11 ($^{2,6\text{-dipp}}$Ar-C), 144.43 ($^{2,6\text{-dipp}}$Ar-CN), 144.59 ($^{2,6\text{-dipp}}$Ar-C), 144.80 ($^{2,6\text{-dipp}}$Ar-C), 144.90 ($^{2,6\text{-dipp}}$Ar-CN), 146.12 ($^{2,6\text{-dipp}}$Ar-C), 157.87 (Ar-CN), 171.92 (Im-CH).

C. X-ray Crystal Structures

Upon isolation, the crystals were covered in polyisobutenes and placed under a 173 K N_2 stream on the goniometer head of a Siemens P4 SMART CCD area detector (graphite-monochromated MoKα radiation, λ = 0.71073 Å, or CuKα radiation, λ = 1.54184 Å). The structures were solved by direct methods (SHELXS). All non-hydrogen atoms were refined anisotropically unless stated, and hydrogen atoms were treated as idealized contributions (Riding model).

(dadi)TiBr$_2$ (1-Br$_2$). A dark green block (0.236 x 0.074 x 0.059 mm) was obtained from benzene/pentane. A total of 57,881 reflections were collected with 10,008 determined to be symmetry independent (R_{int} = 0.0412),

and 9,363 were greater than 2σ(I). A semi-empirical absorption correction from equivalents was applied, and the refinement utilized $w^{-1} = \sigma^2(F_o^2) + (0.0517p)^2 + 3.0107p$, where $p = ((F_o^2 + 2F_c^2)/3)$.

(diamide-benzimidazole)$TiCl_2$ (8). A yellow block (0.2 x 0.1 x 0.06 mm) was obtained from pentane. A total of 26,690 reflections were collected with 6,625 determined to be symmetry independent (R_{int} = 0.0729), and 4,201 were greater than 2σ(I). A semi-empirical absorption correction from equivalents was applied, and the refinement utilized $w^{-1} = \sigma^2(F_o^2) + (0.0375p)^2 + 0.3988p$, where $p = ((F_o^2 + 2F_c^2)/3)$.

(dadi-CH_3)TiCl (6-Cl). A brown plate (0.293 x 0.072 x 0.038 mm) was obtained from benzene-d_6. A total of 67,721 reflections were collected with 6,619 determined to be symmetry independent (R_{int} = 0.0528), and 6,416 were greater than 2σ(I). A semi-empirical absorption correction from equivalents was applied, and the refinement utilized $w^{-1} = \sigma^2(F_o^2) + (0.0813p)^2 + 0.3797p$, where $p = ((F_o^2 + 2F_c^2)/3)$.

[(dadi-CH_2)TiNHAd]$_2$ (9). A brown plate (0.39 x 0.1 x 0.08 mm) was obtained from benzene-d_6. A total of 37,881 reflections were collected with 8,351 determined to be symmetry independent (R_{int} = 0.0684), and 5,674 were greater than 2σ(I). A semi-empirical absorption correction from equivalents was applied, and the refinement utilized $w^{-1} = \sigma^2(F_o^2) + (0.0698p)^2 + 0.8560p$, where $p = ((F_o^2 + 2F_c^2)/3)$.

[(dadi-CH_2)TiNHAd]$_2$ (9). A brown plate (0.39 x 0.1 x 0.08 mm) was obtained from benzene-d_6. A total of 37,881 reflections were collected with 8,351 determined to be symmetry independent (R_{int} = 0.0684), and 5,674 were greater than 2σ(I). A semi-empirical absorption correction from equivalents

was applied, and the refinement utilized $w^{-1} = \sigma^2(F_o^2) + (0.0698p)^2 + 0.8560p$, where $p = ((F_o^2 + 2F_c^2)/3)$.

(DaIm)Ti=NAd(OPMe$_2$Ph) (**10**). A green/red dichroic plate (0.171 x 0.109 x 0.042mm) was obtained from toluene/pentane. The data set was refined as a two-component twin. A total of 17809 reflections were collected with 17,809 determined to be symmetry independent (R_{int} = 0.0605), and 16,185 were greater than $2\sigma(I)$. A semi-empirical absorption correction from equivalents was applied, and the refinement utilized $w^{-1} = \sigma^2(F_o^2) + (0.1211p)^2 + 0.8532p$, where $p = ((F_o^2 + 2F_c^2)/3)$.

References:

(1) Schmidt, V. A.; Kennedy, C. R.; Bezdek, M. J.; Chirik, P. J. *J. Am. Chem. Soc.* **2018**, *140* (9), 3443–3453.

(2) Tom, D. H.; Jörg, D. *Chem. Ber.* **2006**, *117* (2), 694–701.

(3) Takacs, J. M.; Anderson, L. G.; Madhavan, G. V. B.; Creswell, M. W.; Seely, F. L.; Devroy, W. F. *Organometallics*. **1986**, *5* (11), 2395–2398.

(4) Ketterer, N. A.; Fan, H.; Blackmore, K. J.; Yang, X.; Ziller, J. W.; Baik, M.-H.; Heyduk, A. F. *J. Am. Chem. Soc.* **2008**, *130* (13), 4364–4374.

(5) Stanciu, C.; Jones, M. E.; Fanwick, P. E.; Abu-Omar, M. M. *J. Am. Chem. Soc.* **2007**, *129* (41), 12400–12401.

(6) Haneline, M. R.; Heyduk, A. F. *J. Am. Chem. Soc.* **2006**, *128* (26), 8410–8411.

(7) Cotton, F. A.; Wilkinson, G.; Murillo, C. A.; Bochmann, M. *Advanced Inorganic Chemistry*, 6th ed.; Wiley: New York, 1999.

(8) Blackmore, K. J.; Ziller, J. W.; Heyduk, A. F. *Inorg. Chem.* **2005**, *44* (16), 5559–5561.

(9) Allen, F. H.; Kennard, O.; Watson, D. G.; Brammer, L.; Orpen, A. G.; Taylor, R. *J. Chem. Soc. Perkin Trans. 2*. **1987**, No. 12, S1–S19.

(10) Heins, S. P.; Wolczanski, P. T.; Cundari, T. R.; MacMillan, S. N. *Chem. Sci.* **2017**, *8* (5), 3410–3418.

(11) Addison, A. W.; Rao, T. N.; Reedijk, J.; van Rijn, J.; Verschoor, G. C. *J. Chem. Soc., Dalt. Trans.* **1984**, No. 7, 1349–1356.

(12) Griller, D.; Ingold, K. U. *Acc. Chem. Res.* **1980**, *13* (9), 317–323.

(13) Klaus-Peter, L.; Othmar, S.; Norbert, W. *Chem. Ber.* **2006**, *123* (5), 995–999.

(14) Hazari, N.; Mountford, P. *Acc. Chem. Res.* **2005**, *38* (11), 839–849.

(15) Heins, S. P.; Morris, W. D.; Wolczanski, P. T.; Lobkovsky, E. B.; Cundari, T. R. *Angew. Chemie Int. Ed. 54* (48), 14407–14411.

Appendix A

Determining uncertainty in activation parameters obtained from an Eyring plot

Introduction:

The purpose of this appendix is to provide a general overview of the statistics associated with calculating activation parameters using an Eyring analysis. This appendix is not designed to provide a description of the theory behind the statistical analysis. The second, and perhaps more useful, reason for this appendix is to illustrate to an experimental chemist when approximations in uncertainties may be used, without compromising their legitimacy. This section is organized in a way that introduces the rules needed to perform any basic error analysis, followed by a sample calculation of the uncertainty in one data point in the Erying plot, which is used a weighing factor for linear regression. Finally, a sample calculation of the uncertainties in the activation parameters is presented. The data used for this analysis were experimentally determined from the stoichiometric carbonylation of imide (dadi)Ti=NAd (**2**=NAd) (*cf.* Chapter 2).

Discussion:

A.1. Notation

$$\delta x = \text{uncertainty in measured value x}$$

$$\frac{\delta x}{|x|} = \text{fractional uncertainty in measured value x (percentage error)}$$

A.2. Provisional rules[1]

Provisional rules, tend to overestimate uncertainties but require less arithmetic. However, provisional rules should give the maximum possible uncertainties. If various quantities *x*,…,*w* are measured with *independent and random* small uncertainties δx,…,δw, and the measured values are used to calculate some quantity *q*, then the uncertainties in *x*,…,*w* cause an uncertainty in *q* as follows:

A.2.1. Sum and differences

If *q* is the sum and difference (*e.g.*, *q = (x + … + z) – (u + … + w)*) then the uncertainty of the computed value of *q* is the sum of all the original uncertainties as shown in eq 1.

$$\delta q \approx \delta x + \cdots + \delta z + \delta u + \cdots + \delta w \qquad \text{(eq 1)}$$

A.2.2 Product and quotients

If *q* is the product and/or quotient (*e.g.*, *q = (x * … * z) / (u * … *w)* then the fractional uncertainty in the computed value of *q* is the sum of the fractional uncertainties in x, …, w (eq 2).

$$\frac{\delta q}{|q|} \approx \frac{\delta x}{|x|} + \cdots + \frac{\delta z}{|z|} + \frac{\delta u}{|u|} + \cdots + \frac{\delta w}{|w|} \qquad \text{(eq 2)}$$

i.e., When quantities are multiplied or divided the *fractional uncertainties add*.

A.3. General rules[1]

General rules require more arithmetic but are more accurate. Uncertainties found from general rules will *always* be less than or equal to the uncertainties found from using the corresponding provisional rule.

If various quantities *x,…,w* are measured with *independent and random* small uncertainties $\delta x,\ldots,\delta w$, and the measured values are used to calculate some quantity *q*, then the uncertainties in *x*,…,*w* cause an uncertainty in *q* as follows:

A.3.1. Sum and difference

If *q* is the sum and difference (*e.g.*, *q = x + … + z – (u + … + w)*) then:

$$\delta q = \sqrt{(\delta x)^2 + \cdots + (\delta z)^2 + (\delta u)^2 + \cdots + (\delta w)^2} \qquad \text{(eq 3)}$$

A.3.2. Products and quotients

If *q* is the product and/or quotient (*e.g.*, *q = (x * … * z) / (u * … *w))* then:

$$\frac{\delta q}{|q|} = \sqrt{(\frac{\delta x}{|x|})^2 + \cdots + (\frac{\delta z}{|z|})^2 + (\frac{\delta u}{|u|})^2 + \cdots + (\frac{\delta w}{|w|})^2} \qquad \text{(eq 4)}$$

A.3.3. Product of an exact number and measured quantity

If *q* = *Bx*, where B is known exactly, then:

$$\delta q = |B|\delta x \qquad \text{(eq 5)}$$

A.3.4. Functions of one variable

If *q* is a function of one variable (*e.g.*, q(x) = ln(x)) then:

$$\delta q = \left|\frac{dq}{dx}\right| \delta x \quad \text{(eq 6)}$$

A.3.5. Functions of several variables

If *q* is a function of several variables (*e.g.*, *q(x,y) = (x +y)/(x + z)*), then:

$$\delta q = \sqrt{(\frac{\partial q}{|\partial x|}\delta x)^2 + \cdots + (\frac{\partial q}{|\partial z|}\delta z)^2} \quad \text{(eq 7)}$$

A.4. Calculating the uncertainty in activation parameters obtained from an Eyring plot

For quick reference, eq's 8-10 are the equations most useful for chemists seeking to obtain activation parameters, which are transformed from their original form put forth by Eyring and Polyani,[2,3] into terms of $\Delta G^{\ddagger}$ and further into $\Delta H^{\ddagger}$ and $\Delta S^{\ddagger}$.[4,5]

$$ln\frac{k}{T} = \frac{-\Delta H^{\ddagger}}{RT} + \ln\frac{k_B}{h} + \frac{\Delta S^{\ddagger}}{R} \quad \text{(eq 8)}$$

$$-\Delta H^{\ddagger} = slope * R \quad \text{(eq 9)}$$

$$\Delta S^{\ddagger} = \left(intercept - \ln\frac{k_B}{h}\right) * R \quad \text{(eq 10)}$$

In an Eyring plot, both x- and y-axis contain variables with measured quantities. The first step for the error analysis is to find the uncertainties associated with the x-axis, which is a function of two measured quantitates

(temperature, and a rate constant). These will be used as weighting factors for the linear regression needed to obtain the slope and intercept that are required for the determination of activation parameters. The error in temperature (T) is estimated to be 0.5 K, and the standard deviation of the rate constant (*k*) measured from three trials (Table A.1) can used as the error in *k*.[1] An Eyring analysis should span at least 50 K, hence the experimentalist must perform this calculation for each temperature.

25 °C Run	k x 10^3 ($M^{-1}s^{-1}$)
1	1.20
2	1.25
3	1.26
ave	1.25
std. dev.	0.00989

Table A.1. Rate data acquired from the carbonylation of imide (dadi)TiNAd (**2**=NAd).

It should be noted that the errors in the x-axis are typically half or less than those associated with the y-axis, and therefore can be neglected. It has been found that incorporating them into the weighting scheme during linear regression has little effect on the resulting fits.

A.4.1. Calculation of the uncertainty in ln(k/T)

In this case, *q* is a function of two measured quantities (*k*, and T), thus eq 7 can be used to calculate the uncertainty in *q* (δq). Note that for the calculation below, 3σ is used as the uncertainty for the rate constant (*k*), representing a 95% confidence interval.

$$q = ln\frac{k}{T} = ln\frac{1.25 * 10^{-3}}{298} = -12.38 \quad \text{(eq 11)}$$

$$\delta q = \sqrt{(\frac{\partial q}{|\partial k|}\delta k)^2 + (\frac{\partial q}{|\partial T|}\delta T)^2} \quad \text{(eq 12)}$$

$$(\frac{\partial q}{|\partial k|}\delta k)^2 = \left(\frac{1}{k} * \delta k\right)^2 = \left(\frac{1}{1.25 * 10^{-3}} * 9.89 * 10^{-6}\right)^2 = 5.63 * 10^{-4}$$

$$(\frac{\partial q}{|\partial T|}\delta T)^2 = \left(\frac{1}{T} * \delta T\right)^2 = \left(\frac{1}{298} * 0.5 = 2.82\right)^2 = 2.82 * 10^{-6}$$

$$\delta q = \sqrt{5.63 * 10^{-4} + 2.82 * 10^{-6}} = 2.38 * 10^{-3}$$

A.4.2. Uncertainty from linear regression

Once the above calculation has been repeated for each data point, a ln(*k*/T) versus 1/T plot is made (Eyring plot). The uncertainties in the intercept and slope are required to complete this error analysis, which are computed using the least squares method. When fitting the data (linear regression), the uncertainties in each ln(*k*/T) point are used as weighting factors. The result is a better and more accurate fit, as well as a more accurate estimate in the errors for the fit coefficients (*i.e.*, slope and intercept). The uncertainties in the fit coefficients for this analysis were obtained using the error analysis function in Igor Pro 6,[6] and represent a 95% confidence interval (Table A.2.). Alternatively, these errors can be obtained by plotting all the non-averaged data (*i.e.*, each data point from each trial) then applying the “LINEST” function in Microsoft Excel.

b (slope)	- 4458.6 ± 228
a (intercept)	2.55 ± 0.75

Table A.2. Fit coefficients obtained from a weighted linear regression of an Eyring plot. Uncertainties were computed using least squares method and represent a 95% confidence interval (3σ)

A.4.3. Uncertainty in the enthalpy of activation (∆H‡)

As eq 9 states, the enthalpy of activation is the product of two measured values, the slope (b) and the gas constant (R). Hence, the rigorous calculation for the fractional uncertainty in ∆H‡, using eq 4, can be done in the following way:

$$\frac{\delta\Delta H^{\ddagger}}{|\Delta H^{\ddagger}|} = \sqrt{\left(\frac{\delta b}{|b|}\right)^2 + \left(\frac{\delta R}{|R|}\right)^2} = \sqrt{\left(\frac{228}{|-4458.6|}\right)^2 + \left(\frac{5 * 10^{-8}}{|8.3144598|}\right)^2} \qquad \text{(eq 13)}$$

$$= 0.051$$

Therefore:

$$-\Delta H^{\ddagger} = 37.1 \pm 1.9\ kJ/Mol = 8.9 \pm 0.5\ kcal/Mol$$

Realizing that the error in the gas constant is vanishingly small, it can be treated as an exact number. This leads to the following simplification:

$$\delta\Delta H^{\ddagger} = |R|\delta b = 8.314 * 228 = 1.9\ kJ/Mol = 0.5\ kcal/Mol \qquad \text{(eq 14)}$$

A.4.4. Uncertainty in the entropy of activation (∆S‡)

The rigorous calculation for the uncertainty in ∆S‡ requires more arithmetic and is provided below:

$$\frac{\delta\Delta S^{\ddagger}}{|\Delta S^{\ddagger}|} = \sqrt{\left(\frac{\delta\left(a - ln\frac{k_B}{h}\right)}{\left|a - ln\frac{k_B}{h}\right|}\right)^2 + \left(\frac{\delta R}{|R|}\right)^2} \qquad \text{(eq 15)}$$

Breaking it down piecewise:

$$\delta\left(ln\frac{k_B}{h}\right) = \sqrt{\left(\frac{1}{k_B}\delta k_B\right)^2 + \left(\frac{1}{h}\delta h\right)^2}$$

$$= \sqrt{\left(\frac{1}{1.3864052 * 10^{-23}} * (8 * 10^{-32})\right)^2 + \left(\frac{1}{6.626070040 * 10^{-23}} * (8 * 10^{-45})\right)^2}$$

$$= 1.2 * 10^{-11}$$

$$\delta\left(a - ln\frac{k_B}{h}\right) = \sqrt{\left(\frac{\delta a}{|a|}\right)^2 + \left(\frac{\delta ln\frac{k_B}{h}}{\left|ln\frac{k_B}{h}\right|}\right)^2}$$

$$= \sqrt{\left(\frac{0.75}{2.5499}\right)^2 + (1.2 * 10^{-11})^2} = 0.2941$$

Finally:

$$\frac{\delta\Delta S^{\ddagger}}{|\Delta S^{\ddagger}|} = \sqrt{\left(\frac{\delta\left(a - ln\frac{k_B}{h}\right)}{\left|a - ln\frac{k_B}{h}\right|}\right)^2 + \left(\frac{\delta R}{|R|}\right)^2}$$

$$= \sqrt{\left(\frac{0.2941}{|-21.21|}\right)^2 + \left(\frac{5 * 10^{-8}}{|8.3144598|}\right)^2} = 0.0139$$

Therefore:

$$\Delta S^{\ddagger} = -176.35 \pm 6.2\ J/Mol = -42.1 \pm 1.5\ cal/Mol$$

As with $\Delta H^{\ddagger}$, this calculation can be simplified because the errors associated with the Boltzmann, Planck, and gas constants are extremely small relative to that of the slope obtained from linear regression. The uncertainty in

the entropy of activation simplifies to the addition of an exact number and multiplication by an exact number as shown in eq 16.

$$\delta\Delta S^{\ddagger} = \delta\left(a - ln\frac{k_B}{h}\right) * |R| = 0.75 * 8.3144598 = 6.23 \quad \text{(eq 16)}$$

This simplification gives the exact same uncertainty in $\Delta S^{\ddagger}$ that was found from using eq 15.

$$\Delta S^{\ddagger} = -176.35 \pm 6.2\ J/Mol = -42.1 \pm 1.5\ cal/Mol$$

A.4.5. Uncertainty in Gibbs free energy of activation ($\Delta G^{\ddagger}$)

With the uncertainties in $\Delta H^{\ddagger}$ and $\Delta S^{\ddagger}$ on hand, the uncertainty in $\Delta G^{\ddagger}$ can now be calculated using eq 17 derived from eq 3. Note the conversion from fractional uncertainty ($\delta x/|x|$) to uncertainty δx.

$$\delta\Delta G^{\ddagger} = \sqrt{(\delta\Delta H)^2 + (\delta\Delta S^{\ddagger}T)^2} \quad \text{(eq 17)}$$

Again, breaking it down piecewise:

$$\frac{\delta\Delta S^{\ddagger}T}{|\Delta S^{\ddagger}T|} = \sqrt{\left(\frac{\delta\Delta S^{\ddagger}}{|\Delta S^{\ddagger}|}\right)^2 + \left(\frac{\delta\Delta T}{|T|}\right)^2} = \sqrt{0.035^2 + \left(\frac{0.5}{298}\right)^2} = 0.035$$

$$\delta\Delta G^{\ddagger} = \sqrt{(\delta\Delta H)^2 + (\delta\Delta S^{\ddagger}T)^2}$$
$$= \sqrt{(0.5)^2 + (0.035 * (1.5 * 10^{-3}) * 298)^2} = 0.5$$

Therefore:

$$\Delta G^{\ddagger}(298\ K) = 21.7 \pm 0.5\ kcal/mol$$

Conclusions:

In general, any physical constant used in an Eyring analysis can be treated as an exact number. This will simplify the calculation of the uncertainties associated with enthalpy and entropy of activation. It should be noted that using a weighted linear regression will give the most accurate estimations in the errors associated with the slope and intercept. Although, an analysis of the carbonylation rate data (*cf.* Chapter 2) using a non-weighted linear regression found $\Delta H^{\ddagger}$ and $\Delta S^{\ddagger}$ values to deviate from those calculated using a weighted linear regression by only 3% and 2%, respectively. Accordingly, the uncertainty in ln(*k*/T) values can be neglected *as long as a sufficient amount of data is available* (*i.e.*, a temperature range of at least 50 ^{o}C performed in triplicate), and the resulting Eyring analysis will yield useful fit coefficients (slope and intercept) for an experimental chemist.

References:

(1) Taylor, J. R. *An Introduction to Error Analysis: The Study of Uncertainties in Physical Measurements*, 2nd ed.; University Science Books: Sausalito, 1997.

(2) Eyring, H. *J. Chem. Phys.* **1935**, *3* (2), 107–115.

(3) Eyring, H.; Polanyi, M. *Z. Phys. Chem. B*. **1931**, *12*, 279–311.

(4) Laidler, K. J.; King, M. C. *J. Phys. Chem.* **1983**, *87* (15), 2657–2664.

(5) Anslyn, E. V; Dougherty, D. A. *Modern Physical Organic Chemistry*; Murdzec, J., Ed.; University Science Books: Sausalito, 2006.

(6) WaveMetrics Inc.: Lake Oswego 2017.

Appendix B

Reversible C-C Bond Formation with a Redox Non-innocent Diazepane-pyridine Imine Ligand

Introduction:

Transition metal catalyzed carbon-carbon (C-C) bond forming reactions have proven to be some of the most powerful chemical transformations for the agrochemical, pharmaceutical, and fine chemical industries.[1,2] Typically, the catalysts used rely on strong field ligands and closed shell organometallic species to promote the 2-electron changes that form new C-C bonds. In contrast, the use of weak field ligands with first row transition metals have been shown to catalyze C-C bond forming reactions such as ethylene polymerization[3–7] and alkene cycloaddition.[7,8] Furthermore, when coupled to redox non-innocent (RNI) ligands such as pyridine imines[7] or β-diketiminates,[9] a unique opportunity to control the electronic structure of the catalyst and optimize reactions arises. While 2-electron redox processes have shown their utility in industrial and research settings, 1-electron processes such as atom transfer radical polymerization (ATRP) can be equally useful.[10]

While exploring the reactivity of a weak field diazepane ligand with a redox non-innocent pyridine-imine group (**13**, DPyIm = (E)-1-(pyridin-2-yl)-N-(1,4,6-trimethyl-1,4-diazepan-6-yl)methanimine), an interesting reversible C-C bond forming reaction was discovered. In addition, this 1-electron process which exhibits clear ligand RNI, was envisioned to catalyze ATRP. During catalysis, the iron center transfers the halogen atom, and the RNI ligand can be oxidized/reduced by 1-electron to maintain the iron center in its preferred[11] +2 charge state. This unprecedented manifestation of RNI in iron catalyzed

ATRP would represent an expansion of the capabilities of ligand centered redox events. Open shell {(DPyA)FeX}$_2$ complexes (**15**-X; X = Cl, Br) showed modest catalytic activity for ATRP, providing a proof of concept that RNI ligands can be harnessed as radical polymerization catalysts. The reactivity explored has also provided some basic design principles to improve ATRP catalysts that utilize RNI ligands.

Results and Discussion:

B.1. Ligand synthesis

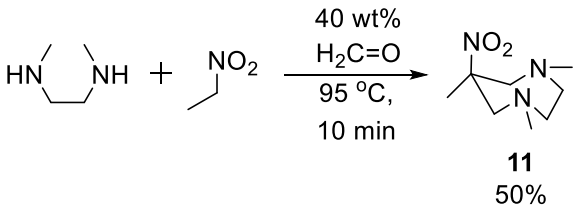

11
50%

(eq 1)

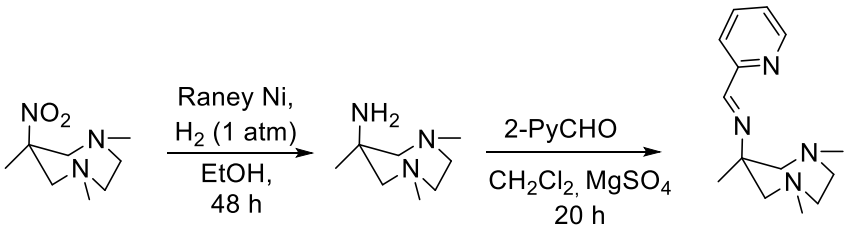

12
95%

DPyIm (**13**)
83%

(eq 2)

The first step in the synthesis of DPyIm (**13**, DPyIm = (E)-1-(pyridin-2-yl)-N-(1,4,6-trimethyl-1,4-diazepan-6-yl)methanimine), a nitro-Mannich reaction,[12] proceeds smoothly under solvent-free conditions (eq 1).[13] After vacuum distillation 1,4,6-trimethyl-6-nitro-1,4-diazepane (**11**) is obtained in 50% yield as a clear liquid. Reduction of **11** using Raney-Ni and H_2 (1 atm),

gives the amine **12** (**12** = 1,4,6-trimethyl-1,4-diazepan-6-amine) as a clear liquid in 95% (eq 2).[13] The amine (**12**) is then condensed onto 2-pyridine carboxaldehyde with $MgSO_4$ as a drying agent, to give the trimethyldiazepane-pyridineimine ligand (DPyIm, **13**) as a faint yellow viscous oil in 83% yield.

B.2. Synthesis and reactivity of (DPyIm)FeX_2 (X = Cl, 14-Cl_2; X = Br, 14-Br_2) complexes

*B.2.1. Synthesis and reactivity of dihalides **14**-Cl_2 and **14**-Br_2*

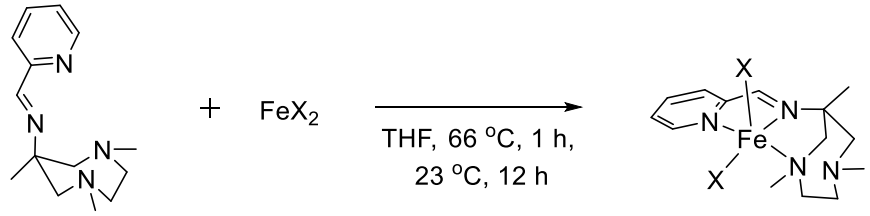

DPyIm (**13**) X = Cl, Br (DPyIm)FeX_2 (**14**-X_2) X = Cl, 92% X = Br, 85%

(eq 3)

The (DPyIm)FeX_2 (X = Cl, **14**-Cl_2; X = Br, **14**-Br_2) complexes were easily synthesized by refluxing a THF suspension of FeX_2 (X = Cl, Br) in the presence of free DPyIm (**13**) ligand (eq 3). After filtration, **14**-Cl_2 and **14**-Br_2 were isolated as blue crystalline solids in 92% and 85% yields, respectively. The ^{1}H NMR spectrum of **14**-Cl_2 displays 10 paramagnetically shifted resonances suggesting a lack of symmetry, and structural evidence for a pseudo square pyramidal iron center has also been obtained in this laboratory. A solution magnetic moment[14,15] of 5.0(1) μ_B in CD_3CN was measured for **14**-Cl_2, consistent with a high spin Fe(II) center. The bromide derivative (**14**-Br_2) displays a similar ^{1}H NMR spectrum with 11 paramagnetically shifted

resonances, and a solution magnetic moment[14,15] of 5.2(1) μ_B that is consistent with a high spin S = 2 iron center.

*B.2.2. Synthesis and reactivity of dimers **15**-X (X = Cl, Br)*

The pyridine-imine unit of the diazepane ligand (DPyIm) was reasoned to be redox active upon reduction of the dihalide complexes **14**-Cl_2 and **14**-Br_2. Hence, **14**-Cl_2 was treated with 1 equiv 1 wt% Na/Hg or KC_8 at -78 °C in THF. Upon warming to room temperature, a color change from blue to red was observed, and a red product with increased solubility in THF was obtained. Through a structural study (*vide infra*), the product of the reduction was identified to be the dimer complex {(DPyA)FeCl}$_2$ (**15**-Cl; DPyA = 1,2-di(pyridin-2-yl)-N1,N2-bis(1,4,6-trimethyl-1,4-diazepan-6-yl)ethane-1,2-diamide), as depicted in eq 4. The bromide derivative can also be synthesized following the same procedure to yield **15**-Br in a slightly lower 67% yield, which is isolated as a red powder. The solution magnetic susceptibilities of **15**-Cl and **15**-Br are 7.4(2) and 7.8(1) μ_B, respectively, indicating modest ferromagnetic coupling between the two high spin Fe(II) centers.

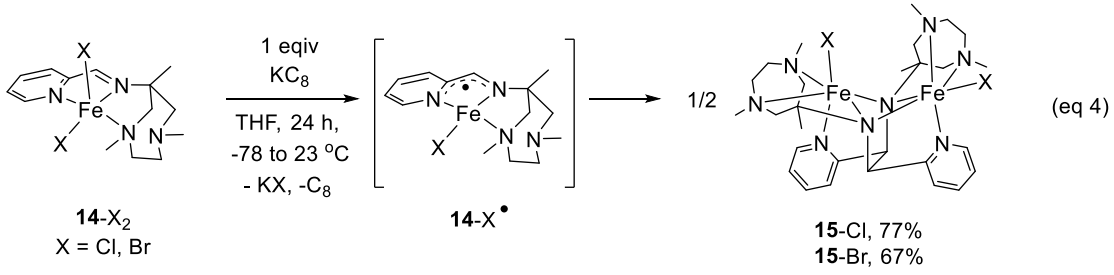

(eq 4)

Complexes (**15**-Xl; X = Cl, Br) were tested in the Fors laboratory at Cornell University for their ATRP activity. Initial results indicate that modest polymerizations can be achieved with PDI's ranging from ~2-4. The

polymerizations appear to be controlled but unfortunately the ligand based radical is likely interfering with the polymerization process (*vide infra*). This suggests that the imine moiety needs to be sterically protected to prevent reactions between the putative ligand based radical (**14**-X$^{\bullet}$) and the propagating polymer or initiator.

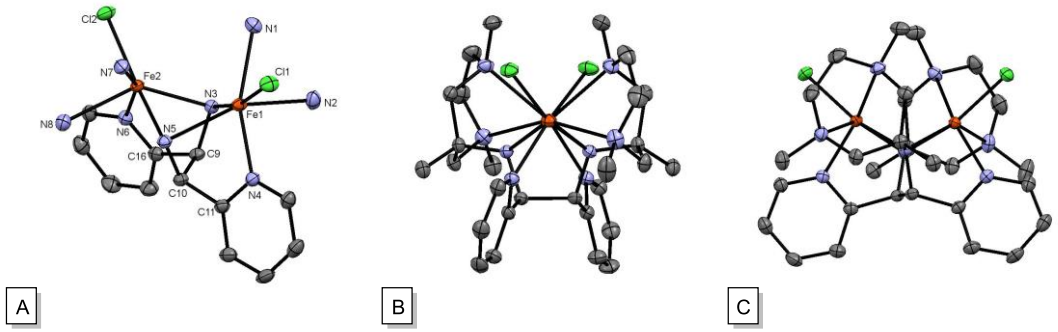

Figure B.1. Molecular views of dimer {(DPyA)FeCl}$_2$ (**15**-Cl); hydrogens omitted for clarity. A) Side view with diazepane carbons omitted for clarity. B) View down the Fe-Fe axis. C) Side view perpendicular to Fe-Fe axis.

*B.2.3. Structure of {(DPyA)FeCl}$_2$ (**15**-Cl; DPyA = 1,2-di(pyridin-2-yl)-N1,N2-bis(1,4,6-trimethyl-1,4-diazepan-6-yl)ethane-1,2-diamide)*

Figure B.1 depicts the solid state structure of dimer {(DPyA)FeCl}$_2$ (**15**-Cl; DPyA = 1,2-di(pyridin-2-yl)-N1,N2-bis(1,4,6-trimethyl-1,4-diazepan-6-yl)ethane-1,2-diamide), revealing two distorted octahedral iron centers. The two μ_2-amide nitrogens are derived from the imine moiety of (DPyIm)FeCl$_2$ (**14**-Cl$_2$). Each bridging amide occupies an axial site trans to the chloride (d(Fe1-N3) = 2.031(2) Å); d(Fe2-N5) = 2.047(2) Å), and an equatorial site, with the latter showing significantly elongated Fe-N$_{am}$ distances (d(Fe1-N5) = 2.354(2) Å; d(Fe2-N3) = 2.316(2) Å). The distortion of the octahedron for both iron centers results from the positioning of the μ_2-amides, which are pulled out of their respective equatorial planes (∠Cl1-Fe1-N5 = 116.17(4)°; ∠Cl2-Fe2-N3

= 122.73(6)°.The tertiary diazepane nitrogens that coordinate to Fe(1) and Fe(2) have bite angles of 67.89(6)° and 68.06(6)°, respectively, and can be described as weakly coordinating (d(Fe1-N1,N2) = 2.441(2) Å, 2.484(2) Å; d(Fe2-N7,N8) = 2.456(2) Å, 2.467(2)Å). The Fe-Fe distance of 3.1312(6) Å falls outside of the sum of the two covalent radii,[16] but well within the sum of the van der Waals radii.[17] Most importantly, the new C-C bond formed in **15**-Cl, containing what was originally the imine carbons of each DPyIm ligand, is relatively long at d(C9-C10) = 1.581(3) Å.[18] This suggests the possibility of reversible C-C bond formation through a reduction/oxidation cycle using a halogen atom source such as N-chlorosuccinamide (NCS) or tritylchlorlide.

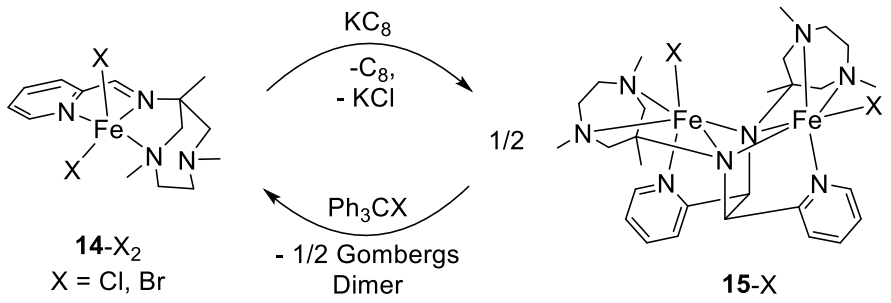

Scheme B.1. Reversible C-C bond formation between monomer **14**-X_2 and **15**-X (X = Cl, Br).

B.3. Reversible C-C bond formation

As outlined in Scheme B.1, the new C-C bond in dimers **15**-X (X = Cl, Br) can be homolytically cleaved upon oxidation using a halogen atom source such as Ph_3CX (X = Cl, Br). This oxidation regenerates the monomer **14**-X_2 (X = Cl, Br) and produces Gomberg's dimer, where the iron center maintains it +2 oxidation state. ^{1}H NMR spectroscopic analysis of the crude reaction mixtures revealed clean conversion to the dihalides (**14**-X_2; X = Cl, Br) when Ph_3CX was used as the oxidant, but the use of other halogen atom sources such as

NCS or NBS produces only trace dihalide. It is possible that the less sterically protected succinamide radical reacts with the ligand resulting in products that have incorporated the succiniamide moiety into the ligand scaffold. Preliminary GC-MS evidence suggests that when dimer **15**-Br is treated with ethyl-α-bromoisobutyrate, the isobutyrate group is incorporated into the ligand (eq 5), consistent with coupling between of the imine based radical (**14**-X$^{\bullet}$) and the organic isobutyrate radical. Thus, current synthetic efforts are focused on protecting the imine position with alkyl or aryl groups. Unfortunately, condensations of the teritiary diazepane amine (**12**), with ketones such as benzoyl pyridine or 2-acetylpyridine have been unsuccessful.

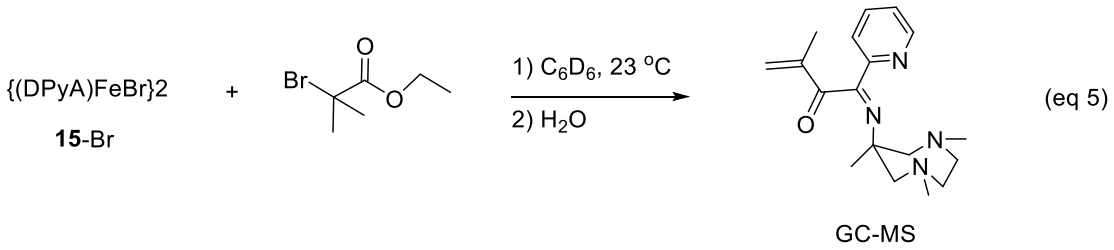

(eq 5)

GC-MS

Conclusions:

The weak field trimethyldiazpane pyridine-imine ligand scaffold undergoes reversible C-C bond formation when chelated to iron. Reactivity between the putative ligand based radical (**14**-X$^{\bullet}$) with organic radicals or ATRP initiators has limited its use as a polymerization catalyst. These preliminary results suggest that protection of the imine carbon will be required to prevent the reactions between radicals generated from halogen atom sources and the ligand. While standard condensation routes have been unsuccessful, other promising routes such as β-H elimination from the amine, and the use of a secondary diazepane-amine are actively being explored.

*Experimental***:**

A. General Considerations

All manipulations were performed using either glovebox or high vacuum line techniques. All glassware was oven dried. THF and diethyl ether were distilled under nitrogen from purple sodium benzophenone ketyl and vacuum transferred from the same prior to use. Hydrocarbon solvents were treated in the same manner with the addition of 1-2 mL/L tetraglyme. Benzene-d_6 was dried over sodium, vacuum transferred and stored over activated 4Å molecular sieves. THF-d_8 was dried over sodium and stored over purple sodium benzophenone ketyl. Acetonitrile-d_3 was dried over activated 4 Å molecular sieves then stored over fresh 4 Å molecular sieves. Nitroethane (EMD Millipore), N,N'-dimethylethylenediamine (Sigma-Aldrich), 40 wt % formaldelhyde solution (Macron), Raney-Ni (Sigma-Aldrich), 100 % ethanol (Fischer Scientific), and H_2 (Prepurified, Airgas) were used as received from their commercial sources.

1,4,6-trimethyl-6-nitro-1,4-diazepane (**11**)[13] and 1,4,6-trimethyl-1,4-diazepan-6-amine (**12**)[13] were prepared following literature procedures. NMR spectra were acquired using Mercury 300 MHz, INOVA 400 MHz, or Bruker AV III HD 500 MHz (equipped with a 5 mm BBO Prodigy cryoprobe) spectrometers. Chemical shifts are reported relative to benzene-d_6 (^{1}H δ 7.16; ^{13}C{^{1}H} δ 128.06), THF-d_8 (^{1}H 3.58), or CD_3CN (^{1}H 1.94). NMR spectra were processed using MNova 12.0.

B. Procedures

1. *(E)-1-(pyridin-2-yl)-N-(1,4,6-trimethyl-1,4-diazepan-6-yl)methanimine (**13**, DPyIm).* To a 100 mL round bottom flask, charged with **12** (1.000 g, 6.36

mmol), CH_2Cl_2 (45 mL), and $MgSO_4$ (*ca.* 3 g) was added 2-pyridine carboxaldehyde (681 mg, 6.36 mmol). The reaction mixture was stirred for 24 hours, filtered then concentrated to a yellow oil. The product was purified by vacuum distillation (1 x 10^{-5} torr, b.p. = 81 ^{o}C) yielding **13** as a light yellow oil (1.28 g, 83%). ^{1}H NMR (500 MHz, Benzene-d_6) δ 1.32 (s, 3H), 2.19 (s, 6H), 2.30 – 2.45 (m, 4H), 2.49 (d, *J* = 13.3 Hz, 2H), 2.78 (d, *J* = 13.3 Hz, 2H), 6.70 (ddd, *J* = 7.5, 4.8, 1.4 Hz, 1H), 7.14 (td, *J* = 7.7, 1.8 Hz, 1H), 8.18 (dt, *J* = 8.0, 1.2 Hz, 1H), 8.50 (dt, *J* = 4.7, 1.4 Hz, 1H), 8.86 (s, 1H). ^{13}C NMR (126 MHz, Benzene-d_6) δ 26.23, 48.84, 61.90, 64.35, 69.80, 120.42, 124.25, 135.92, 149.48, 156.74, 158.88.

2. *(DPyIm)$FeCl_2$ (**14**-Cl_2).* To a 50 mL round bottom flask was charged with DPyIm (200 mg, 0.812 mmol) and THF (ca. 25 mL), was added anhydrous $FeCl_2$ (102 mg, 0.805 mmol). The reaction mixture was heated to reflux for 1 h, then cooled to 23 °C and stirred for an additional 12 h. The suspension of blue crystalline solid was filtered and washed (3x) with THF. After removal of all volatiles **14**-Cl_2 was collected as a blue crystalline solid (279 mg, 92%). ^{1}H (400 MHz, Acetonitrile-d_3) δ 19.89 ($\Delta\nu_{1/2}$ = 80 Hz, 6H), 32.65 ($\Delta\nu_{1/2}$ =405 Hz, 2H), 37.01 ($\Delta\nu_{1/2}$ = 43 Hz, 1H), 38.49 ($\Delta\nu_{1/2}$ = 23 Hz, 1H), 56.77 ($\Delta\nu_{1/2}$ = 335 Hz, 6H), 61.90 ($\Delta\nu_{1/2}$ = 51 Hz, 1H), 103.83 ($\Delta\nu_{1/2}$ = 247 Hz, 2H), 141.16 ($\Delta\nu_{1/2}$ = 312 Hz, 1H), 210.68 ($\Delta\nu_{1/2}$ = 1135 Hz, 1H), 279.27 ($\Delta\nu_{1/2}$ = 547 Hz, 1H). μ_{eff} = 5.0(1) μ_B.

3. *(DPyIm)$FeBr_2$ (**14**-Br_2).* To a 50 mL round bottom flask was charged with DPyIm (1.099 g, 4.465 mmol) and THF (ca. 25 mL), was added anhydrous $FeBr_2$ (875 mg, 4.059 mmol). The reaction mixture was heated to reflux for 1 h, then cooled to 23 °C and stirred for an additional 12 h. The suspension of blue crystalline solid was filtered and washed (3x) with THF.

After removal of all volatiles **14**-Br_2 was collected as a blue crystalline solid (1.600 g, 85%). ^{1}H NMR (400 MHz, Acetonitrile-d_3) δ 18.45 ($\Delta\nu_{1/2}$ = 70 Hz, 3H), 25.67 ($\Delta\nu_{1/2}$ = 450 Hz, 2H), 29.74 ($\Delta\nu_{1/2}$ = 380 Hz, 2H), 34.73 ($\Delta\nu_{1/2}$ = 26 Hz, 1H), 35.24 ($\Delta\nu_{1/2}$ = 45 Hz, 1H), 64.72 ($\Delta\nu_{1/2}$ = 63 Hz, 1H), 67.08 ($\Delta\nu_{1/2}$ = 367 Hz, 6H), 113.90 ($\Delta\nu_{1/2}$ = 292 Hz, 2H), 160.10 ($\Delta\nu_{1/2}$ = 436 Hz, 2H), 207.01 ($\Delta\nu_{1/2}$ = 713 Hz, 1H), 301.12 ($\Delta\nu_{1/2}$ = 488 Hz, 1H). μ_{eff} = 5.2(1) μ_B

4. *{(DPyA)FeCl}$_2$ (**15**-Cl).* To a 100 mL round bottom flask charged with **14**-Br_2 (500 mg, 1.34 mmol) and KC8 (185 mg, 1.34 mmol) was added THF (ca. 30 mL) at -78 °C. The reaction solution was allowed to warm to 23 °C and stirred for an additional 60 h. The red reaction mixture was filtered and washed (1x). The resulting red solution was concentrated to ~ 5 mL, and the product was precipitated with pentane (ca. 30 mL) at -78 °C. The resulting suspension was warmed to room temperature, filtered, and all volatiles removed by vacuum. **15**-Cl was collected as a red solid (297 mg, 66%). A crystal suitable for X-Ray diffraction was obtained by diffusion of pentane vapor into a concentrated THF solution. ^{1}H NMR (300 MHz, THF-d_8) δ -37.56 ($\Delta\nu_{1/2}$ = 320 Hz, 2H), -8.31 ($\Delta\nu_{1/2}$ = 720 Hz, 2H), 32.86 ($\Delta\nu_{1/2}$ = 211 Hz, 7H), 34.41 ($\Delta\nu_{1/2}$ = 71 Hz, 3H), 37.86 ($\Delta\nu_{1/2}$ = 33 Hz, 3H), 40.00 ($\Delta\nu_{1/2}$ = 680 Hz, 2H), 41.54 ($\Delta\nu_{1/2}$ = 214 Hz, 8H), 53.49 ($\Delta\nu_{1/2}$ = 127 Hz, 3H), 64.18 ($\Delta\nu_{1/2}$ = 61 Hz, 3H), 72.82 ($\Delta\nu_{1/2}$ = 189 Hz, 2H), 113.92 ($\Delta\nu_{1/2}$ = 163 Hz, 2H), 126.92 ($\Delta\nu_{1/2}$ = 136 Hz, 3H), 178.31 ($\Delta\nu_{1/2}$ = 568 Hz, 2H), 283.48 ($\Delta\nu_{1/2}$ = 468 Hz, 2H). μ_{eff} = 7.4(2) μ_B.

5. *{(DPyA)FeBr}$_2$ (**15**-Br).* To a 100 mL round bottom flask charged with **14**-Br_2 (500 mg, 1.08 mmol) and KC8 (146 mg, 1.08 mmol) was added THF (ca. 30 mL) at -78 °C. The reaction solution was allowed to warm to 23 °C and stirred for an additional 60 h. The red reaction mixture was filtered and washed (1x). The resulting red solution was concentrated to ~ 5 mL, and the product

was precipitated with pentane (ca. 30 mL) at -78 °C. The resulting suspension was warmed to room temperature, filtered, and all volatiles removed by vacuum. **15**-Br was collected as a red solid (257 mg, 67%). ^{1}H NMR (300 MHz, THF-d_8) δ -49.69 ($\Delta\nu_{1/2}$ = 303 Hz, 2H), -7.58 ($\Delta\nu_{1/2}$ = 410 Hz, 7H), 10.58 ($\Delta\nu_{1/2}$ = 226 Hz, 2H), 30.30 ($\Delta\nu_{1/2}$ = 58 Hz, 2H), 36.02 ($\Delta\nu_{1/2}$ = 216 Hz, 6H), 37.39 ($\Delta\nu_{1/2}$ = 25 Hz, 4H), 46.09 ($\Delta\nu_{1/2}$ = 160 Hz, 6H), 64.79 ($\Delta\nu_{1/2}$ = 40 Hz, 3H), 66.37 ($\Delta\nu_{1/2}$ = 103 Hz, 2H), 67.03 ($\Delta\nu_{1/2}$ = 150 Hz, 2H), 110.97 ($\Delta\nu_{1/2}$ = 130 Hz, 2H), 127.15 ($\Delta\nu_{1/2}$ = 105 Hz, 2H), 188.27 ($\Delta\nu_{1/2}$ = 400 Hz, 2H), 255.59 ($\Delta\nu_{1/2}$ = 480 Hz, 2H). μ_{eff} = 7.8(1) μ_B.

6. *Dimer (**15**-X; X = Cl, Br) to monomer (**14**-X_2; X = Cl, Br) oxidation.*

***15**-Cl to **14**-Cl_2:* To a scintillation vial charged with **15**-Cl (24 mg, 0.036 mmol) and THF (ca. 12 mL) was added solid Ph_3CCl (20 mg, 0.072 mmol), whereupon a color change from red to blue was observed. The reaction mixture was stirred for 16 h then filtered. The resulting blue filter cake was dissolved in CD_3CN for ^{1}H NMR spectroscopic analysis, which was consistent with the formation of complex **14**-Cl_2 and Gomberg's dimer.

***15**-Br to **14**-Br_2:* To a scintillation vial charged with **15**-Br (23 mg, 0.030 mmol) and THF (ca. 5 mL) was added solid Ph_3CBr (20 mg, 0.062 mmol), whereupon a color change from red to blue was observed. The reaction mixture was stirred for 16 h then filtered. The resulting blue filter cake was dissolved in CD_3CN for ^{1}H NMR spectroscopic analysis, which was consistent with the formation of complex **14**-Br_2 and Gomberg's dimer.

C. X-ray Crystal Structure

Upon isolation, the crystals were covered in polyisobutenes and placed under a 173 K N_2 stream on the goniometer head of a Siemens P4 SMART

CCD area detector (graphite-monochromated Cu radiation, λ = 1.54184 Å). The structures were solved by direct methods (SHELXS). All non-hydrogen atoms were refined anisotropically unless stated, and hydrogen atoms were treated as idealized contributions (Riding model).

*{(DPyA)FeCl}$_2$ (**15**-Cl).* A red plate (0.225 x 0.095 x 0.037 mm) was obtained from THF/pentane. A total of 34,256 reflections were collected with 6,389 determined to be symmetry independent (R_{int} = 0.0458), and 5,868 were greater than 2σ(I). A semi-empirical absorption correction from equivalents was applied, and the refinement utilized $w^{-1} = \sigma^2(F_o^2) + (0.0556p)^2 + 2.7354p$, where $p = ((F_o^2 + 2F_c^2)/3)$.

References:

(1) Torborg, C.; Beller, M. *Adv. Synth. Catal.* **2009**, *351* (18), 3027–3043.

(2) Magano, J.; Dunetz, J. R. *Chem. Rev.* **2011**, *111* (3), 2177–2250.

(3) Bennett, A. M. A. US 6214761 B1, 1989.

(4) J. P. Britovsek, G.; C. Gibson, V.; J. McTavish, S.; A. Solan, G.; J. P. White, A.; J. Williams, D.; J. P. Britovsek, G.; S. Kimberley, B.; J. Maddox, P. *Chem. Commun.* **1998**, No. 7, 849–850.

(5) Small, B. L.; Brookhart, M.; Bennett, A. M. A. *J. Am. Chem. Soc.* **1998**, *120* (16), 4049–4050.

(6) Chirik, P. J.; Schaefer, B. A.; Margulieux, G. W. *Bull. Japan Soc. Coord. Chem.* **2016**, *67*, 19–29.

(7) J., C. P. *Angew. Chemie Int. Ed.* **2017**, *56* (19), 5170–5181.

(8) Bouwkamp, M. W.; Bowman, A. C.; Lobkovsky, E.; Chirik, P. J. *J. Am. Chem. Soc.* **2006**, *128* (41), 13340–13341.

(9) Holland, P. L. *Acc. Chem. Res.* **2015**, *48* (6), 1696–1702.

(10) Matyjaszewski, K. *Macromolecules*. **2012**, *45* (10), 4015–4039.

(11) Wolczanski, P. T. *Organometallics*. **2017**, *36* (3), 622–631.

(12) Noble, A.; Anderson, J. C. *Chem. Rev.* **2013**, *113* (5), 2887–2939.

(13) Appel, A. C. M.; Hage, R.; Russel, S. W.; Tetard, D. WO 2001085717, 2001.

(14) Evans, D. F. *J. Chem. Soc.* **1959**, 2003–2005.

(15) Schubert, E. M. *J. Chem. Educ.* **1992**, *69* (1), 62.

(16) Cordero, B.; Gomez, V.; Platero-Prats, A. E.; Reves, M.; Echeverria, J.; Cremades, E.; Barragan, F.; Alvarez, S. *Dalt. Trans.* **2008**, No. 21, 2832–2838.

(17) Bondi, A. *J. Phys. Chem.* **1964**, *68* (3), 441–451.

(18) Allen, F. H.; Kennard, O.; Watson, D. G.; Brammer, L.; Orpen, A. G.; Taylor, R. *J. Chem. Soc. Perkin Trans. 2*. **1987**, No. 12, S1–S19.